FULL CAPABILITY FORMATION FLIGHT CONTROL

THESIS

Ryan K. Osteroos, Major, USAF

AFIT/GAE/ENY/05-M16

DEPARTMENT OF THE AIR FORCE
AIR UNIVERSITY

AIR FORCE INSTITUTE OF TECHNOLOGY

Wright-Patterson Air Force Base, Ohio

APPROVED FOR PUBLIC RELEASE; DISTRIBUTION UNLIMITED

The views expressed in this thesis are those of the author and do not reflect the official policy or position of the United States Air Force, Department of Defense, or the United States Government.

AFIT/GAE/ENY/05-M16

FULL CAPABILITY FORMATION FLIGHT CONTROL

THESIS

Presented to the Faculty

Department of Aeronautics and Astronautics

Graduate School of Engineering and Management

Air Force Institute of Technology

Air University

Air Education and Training Command

In Partial Fulfillment of the Requirements for the

Degree of Master of Science in Aeronautical Engineering

Ryan K. Osteroos, BS

Major, USAF

February 2005

APPROVED FOR PUBLIC RELEASE; DISTRIBUTION UNLIMITED.

AFIT/GAE/ENY/05-M16

FULL CAPABILITY FORMATION FLIGHT CONTROL

Ryan K. Osteroos, BS
Major, USAF

Approved:

/signed/	2 Feb 05
Dr. David Jacques (Co-Chairman)	date
/signed/	2 Feb 05
Dr. Meir Pachter (Co-Chairman)	date
/signed/	2 Feb 05
Maj Russell Adelgren (Member)	date

Abstract

The subject of automatic formation flight control is of current interest to the development of Unmanned Aerial Vehicles (UAV). Previous control approaches have been refined in this work to allow more robust maneuvering and to include a fourth control parameter. The equations of motion for each aircraft as a point mass, expressed in a wind-axes coordinate system, are coupled into differential equations that model the two aircraft system dynamics. Control laws are developed that include proportional and integral action. Gains are determined based on formation performance. Lead maneuvers are simulated and the controller is gauged on its ability to maintain the commanded formations in and out of the vortex wake generated by the lead aircraft. A Dryden wind model at varying intensities is applied to the system. In simulation the controller maintained acceptable performance in all maneuvers tested.

A slightly modified controller was applied to the USAF NF-16D aircraft for flight testing. Utilizing a data link system and a virtual lead aircraft generated from a ground based control station, the NF-16D was able to flight test the controller. In-flight the precision of control was affected by winds, atmospheric turbulence, and data-link dropouts, but the controller was stable, and able to perform all of the desired formation hold and change maneuvers.

To my Wife, my Life and Inspiration

Acknowledgments

I would like to express my sincere appreciation to Dr. Meir Pachter for all of his insight and guidance both during this endeavor and in the class room. His wisdom and understanding of the subject of formation flight and navigation is unparalleled. Dr. Dave Jacques has been invaluable as my advisor during my stay at AFIT and the rail that has kept me on track. Thank you for your persistence and patience. The flight test portion of this thesis would not have been possible without the technical competency and support of Mr. Andrew Markofski, whose knowledge and skill are a true asset to the students and faculty of the USAF Test Pilot School. I cannot thank Dr. John Raquet enough for his moral support and inspiration over the last two years. Dr. Raquet's ability to see the crux of a problem and formulate solutions is only surpassed by his technical competency. He is a truly gifted scholar and teacher. Thank you for being a great role model, advisor and friend. Special thanks is given to Finley Barfield for his patient help with the D-Six simulation software given during off-duty hours and even on the weekends. The success of the project would have been doubtful without his support.

Finally I would like to thank the two most important people in my life, my wife and daughter. You have been my rock, and mean more to me than life itself. You are both truly a gift from God. Thank you for your love, support, encouragement and most importantly, laughter.

Finally, I would like to thank God, in whom all things are possible.

Ryan K. Osteroos

Table of Contents

List of Figures

Page

Page

Page

Page

Page

List of Tables

List of Symbols

Symbol	Definition
C	DCM (Direction Cosine Matrix)
C_D	Drag Coefficient
C_L	Lift Coefficient
C_Y	Side Force Coefficient
D	Drag
F_Y	Side Force
H	Course
K	Drag Polar
L	Lift
M	Mass of Aircraft
P	Angular Rate of Wind Axis(x-component)
q	Dynamic Pressure
Q	Angular Rate of Wind Axis(y-component)
R	Angular Rate of Wind Axis (z-component)
$\overline{R}$	Position Vector of Lead in Wing Reference System
$\bar{r}$	Position Vector of Lead in Inertial Reference System
R_o	Position Vector of Wing in Inertial Reference System
S	Wing Area
V	Velocity

x_d .....Wing/Lead Separation in Wing Reference System (x-component)

y_d .....Wing/Lead Separation in Wing Reference System (y-component)

z_d .....Wing/Lead Separation in Wing Reference System (z-component)

$\alpha / \alpha_{OL} / \alpha_o$ ..... Angle of Attack(AOA)/AOA zero lift/AOA in steady flight

β / β_o ..... Side-slip Angle/Side-slip Angle in steady flight

γ / γ_o .....Flight Path Angle/Flight Path Angle in steady flight

ρ .....Air Density

ϖ ..... Angular Rate Vector

$\bar{\phi}_V$ ..... Velocity Vector Roll Angle

μ / μ_o ..... Throttle Setting(0-1)/Steady flight throttle setting

L .....Subscript for Leader

W .....Subscript for Wingman

wa ..... Subscript for Wind Axis Reference System

n .....Subscript for Navigation Axis (Psuedo-Inertial Axis) Reference System

I_Z ..... Moment of Inertia About the aircraft body frame z axis

FULL CAPABILITY FORMATION FLIGHT CONTROL

I. Introduction

Background

The subject of automatic formation flight control is of current interest to the development of unmanned aerial vehicles (UAV) for the purposes of worldwide deployment and in-theatre operations. It is also of current interest to operational unmanned combat aerial vehicles (UCAV) for the purposes of attack formation control and general formation operations. The benefits of formation flight include fuel savings at certain close formation positions, tanker formation operations where flights of UAV's are ferried by a single tanker, and kill container operations for UCAV's. Long duration automatic formation flight for fuel savings or weather penetration is also of interest to manned flight operations. The Air Force Institute of Technology has a long history of MS thesis in formation flight control. In 1991 Paul Rohs designed and simulated an automated formation control system using proportional and integral control (17). It was initially developed to maintain a formation of C-130 aircraft and later applied to a formation of H-53 aircraft. The control system was based on one-way received information from a lead aircraft and the desired formation to be maintained. It was determined from this initial set of tests that a performance mismatch between different aircraft would cause controller issues that were overcome by attenuating the lead aircraft's performance. John Dargan continued the effort with the formation of C-130 aircraft in his AFIT MS thesis presented in December of 1991 (4). The control system in

simulation was able to correct to zero steady state errors for the C-130 formations and was proven to be feasible for any type of aircraft flying in wide formations. In December of 1992 Louis Buzogany developed, for his MS thesis, a control system used to determine optimum controller parameters for the previously tested C-130 formation in an effort to reduce fuel consumption and formation transients (3). In March of 1994 Vincent Reyna conducted an exploration of several automatic formation controller algorithms and compared their results (16). His study concluded that integral control was needed for precise formation control. He also looked at the different algorithms to compare their usefulness during different aircraft tasks. The results of this thesis were incorporated into the MS thesis work of Michael Veth in December of 1994 (19). Veth utilized higher order aircraft models, a proportional only control law, and an energy tracking algorithm that was able to minimize, through simulation, aircraft energy excursions. A year later in December of 1995, Shawn McCamish developed a constrained optimization algorithm to optimize the gain set of a fixed controller architecture for the purposes of increased controller robustness in the face of formation maneuvers and system non-linearities (11). In March of 1999 Andrew Proud presented his MS thesis in which he tackled the problems of close formation flight within the vortex of the lead aircraft (15). One conclusion of his work was that formation controllers designed to conduct wide formation maneuvering have sufficient control authority to overcome the additional forces of a close formation position, including those positions within the vortex of the lead aircraft (15:Sec 6,3). The MS thesis of James Hall was presented in March of 2000, in which the dynamics of two aircraft were computer modeled and simulated in three dimensions with three control parameters, lift, roll rate, and thrust (7). Hall included the

contributions of the lead wake by integrating the forces along the wing aircraft to determine the overall change in lift and drag. These values were then included in the model. He also found the controller was able to overcome the wake forces without significant additional error. His simulations included a displacement recovery maneuver, where the trail aircraft was initialized away from the commanded position and the controller was allowed to fix the initial errors. He also conducted velocity changes, altitude changes, heading changes, and a climbing-turning maneuver while the trail aircraft held a commanded formation. The control laws included proportional, integral, derivative and, in some cases, second-derivative feedback. His simulation results indicated errors of approximately 12 feet in the x direction for 30 foot per second velocity changes, approximately 24 and 9 feet in the x and y directions for lead climbs of 450 meters and errors of less than 7 feet in all three directions during 15 degree heading change maneuvers using 20 degrees of bank (7:Sec 5). It was determined that this level of precision would not be sufficient for the purposes of close formation flight considering the real world disturbances that will be encountered in flight test.

Problem Statement

The ultimate goal of this work is to control actual assets, namely two USAF F-16's, in automatic formation flight. Previous control designs did not demonstrate the robustness and precision required for flight test success. Thus, the problem was to create a three dimensional controller that would be more precise and capable of long term formation flight. In an attempt to increase the robustness of the system and decrease excessively noisy inputs, the controller will not utilize any control parameters that rely

upon the derivative of a sensor based signal. In addition, it is necessary to model the significant real world dynamics, such as the vortex airflow generated by the lead aircraft and atmospheric disturbances to gain a greater probability of success when the controller is implemented in flight test.

Research Objectives

The first objective is that a mathematical model of a two-aircraft system be derived. The next objective is to create this model in Simulink and develop a controller that displays stability in all maneuvers tested. The tested maneuvers include maintaining a given position off of the lead aircraft while the lead aircraft performs unlimited climbs or descents at a flight path angle of less than ±30 degrees. The lead aircraft will then perform unlimited turning maneuvers with a roll angle of not greater than 30 degrees and a roll rate of not greater than 30 degrees/sec. Finally the lead aircraft will perform unlimited airspeed accelerations/decelerations with a minimum of 5% and a maximum of 95% of the maximum, non-afterburner power setting. The controller will be designed to achieve a maximum error of 1 foot from the commanded position during all of the above lead maneuvering. The capability to change formations is also an objective of this work. The controller must be able to provide a position change of up to 30 feet in any direction with an overshoot of no more than 2 feet. The wing aircraft is further required to reach 95% steady state position by 30 seconds. After a controller has been created to meet the above criteria, it is an objective of this research that wind disturbances be applied, and that the controller maintain a position error of ≤ 1 foot during normal turbulence, ≤ 3 feet during moderate turbulence, and ≤ 5 feet during thunderstorm level turbulence. Next, the

vortex wake of the lead aircraft will be modeled and the controller will be expected to maintain the given formation with an error, or overshoot, of < 2 feet while holding, or moving too, respectively, a position within the vortex wake. These error objectives were chosen based on the author's opinion of acceptable errors for close formation flight. When wind and vortex disturbances are applied simultaneously during lead maneuvers or formation changes, the greatest error objective from the applicable objectives given above will be used as the error objective for that simulation run.

Table 1. Maneuver and Position Change Limitations

Maneuver Limitations	
Climbs	±30° Flight Path Angle Limit
Turns	≤ 30° Bank, ≤ 30°/sec Roll Rate
Accel	5% ≤ Military Power ≥ 95%
Position Change Limitations	
Position Change	≤ 30 feet

The final objective of this work is that all or a portion of the controller be applied to the Variable In-Flight Stability Aircraft (VISTA) NF-16D (5) for flight testing in an attempt to validate this research.

Assumptions

It was assumed based on previous work by Hall (7) and Proud (15) that a formation controller given operationally representative cruise airspeeds would have the control authority to overcome the forces generated in the vortex field of the lead aircraft. This assumption is based on the vortex string method where the changed airflow

generated by the lead aircraft can be represented as two string vortices of infinite length trailing and attached to positions near the tips of the lead aircraft's wings (9:169-172). The assumption that there exists enough control authority will be proved as part of the objectives of the research, as the vortex interaction will not be specifically countered in the design of the controller, unless required to provide acceptable performance. To represent the forces present in the vortex field of the lead aircraft, the panel method results obtained by Morgan (12) are modeled via a cosine function where the vortex generated forces are reduced to zero when the trail aircraft is located nine feet laterally away from the position of greatest force. It must be noted that these distances and values would be aircraft dependant and are valid only for the exact two ship formation modeled in Morgan's work. This approach is meant to present the worse case vortex generated aerodynamic forces at the given speed. For the calculation of equilibrium angle of attack and thrust setting it is assumed that the aircraft is in un-accelerated, steady level flight, such that lift equals weight and thrust equals drag. It is also assumed that the force of gravity is a constant, that the aircraft thrust acts along the x wind axis, and for computer simulations, the mass of the aircraft is constant.

Methodology

The equations of motion for each aircraft, as a point mass, are expressed in a wind axis coordinate system. The two coordinate systems are coupled into differential equations that model the two aircraft system dynamics. Previous control schemes will be refined to allow more robust control and precise maneuvering. Four control parameters, thrust, alpha, beta, and roll rate will be used to control the wing aircraft. Control laws are

developed that include proportional and integral action. Gains are determined based on the desired formation performance. Lead maneuvers will be simulated and the controller will be analyzed based on its ability to maintain the prescribed position. In addition, formation position changes, including maneuvers into and out of the vortex region generated by the lead aircraft, will be analyzed. A Dryden wind model will be applied to the lead and wing aircraft and assessed at varying intensities. The controller will then be modified and applied to the VISTA NF-16D aircraft (5). Utilizing a data link system and a virtual lead aircraft generated from a ground based control station, the VISTA will test a slightly modified version of the developed control laws. Finally, the controller's in-flight performance will be analyzed and measured against the simulation results, and overall conclusions will be presented.

Overview of Thesis

The following chapter details the theory and development of the equations governing the system. Next the disturbances that the controller must overcome are developed in Chapter III. Details of the controller design and implementation are presented in Chapter IV. The simulation results are located in Chapter V. The system and controller as modified for flight testing are presented subsequently in Chapter VI. Finally, Chapter VII details the flight test results and analysis.

II. System Development

Single A/C Dynamics

It must first be noted that the system is comprised of two rotating and translating reference frames attached to each aircraft in the two ship formation. The pseudo inertial reference frame, referred subsequently as the navigation frame, is attached to the non-moving earth in the North, East and down directions. Each aircraft's reference frame is related to the navigation frame through the Course angle (H), Flight Path angle (γ), and Velocity Vector Roll angle (ϕ_V). These angles are defined by each aircraft's wind axis reference frame. The x component of the velocity vector reference system is aligned with the velocity vector of the aircraft. The y component is aligned with the right wing of the aircraft and the z component completes the right handed reference system and points generally in a downward direction for straight and level flight. Figure 1 below shows the navigation and wind axes reference systems, and the vector relationship.

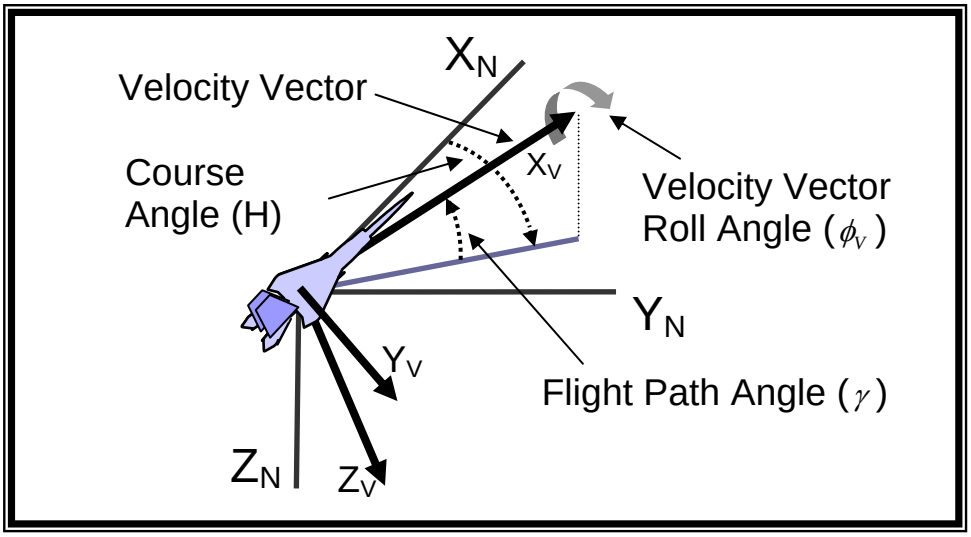

Figure 1. Navigation To Wind Axes Transformation Angles

The aircraft motion is driven by the aerodynamic and thrust forces acting on the aircraft. These forces are presented in the equations below. In general form these equations are the same for both the lead aircraft and wing aircraft:

$$L = \bar{q}SC_{L\alpha}(\alpha - \alpha_{OL}) \tag{1}$$

$$D = \bar{q}S(C_{Do} + KC_L{}^2) \tag{2}$$

$$C_L = C_{L\alpha}(\alpha - \alpha_{OL}) \tag{3}$$

$$F_Y = \bar{q}S_t C_{Y\beta}\beta \tag{4}$$

$$\bar{q} = \frac{1}{2}\rho V^2 \tag{5}$$

$$T = T_{Mil}\mu \tag{6}$$

Where

L = Lift
D = Drag
$\bar{q}$ = Dynamic Pressure
S = Wing Surface Area
S_t = Tail Surface Area
K = Drag Polar Constant
C_L = Lift Coefficient
$C_{L\alpha}$ = Lift Coeffient/unit AOA
C_{Do} = Base Drag Coefficient
$C_{Y\beta}$ = Side Force Coefficient/unit β
ρ = Density
T = Thrust
V = Velocity
T_{Mil} = Military Power Thrust
μ = Thrust Control Value
β = Sideslip Angle
F_Y = Side Force
α = AOA
α_{OL} = Zero Lift AOA

The above force equations are used in the model to give dynamics, and are also used initially to find the trim values for alpha (α_o) and thrust (μ_o). This is accomplished by assuming that the aircraft is in steady un-accelerating flight. In this case, lift equals

weight (L=W) and thrust equals drag (T=D). With this assumption, the equations for equilibrium alpha and thrust become

$$\alpha_o = \frac{(32.2)M}{\bar{q}SC_{L\alpha}} + \alpha_{OL} \tag{7}$$

$$\mu_o = \frac{\bar{q}S(C_{DO} + K[C_{L\alpha}(\alpha_o - \alpha_{OL})]^2)}{T_{Mil}} \tag{8}$$

where M is the mass of the aircraft. The relationships between the body aerodynamic angles and the wind axes angles are shown in Figure 2. below.

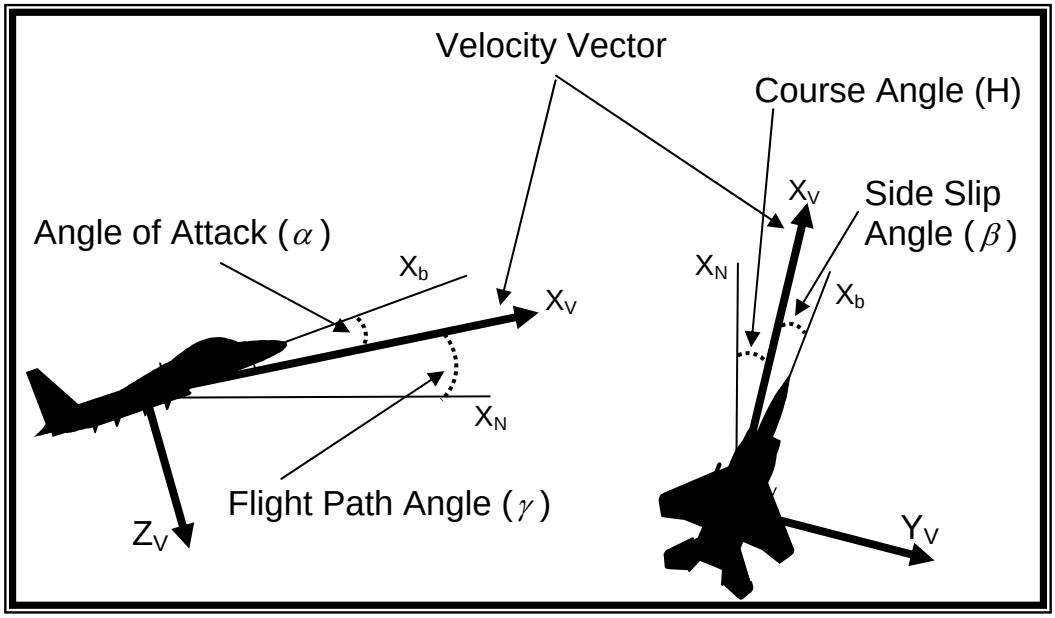

Figure 2. Body to Wind Axes Relationship

The wind axes to navigation axes transformation is given by the direction cosine matrix (DCM), C_{wa}^{n}. This matrix is found by a negative rotation of the velocity vector roll angle about the x-wind axis, followed by a negative rotation of the flight path angle about the new y-axis, and finally a negative rotation of the coarse angle about the new z-axis. The DCM then becomes

$$C_{wa}^{n} = \begin{bmatrix} \cos\gamma\cos H & \sin\phi_V \sin\gamma\cos H - \cos\phi_V \sin H & \cos\phi_V \sin\gamma\cos H + \sin\phi_V \sin H \\ \cos\gamma\sin H & \sin\phi_V \sin\gamma\sin H - \cos\phi_V \cos H & \cos\phi_V \sin\gamma\sin H - \sin\phi_V \cos H \\ -\sin\gamma & \sin\phi_V \cos\gamma & \cos\phi_V \cos\gamma \end{bmatrix} \tag{9}$$

The transpose of the above matrix yields a transformation matrix from the navigation axes to the wind axes. This would be

$$C_{n}^{wa} = \begin{bmatrix} \cos\gamma\cos H & \cos\gamma\sin H & -\sin\gamma \\ \sin\phi_V \sin\gamma\cos H - \cos\phi_V \sin H & \sin\phi_V \sin\gamma\sin H + \cos\phi_V \cos H & \sin\phi_V \cos\gamma \\ \cos\phi_V \sin\gamma\cos H + \sin\phi_V \sin H & \cos\phi_V \sin\gamma\sin H - \sin\phi_V \cos H & \cos\phi_V \cos\gamma \end{bmatrix} \tag{10}$$

Euler's rate equations are required and presented here:

$$P = \dot{\phi}_V - \dot{H}\sin\gamma \tag{11}$$

$$Q = \dot{\gamma}\cos\phi_V + \dot{H}\cos\gamma\sin\phi_V \tag{12}$$

$$R = -\dot{\gamma}\sin\phi_V + \dot{H}\cos\gamma\cos\phi_V \tag{13}$$

where

P = Roll Rate
Q = Pitch Rate
R = Yaw Rate
ϕ_V = Velocity Vector Roll Angle
H = Velocity Vector Heading Angle
γ = Velocity Vector Flight Path Angle

Wind Axes Equations of Motion

The wind axes equations of motion for a single aircraft are presented here and are applicable to both wing and lead:

$$\dot{V} = \frac{T - D}{M} - g\sin\gamma \tag{14}$$

$$\dot{\gamma} = \frac{L\cos\phi_V - F_Y \sin\phi_V}{MV} - \frac{g}{V}\cos\gamma \tag{15}$$

$$\dot{H} = \frac{L\sin\phi_V + F_Y \cos\phi_V}{MV\cos\gamma} \tag{16}$$

$$\dot{\phi}_V = P + \tan\gamma\left(\frac{L\sin\phi_V + F_Y \cos\phi_V}{MV}\right) \tag{17}$$

where

V = Velocity
T = Thrust
D = Drag
M = Mass
g = Gravity Force
L = Lift Force
F_y = Side Force

Separation Dynamics

The last differential equations we will need are those that relate the separation of the lead aircraft from the wing aircraft written in the wing aircraft wind axes reference frame.

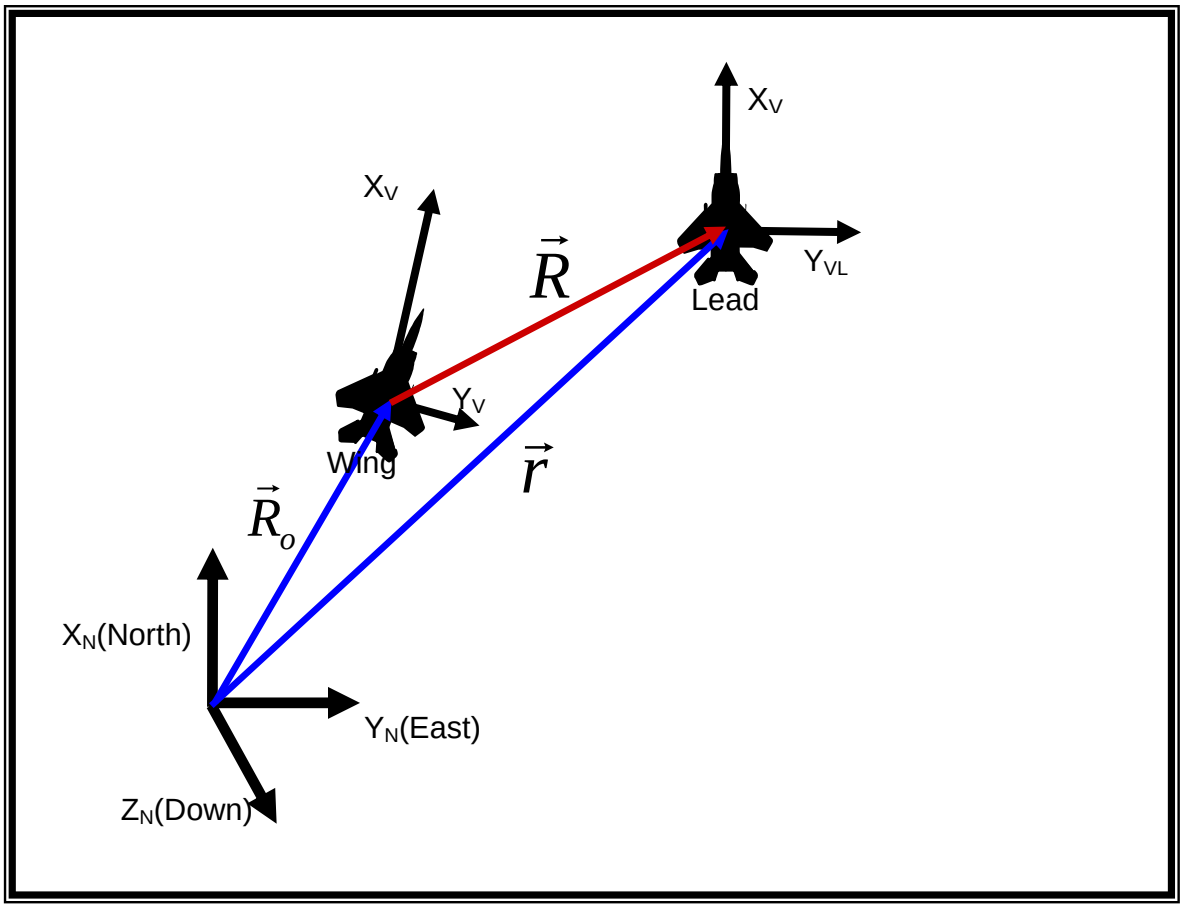

Figure 3. Two Aircraft Formation Vector Relationship

This is accomplished by using Figure 3 above, and noting that the vector equations connecting the two aircraft can be written

$$\bar{r} = \bar{R}_o + \bar{R} \tag{18}$$

The total derivative of the above equation can be written

$$\frac{D\bar{r}}{Dt} = \frac{D\bar{R}_o}{Dt} + \frac{D\bar{R}}{Dt} \tag{19}$$

$\frac{D\bar{R}}{Dt}$ is next found utilizing the Coriolis effect:

$$\frac{D\bar{R}}{Dt} = \frac{d\bar{R}}{dt} + \bar{\omega}_W \times \bar{R} \tag{20}$$

Substituting equation (20) into equation (19) above becomes

$$\frac{D\bar{r}}{Dt} = \frac{D\bar{R}_o}{Dt} + \frac{d\bar{R}}{dt} + \bar{\omega}_W \times \bar{R} \tag{21}$$

where the angular velocity vector of the wing aircraft is

$$\bar{\omega}_W = \begin{bmatrix} P_W \\ Q_W \\ R_W \end{bmatrix} \tag{22}$$

Also, the separation vector is defined as

$$\bar{R} = \begin{bmatrix} x_d \\ y_d \\ z_d \end{bmatrix} \tag{23}$$

The lead and wing aircrafts' inertial velocities, $\frac{D\bar{r}}{Dt}$, and $\frac{D\bar{R}_o}{Dt}$ respectively are related to the wind axis velocities by

$$\frac{D\bar{r}}{Dt} = C_{L\,wa}^{\;\;n} \begin{bmatrix} V_L \\ 0 \\ 0 \end{bmatrix} = V_L \begin{bmatrix} \cos\gamma_L \cos H_L \\ \cos\gamma_L \sin H_L \\ -\sin\gamma_L \end{bmatrix} \tag{24}$$

$$\frac{D\bar{R}_o}{Dt} = C_{W\,wa}^{\;\;n} \begin{bmatrix} V_W \\ 0 \\ 0 \end{bmatrix} = V_W \begin{bmatrix} \cos\gamma_W \cos H_W \\ \cos\gamma_W \sin H_W \\ -\sin\gamma_W \end{bmatrix} \tag{25}$$

Note that the velocity of the separation vector in the wind axis frame would be

$$\frac{d\bar{R}}{dt} = \begin{bmatrix} \dot{x}_d \\ \dot{y}_d \\ \dot{z}_d \end{bmatrix} \tag{26}$$

Substituting equations (24-26) into equation (21) in the navigation frame yields

$$V_L\begin{bmatrix}\cos\gamma_L\cos H_L\\ \cos\gamma_L\sin H_L\\ -\sin\gamma_L\end{bmatrix}=V_W\begin{bmatrix}\cos\gamma_W\cos H_W\\ \cos\gamma_W\sin H_W\\ -\sin\gamma_W\end{bmatrix}+C_{W\,wa}^{\;\;n}\left[\begin{bmatrix}\dot{x}_d\\ \dot{y}_d\\ \dot{z}_d\end{bmatrix}+\begin{bmatrix}P_W\\ Q_W\\ R_W\end{bmatrix}\times\begin{bmatrix}x_d\\ y_d\\ z_d\end{bmatrix}\right] \tag{27}$$

Noting that

$$C_{W\,n}^{\;\;wa}V_W\begin{bmatrix}\cos\gamma_W\cos H_W\\ \cos\gamma_W\sin H_W\\ -\sin\gamma_W\end{bmatrix}=V_WC_{W\,n}^{\;\;wa}\begin{bmatrix}\cos\gamma_W\cos H_W\\ \cos\gamma_W\sin H_W\\ -\sin\gamma_W\end{bmatrix}=V_W\begin{bmatrix}1\\ 0\\ 0\end{bmatrix} \tag{28}$$

allows equation (27) above, to be rewritten. With the desired separation derivatives on the left, the equation becomes

$$\begin{bmatrix}\dot{x}_d\\ \dot{y}_d\\ \dot{z}_d\end{bmatrix}=\begin{bmatrix}R_Wy_d-Q_Wz_d\\ P_Wz_d-R_Wx_d\\ Q_Wx_d-P_Wy_d\end{bmatrix}-V_W\begin{bmatrix}1\\ 0\\ 0\end{bmatrix}+V_LC_{W\,n}^{\;\;wa}\begin{bmatrix}\cos\gamma_L\cos H_L\\ \cos\gamma_L\sin H_L\\ -\sin\gamma_L\end{bmatrix} \tag{29}$$

The transpose of the DCM $C_{W\,wa}^{\;\;n}$ yields the DCM

$$C_{W\,n}^{\;\;wa}=\begin{bmatrix}\cos\gamma_W\cos H_W & \cos\gamma_W\sin H_W & -\sin\gamma_W\\ \sin\phi_{VW}\sin\gamma_W\cos H_W-\cos\phi_{VW}\sin H_W & \sin\phi_{VW}\sin\gamma_W\sin H_W+\cos\phi_{VW}\cos H_W & \sin\phi_{VW}\cos\gamma_W\\ \cos\phi_{VW}\sin\gamma_W\cos H_W+\sin\phi_{VW}\sin H_W & \cos\phi_{VW}\sin\gamma_W\sin H_W-\sin\phi_{VW}\cos H_W & \cos\phi_{VW}\cos\gamma_W\end{bmatrix} \tag{30}$$

Now we calculate

$$C_{W\,n}^{\;\;wa}\begin{bmatrix}\cos\gamma_L\cos H_L\\ \cos\gamma_L\sin H_L\\ -\sin\gamma_L\end{bmatrix}=\begin{bmatrix}\cos\gamma_W\cos\gamma_L\cos H_e+\sin\gamma_W\sin\gamma_L\\ \sin\phi_{VW}\sin\gamma_W\cos\gamma_L\cos H_e+\cos\phi_{VW}\cos\gamma_L\sin H_e-\sin\phi_{VW}\cos\gamma_W\sin\gamma_L\\ \cos\phi_{VW}\sin\gamma_W\cos\gamma_L\cos H_e-\sin\phi_{VW}\cos\gamma_L\sin H_e-\cos\phi_{VW}\cos\gamma_W\sin\gamma_L\end{bmatrix} \tag{31}$$

where

$$H_e=H_L-H_W \tag{32}$$

Now we can insert equation (31) into equation (29), such that

$$\begin{bmatrix}\dot{x}_d\\ \dot{y}_d\\ \dot{z}_d\end{bmatrix}=\begin{bmatrix}R_Wy_d-Q_Wz_d-V_W+V_L(\sin\gamma_W\sin\gamma_L+\cos\gamma_W\cos\gamma_L\cos H_e)\\ P_Wz_d-R_Wx_d+V_L(\sin\phi_{VW}\sin\gamma_W\cos\gamma_L\cos H_e+\cos\phi_{VW}\cos\gamma_L\sin H_e-\sin\phi_{VW}\cos\gamma_W\sin\gamma_L)\\ Q_Wx_d-P_Wy_d+V_L(\cos\phi_{VW}\sin\gamma_W\cos\gamma_L\cos H_e-\sin\phi_{VW}\cos\gamma_L\sin H_e-\cos\phi_{VW}\cos\gamma_W\sin\gamma_L)\end{bmatrix} \tag{33}$$

Lastly we need to relate the rate values Q_W and R_W to the aerodynamic force equations so that the above separation equations can be related to each aircraft's forces. The roll rate, P_W, is to be directly controlled and will not be converted to aerodynamic force equations. The rate equations are found by using Euler's equations (11-13) presented above and the equations of motion (15) and (16) for $\dot{\gamma}_W$ and $\dot{H}_W$ respectively. They are

$$Q_W = \frac{L_W}{M_W V_W} - \frac{g}{V_W}\cos\gamma_W \cos\phi_{VW} \tag{34}$$

$$R_W = \frac{F_{YW}}{M_W V_W} + \frac{g}{V_W}\cos\gamma_W \sin\phi_{VW} \tag{35}$$

These two equations and the roll rate, P_W, are now substituted into equation (33) to finally yield the desired separation dynamics in terms of the aerodynamic force equations of both aircraft:

$$\begin{aligned}\dot{x}_d = &\left(\frac{g}{V_W}\cos\gamma_W \sin\phi_{VW} + \frac{F_{YW}}{M_W V_W}\right) y_d + \left(\frac{g}{V_W}\cos\gamma_W \cos\phi_{VW} - \frac{L_W}{M_W V_W}\right) z_d \\ &- V_W + V_L\left(\sin\gamma_W \sin\gamma_L + \cos\gamma_W \cos\gamma_L \cos H_e\right)\end{aligned} \tag{36}$$

$$\begin{aligned}\dot{y}_d = &P_W z_d - \left(\frac{F_{YW}}{M_W V_W} + \frac{g}{V_W}\cos\gamma_W \sin\phi_{VW}\right) x_d \\ &+ V_L\left(\sin\phi_{VW} \sin\gamma_W \cos\gamma_L \cos H_e + \cos\phi_{VW} \cos\gamma_L \sin H_e - \sin\phi_{VW} \cos\gamma_W \sin\gamma_L\right)\end{aligned} \tag{37}$$

$$\begin{aligned}\dot{z}_d = &\left(\frac{L_W}{M_W V_W} - \frac{g}{V_W}\cos\gamma_W \cos\phi_{VW}\right) x_d - P_W y_d \\ &+ V_L\left(\cos\phi_{VW} \sin\gamma_W \cos\gamma_L \cos H_e - \sin\phi_{VW} \cos\gamma_L \sin H_e - \cos\phi_{VW} \cos\gamma_W \sin\gamma_L\right)\end{aligned} \tag{38}$$

With the above separation dynamics equations (36-38), and the single ship wind axes equations of motion (14-17) all written in terms of the aerodynamic force values of lead and wing, the two aircraft system model can be developed.

System States and Control Vectors

With all required equations derived, the system state vector will be

$$STATEVEC = \left[x_d, y_d, z_d, V_L, V_W, H_L, H_W, \phi_L, \phi_W, \gamma_L, \gamma_W, Alt_L, Alt_W\right]^T \tag{39}$$

The system is driven by the lead and wing control parameters that are embedded in the state equations listed above. They are

$$Controlvec_{LEAD} = \left[\alpha_L, \beta_L, \mu_L, P_L\right]^T \tag{40}$$

$$Controlvec_{WING} = \left[\alpha_W, \beta_W, \mu_W, P_W\right]^T \tag{41}$$

The above control vectors include angle of attack, sideslip angle, thrust, and roll rate of each aircraft.

III. Disturbances

To more closely model the actual conditions the controller will encounter during flight test, two main disturbances to the system were developed and applied. The first disturbance is the random effects of wind turbulence on the lead and wing aircraft. The second disturbance is the aerodynamic forces that result on the wing aircraft when it is flying in the lead aircraft's wake.

Dryden Wind Model

The Dryden wind model will be used to simulate the random effects of wind turbulence on the system. This model allows for the input of wind turbulence at three different levels of intensity; normal, cumulous clouds, and thunderstorms (1:778-779). The first order differential model of wind turbulence is driven with continuous white noise that has a zero mean. The wind state $w(t)$ is normalized by the velocity of the aircraft and given as an angle of attack disturbance, $\alpha_T(t)$, for the longitudinal dynamics, and as a sideslip angle disturbance, $\beta_T(t)$, for the lateral dynamics. The differential equation that represents the dynamics of the Dryden wind disturbance model is given by

$$\dot{\alpha}_T(t) = -2\left(\frac{V}{L}\right)\alpha_T(t) + \frac{2\sigma}{\sqrt{\pi L V}}\varepsilon(t) \tag{42}$$

Here, $\varepsilon(t)$ is continuous white noise with unity intensity. The scale length L, models the differences in turbulence as a result of altitude by the relationship:

$$L = \begin{cases} (\text{if alt} = 0 \text{ ft.}) \Rightarrow 200 \\ (\text{if } 0 \text{ ft.} \lhd \text{alt} \lhd 2500 \text{ ft.}) \Rightarrow \text{Interpolate between 200 and 2500} \\ (\text{if alt} \geq 2500 \text{ ft.}) \Rightarrow 2500 \end{cases} \tag{43}$$

The level of turbulence is controlled by the σ value in equation (42) above. The values of turbulence are given by

$$\sigma = \begin{cases} 6 \text{ ft/s normal turbulence} \\ 15 \text{ ft/s cumulus clouds} \\ 30 \text{ ft/s thunderstorm turbulence} \end{cases} \tag{44}$$

The above equations also apply to the sideslip angle, $\beta_T(t)$, for the lateral dynamics. These wind disturbance equations are now ready to be inserted into the model. The details of their inclusion are presented in the Chapter IV below.

Close Formation Vortex Interactions

The other significant disturbance to be included in the two aircraft dynamic model is the effect of lead's vortex wake on the trail aircraft. It has been discussed above that previous work by Hall and Proud have shown that the wind effects of the lead aircraft on the trail aircraft are not significant from a control standpoint when formations of similar aircraft are considered. This conclusion will allow a more relaxed approach to the issue of vortex interactions but does not negate the requirement to account for the forces if an accurate estimation of performance is to be achieved. Therefore the aerodynamic effects will not be explicitly calculated in the model but will instead be accounted for as a disturbance with which the controller must contend. In an MS thesis work, Morgan modeled a two ship formation of F-16 aircraft (12). The lead aircraft was an F-16C with

the VISTA NF-16D as the wing aircraft. Morgan utilized the most robust vortex panel method available at the time of this writing and provides the wind forces present on the trail aircraft given different positions behind lead. Since this is the exact formation the controller will be expected to control in flight tests, the author chose to utilize these results to simulate the vortex forces affecting the wing aircraft. The results of Morgan's work provide estimated roll moment, yaw moment, and side-force disturbances as dimensionless coefficients similar to an aileron or rudder input. The greatest fuel savings are expected to occur where the beneficial aerodynamic forces are the greatest. The commanded formation vector below represents 86.5% of the wingspan separation in the lateral direction and is expected to yield the greatest fuel savings:

$$Commvec = \begin{bmatrix} x_{Comm} \\ y_{Comm} \\ z_{Comm} \end{bmatrix} = \begin{bmatrix} 60 \\ 26.815 \\ 0 \end{bmatrix} \text{ft.} \tag{45}$$

This position will be defined as the optimum fuel formation. The greatest aerodynamic forces occur at a formation position slightly wider than this, at approximately 95% of the wingspan which corresponds to 29.45 ft of lateral separation between each aircraft's centerline. Assuming the wing aircraft maintains a level vertical position, $z_d = 0\,\text{ft}$, the above mentioned coefficients can be suitably modeled by a cosine function with a half period of nine ft. The coefficients are set to zero when the wing's position is greater than nine feet from the above given lateral separation of $y_d = 29.45\,\text{ft}$, both inward and outward from this position. The maximum coefficients centered about the above given position, placing the wingman behind lead's left wing, are

$$C_{l\max} = -.0075 \tag{46}$$

$$C_{n\max} = -.0038 \tag{47}$$

$$C_{F_Y\max} = .011 \tag{48}$$

Thus, while in the optimum fuel position behind lead's left wing, the wing aircraft experiences a left rolling and yawing tendency, and a right side force. The model of these coefficients is then found, using the cosine function for values less than 9 feet laterally from the optimum fuel position, to be

$$C_l = \left(\frac{C_{l\max}}{2}\right)\left(\cos\left(\left|y_{dL} - 29.45\right|\left(\frac{\pi}{9}\right)\right)+1\right) \tag{49}$$

$$C_n = \left(\frac{C_{n\max}}{2}\right)\left(\cos\left(\left|y_{dL} - 29.45\right|\left(\frac{\pi}{9}\right)\right)+1\right) \tag{50}$$

$$C_{F_Y} = \left(\frac{C_{F_Y\max}}{2}\right)\left(\cos\left(\left|y_{dL} - 29.45\right|\left(\frac{\pi}{9}\right)\right)+1\right) \tag{51}$$

where the above value, y_{dL}, is the lateral separation distance of the two aircraft written in lead's reference frame. A plot of the coefficient values as a function of the lateral separation in the lead reference plane is plotted in Figure 4 below. The distance must be calculated in lead's reference frame since the vortex is attached to the lead aircraft's wing. The above coefficients are taken from Morgan's work and presented as a function of the lateral spacing only. This is a fairly good assumption for our purposes since we are looking to see controller performance with the worse case disturbance values and not trying to predict fuel savings or lift and drag changes as in previous work (15,7,8,20,10). This simplifies the disturbance model, but it must be appreciated that the model

represents a plane of disturbances on the wing aircraft and does not consider the effect of varying z positions on the disturbances.

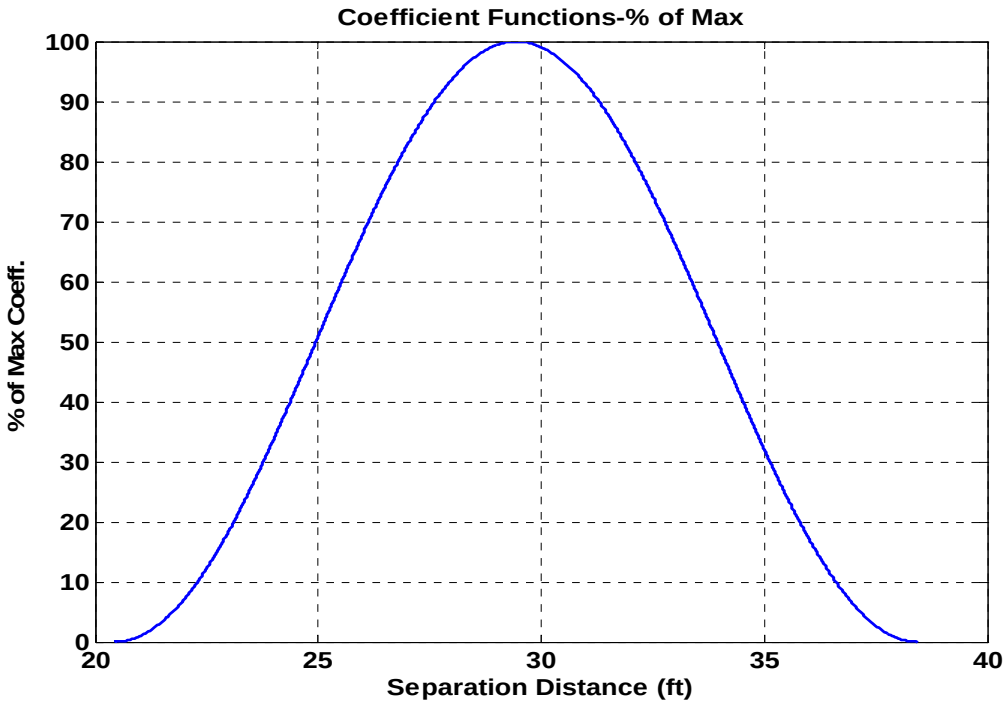

Figure 4. Coefficients vs. Lateral Separation

It is expected that this approach is acceptable since the wing aircraft will be entering the optimum fuel position from a lateral direction, maintaining the z component separation at zero. Maintaining the z component separation at zero while lead flies straight and level allows us to simplify the transformation of the lateral spacing from y_{dL} into the lead reference frame. It is simply the equation

$$y_{dL} = \frac{y_d \cos\phi_L}{\cos\phi_W} \tag{52}$$

This is then substituted into equations (49-51) above so that the vortex coefficients can be calculated. Next it is necessary for these coefficients to be expressed as forces that affect the wing aircraft. To accomplish this, the stability derivatives of the VISTA NF-16D at

the flight test conditions must be utilized. The simplest disturbance to model will be induced roll rate that results from the roll moment coefficient, C_l. Since the optimum fuel position will be entered from outside of the effects of the vortex disturbance it is assumed that the dynamics of the roll force will be negligible and only the resulting steady state rate will need to be countered. Using aircraft coefficients a steady state approximation of roll rate can be written as

$$P_{SS} = \frac{2V}{b}\left(-\frac{C_l}{C_{l_p}}\right) \tag{53}$$

Where C_l is the induced roll moment coefficient and C_{l_p} is the aircraft dependent roll damping coefficient. The induced steady state roll rate can now be input into the model.

The lateral coefficients presented above, C_n and C_{F_Y}, are valid only when the wing aircraft is maintaining a nose position alignment with the lead aircraft. If we assume the yaw and side forces are simply the results of an induced side slip angle, then we must include the yaw angle and the yaw stability derivatives to determine the resulting sideslip condition. The sideslip condition can be determined independently from both the coefficients. If our assumption that these forces are simply a result of the sideslip condition of the vortex only, then the resulting sideslip that is calculated in both cases should agree. Using each of the above lateral coefficients, C_n and C_{F_Y}, and the standard coefficients from Table 2 in Chapter V below based on the proposed test conditions of 20,000 ft. and 667 ft/sec true airspeed, it was found that calculations of the steady state sideslip condition as a result of each coefficient do not agree. Obviously there is more to the actual dynamics than can be accounted for when making the

assumption that all forces are a result of the sideslip condition. In the interest of presenting the worse case condition, the C_n coefficient will be used as it yielded a steady state sideslip angle of -.0905 radians, while the C_{F_Y} coefficient yielded a steady state side slip angle of -.0096 radians.

Unlike the roll rate disturbance, it is not prudent to disregard the aircraft yaw dynamics as they will significantly affect the lateral position as the wing aircraft attempts to maintain the same velocity vector headings despite a continuously increasing yaw angle as compared to lead. To obtain the required sideslip angle as a result of the changing yaw moment, the current yaw angle of the wing aircraft, ψ, will be differenced from the induced wind angle. This wind angle is derived from the steady state yaw angle, ψ_{SS}, as a result of the yaw moment coefficient, C_n. Simply put, if the wing aircraft is allowed to weathervane into the wind, the steady state angle that results is essentially the angle of the wind. Since the system models each aircraft as a point mass, the yaw angle of the wing aircraft will not be explicitly available. Thus, in order to have the information required to calculate the yaw disturbance, a second order yaw only equation of motion for the wing aircraft will supplement the model. An equation of this type can be found in Nelson's book, and modified such that it is driven by the yaw moment, N_{Vort} created by the vortex and the second derivative of the commanded sideslip, $\ddot{\beta}_{Comm}$, (13:191). It is presented below

$$\ddot{\psi} - N_r\dot{\psi} + N_\beta\psi = N_{Vort} - \ddot{\beta}_{Comm} \tag{54}$$

N_r and N_β are the yaw moment stability derivatives on the aircraft as a result of the yaw damping, C_{n_r}, and weathercock stability, C_{n_β}, coefficients. They are derived as

$$N_r = \frac{C_{n_r}\left(\frac{b}{2V}\right)qsb}{I_Z} \tag{55}$$

$$N_\beta = \frac{C_{n_\beta}qsb}{I_Z} \tag{56}$$

The driving yaw moment, N_{Vort}, similar to a rudder input, is derived as

$$N_{Vort} = \frac{C_n qsb}{I_Z} \tag{57}$$

The initial condition for ψ, and all of it's derivatives are zero since it is assumed that no steady state yaw exists before the wing aircraft is subjected to the vortex flow. I_z is the wing aircraft's moment of inertia about the yaw axis. It should be noted that the velocity, *V*, in the above equation is the point mass velocity of the wing aircraft and not the usual body axis u_o as Nelson originally termed the equation (13:191). Equation (54) above can now be calculated in the model and the yaw angle of the wing aircraft relative to the lead aircraft can be pulled from this supplemental system. Subtracting the yaw angle from the relative wind yields a sideslip angle input, β_{Vort}, that can be input directly into the model as an additional sideslip angle:

$$\beta_{Vort} = (\psi_{SS} - \psi) \tag{58}$$

IV. Controller Design and Model Development

This chapter is meant to detail the control design of the system model. It represents what would be required on an aircraft to perform the formation control, while previous chapters included the modeling scheme used to test these control algorithms. It should be noted that the control design presented in this chapter is not to the detail required for actual aircraft implementation and testing, but is meant to be more generic in its application and appropriate for computer simulation with a wide variety of aircraft types.

Error Signal

Simply put, the controller is given a position to maintain or go to that is represented as a separation in the x, y and z directions written in the wing axes system. The current separation is calculated via the model. The difference between these two separations in each axis represents the errors that must be forced to zero. A pilot flying formation knows that the first step to maintaining a given position is to match the lead aircraft. In other words, errors are managed and kept small by always attempting to match lead's angles and orientation. Thus, assuming the wing aircraft is in the correct position and that it is of similar type, we would like for the bank angles, angles of attack, heading angles, and roll angles to all simultaneously match. In fact, if we match all of these parameters with no error or lag, the two aircraft would always have the same inertial spacing. Obviously the inclusion of disturbances, lag, and error, and maintaining the formation in the wing reference frame drives the need for the formation controller.

Another error that will be used for control is the error between the velocities of the lead and wing aircraft. It is true that when there is a lateral separation between the two aircraft and a turn is initiated, the outside aircraft must increase its velocity to maintain the formation, but this issue will be addressed in the control laws. Thus, in addition to the positional errors presented above, the error between the lead and wing flight path angle, heading angle, velocity vector roll angle, and velocities will used to control the wing aircraft, and in most cases be expected to be driven to zero. The error vector is then calculated

$$Errorvec = \begin{bmatrix} x_e \\ y_e \\ z_e \\ V_e \\ H_e \\ \phi_{Ve} \\ \gamma_e \end{bmatrix} = \begin{bmatrix} x_d - x_{Comm} \\ y_d - y_{Comm} \\ z_d - z_{Comm} \\ V_L - V_W \\ H_L - H_W \\ \phi_{VL} - \phi_{VW} \\ \gamma_L - \gamma_W \end{bmatrix} \tag{59}$$

where x_{Comm} , y_{Comm} , and z_{Comm} are the commanded separation distances.

Control Parameters

The four control parameters for lead and wing were presented above and are repeated here for clarity:

$$Controlvec_{LEAD} = \left[\mu_L, \alpha_L, \beta_L, P_L\right]^T \tag{60}$$

$$Controlvec_{WING} = \left[\mu_W, \alpha_W, \beta_W, P_W\right]^T \tag{61}$$

The above control vectors include angle of attack, sideslip angle, thrust, and roll rate of each aircraft.

Before each control parameter is given a control law to define how the control is generated, it is necessary to first set limits on the parameters based on sound engineering judgment of the system being controlled. It should be noted that the limits presented below are not of the controller alone, but of the total parameter that the aircraft will experience. In other words, the equilibrium values of the flight condition for straight and level flight are added to the control parameters and it is this value that is limited as prescribed below.

Lead Parameter Limits.

The lead aircraft will be limited based on the objectives given in Chapter I that described how aggressive lead is allowed to maneuver. As any good formation flight leader knows, the wingman must always have a range of power control that is greater than the lead's range of power control. Along those lines, thrust control, μ_L will be used as necessary to provide airspeed control during lead maneuvering, but will not be greater than 95% or less than 5% of military power for the given conditions. In addition, the lead aircraft will be limited to a thrust maximum rate of ±10% of military power per second. α_L will be limited to a maximum rate of ±30 deg/sec, and will not be allowed to generate a flight path angle greater than ±30 degrees. β_L will not be controlled except to help affect coordinated flight during the lead turn maneuvers. Finally, P_L will not exceed ±30 deg/sec with a roll acceleration not to exceed ±10 deg/sec^2 and the resulting roll angles of lead , ϕ_{VL} will not exceed ± 30 degrees.

Wing Parameter Limits.

The wingman will be limited in a similar fashion, but is meant to have more controllability overall such that corrective control action is always possible. The wing aircraft's power level, μ_W, is constrained from 0-100% of mil power at the given conditions. The wing's angle of attack, α_W, will not exceed ±90 degrees and will not exceed a rate of ±60 deg/sec. In addition the angle of attack of the wingman will not be allowed to generate a flight path angle, γ_W of greater than ±90 degrees. β_W will be constrained to values less than ±5 degrees with no rate limit. Finally the roll rate, R_W will not be limited, although the velocity vector roll angle will be limited to less than ±90 degrees.

Control Laws

This section details how the error vector presented above is converted into an actual command input to the aircraft. There is a section detailing the lead control first since the lead states are not driven by direct position values, but are more or less "flown" by the lead inputs.

Lead control.

Since the equations of motion for both aircraft are included in the model it is to be noted that the lead aircraft must be "flown" via inputs to the system. This will provide greater model accuracy from the standpoint that it will model an actual aircraft as it performs the lead maneuvers, ie no discontinuous accelerations or heading changes. The drawback of this kind of arrangement is the need to build a lead autopilot in order for the

lead aircraft to perform simple maneuvers like holding a given altitude, heading, climb or descent. In simple terms, an error vector for the lead aircraft is used as feedback for the given maneuver that is meant to be performed and the control parameters presented above are used to minimize the errors. For our purposes, how the control is accomplished is insignificant, only that the resulting maneuvers are what a typical pilot would fly and fall within the aggressiveness parameters presented in the objectives of Chapter I. The autopilot used to fly the lead aircraft through the maneuvers is included in the Simulink model of the system found in Appendix B which details the model development below, but does not include the theory behind the control schemes. For an explanation of standard aircraft autopilots the reader is directed towards Stevens and Lewis (18).

Wing Control.

Because of the multiple tasks the controller is meant to perform, it is prudent to further divide the discussion of control laws into nominal formation flight and close formation vortex flight.

The basic form of the control laws will include proportional and integral control. From above the seven error states we intend to control include

$$Errorvec = \begin{bmatrix} x_e \\ y_e \\ z_e \\ V_e \\ H_e \\ \phi_{Ve} \\ \gamma_e \end{bmatrix} \tag{62}$$

These are to be controlled by four delta control parameters which are added to the equilibrium values required for straight and level flight such that

$$Controlvec_{WING} = \begin{bmatrix} \mu_W \\ \alpha_W \\ \beta_W \\ P_W \end{bmatrix} = \begin{bmatrix} \mu_{oW} + \Delta\mu_W \\ \alpha_{oW} + \Delta\alpha_W \\ \beta_{oW} + \Delta\beta_W \\ P_{oW} + \Delta P_W \end{bmatrix} \tag{63}$$

The first control law for delta thrust includes proportional and integral control on the x error separation and proportional control on the velocity error. There is no integral control on the velocity error as this would be redundant with the proportional x error separation control, since integrating the velocity error would yield the position error. The thrust law is

$$\Delta\mu_W = K_{XP}x_e + K_{XI}\int x_e + K_{VP}V_e \tag{64}$$

The angle of attack control law includes proportional and integral control on z separation error and flight path error and is found by the equation

$$\Delta\alpha_W = K_{ZP}z_e + K_{ZI}\int z_e + K_{\gamma P}\gamma_e + K_{\gamma I}\int \gamma_e \tag{65}$$

In a similar matter, the roll rate control law is proportional and integral in both the y separation error and the velocity vector roll angle error:

$$\Delta P_W = K_{YP}y_e + K_{YI}\int y_e + K_{\phi P}\phi_{Ve} + K_{\phi I}\int \phi_{Ve} \tag{66}$$

It can be seen from the above three control laws that there is a balance that occurs between the two different error values represented in each law. The objective is to find the correct gains to balance the two errors in a way that causes the aircraft to perform adequately. For example, the angle of attack law will continuously try to drive the flight path angles to the same value, but a separation error that is big enough in the z direction

will take precedence over the angle error and both will be corrected until a steady state of zero is reached.

Sideslip control is previously unaccomplished in automatic formation flight control. The sideslip control law presented below controls only the course error but is somewhat more complex than the other three laws. It is given here

$$\Delta\beta_W = \left(\frac{1}{1 + \frac{|y_e|}{K_{\beta HG}}} \right) \left(K_{He} H_e \left(e^{-12|He|} - e^{-60000|He|} \right) \right) \tag{67}$$

It is understood that the use of rudder control in a high performance aircraft for more than coordinated flight is not normally done. The purpose of this control is to fix small angle errors in course while minimizing the disturbances in other channels. The advantage to be gained by using sideslip angle to control course angle error is that the dynamics of the aircraft in the directional axis is lightly coupled to the other axes of the aircraft. Thus, when an input is made to correct heading, minimal disturbances are realized in the other axes. The largest challenge to using this control is to limit its use to reasonable levels and at appropriate places. The controller, nor the pilot flying in the aircraft, desire a large yaw angle or even slight yaw angles for long periods of time. A sideslip controller was desired to have a somewhat proportional response at course angle errors of less than five degrees and a diminishing response as the error increased in size. Simply put, sideslip correction is only to be accomplished when the wing and lead course headings are near each other, otherwise roll correction as a result of the roll rate control law is allowed to drive the course until a lower course error is achieved and sideslip control is again activated. An exponential based function was synthesized by the author to provide this

type of control, and can be seen in equation (67) above. The exponential type responses of the controller to varying Heading angle errors, H_e , at different lateral separation errors, y_e are plotted in the graph below:

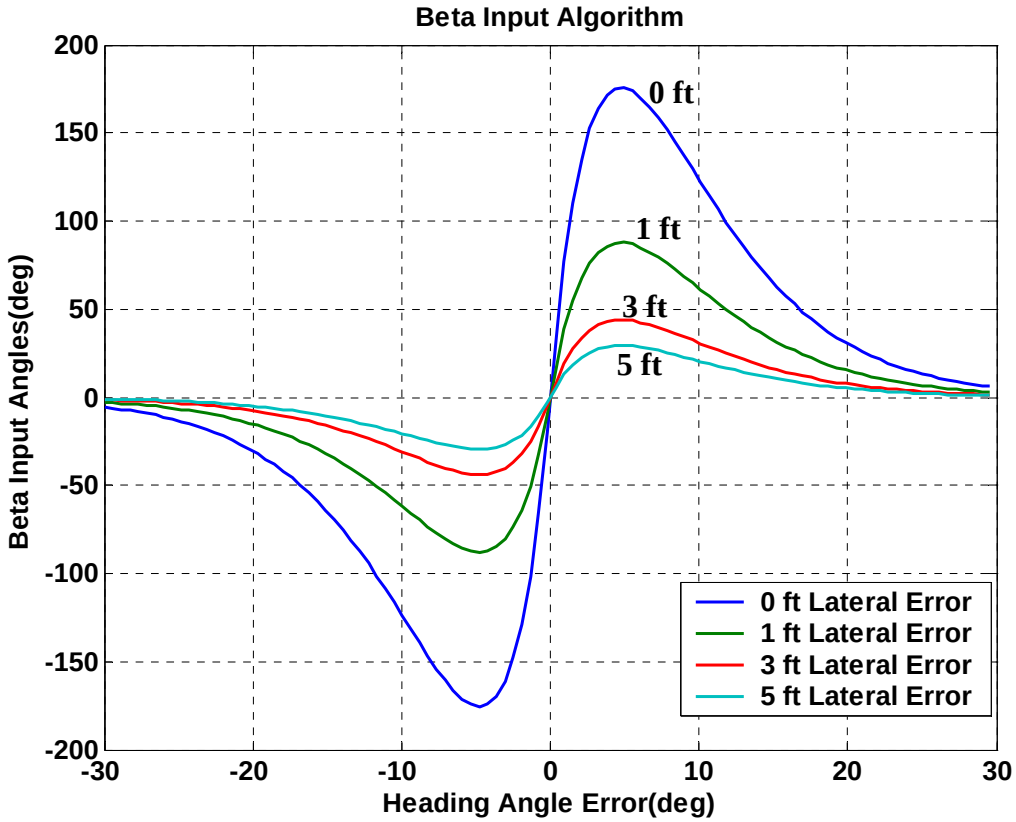

Figure 5. Exponential Curve for Beta Control

Sideslip control cannot be applied in all occasions, even if the course error is low, since there are occasions when this could result in a cross controlled situation. If the wing aircraft was in a position far to the left of the commanded y separation distance, a cross controlled situation would arise as the roll rate control attempted to fix the position error with right roll, while the sideslip control attempted to match lead's course angle with an increasing left correction. Thus, inverse proportional control to the y separation error was implemented and can be seen in the sideslip control equation (67). As the y

separation error increases the use of sideslip is proportionally decreased. This rate of decrease is controlled via a gain, $K_{\beta HG}$ that represents the distance in the y direction where sideslip gain, K_{He} is half of its value.

It is clear that the above control laws are capable of driving all of the error states to zero, assuming that we desire the angles and velocities of both aircraft to match. A full discussion of the subject must then include any situations where it is desired that the angles or velocities be different. In these cases we desire a steady state error in one of our error states. An example of this occurs when lead begins a significant turn and the wing aircraft is required to make a larger or smaller turn radius due to an offset in the y direction. If the turn takes long enough, the wing aircraft will have enough time to settle into a steady state value during the turn. Due to the balancing nature of the above control laws, the gains placed on the velocity error versus the gain placed on the x separation error will determine a steady state offset in the x separation distance as the velocity error stabilizes at a steady state to compensate for the two different radius' of flight. There are three options to control this situation. The first option is to build a velocity required estimator that is based on the lead aircraft's roll angle and acceleration and the wing aircraft's lateral spacing. The second option is to simply test the controller in sustained turns to determine the steady state error that will result and decide if the error is acceptable. The final option is to design a continuously trimming function that continuously determines the steady state error and applies that error to the steady flight equilibrium values. This option would be somewhat complex to implement and will be

listed as a subject of future development in the area of automatic formation flight. The author simulated the second option above, and the results are discussed in Chapter V.

It was presented above that a steady state error will occur in an error state when a control law is balancing two error states and one of them is forced to a non-zero steady state value. This same condition could exist in close formation flight depending on the techniques used to counter the different wind angles the trail aircraft will experience as a result of the lead aircraft's wake. As presented in Chapter III above, the close formation disturbances will occur as a roll moment, a yaw moment and a side force. The roll rate that is induced by the roll moment will not be difficult to control since roll rate is a control variable. The induced roll rate will simply be countered by roll rate inputs. As presented above we assume the yaw rate and side force induced are a result of the sideslip angle created because of the modified airflow. The wing aircraft must negate these additional forces if it is to maintain the same inertial flight path as that of the lead aircraft. The problem of yaw and side force is much akin to the problem of a crosswind landing. Similar to a crosswind landing where the pilot has the well known options of crabbing into the wind or using a wing low method, the controller must perform one of the same two options. The crab method would allow the wing aircraft to weathervane into the wind with a slightly different yaw angle than lead, but with the same velocity vector heading angle. With this option, besides wind disturbances and the aileron input required to counter roll rate, there is no further control input required to maintain the formation. In addition, there would be no steady state errors induced in any of the control laws. Alternatively, the wing low option uses a continuous rudder input to force the nose of the wing aircraft in alignment with the lead aircraft. Then, to counter the drift that will occur

due to the sideslip angle of the airflow, a continuous wing low roll angle will be maintained. With this option, besides wind disturbance inputs and the aileron input required to counter roll rate as before, the controller must also include a constant rudder input and a constant roll angle mismatch between lead and wing. Similar to the sustained turn situation given above, the sustained error in velocity vector roll angle will induce a y separation error as a result of the roll rate control law repeated here:

$$\Delta P_W = K_{YP} y_e + K_{YI} \int y_e + K_{\phi P} \phi_{Ve} + K_{\phi I} \int \phi_{Ve} \tag{66}$$

Thus, the sustained velocity vector roll angle error that is necessary to maintain the wing low correction will cause a sustained error in the y direction. As discussed above, three options could be used to counter the steady state error problem. The first option is to build a steady state roll error estimator either based on formation flight data or a formation vortex model. The estimated error could then be subtracted from the actual error, and this value minimized. In this case, the roll angle error would no longer compete with the y separation error, which could then be driven to zero. The only error that would present itself becomes a function of the validity of the flight data or the fidelity of the model. As before, the second option would be to simply test the controller to determine the steady state error that will result if no compensation is made. Since we will be trying to maintain a fuel savings position, this option will most likely not be possible, but will be tested regardless. The last option is to implement a trimming function to determine the steady state errors in real time and continuously add them as corrections to the steady level flight equilibrium values. As before, this option will be left as a further development to automatic formation flight control and will not be attempted here.

The best overall option to maintain the correct formation while in the vortex of the lead aircraft appears to be the crab method. No steady state errors occur when using this option and because fewer control inputs correlates to less drag, the crab method is expected to be the best solution to counter the vortex disturbance, maintain the optimum fuel position, and reduce the required fuel flow. Regardless of the author's expectations, both the wing low and crab method will be simulated and the results analyzed.

Model Development

Appendix B includes all figures relating to the Simulink® model that was developed for simulating the system. The top level view of the system is found in Figure 96 of Appendix B. The equilibrium parameters for the lead and wing aircraft are utilized separately so that different aircraft types could be explored in the future. For all of the simulations presented, the same equilibrium values for lead and wing, (both F-16's) are input into their respective control calculator and limiter, "L Param w/ Limits" and "W Param w/Limits" blocks shown in Figure 96 of Appendix B.

The control values are added to the steady flight equilibrium values, limited and then fed into the each aircraft's state calculator. If an actual control signal is being simulated, a signal limiter and/or rate limiter block is used to limit lead or wing control values. For lead, this simulates that the lead pilot will not exceed certain values or rates. For the wing aircraft, this simulates what the controller will be limited to command from its control surfaces. State values are limited through the use of saturation values in the state vector integrator block.

The state of each aircraft as a result of the control inputs driving the aerodynamic force equations is calculated in the "Lead A/C Model" and "Wing A/C Model" blocks found in Figure 106 of Appendix B. The lead and wing aircraft states are then fed into three blocks titled "Lead Angle & Vdot", "Wing Angle & Vdot", and "Position Delta Dots". The dot values for each state are then collected and integrated to yield the formation state vector. The formation state vector is written to the workspace at each time step, and is used in this way to view and analyze the system and controller results.

The two main disturbances are calculated in the same "Wind/Vortex Gen" block found in Figure 103 of Appendix B. For the wind disturbances, two random white noise signals with zero bias are fed into their own integration loops to continuously calculate the differential wind angle equations presented above. Two separate signals represent angle of attack and side-slip disturbances. We assume the rate of change of the wind at a given position is much less than the velocity of the aircraft. This assumption implies that the aircraft are flying through a wind field that is not moving relative to inertial space. The x separation distance and velocity of the wing aircraft is used to calculate a time delay. This time delay is applied to the wind disturbance signals for the wing aircraft. In this way, the same air mass disturbances are applied at different times, simulating the real world effect of being in close formation and flying through an atmospheric disturbance.

The vortex forces are calculated as a function of the y separation in the leader's reference frame. The induced roll rate is calculated and output. The sideslip disturbance is calculated by a separate feedback loop to capture the second order yaw rate dynamics of the F-16 aircraft when the yaw moment is applied. In addition, the second derivative of the controller's sideslip commands are also fed into the differential equation. When

steady state errors are to be compensated for, the model has perfect knowledge of what roll rate is required to negate the error. This is accomplished by running the simulation without compensation to see what the steady state error is, and then applying this steady state error as the "model data". The effects of the poor model can then be determined by changing the compensating error a certain percentage and noting the effect.

V. Simulation Results

Aircraft Parameters and Maneuvers

For all tests the lead and wing aircraft parameters were the same to represent a two ship of similar F-16's, and were taken from Stevens and Lewis (18:584-592). The actual parameters used are presented in Table 2 below:

Table 2. Aircraft Parameters @ 20,000 ft & 667 ft/sec

Surface Area (S)	300 f t^2	**Tail Span (b_{Vt})**	10 ft
Wing Span (b)	31 ft	$C_{Y\beta}$	1.146/rad
Aspect Ratio	3	**Tail Eff. Factor(η)**	.95
$C_{L\alpha}$	5.3/rad	**Mass (M)**	776.4 Slugs
C_{Do}	.015	**Force Gravity (W)**	25,000 lbs
Drag Polar (K)	.02	**Density (ρ_{20K})**	.001267 slug/ft
Surface Area Vertical Tail (S_{Vt})	54.75 ft^2		

The controller's performance was tested using five different simulation sets. Each simulation set represents a series of maneuvers that were used to measure the controller's performance and determine a set of gains that give the best performance for the given series of maneuvers or tasks. The first set was used to test only the controller's ability to maintain a given formation, out of the vortex and with no wind. The second set had the lead fly straight and level while the wing aircraft changed its formation separation. Again no wind or lead vortex disturbances were investigated. The third

simulation set looked at maintaining and changing formations with varying levels of wind turbulence. The fourth simulation set looked specifically at the effects of close formation flight and was used to determine what control options presented above would provide the best controller performance. Finally, the fifth simulation set utilized varying wind effects while the wing aircraft attempted to both maintain and maneuver through the vortex field. This final simulation set also used the best case gains as determined from the previous simulation sets. The following sections give a brief description of the simulation set, a table to describe the maneuvers and gains used and finally present the actual simulation results in graphical format. Following the fifth simulation set, the overall results are summarized and conclusions are made.

Gain Selections and Controller Modifications

In every simulation set presented below something interesting was discovered and the controller gains or even the controller itself was modified to provide acceptable performance. Since the controller was modified as the tests were conducted, it was unrealistic to present all of the previous results as the controller was changed in later simulation sets. Because of this, the simulation sets below are all run utilizing the overall best set of gains and the controller setup optimized for all simulation sets. The process of determining the overall best setup is a balancing act between the different maneuvers and the author's view of what is acceptable error. The two main trade-offs when selecting gains are the requirements for stiffness when holding formation position through lead maneuvers, and the ability to change the formation separations. The initial gains were set according to the minimum error that could be achieved while holding formation during

lead maneuvering. During simulations 1-5 and 1-6, lead turn maneuvers found in Figures 10 and 11 respectively, it was discovered that a steady state heading error will develop during a sustained turning maneuver that the controller will attempt to counter with sideslip. The sideslip is then countered by a steady state roll angle to compensate for the side-force. Due to the balancing nature of the roll rate control law, the y separation is reduced to compensate for the steady state error. Since the sideslip control was only meant to be applied during fine tune correcting of the aircraft course angle in near level flight, and the above situation represents an unwanted cross control situation, a limiter as a function of the wing roll angle, was built and applied to the wing aircraft's sideslip control. The control utilizes a cosine function to allow sideslip control only when the wing aircraft has a near zero velocity vector roll angle. The function drives the sideslip control to zero by 5 degrees of wing roll angle. The tightest lateral control that could be achieved was used for these gains. The gains after first running simulation set#1 were thus initially set to

Table 3. Gains For Simulation Set #1-Tight Lateral Control

Gain	K_{XP}	K_{XI}	K_{ZP}	K_{ZI}	$K_{\gamma P}$	$K_{\gamma I}$	K_{YP}	K_{YI}	$K_{\varphi P}$	$K_{\varphi I}$	K_{VeP}	$K_{\beta HG}$	K_{He}
Value	.25	.06	.025	.02	25	20	.09	.02	2	5	.3	1	100

Simulation set #2 was next run to determine how the controller would respond to formation separation changes. The first of two main changes made to the system because of simulation set #2 was the addition of velocity error integral control. It was found that a position change in the longitudinal direction had very poor damping, and resulted in a large overshoot and long settling times. Earlier, in Chapter IV during a discussion of the control laws, it was stated that integral action on the velocity error is redundant since the

integral of velocity is position. This is a correct statement when we are considering a position hold situation where the velocity error is explicitly defined as time rate of change of a continuous position error. This is not the case when a formation position change is considered. During a commanded position change the position error can be instantly changed to 30 feet, while the velocity error has not changed. In this case, the integral of the velocity error is zero, while the x position error is 30. In essence the controller is tracking a type 0 signal in the position hold case and a type 1 signal in the case of the step position input. According to well known tracking theory the controller requires another integrator to affect the control with zero steady state error. Thus the author changed the controller to include velocity error integral action and ran the simulation again. The longitudinal damping was greatly increased. More importantly the damping can now be adjusted as necessary for the desired performance. It should be noted that the addition of the velocity error integral action affected the position hold schemes presented in simulation set #1. There is now a balancing effect in the x channel as in the y and z channels. Specifically, for the turning maneuvers in simulation set #1, a steady state error in the x separation will be the result of the lateral offset and the different velocities required to maintain the formation during the turn. The second main discovery when initially running the simulation set #2 with the gains determined during simulation set #1, was instability in the system due to the tight lateral control given by the above lateral gains. Thus, these gains were relaxed for stability when a lateral position change was commanded. Relaxing these gains increased the error of the formation hold maneuvers slightly. This solved the stability problem but did not satisfy the error objectives, yet it was becoming difficult to make gain changes that would not degrade the formation hold

capability of the controller. One technique to decrease the overshoot and settling time of the response is to limit the size of the y error the controller sees. This was a simple approach that did not affect the formation hold capability of the controller as long as the errors while trying to hold the formation position did not exceed what the error had been limited too. This technique was applied to determine how much the error had to be limited and what kind of performance would result. It was found that a y error limit of 10 feet met the objectives. The final gain values used for simulation sets one and two, with the new gain variables and the y error limit are presented in Table 4 below with the changed and new values highlighted in bold.

Table 4. Gains Optimized For Simulation Set #1 and #2

Gain	$\boldsymbol{K_{XP}}$	K_{XI}	K_{ZP}	K_{ZI}	$K_{\gamma P}$	$K_{\gamma I}$	$\boldsymbol{K_{YP}}$	K_{YI}
Value	**.03**	.06	.025	.02	25	20	**.05**	.02
Gain	$\boldsymbol{K_{\varphi P}}$	$K_{\varphi I}$	K_{VeP}	$\boldsymbol{K_{VeI}}$	$K_{\beta HG}$	K_{He}	***Yerr Lim***	
Value	**3**	5	.3	**.23**	1	100	**10**	

The gains presented Table 4 above were then used to generate the final results for all of the simulation sets below, since no further changes to the controller were needed while performing the last three simulation sets.

Simulation Set #1

Simulation Set #1 included the following maneuvers flown by the lead aircraft with the trail aircraft attempting to maintain the commanded formation. The wind generator was not initiated for this set of simulations so that the controller's performance could be clearly seen. The performance objectives as provided in Chapter I are presented in the table as an indication of the performance goal for the given maneuver. The simulation set included

Table 5. Simulation Set #1: No Wind/Vortex Disturbances

Sim Num	Lead Aircraft Maneuvers	Wing Aircraft Maneuvers	Initial Form (*x/y/z*)ft	Final Form (*x/y/z*)ft	Error Objective
1	5000' Climb	Maintain Form	30/30/30	Same	≤ 1 ft
2	5000' Descent	Maintain Form	30/30/30	Same	≤ 1 ft
3	100 ft/sec Accel	Maintain Form	30/30/30	Same	≤ 1 ft
4	100 ft/sec Decel	Maintain Form	30/30/30	Same	≤ 1 ft
5	360 degree Rt 30 deg Bank	Maintain Form	30/30/30	Same	≤ 1 ft
6	360 degree Lt 30 deg Bank	Maintain Form	30/30/30	Same	≤ 1 ft

Gain	K_{XP}	K_{XI}	K_{ZP}	K_{ZI}	$K_{\gamma P}$	$K_{\gamma I}$	K_{YP}	K_{YI}
Value	.03	.06	.025	.02	25	20	.05	.02
Gain	$K_{\varphi P}$	$K_{\varphi I}$	K_{VeP}	K_{VeI}	$K_{\beta HG}$	K_{He}	*Yerr Lim*	
Value	3	5	.3	.23	1	100	10	

During simulation runs one and two it was found that a lead flight path angle limit of 30 degrees created a climb faster than the targeted 5,000 feet in 60 seconds. It was

found that a 15 degree flight path angle limit was more appropriate and an angle of about 8 degrees yielded a 5,000 foot climb in approximately 60 seconds. The results of the climb and descent simulations, presented in Figures 6 and 7 below, show an error of less than 1 foot. It was an objective that the aircraft settle to within one foot of the desired position within 5 seconds. Since no errors were greater than 1 foot, the settling time was not an issue. Although there appears to be a large amount of error in each of the position channels individually, it must be remembered that this is due in large part to the separation values being attached to the wing aircraft. Thus, as the wing aircraft pitches up to follow lead it is also changing the separation values. The last plot for each of the simulations shows the total separation as a function of time. The true error can be easily seen on this plot, since the total distance will not change despite the changing wing reference frame angles.

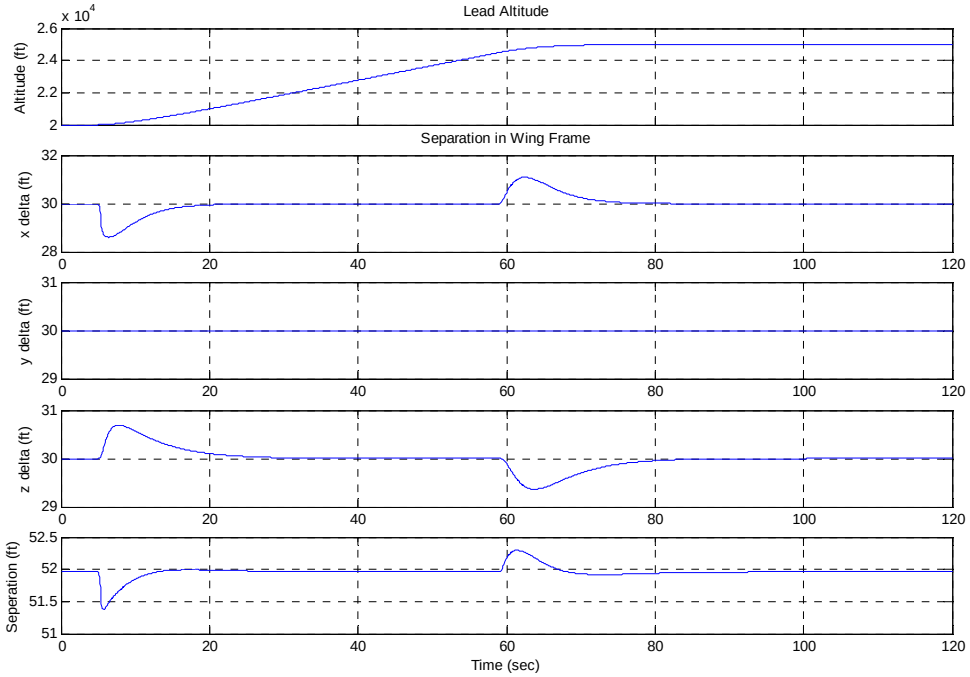

Figure 6. Sim:1-1 (20,000' to 25,000' Lead Climb at 5")

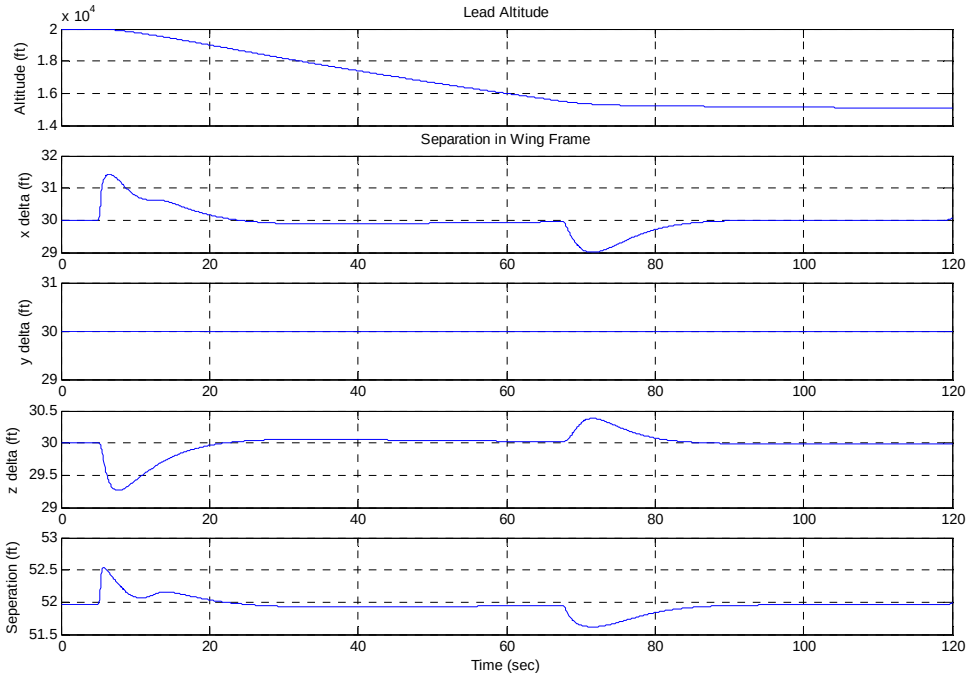

Figure 7. Sim:1-2 (20,000' to 15,000' Lead Descent at 5")

For the acceleration and deceleration simulations it was found that a 5% of mil power thrust limit for lead was too restrictive, requiring an excessive amount of time to decelerate 100 ft/sec. The min thrust limit was changed to 1% of mil power. This change still provided enough of a thrust advantage for the wing aircraft to maneuver appropriately. It was also found that the thrust control rate of 10%/sec for lead was also unnecessarily restrictive and a rate of 20%/sec was acceptable, allowing a more realistic throttle control from the lead aircraft. The results of simulations 1-3 and 1-4 are presented in the Figures 8 and 9 below. Again for both simulations all total separation errors were less than 1 foot.

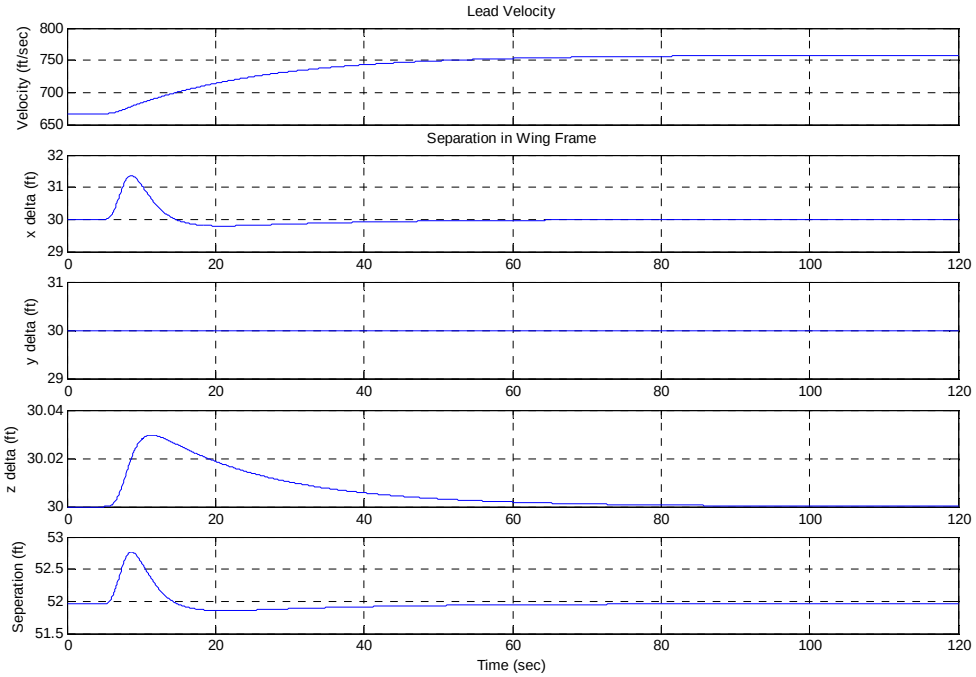

Figure 8. Sim:1-3 (100 ft/sec Lead Accel at 5")

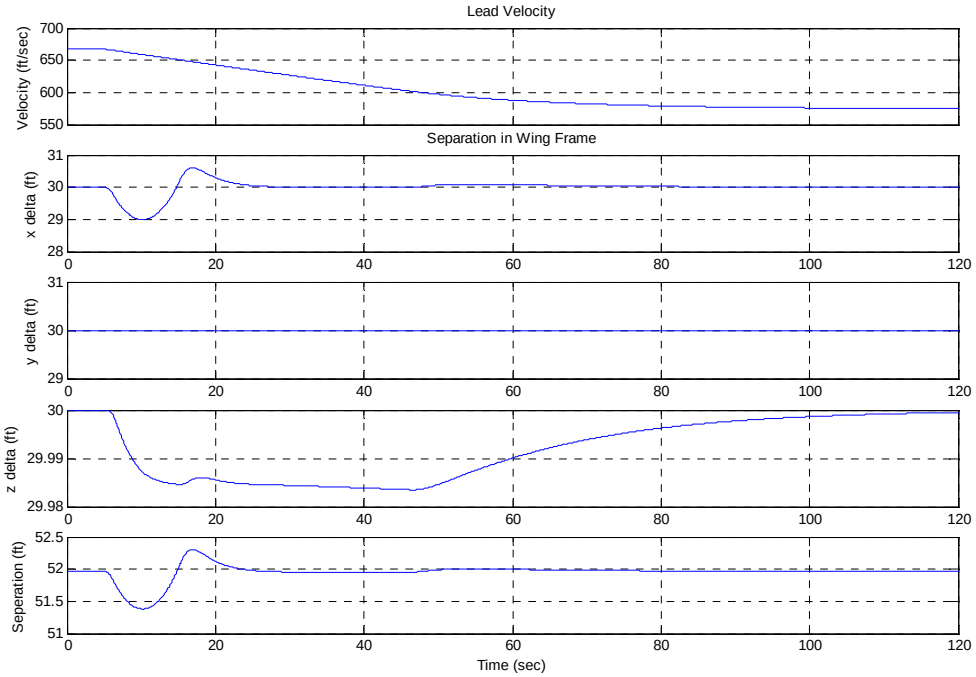

Figure 9. Sim:1-4 (100 ft/sec Lead Decel at 5")

The last two simulations for this simulation set were the most difficult to find acceptable control gains since the lateral motion of the aircraft is more closely coupled to the dynamics in other axes. First, it was discovered that a 10 deg/sec roll rate limit on the lead aircraft more closely approximates a conservative pilot roll rate than the originally planned 30 deg/sec rate. Figures 10 and 11 below show the results of the turning maneuver simulations. Here again, the only true measure of performance is the total separation distance presented in the bottom plot of these figures since the reference system is attached to the wing aircraft.

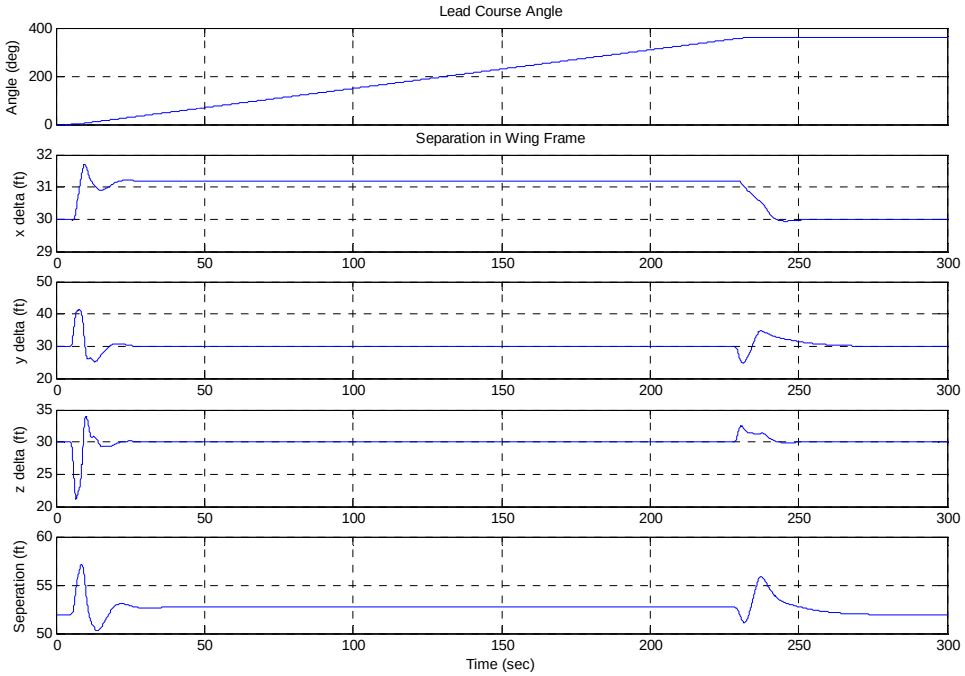

Figure 10. Sim:1-5 (360 deg Lead Right Turn Away at 5")

It is clear from the above figure that a maximum error of approximately 5 feet develops upon roll in for the turn away maneuver of simulation 1-5. From the figure below a maximum error of approximately 6 feet develops upon roll in for the turn into maneuver of simulation 1-6.

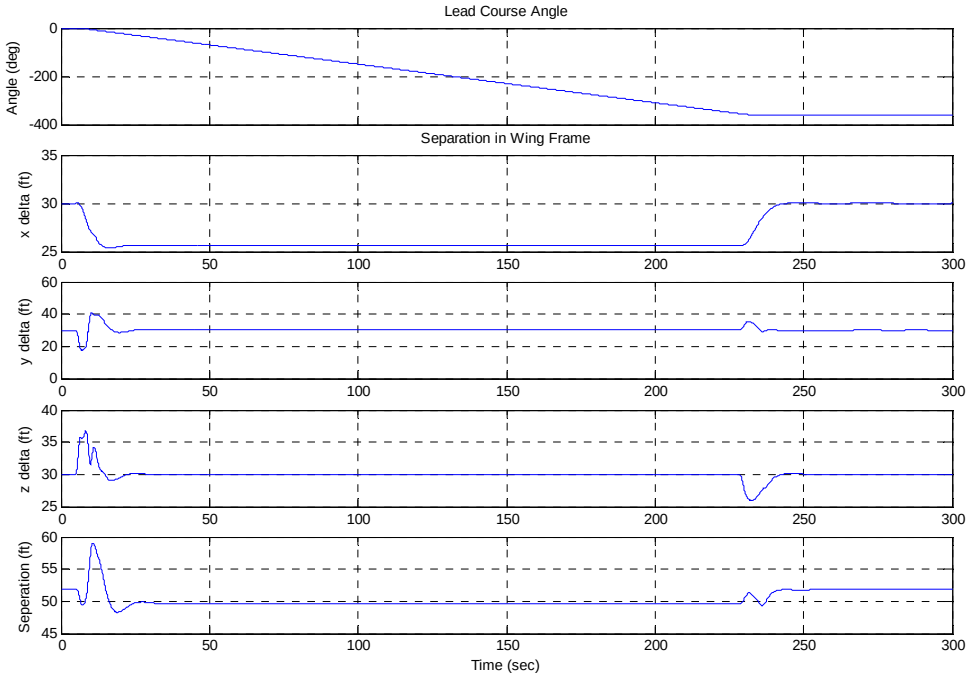

Figure 11. Sim:1-6 (360 deg Lead Left Turn Into at 5")

Clearly the controller is not behaving as stiffly in the lateral channel as was set forth in the objectives, but two considerations help mitigate the impact of these errors. First, in both turning maneuvers, the maximum errors occur in a direction away from the lead aircraft. Secondly, the smaller the separation, the smaller the errors can be expected. As was mentioned, it was possible to get better performance with the set of gains first presented in the previous section, but instead a second set of gains were chosen as a good compromise because of the formation change maneuvers to follow in simulation set two. It should also be noted that a steady state error in the x channel of 1.2 feet is now apparent for the turn away maneuver and 4 feet for the turn into maneuver as a result of the velocity error integral control previously discussed.

Simulation Set #2

Simulation Set #2 included the lead aircraft flying straight and level while the wing aircraft was commanded from one formation position to another. The wind generator was again not initiated for this simulation so that the basic performance of the controller could be assessed. In addition, the wing aircraft was not commanded to, or through, any portion of the lead aircraft's vortex wake. The simulation set included

Table 6. Simulation Set #2: No Wind/Vortex Disturbances

Sim Num	Lead Aircraft Maneuvers (Hold)	Wing Aircraft Maneuvers	Initial Form (*x/y/z*) ft	Final Form (*x/y/z*) ft	Error Objective
1	20,000' 667 ft/sec	Vertical Pos Change Up	30/30/0	30/30/30	≤ 2 ft Overshoot Settle ≤ 1 ft by 15"
2	20,000' 667 ft/sec	Long. Pos Change Aft	0/30/30	30/30/30	≤ 2 ft Overshoot Settle ≤ 1 ft by 15"
3	20,000' 667 ft/sec	Long. Pos Change Forward	30/30/30	0/30/30	≤ 2 ft Overshoot Settle ≤ 1 ft by 15"
4	20,000' 667 ft/sec	Lateral Pos Change Away	30/30/30	30/60/30	≤ 2 ft Overshoot Settle ≤ 1 ft by 15"
5	20,000' 667 ft/sec	Lateral Pos Change Into	30/60/30	30/30/30	≤ 2 ft Overshoot Settle ≤ 1 ft by 15"

Gain	K_{XP}	K_{XI}	K_{ZP}	K_{ZI}	$K_{\gamma P}$	$K_{\gamma I}$	K_{YP}	K_{YI}
Value	.03	.06	.025	.02	25	20	.05	.02
Gain	$K_{\varphi P}$	$K_{\varphi I}$	K_{VeP}	K_{VeI}	$K_{\beta HG}$	K_{He}	*Yerr Lim*	
Value	3	5	.3	.23	1	100	10	

This simulation set began with the vertical formation change maneuver. The simulation results show no overshoot and crosses within 1 foot of the steady state value by 5.4 seconds. Figure 12 below displays these results.

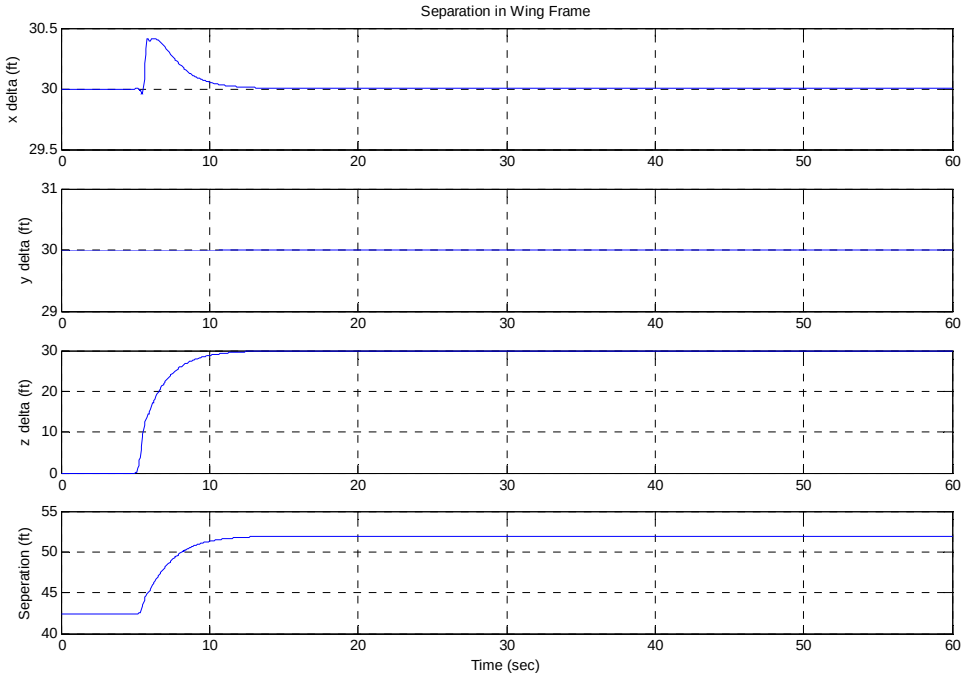

Figure 12. Sim:2-1 (Vertical Formation Change Up 30 feet)

The next simulation in this set was a longitudinal formation change of 30 feet aft. The simulation results in an overshoot of approximately .615 feet and a settling time (≤1 foot of steady state) of exactly 6.48 seconds. Again, the formation change maneuver begins at 5 seconds simulation time. The results of this run are presented below in Figure 13. This simulation set also includes a formation change forward from 30 feet to 0 feet of x separation. The results of this simulation are presented in Figure 14 below. For this simulation there was no overshoot, and the settling time (≤1 foot of steady state) was 10.7 seconds.

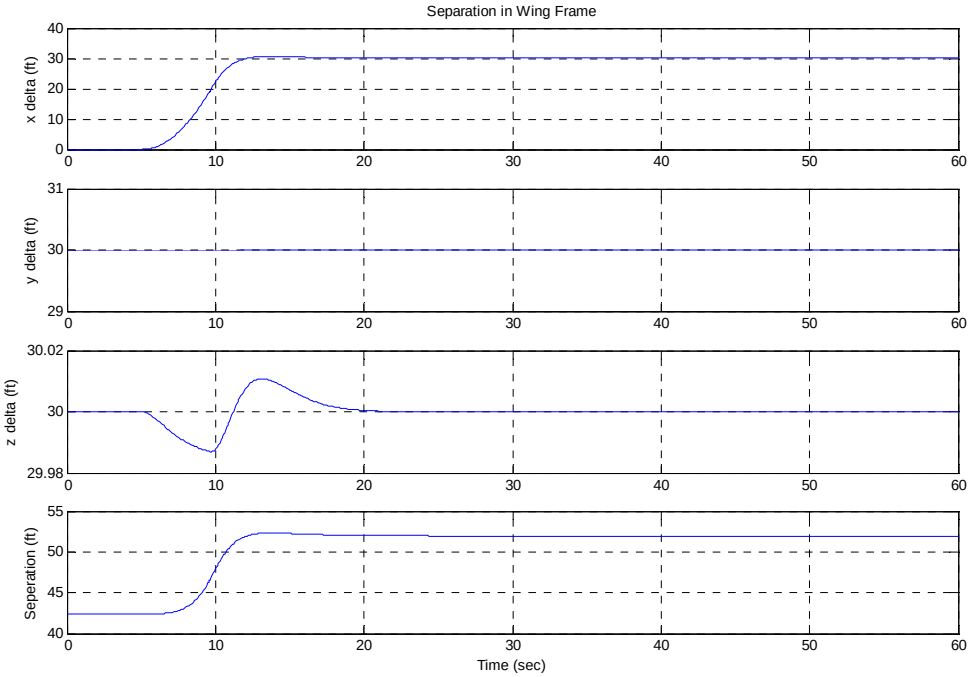

Figure 13. Sim:2-2 (Longitudinal Formation Change Aft 30 feet)

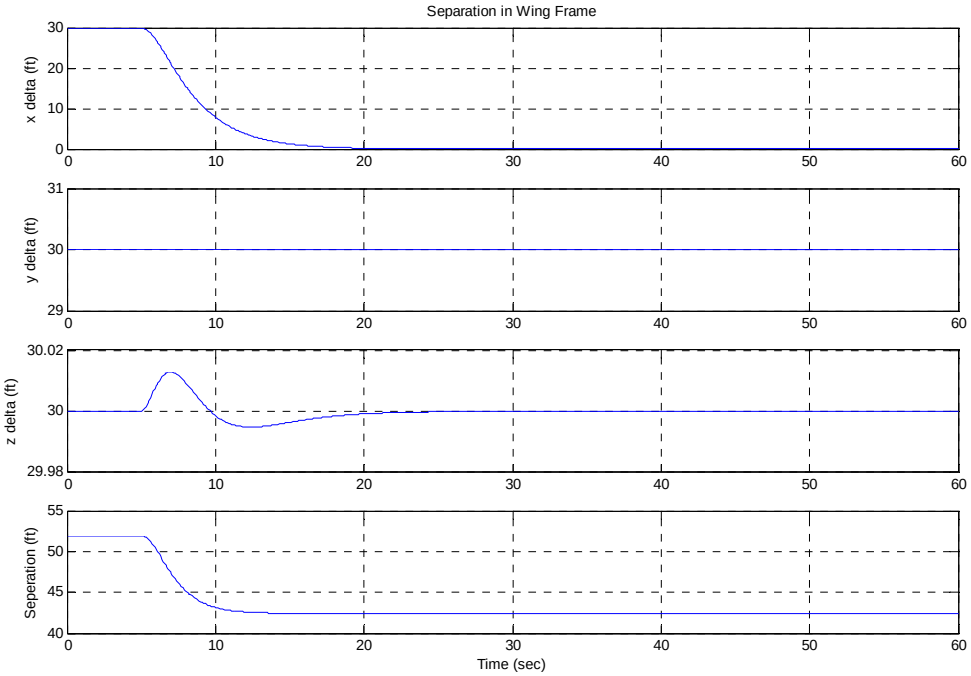

Figure 14. Sim:2-3 (Longitudinal Formation Change Forward 30 feet)

The first lateral motion of this simulation set was a formation change away from the lead aircraft. The gain set given in Table 4, which included a relaxed value of $K_{YP} = .05$, did not yield instability until a lateral position change of approximately 78 feet was commanded. Thus, our required lateral step of 30 feet has a significant margin of stability. The first run of the lateral position changed maneuver showed a significant overshoot of 12.654 feet, and a settling time (≤1 foot of steady state) of 18 seconds, both much greater than the desired objectives for each. This simulation run is presented in Figure 15 below. It is noted that the positional error results are most clearly represented by the bottom total separation plot, since the y and z separation plots are affected by the rotating of the reference frame attached to the wing aircraft.

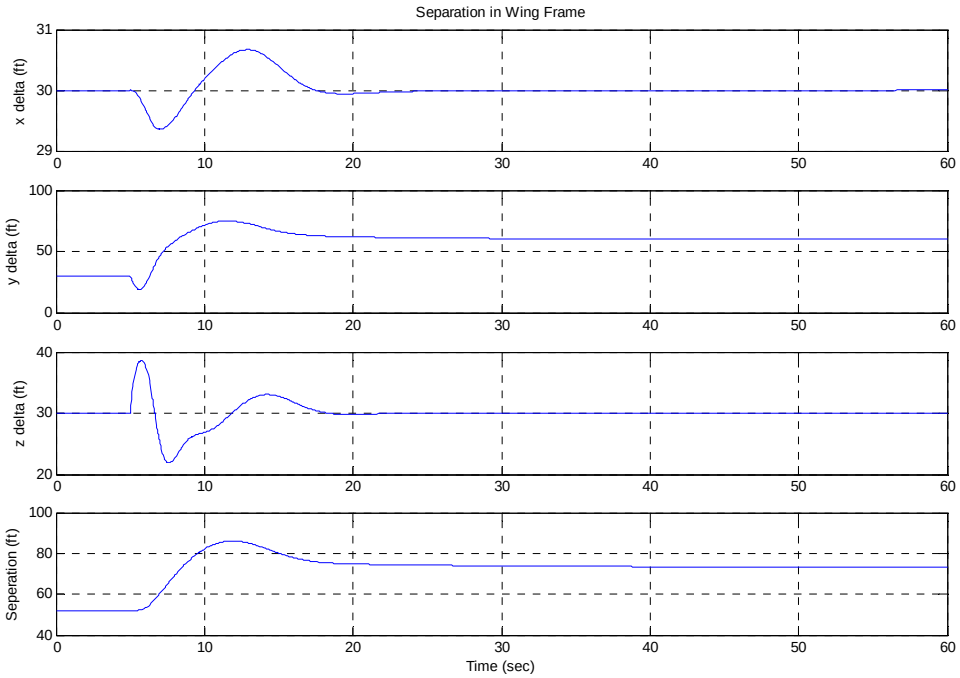

Figure 15. Sim:2-4 (Lateral Formation Change 30 feet Away from Lead)

Clearly the lateral maneuver is far from the overshoot and settling time objectives. As was previously mentioned, a y error limit of 10 feet was applied. With the y error

limit in place the simulation yielded an overshoot of 2 feet and a settling time (≤ 1 ft of steady state) of 13.8 seconds. The plot of the response is presented in Figure 16 below.

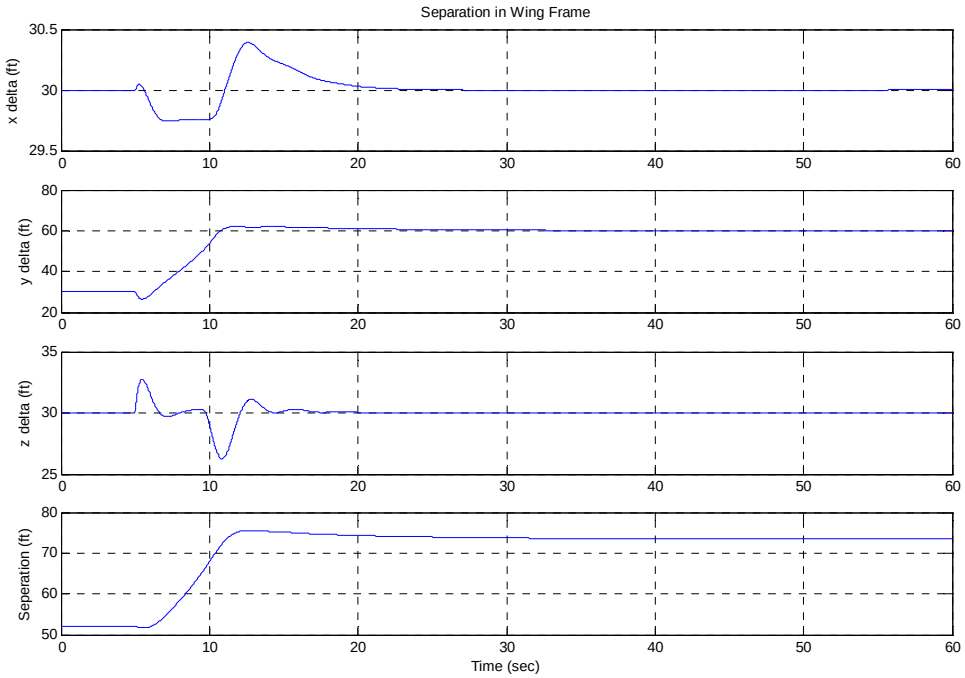

Figure 16. Sim:2-4 (Lateral Formation Change 30 feet Away from Lead) with 10 ft y error limit

It is clear from the above plot that the move to the new position is direct, with little overshoot. The initial y channel dip separation is a result of the trading of y separation with z separation during the bank to the left to affect the formation change. This is apparent in the overall separation distance in the bottom plot that does not show the same characteristic dip.

Simulation Set #3

Simulation Set #3 looked at maintaining and changing formations with varying levels of wind turbulence.

Table 7. Simulation Set #3: No Vortex Disturbances

Sim Num	Lead Aircraft Maneuvers	Wing Aircraft Maneuvers	Initial Form (*x/y/z*) ft	Final Form (*x/y/z*) ft	Error Objective	Wind Dist
1	Hold:20,000' V=667 ft/sec	Hold Form	30/30/30	30/30/30	≤ 1 ft	Norm
2	Hold:20,000' V=667 ft/sec	Hold Form	30/30/30	30/30/30	≤ 3 ft	Cum Clds
3	Hold:20,000' V=667 ft/sec	Hold Form	30/30/30	30/30/30	≤ 5 ft	Thndr Storm
4	Hold:20,000' V=667 ft/sec	Vert Pos ChangeUp	0/30/30	30/30/30	≤ 2 ft Overshoot Settle by 15"	Norm
5	Hold:20,000' V=667 ft/sec	Long. Pos Change Aft	0/30/30	30/30/30	≤ 2 ft Overshoot Settle by 15"	Norm
6	Hold:20,000' V=667 ft/sec	Lateral Pos Change Away	30/30/30	30/60/30	≤ 2 ft Overshoot Settle by 15"	Norm
7	Climb 5,000' Vel=667 ft/sec	Hold Form	30/30/30	Same	≤ 1 ft Settle by 5"	Norm
8	Accel 100 ft/sec 20,000 ft	Hold Form	30/30/30	Same	≤ 1 ft Settle by 5"	Norm
9	360 deg Rt Turn, 20,000 ft	Hold Form	30/30/30	Same	≤ 1 ft Settle by 5"	Norm

Gain	K_{XP}	K_{XI}	K_{ZP}	K_{ZI}	$K_{\gamma P}$	$K_{\gamma I}$	K_{YP}	K_{YI}
Value	.03	.06	.025	.02	25	20	.05	.02
Gain	$K_{\varphi P}$	$K_{\varphi I}$	K_{VeP}	K_{VeI}	$K_{\beta HG}$	K_{He}	*Yerr Lim*	
Value	3	5	.3	.23	1	100	10	

It should be noted that the errors presented in the text below are based on the observations of a single run of the simulation. A more precise approach would be to conduct a statistical determination of the root mean square of the errors with an associated confidence level. This further level of analysis was not conducted based on the relatively small error values observed. The vortex dynamics of lead were still not included in these tests. The error objectives for the wind disturbance simulations were chosen based on the author's opinion of acceptable error given the size of the disturbance. The first three simulations in this set has the lead aircraft hold altitude and velocity while the wing aircraft holds a formation. The wind disturbances are added at increasing severity levels. The results of simulation 3-1 with normal turbulence are presented in Figure 17 below, which was run for 120 seconds and shows a maximum of approximately ± .1 feet of error. Well within the 1 foot error set as an objective.

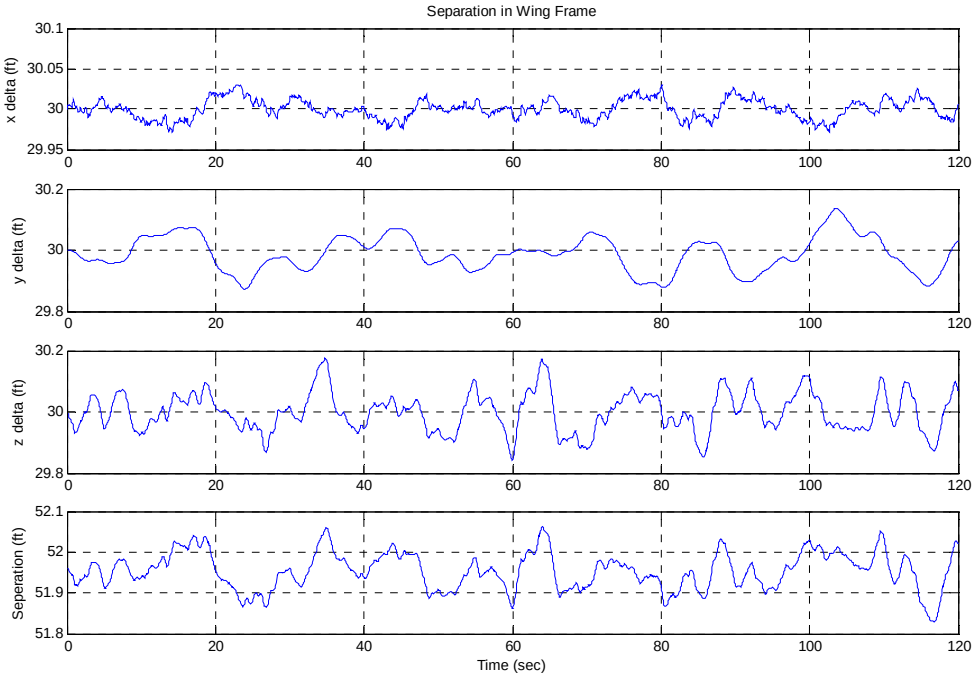

Figure 17. Sim: 3-1 (Formation Hold With Wind at Normal Level)

Simulation 3-2, with cumulous clouds turbulence yielded an error of approximately ± .25 feet and is presented in Figure 18 below. Again this error is well within the 3 foot error objective.

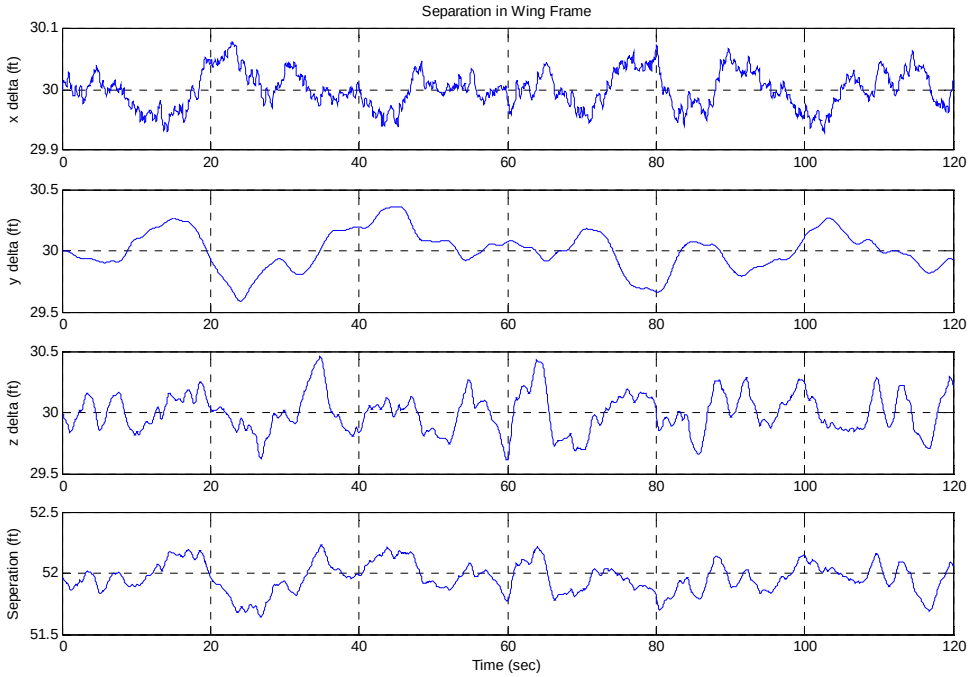

Figure 18. Sim: 3-2 (Formation Hold With Wind at Cumulous Cloud Level)

The third simulation in this set, utilizing thunderstorm level turbulence shows a maximum error of approximately ± .6 feet according to the results presented in Figure 19. The thunderstorm turbulence level error objective of 5 feet was easily met.

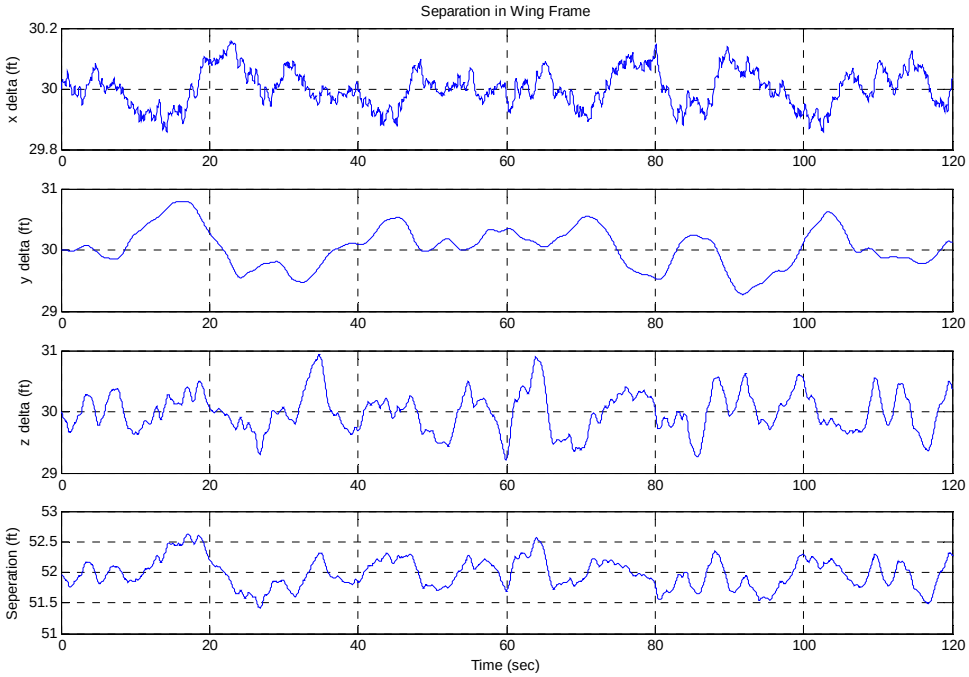

Figure 19. Sim: 3-3 (Formation Hold With Wind at Thunderstorm Level)

The next series of simulations in this set included three formation changes, a vertical position change up, a longitudinal position change aft, and a lateral position change away. The tests were all conducted as a worst case scenario with thunderstorm level turbulence and are presented in Figures 20, 21, and 22 below. It is clear from the plots that the thunderstorm turbulence merely added noise on top of the results previously determined in simulation set two.

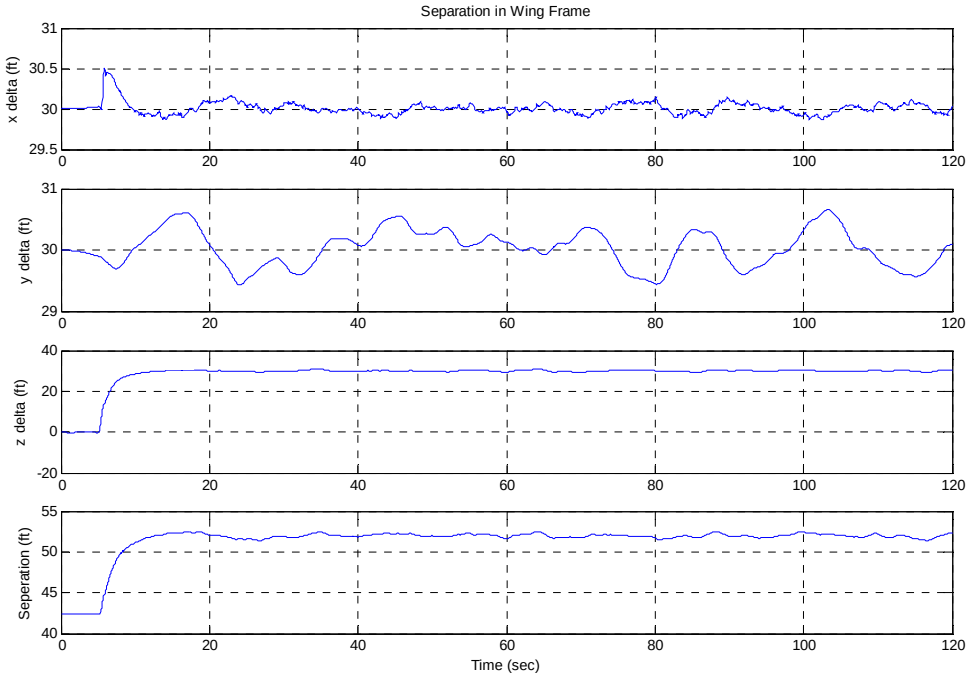

Figure 20. Sim: 3-4 (Vertical Position Change, Wind at Thunderstorm Level)

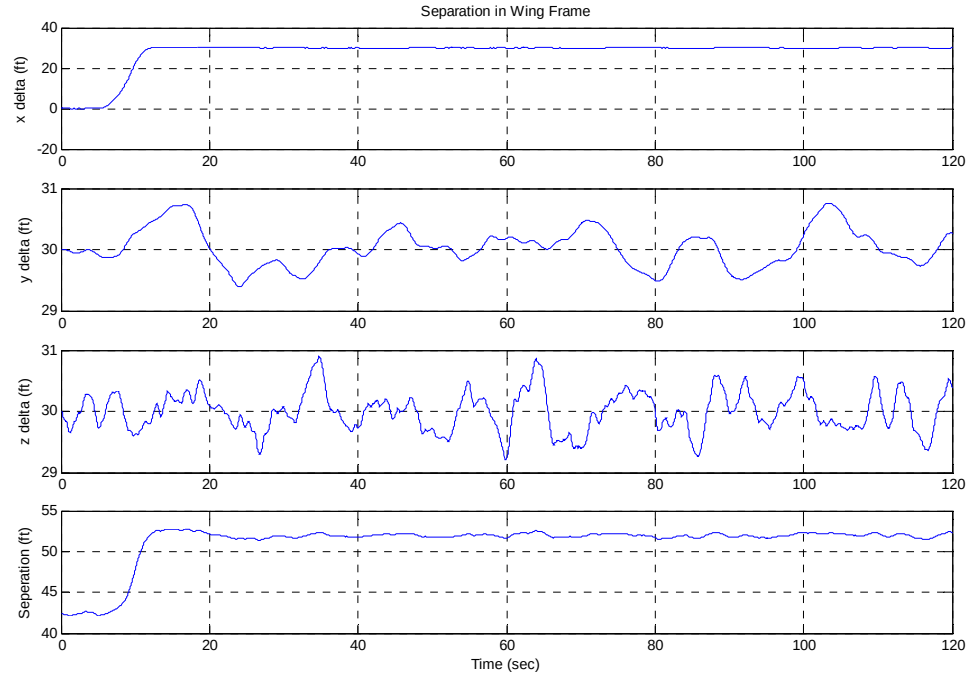

Figure 21. Sim: 3-5 (Longitudinal Position Change Aft, Wind at Thunderstorm Level)

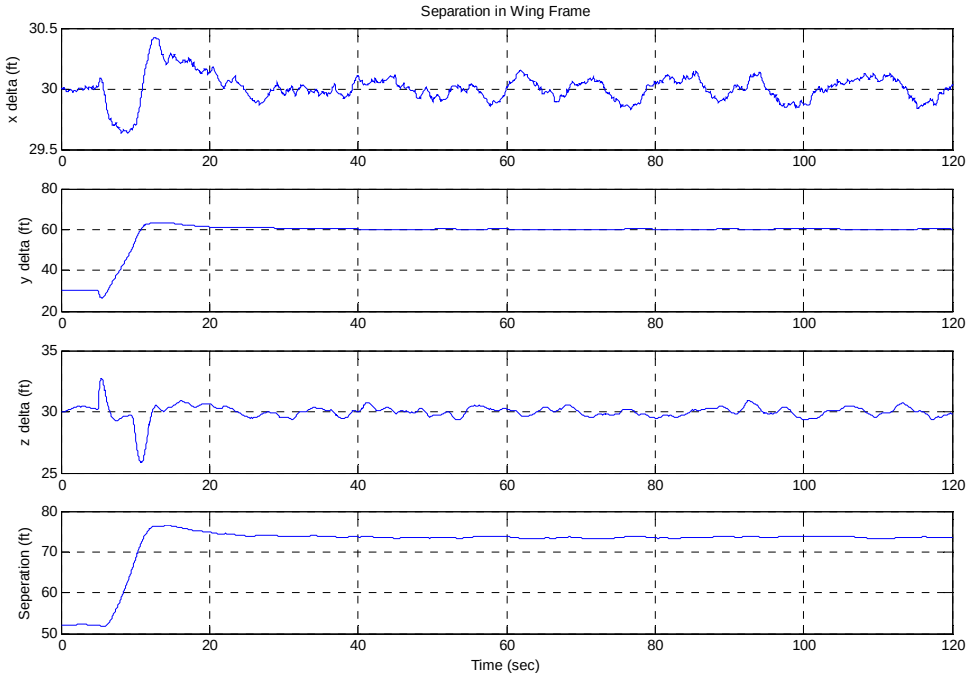

Figure 22. Sim: 3-6 (Lateral Position Change Away, Wind at Thunderstorm Level)

The last three simulations in this set are lead maneuvers while the controller is commanded to maintain position with thunderstorm level wind disturbances. The maneuvers include a 5,000' climb, a 100 foot per second acceleration, and a 360 degree right turn away. The simulation results are presented in Figures 23, 24, and 25 below. Again, the maneuvers are approximately the same with the addition of the wind noise on the result.

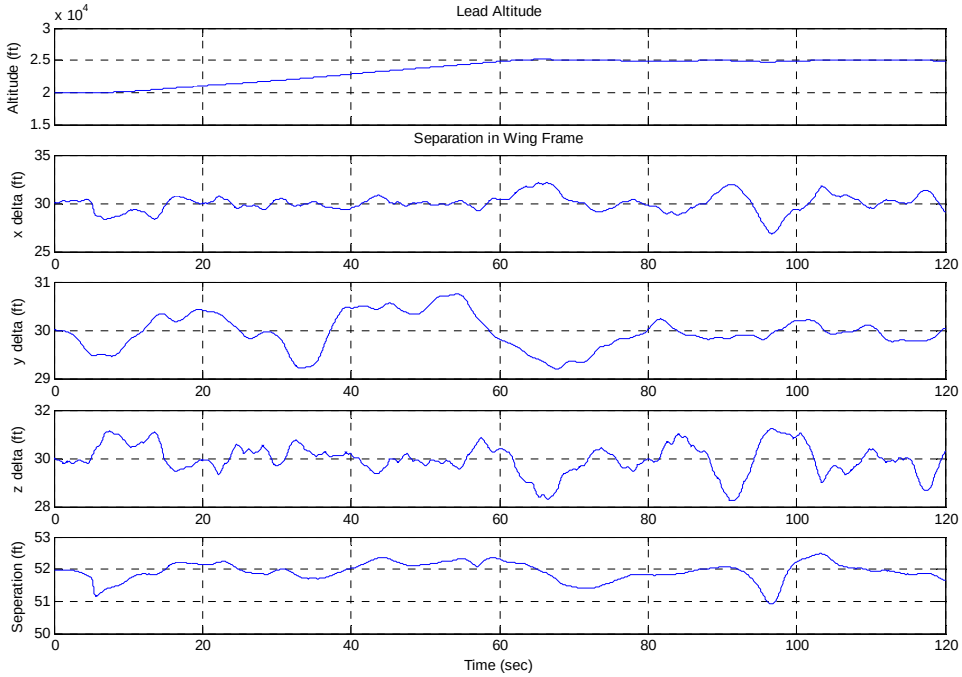

Figure 23. Sim: 3-7 (Lead 5,000' Climb With Wind at Thunderstorm Level)

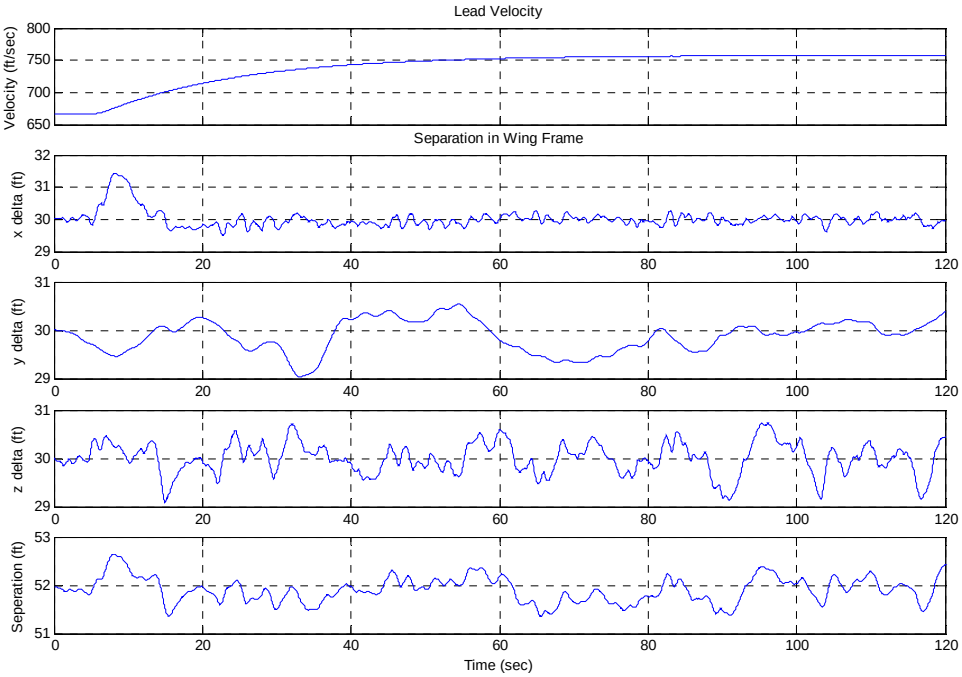

Figure 24. Sim: 3-8 (Lead 100 ft/sec Accel With Wind at Thunderstorm Level)

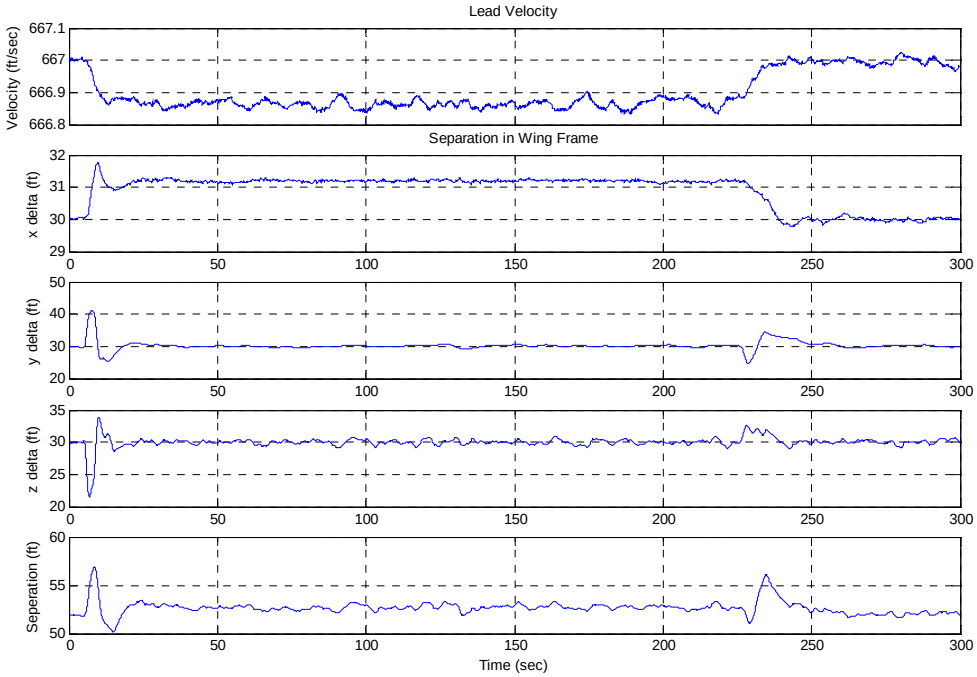

Figure 25. Sim: 3-9 (Lead 360 deg Right Turn Away With Wind at Thunderstorm Level)

Simulation Set #4

Simulation Set four looked at the close formation control options to counter vortex forces. The two options previously discussed were tested. The crab option was simulated first, followed by the wing low option, with and without steady state error compensation. Finally, the wing low method with a 10% error in the model was simulated. Wind disturbances were not applied in this section. The simulation set included:

Table 8. Simulation Set #4: No Wind/ With Vortex Disturbances

Sim Num	Lead Aircraft Maneuvers	Wing Aircraft Maneuvers	Initial Form (*x/y/z*) ft	Final Form (*x/y/z*) ft	Error Objective
1	Hold: 20,000' 667 ft/sec	Hold Form Crab Option	60/40/0	60/26.815/0	≤ 2 ft Overshoot
2	Hold: 20,000' V=667 ft/sec	Hold Form Wing Low Opt No Comp	60/40/0	60/26.815/0	≤ 2 ft Overshoot
3	Hold: 20,000' V=667 ft/sec	Hold Form Wing Low Opt Model Comp	60/40/0	60/26.815/0	≤ 2 ft Overshoot
4	Hold: 20,000' V=667 ft/sec	Hold Form Wing Low Opt Overcomp 10%	60/40/0	60/26.815/0	≤ 2 ft Overshoot

Gain	K_{XP}	K_{XI}	K_{ZP}	K_{ZI}	$K_{\gamma P}$	$K_{\gamma I}$	K_{YP}	K_{YI}
Value	.03	.06	.025	.02	25	20	.05	.02
Gain	$K_{\varphi P}$	$K_{\varphi I}$	K_{VeP}	K_{VeI}	$K_{\beta HG}$	K_{He}	*Yerr Lim*	
Value	3	5	.3	.23	1	100	10	

The first simulation in the set commanded the wing aircraft to move from a position outside the effects of the vortex to the optimum fuel position located in the vortex created by the lead aircraft. In this test, the wing aircraft is allowed to yaw into

the wind, such that the only forces on the wing aircraft are the side-forces that result from the sideslip angle prior to the aircraft reaching the steady state condition. The building roll rate disturbance is also experienced and countered with opposite roll rate. As a worse case response to the increasing sideslip angle, the bare aircraft dynamics of the f-16 as presented in Stevens and Lewis are used in the simulation (18:584-592). The results of simulation 4-1, utilizing the crab option, are presented in Figure 26 below. The first two plots are the induced roll rates and sideslip angles as a result of moving into the vortex field. It can be seen from the plot that all states eventually drive to the desired optimum fuel formation, with no overshoot and a settling time ($\leq$ 1 foot of steady state) of 17.1 seconds. The settling time places us just outside the desired 15 second settling time objective.

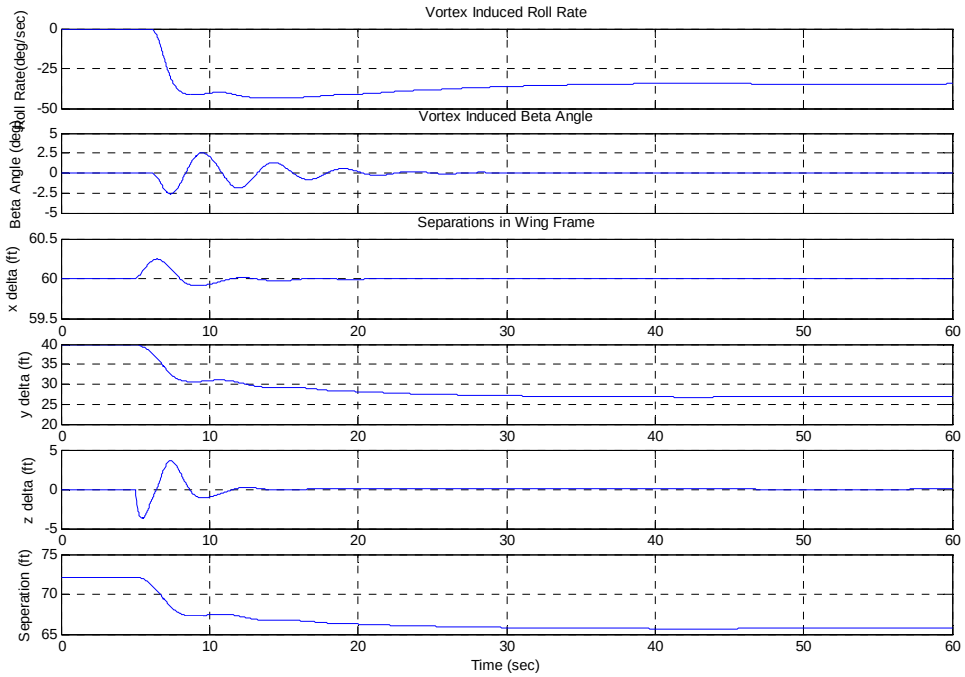

Figure 26. Sim: 4-1 Lateral Move to Optimum Fuel Formation-(Crab Option)

The second simulation in this set was meant to test the performance of the controller using a wing low method to counter the induced yaw moment. To reiterate, we expect a steady state roll and sideslip angle input will be required to counteract the yaw moment. As before, an additional steady state roll rate will also be required to counter the induced roll rate from the vortex. To help isolate the effects of the disturbances, the wing low method was accomplished first with only the induced sideslip effects and then with the induced sideslip and roll rate effects. No steady state roll error compensation was input for either of these runs. In this way the controller was allowed to perform assuming no test information, model, or trimmer function was available to estimate the roll error. The only significant dynamics occurred in the y separation channel. The results of the simulation are presented in Figure 27 below first without the roll rate disturbance so that the effects of the yaw moment disturbance can be clearly seen. The plots include only the disturbances, the wing roll angle and the y separation channel. From the plots it can be seen that there is a steady state roll angle and y separation error of - 0.815 degrees and 3.56 feet respectively. Thus we would be 3.56 feet from the optimum fuel formation position and not receive all of the fuel saving benefits. In addition the error is inward of the optimum position which, according to Wagner (20), places the trail aircraft nearer to significantly stronger rolling moments found inside of the 75% of wingspan position.

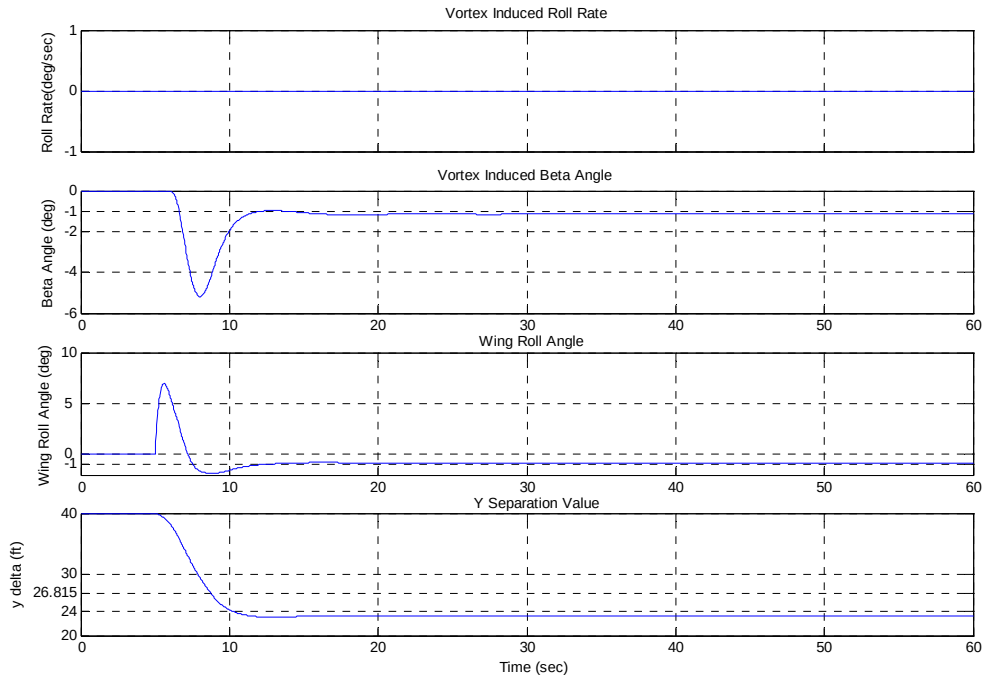

Figure 27. Sim: 4-2 Lateral Move to Opt Fuel Formation (Wing Low Option/No Compensation/No Roll Rate Disturbance)

The next run in Figure 28 below includes both the induced sideslip and the induced roll rate disturbances, but still includes no steady state compensation for roll errors. The results are the same except the damping in the y channel, provided by the sideslip controller, is minimized due to the previously discussed roll angle filter that was applied to the controller. The overall result apparent in Figure 28 below, is a lightly damped y channel. The next simulation used the same wing low option to control position, but this time a model of the expected roll error was applied to compensate for the roll error. In this simulation the controller had perfect knowledge of what the errors were since the simulation was run once to determine what the error would be and then run a second time with the error compensation included.

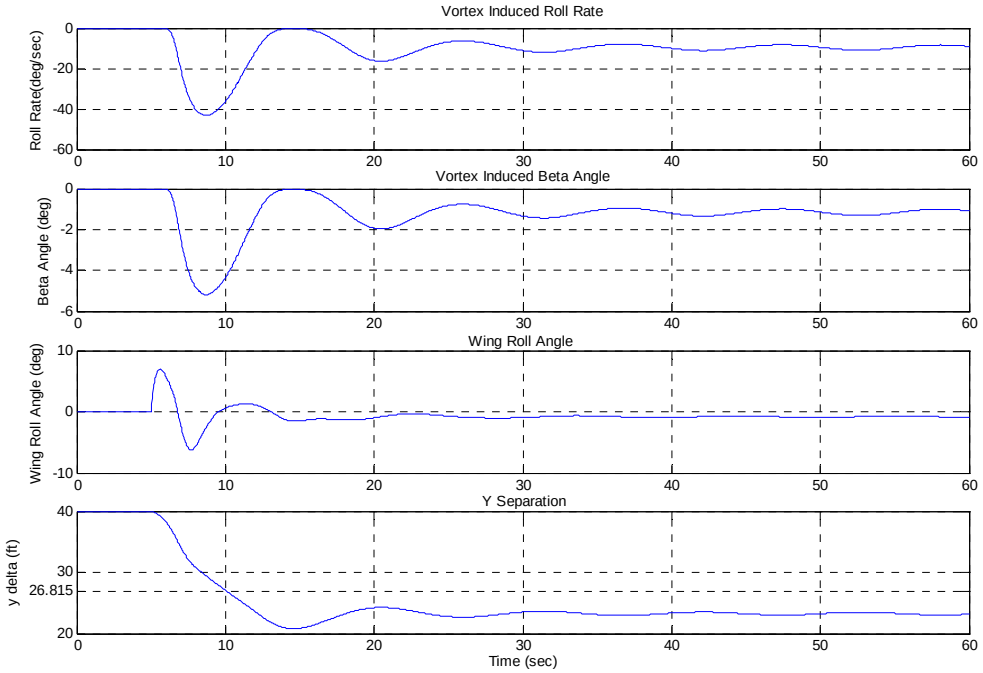

Figure 28. Sim: 4-2 Lateral Move to Opt Fuel Formation (Wing Low Option/No Compensation/With Roll Rate Disturbance)

This second run, with the modeled roll error input into the controller, is presented in Figures 29 and 30 below. Again, they are presented with only the sideslip disturbance first and then with both the sideslip and roll rate disturbances together. It is clear from the plots that modeling the roll error and including it in the system allowed the controller to drive the y separation error to zero, which would allow the aircraft to maintain the optimum fuel position. It is also apparent from the top two plots of Figure 30 that the roll rate and yaw moment are greater now that y separation error is kept closer to the maximum disturbance position of 29.54 feet

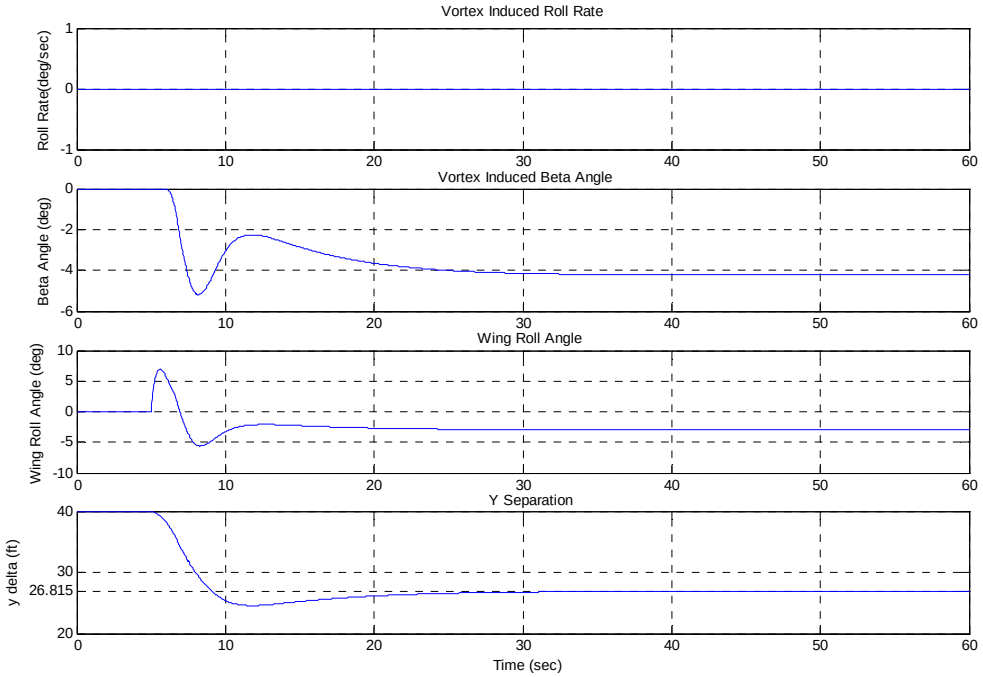

Figure 29. Sim: 4-3 Lateral Move to Optimum Fuel Formation (Wing Low Option/Model Compensated/No Roll Rate Disturbance)

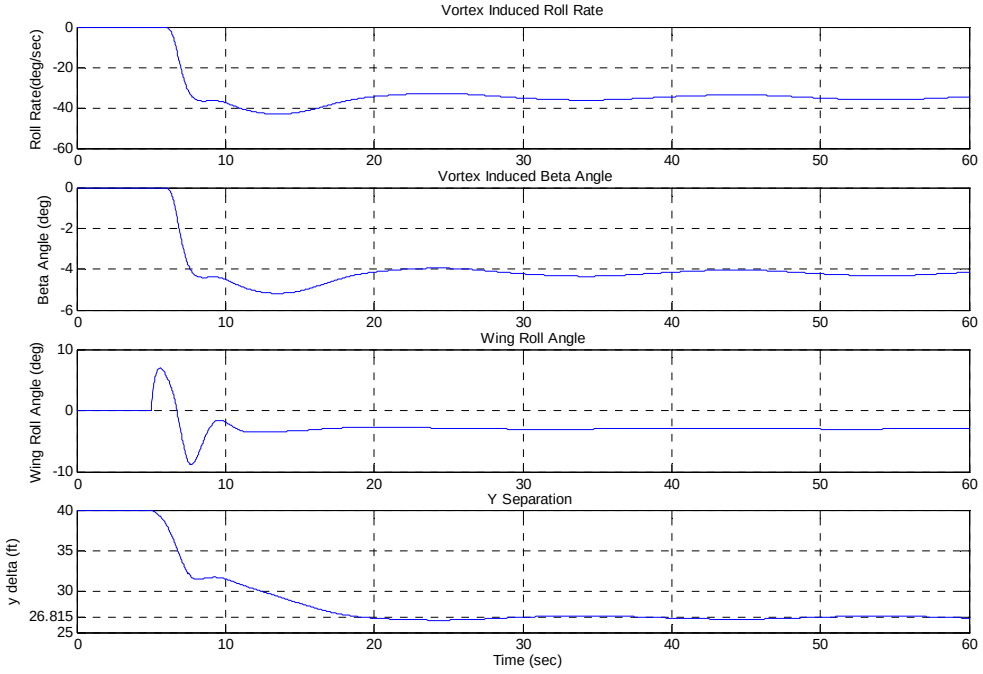

Figure 30. Sim: 4-3 Lateral Move to Optimum Fuel Formation (Wing Low Option/Model Compensated)

With a perfect model, the steady state y separation error was zero. It was simple to simulate the effects of a model being 10% off of the true required roll error compensation. This is accomplished in Figure 31 as the fourth simulation in this set, and clearly shows the y separation settling at a steady state value of 28.36 feet.

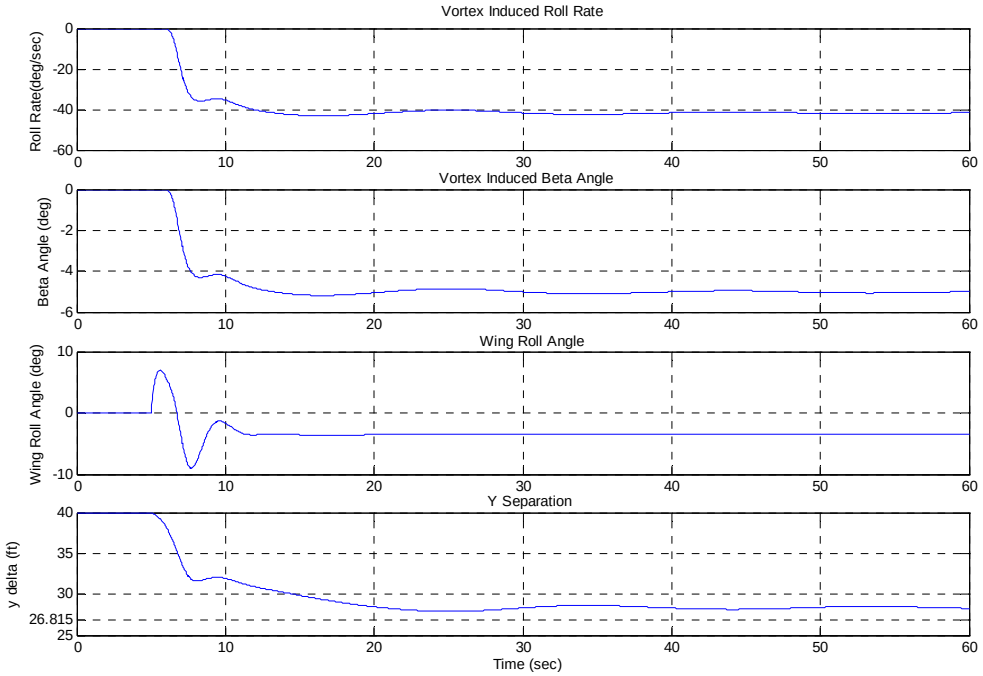

Figure 31. Sim: 4-4 Lateral Move to Optimum Fuel Formation (Wing Low Option/Model Compensated with 10% error)

In this simulation the steady state error from the commanded position of 26.85 feet is 1.55 feet. Thus, the incorrect model that was overcompensating for the roll angle error by 10% yielded a steady state error of 1.55 feet. If the intended purpose of the controller is to maintain a tight formation for fuel savings, this error could significantly decrease the realized fuel savings. Clearly, the precision of the controller will be greatly dependent upon the model or the test data used to generate any roll compensation required. Because of this dependency, and the added drag that will result from the above control inputs to maintain the wing low formation, it is determined that the crab option is the better overall

solution. It will also allow the sideslip control law, which provides extra lateral damping, to be more effective as it will not be reduced by the roll angle filter previously described.

Simulation Set #5

Finally, Simulation Set five was intended to test the overall controller using the gains that were determined to provide the best performance. As detailed in Table 9 below, the set included lead maneuvers while the wing aircraft held the optimum fuel formation position. Each test was accomplished first without the wind and then with the wind disturbances set to varying intensity levels. The set was intended to provide the best prediction of how the controller will perform in the real world. All of the simulations in this set used the crab option to control the aircraft. To ensure good trim values for all of the simulations in set five, the wing aircraft will be started from a position outside the vortex and flown to the optimum fuel formation position. The lead aircraft began the maneuver at twenty seconds simulation time, 15 seconds after the commanded formation change.

Table 9. Simulation Set #5: With Vortex Disturbances

Sim Num	Lead Aircraft Maneuvers	Wing Aircraft Maneuvers	Initial Form (*x/y/z*) ft	Final Form (*x/y/z*) ft	Error Objective	Wind Dist
1	Climb 5,000' Vel=667 ft/s	Hold Form Crab Opt	60/40/0	60/26.8/0	≤ 2 ft Overshoot	Norm
2	Climb 5,000' Vel=667 ft/s	Hold Form Crab Opt	60/40/0	60/26.8/0	≤ 5 ft Overshoot	Thnder Storm
3	Accel 100 ft/s 20,000 ft	Hold Form Crab Opt	60/40/0	60/26.8/0	≤ 2 ft Overshoot	Norm
4	Accel 100 ft/s 20,000 ft	Hold Form Crab Opt	60/40/0	60/26.8/0	≤ 5 ft Overshoot	Thnder Storm
5	360 deg Rt Turn, 20,000 ft	Hold Form Crab Opt	60/40/0	60/26.8/0	≤ 2 ft Overshoot	Norm
6	360 deg Rt Turn 20,000 ft	Hold Form Crab Opt	60/26.8/0	Same	≤ 5 ft Overshoot	Thnder Storm

Gain	K_{XP}	K_{XI}	K_{ZP}	K_{ZI}	$K_{\gamma P}$	$K_{\gamma I}$	K_{YP}	K_{YI}
Value	.03	.06	.025	.02	25	20	.05	.02

Gain	$K_{\varphi P}$	$K_{\varphi I}$	K_{VeP}	K_{VeI}	$K_{\beta HG}$	K_{He}	*Yerr Lim*
Value	3	5	.3	.23	1	100	10

The first simulation in this set was with normal wind and a lead climb maneuver of 5,000 feet. The simulation results are presented in Figure 32 below and indicates acceptable performance.

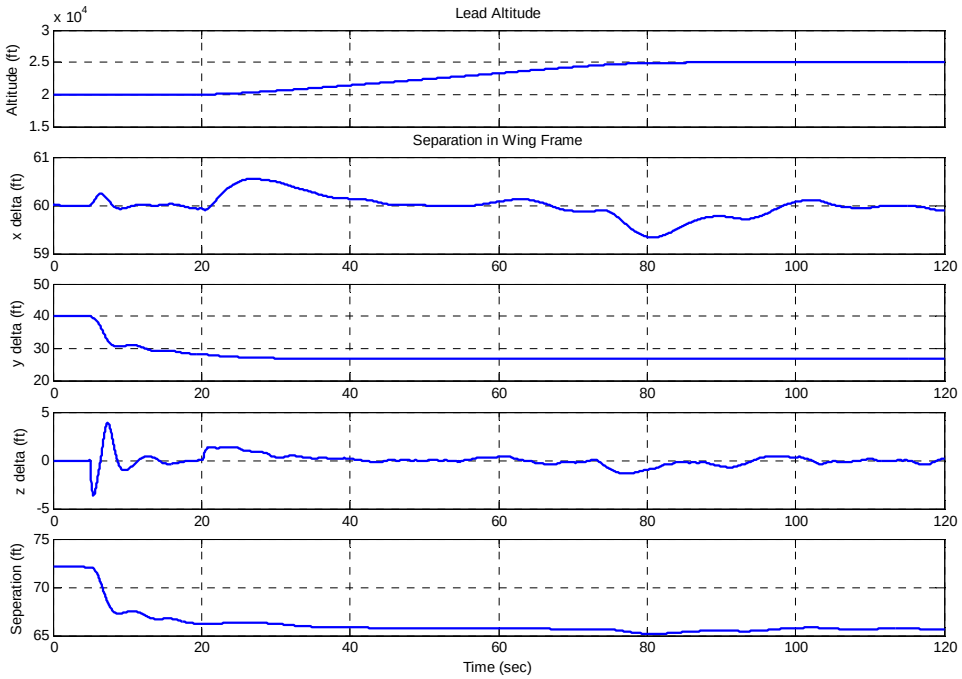

Figure 32. Sim: 5-1 Lead Climb Maneuver (Normal Wind Turbulence)

Next, the lead climb maneuver was again simulated, but with thunderstorm level turbulence. The results are shown in Figure 33 below. The controller's performance was acceptable and within the ≤ 5 foot error tolerance.

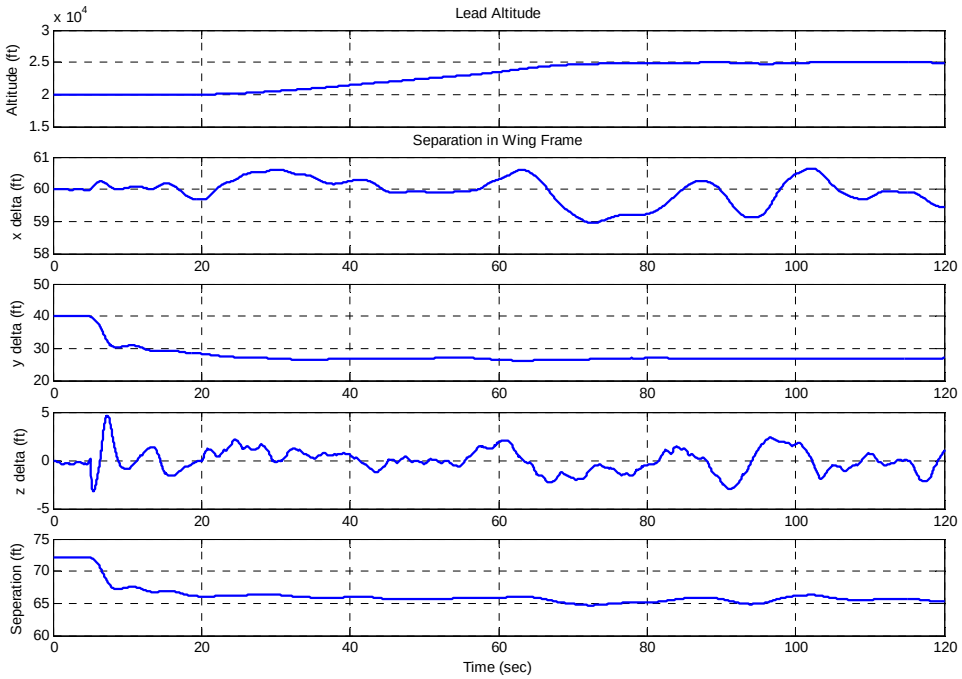

Figure 33. Sim: 5-2 Lead Climb Maneuver (Thunderstorm Wind Turbulence)

The next simulations were an airspeed change from lead at normal and thunderstorm level wind turbulence. The controller showed acceptable performance and the simulations are presented in Figures 34 and 35 below.

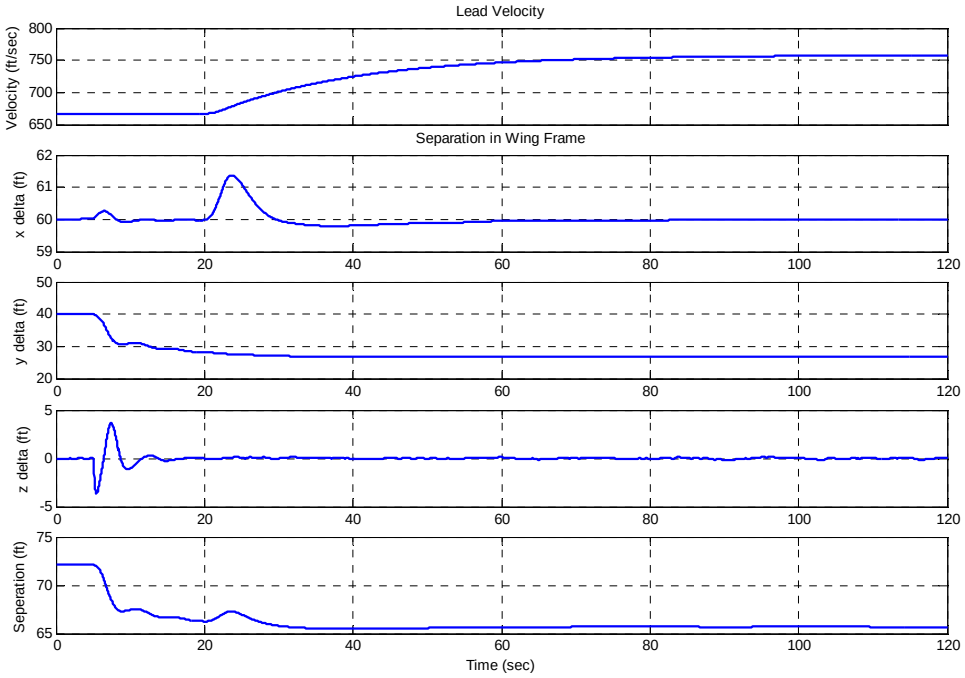

Figure 34. Sim: 5-3 Lead Acceleration Maneuver (Normal Wind Turbulence)

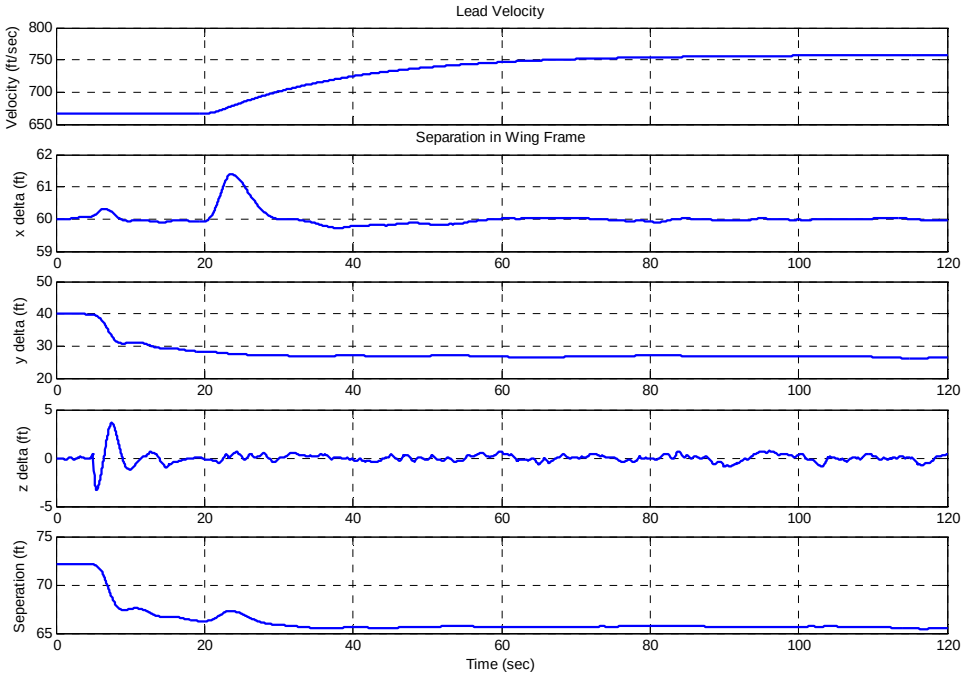

Figure 35. Sim: 5-4 Lead Acceleration Maneuver (Thunderstorm Turbulence)

Finally, the last two simulations included 360 degree right turn-away maneuvers from lead. The maneuvers were conducted at 30 seconds simulation time, 25 seconds after the lateral formation change command, to ensure the dynamics of the position change had a chance to settle. The results of the simulations are shown in Figures 36 and 37 below. As before, the controller's performance did not meet the ≤ 2 foot error during the roll in maneuver, although it is not easily seen in the plots to follow because of the additional noise added as a result of the wind turbulence. The controller did not meet the thunderstorm performance objective of ≤ 5 feet error since the roll-in error during the maneuver was approximately 5.8 feet.

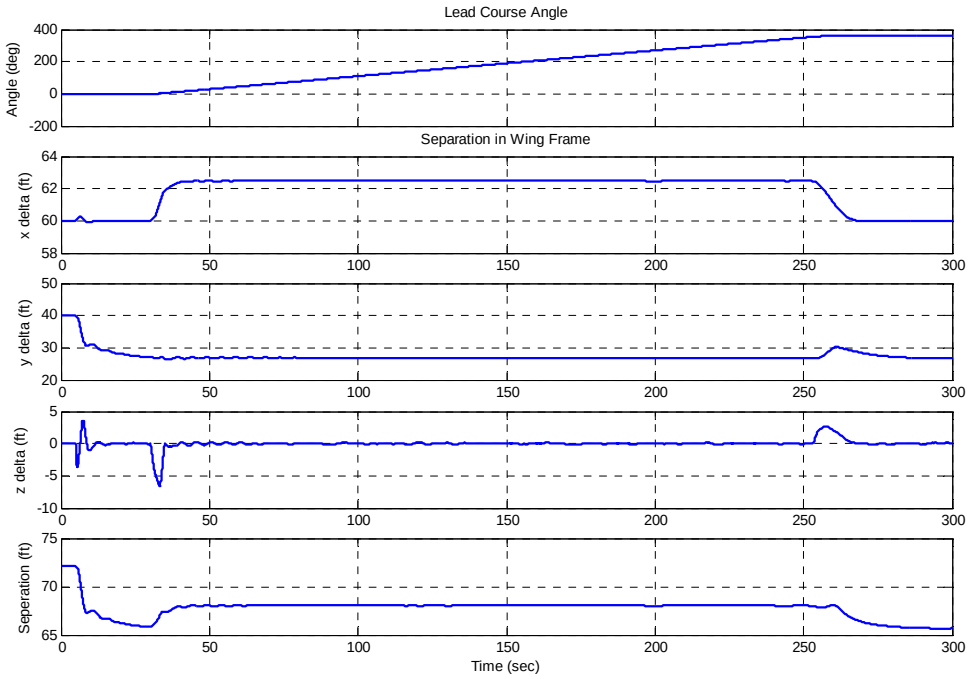

Figure 36. Sim: 5-5 Lead 360 degree Right Turn Away (Normal Turbulence)

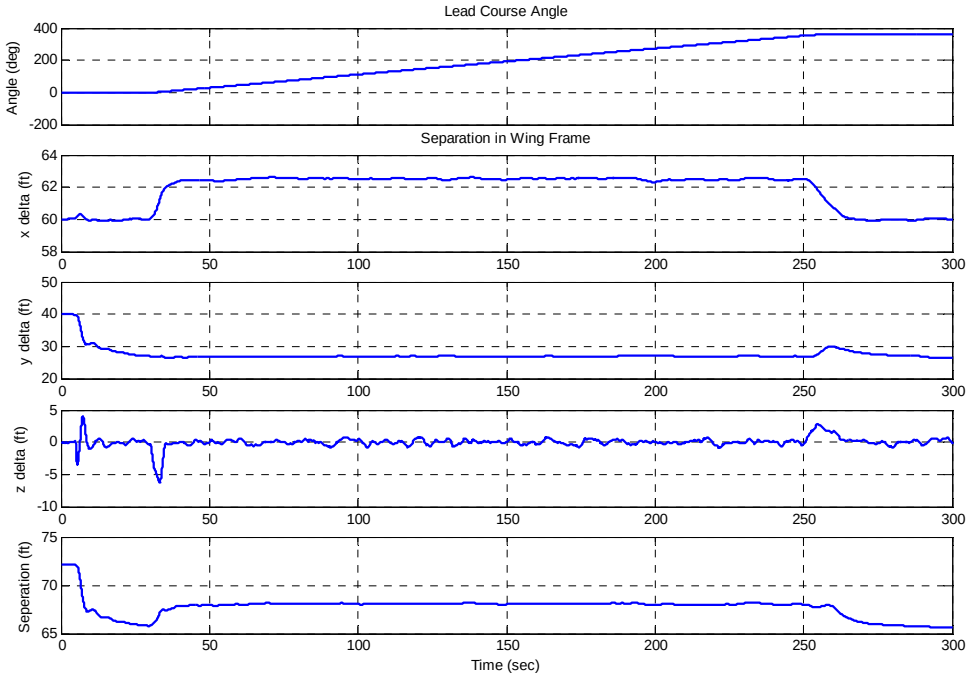

Figure 37. Sim: 5-6 Lead Right Turn Away (Thunderstorm Wind Turbulence)

Conclusions

In conclusion, there is always a trade off to be made when deciding what gains to use when multiple tasks are to be performed. Most of the maneuvers easily met the desired performance objectives. The only failure was the lateral error during the lead 360 degree maneuver. It was mentioned that a set of gains, given in Table 3, were developed that gave an error of approximately one foot, but showed severe instability when a step of more than three feet was commanded. It is the author's conclusion that the additional stability provided by the relaxed lateral gains more than offsets the 4 feet of extra error as a result. This is especially true when considering the effect of turbulence at wide formation distances. A small disturbance in the angles could easily cause instability due to the large moment arm of the system. Other lessons that were learned included the need for velocity error integral control action and the roll angle filter placed on the sideslip control law. It was an objective of simulation set four to determine the best

option when trying to counter the lead induced vortex forces. Because of the complexity of the control and the drag increase as a result of the additional control inputs, the best choice to control the sideslip condition was determined to be the crab option. This concludes the theory and simulation portion of the thesis. The application and in-flight testing of the controller follows in subsequent chapters.

VI. Flight Testing

Flight testing of the control system was conducted at the USAF Test Pilot School. Five test sorties were flown from 25 to 27 October 2004 for a total of 8.0 flight test hours. All test missions operated out of Edwards AFB, CA within the Air Force Flight Test Center's (AFFTC) open-air range in Restricted Area R-2508. Details of this testing are presented in AFFTC Technical Information Memorandum (TIM) 04-08 (14). This chapter initially details the test configuration and setup. The modifications required to test the controller are then given. Next, the procedures used and the maneuvers flown during flight test are briefly presented. Finally, any testing issues that were encountered and how they were overcome, or their impact on the results, are explained.

Test Configuration

The test setup consisted of the control algorithm loaded on the NF-16D VISTA and a virtual lead aircraft transmitted to the VISTA from a ground station running D-Six simulation software (2). The NF-16D VISTA(USAF S/N 86-0048) aircraft is a modified F-16D Block 30 Peace Marble II (Israeli version) aircraft with a Digital Flight Control System (DFLCS) using Block 40 avionics and powered by the F110-GE-100 engine. The on board variable stability system (VSS) computers hosted the flight control laws, allowing the VISTA to generate closed-loop inputs to the flight control system, based on controller commands. VISTA had the capability to change selected flight control gains during the course of a flight, but was used only once to troubleshoot an in-flight controller error. The VSS also included built-in test functions, Vehicle Integrity Monitor

(VIM) and disengagement logic, disengagement reporting, and manual disengagement capability (5). The virtual lead aircraft was a nonlinear, six-degree-of-freedom model simulated by D-Six simulation software using USAF Innovative Control Effector (ICE) UAV dynamics (6). Although another F-16 was initially planned as the lead aircraft, budget and time constraints made utilization of a previously developed model, the ICE UAV, necessary for testing. The most significant issue that arose from the lead aircraft change was the relative inconsistency of maneuvering capability between the lead and wing aircraft. The ICE UAV is a stealthy, tail-less design and thus had different flying characteristics when compared to the VISTA aircraft. Virtual lead aircraft data were calculated by the D-Six simulation software program running on a computer in USAF TPS Control Room A. This signal was output via cable to a situational awareness data link (SADL) system for remote broadcast to the VISTA aircraft flying in the test airspace. In addition, to aid pilot situational awareness during test initialization and execution, the current position of the virtual lead aircraft relative to the current position of the VISTA aircraft was displayed in (x, y, z) format on the VISTA heads up display (HUD).

Controller Modifications For Flight Test

The first task was to produce another Simulink® model that included a General Dynamics Advanced Information Systems (GD-AIS) provided model of the VISTA aircraft to replace the generic F-16 model utilized previously. This new model was used for ground simulation of the flight test setup and provided an opportunity to implement and ground test the controller changes that are presented below. Several modifications

to the controller logic were required for implementation. The following changes were made because of time and resource limitations and not because of control issues. The changes resulted in a reduction in controller precision, but were required if any testing was to be accomplished. Modifications to the controller occurred in three main areas. They included changes to the state information, removing the beta control, and implementing changes to the x channel and y channel control laws to accommodate VISTA control parameter requirements.

State Changes.

Implementing the controller on the VISTA aircraft required the use of aircraft positional information generated from the onboard inertial navigation system (INS) and global positioning system (GPS). The rest of the state information for the VISTA was generated from on board sensors. The state vector presented previously required the velocity vector roll angle be matched for both the lead and wing aircraft. This was acceptable during simulation as the velocity vector roll angle could be easily calculated or commanded in the wing case. In the real world determining a velocity vector roll angle depends upon several measured angles and several coordinate transformations. The result of these calculations was not expected to be precise enough for flight test. In addition the D-Six aircraft simulation program that was providing the virtual lead aircraft did not provide velocity vector roll angle information. Time and budget constraints did not allow the modification required to add the necessary aircraft states to calculate the velocity vector roll angle. Therefore, it was decided that the body to inertial axes roll angle, phi, would instead be used for both of the aircraft. For most straight and level flight situations the change would have minimal effect since the lead aircraft, and

consequently the VISTA aircraft, would be striving for a zero roll value. The main effect would be observed during turning flight. The differences in aircraft turn rates for a given bank angle would cause a positional error even if the roll axis angles were matched. Because the ICE UAV had no tail, it tended to skid through turns and yield a lower turn rate when compared to the VISTA aircraft. Since testing was not going to include continuous turns, only 30 degree heading changes, the change to body roll angle versus velocity vector roll angle, and the errors that would be generated during turning flight, were accepted.

Removing Beta Control.

The beta control law was not able to be implemented due to time and budget constraints. It would have required GD-AIS to perform a significant amount of work to the current lateral control channel of the VISTA aircraft. The test budget would not allow this control feature in addition to the other three main control parameters. It was determined through previous simulations presented above that not including the beta control would reduce the damping of the lateral channel, but would not affect lateral stability. The change was then accepted despite the decreased damping and overall decreased performance of the controller.

Changes to Control Laws.

A significant change to the control laws also came about as a result of time and budget constraints. Previous test programs had utilized the VISTA for the purposes of formation flight and control logic for these programs had been developed. Previous programs had developed velocity command and roll angle command systems and had proven them in flight test. In the interest of time and cost, velocity control instead of

thrust control and roll angle control instead of roll rate control were implemented. Both of these differences, in simulation, resulted in a slower responding controller. The change to these control parameters required a reworking of the control laws in the x and y channels. The new control vector now became

$$Controlvec_{VISTA} = [Vel_V, \alpha_V, \phi_V]^T \tag{68}$$

which included velocity, angle of attack, and bank angle. The error vector remained unchanged and is repeated here:

$$Errorvec = [x_e, y_e, z_e, V_e, \phi_e, \gamma_e]^T \tag{62}$$

For the x channel, the change to velocity command instead of thrust command required that the desired lead velocity be included as the base velocity to continually strive towards. Proportional and integral control was still included on the velocity error. With the lead baseline velocity included, the x channel or velocity control law became

$$\Delta Vel_V = (Vel_L - Vel_{oV}) + K_{XP}x_e + K_{XI}\int x_e + K_{VP}V_e + K_{VI}\int V_e \tag{69}$$

where Vel_L is the lead velocity and Vel_{oV} is initial velocity of VISTA when the controller is engaged. This change was not expected to affect the performance of the controller significantly except to add a slight amount of time delay, since the control parameter now matched the error parameter exactly. In this way, a velocity correction is now fixing a velocity error. It was also related from GD-AIS that the VISTA velocity control law was a simple proportional feedback system, such that the dynamic effects of the change would be minimal.

Similar changes were required in the y channel control law, but the effects of these changes would be much more significant. The lateral control law was changed to

command bank angle and included leads bank angle as the angle to strive towards. Proportional and integral control was placed on the bank angle error and was kept on the y separation error as before. The lateral or bank angle control law became

$$\Delta\phi_V = (\phi_L - \phi_{oV}) + K_{YP} y_e + K_{YI} \int y_e + K_{\phi P} \phi_{Ve} + K_{\phi I} \int \phi_{Ve} \tag{70}$$

where ϕ_L is the lead bank angle and ϕ_{oV} is the VISTA bank angle when the controller is initiated. The expected results of the bank angle control parameter change were more significant primarily because the dynamics of the bank command feedback system were second order in nature and showed significant time delay. The damping of the lateral channel had already been reduced by the removal of the beta control and was expect to worsen with inclusion of bank angle control. In simulation, the controller was found to be stable, but showed significant overshoots and long settling times, well beyond the desired initial objectives of the controller. Again, time and budget constraints necessitated the use of this type of control. The angle of attack control law remained unchanged and is repeated here:

$$\Delta\alpha_V = K_{ZP} z_e + K_{ZI} \int z_e + K_{\gamma P} \gamma_e + K_{\gamma I} \int \gamma_e \tag{65}$$

After the final form of the controller had been developed and simulated, a final "flight ready" version was required. This version was simply the controller rewritten such that controller input and output requirements were matched to VISTA input and output requirements and removed the aircraft and environmental models. This model also required that limits be placed on all of the calculated errors so that stability could be maintained regardless of data dropouts or corrupted information. Limits placed on the values of x, y, and z errors were ±10, ±20, and ±20 feet respectively. The final

Simulink® model was loaded into the VISTA aircraft's onboard memory for flight testing and represented a general rearranging of the controller presented in Figure 38 below.

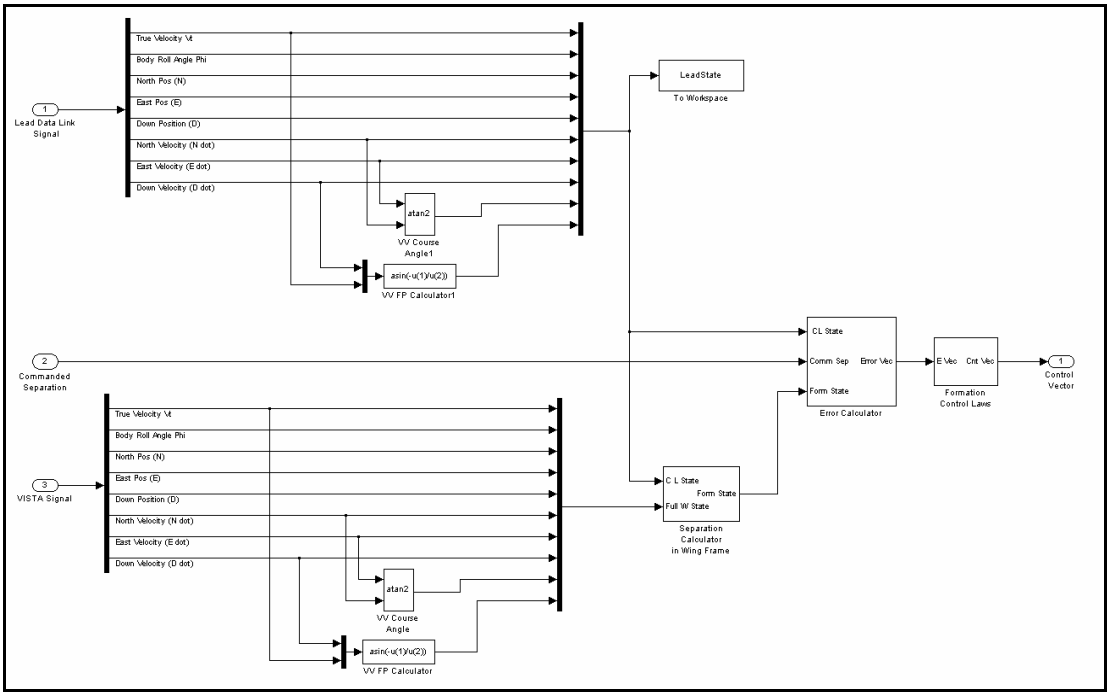

Figure 38. Final Controller Simulink® Model

Test Setup

The two SADL systems, one located adjacent to the ground station in the control room and one in the spine of the VISTA aircraft, each sent and received the same message format for their respective aircraft. The message was recorded at each end of the link and then the required information was pulled from the signal at each end of the link depending upon what information was required. The signal was transmitted at a rate of 30 Hertz. In addition to the internal data recording accomplished by D-Six and VISTA onboard computers, the control room telemetry station was configured to receive and record VISTA aircraft information on a separate telemetry signal. Figure 39 below illustrates the test setup.

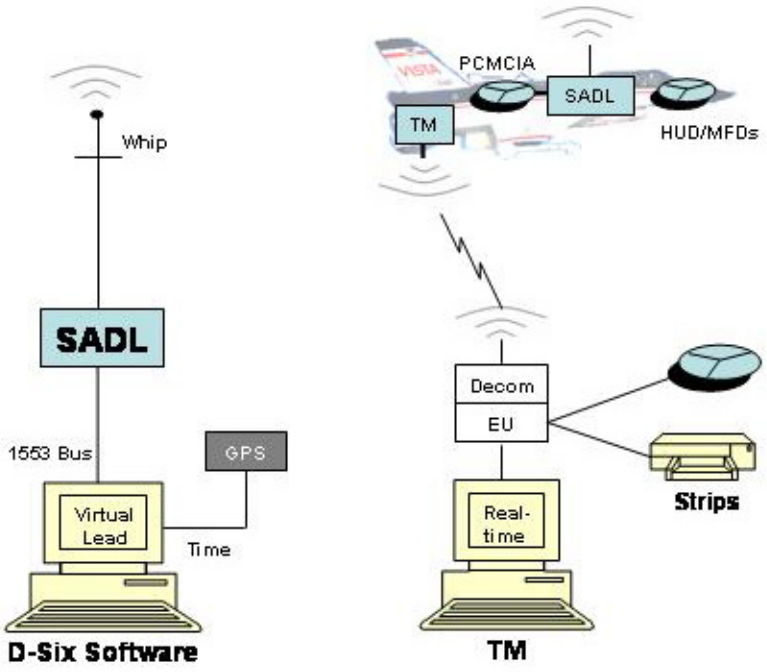

Figure 39. Solo Form TM Room Setup

After decoding the SADL signal, the following set of information was available:

$$SADLEVEC = \begin{bmatrix} GPS\_Time \\ A/C\_Num \\ LAT\_1st \\ LAT\_2nd \\ LON\_1st \\ LON\_2nd \\ Altitude \\ North\_Vel \\ East\_Vel \\ Down\_Vel \\ AOA \\ Beta \\ Roll\_Angle \\ Roll\_Rate \end{bmatrix} \tag{71}$$

The latitudes and longitudes for each aircraft were decoded and calculated as North, East, and Down positions utilizing the same position algorithm, resident on both the VISTA and D-Six computers. The ground station required the VISTA positional information so that it could initialize the virtual lead in a position, relative to the VISTA aircraft, that was commanded by the ground station operator. This would allow the two aircraft to be relatively close to the commanded formation position when the lead aircraft's position was transmitted. Once the VISTA was receiving a virtual lead aircraft, onboard software developed by GD-AIS would calculate the inertial reference frame (NED) positions and velocities of the virtual and VISTA aircraft and provide these values, along with the body roll angles, to the controller. These values were then taken by the controller and converted to errors in the pseudo-wind axis reference frame previously discussed, and the controller would begin generating the required commands

to maintain formation. Whether the VISTA aircraft was allowed to follow the generated commands was selectable by the crew, which aided in successful and timely engagements of the automatic formation hold.

Test Procedures

The flight test was controlled from Test Pilot School (TPS) Control Room A. The procedures used to test the controller were primarily based on the need to maintain a good data link. This meant that all of the maneuvers had to be accomplished within approximately 20 nautical miles from the ground station and generally required a heading directly away from the station as antenna reception was better from the rear of the VISTA aircraft. In addition it was found that the test aircraft was required to be on a specific heading if aircraft velocity errors, explained in detail in the Testing Issues section below, were to be minimized. Prior to commencing each test point, the VISTA was allowed to stabilize in level, un-accelerated flight on a heading that minimized the headwind component of the winds aloft. Whenever the data link was good, the VISTA aircraft was constantly providing its position to the ground station. The nominal flight condition for all of the testing was 20,000 feet pressure altitude and 667 feet per second ground speed (396 knots true airspeed in still air) with gear up, exactly as simulated. When the data link was confirmed acceptable by the control room, the ground station operator would command a virtual lead to be transmitted. The initial position and heading of the virtual lead would be based on the current VISTA coordinates and the desired offset position that was input by the ground station operator. Once the virtual lead was received by the VISTA it was presented to the aircrew on the HUD. It was then possible for the aircrew

to fine tune the formation without the controller engaged, using the HUD displayed positional values as shown in Figure 40 below.

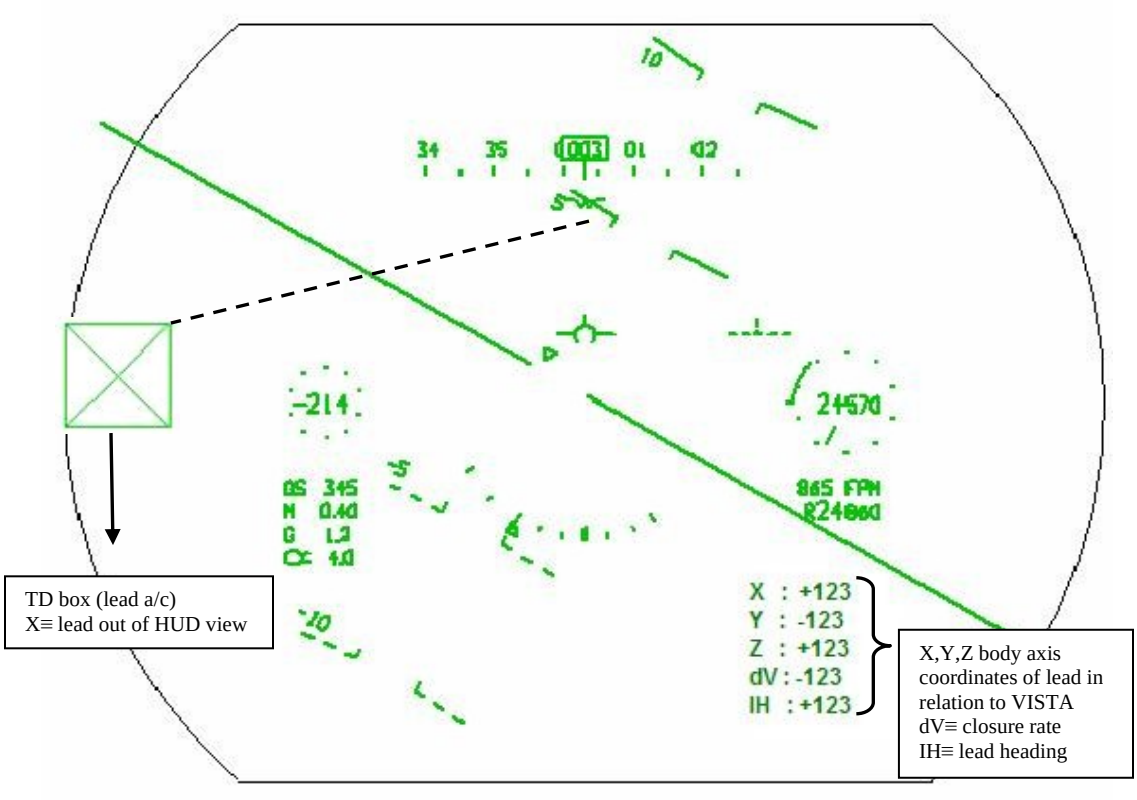

Figure 40. VISTA HUD Test Setup

It was soon found, during the course of testing, that the lateral and vertical channels could correct themselves faster than the aircrew could correct any errors, but the fore and aft channel was slow to correct. To minimize engagement time the aircrew would allow the controller to make lateral and vertical corrections to position, but kept the throttle disengaged. The crew would then hand-fly the fore-aft position with the throttle, until in the commanded position. The throttle control would finally be engaged and the controller was then allowed to operate hands off. Once on full automatic control the ground station would command a lead maneuver, or the aircrew would command a

position change via the VISTA's data entry display (DED) interface. After the maneuver or position change was completed, the test crew would move on to another maneuver or position change from the current formation without the need to re-engage the controller. Data for each test run were collected both on the ground for the virtual lead aircraft and onboard the VISTA for all of the input and control parameters as well as some parameters internal to the controller itself.

Test Maneuvers Flown

The maneuvers flown were broken up into three main categories. The first category was lead maneuvers while the VISTA aircraft was commanded to hold a given formation. The second category was lead holds straight and level, un-accelerated flight, while VISTA is commanded to different formation positions. The final category of maneuvers included complex combinations of the above maneuvers. Several issues presented in the Testing Issues section below decreased the number of runs that could be accomplished during each sortie and limited the available heading change maneuvers that could be accomplished. Due to these constraints the test team decided to limit the number of complex maneuvers that were accomplished in favor of gathering more data for the basic lead maneuvers and formation changes. The complex maneuvers that were accomplished included combination lead maneuvers, such as an acceleration, climb, and heading change while VISTA held a commanded position. The combination runs not accomplished included those where VISTA changed formation while the lead aircraft was maneuvering.

Testing Issues

The first issue that did not impact testing of the controller but did impact controller performance was the inability to accomplish final tuning of the controller because of time and budget constraints. Verifying proper installation of the controller utilized all of the installation time and dollar resources of the project and did not allow the final tuning that was desired. The controller was found to be stable and predictable with the gains selected based upon pre-flight simulations, but did not represent the best possible results that could be attained by fine tuning the controller with flight test results. The iterative process of fly, simulate, adjust gains, and fly again was not allowed by the testing timeline. Given the changes to the lateral control laws, this channel would have seen the most benefit from gain tuning.

The next large testing issue was the fact that the virtual ICE model could generate a rate of deceleration much greater than the actual VISTA aircraft could generate. Thus, the VISTA aircraft would overrun the virtual lead during any lead deceleration maneuvers. Despite the controller commanding idle from the throttle, it would be unable to maintain the formation position and the VISTA aircraft would drift forward until the deceleration was complete. It was found that the VISTA's speed brake could be used to increase the rate of deceleration, such that it was greater than the ICE model's deceleration. In fact, with the speed brake extended by the crew, the controller was able to command the required deceleration rate and maintain the desired formation. Despite this capability, and because the effects of the speed brake were not fully known, the test team elected to consider all deceleration data corrupt and therefore was not included in

the test report. The issue highlights the previously mentioned fact that the lead and trail aircraft must be of similar performance levels, and the wing aircraft must always have a control power advantage in every channel if successful tight formation control is to be accomplished. Lead acceleration maneuvers did not have these errors and were considered good data.

The third testing issue was the data link. In addition to the previously discussed heading dependency, it also experienced frequent data dropouts. This reduced the amount of data that could be collected on each sortie. These dropouts were smoothed by a filter onboard the VISTA aircraft, but represented a significant source of error that the controller was required to reduce. A typical data link dropout is highlighted below in Chapter VII, Flight Test Results and Analysis. These data link dropouts made analysis of the controller performance difficult. It is clear that a more robust data link would reduce position keeping errors and result in better overall system performance. The effects of this issue were minimized through proper test setup on a good heading and recognizing the onset of data dropouts from spikes in the HUD displayed positions. Despite the team's best efforts, airspace constraints and extended ranges from the ground station would often force the test team to move on to the next test point or terminate the run without letting the dynamics of the aircraft fully settle.

The last, and most significant issue that developed during flight testing, was the introduction of error into the VISTA velocities as a function of heading. Prior to flight test, it was determined that the virtual lead aircraft, operating in a windless environment, would not experience the same conditions as the VISTA aircraft as it operated in the real airspace. To solve this problem, inertial positions and velocities for the VISTA aircraft

were given to the controller. In this way the motion of both aircraft would be presented in the same inertial reference system and the controller would not see the aloft winds, only a set of inertial velocity vectors. The problem that was discovered during flight test was that the state information was not always correlated even when using the inertial positions and velocities described above. A correlated state vector would have the integrated velocity values exactly match the position values of the state vector at each time step. It was found that the state vector did not exactly correlate and errors in velocity would be introduced to the system as a function of the heading of the aircraft in relation to the direction of the winds aloft. If the VISTA aircraft was commanded to a heading where the winds aloft were in direct crosswind, the state vector would be well correlated. If any component of the winds aloft were a headwind, then the state vector would be uncorrelated with the inertial velocity being faster than the actual ground track. A tailwind component would yield the opposite effect. The difficulty this presents to the controller can be clearly illustrated when the velocity control law is examined. The law is based on the assumption that matched inertial airspeeds will yield no relative velocity between the two aircraft and thus no change in the x separation. If the wing inertial velocity is in error, the matched airspeeds will generate no velocity corrections and yet the controlled aircraft will drift out of position. The position error portion of the control law will try to correct the drift as it grows, but the overall effect will be, at best, a steady state position error or, in the worse case, an unstoppable drift. This issue limited the amount and type of data that were collected; any time the aircraft was commanded more than twenty degrees off of the direct crosswind heading, the VISTA aircraft would begin a drift either forward or aft of the commanded position. If a real lead aircraft had been in

the formation, this problem would have created a safety issue and flight testing would have likely been stopped until the source of the x-channel drift had been found. A simulation of this problem and some proposed solutions are presented in the analysis portion of Chapter VII below.

VII. Flight Test Results and Analysis

This chapter initially presents the flight test results as a summary of the controller performance for each of the two maneuver types, lead maneuvers and formation changes. Since the complex maneuvers only include combination lead maneuvers they will be presented in the lead maneuvers section. After detailing the results, an analysis of the controller performance for the maneuver type will be made in each section. A summary of each channel's characteristic response, followed by an analysis of the issues that arose during flight test are presented next. Finally, conclusions and suggestions for future controller development and testing are presented. A standard formation position was defined to help identify the aircraft location as maneuvers were accomplished. Presented in Figure 41 below, the standard position was defined as 30 feet aft of lead (+30 feet x axis), 30 feet to the left of lead (+30 in y axis), and level with lead vertically (0 feet z axis). All separations are represented in the VISTA aircraft's reference frame.

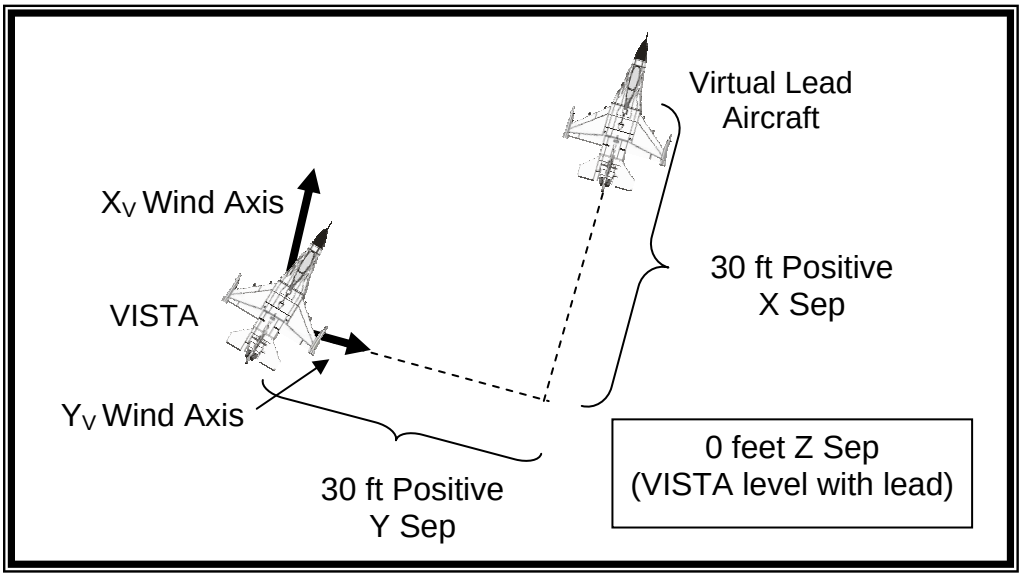

Figure 41. Test Standard Formation Position (30, 30, 0)

All lead maneuvering was accomplished while the VISTA aircraft held in the standard position. In addition, all formation change maneuvers were begun from, or finished at, the standard position. To help clarify the source of any plots subsequently presented, all actual flight test time history plots, taken directly from the flight test report AFFTC-TIM-04-08 (14), will be presented only in Appendix A. Simulation plots used for post flight analysis will be presented in the text. For the flight test time history plots in Appendix A, each figure is labeled as a) through c) showing the lead and wing aircraft states on the same plot so that the maneuver start and stop points can be identified. Plots d) through f) display the x, y, and z channel separations. Finally, the g) labeled plot depicts the total separation of the two aircraft.

Lead Maneuvers

Basic lead maneuvers will be presented first and include lead accelerations of 50 knots, lead climbs and descents of 100 feet, and finally lead turns of 30 degrees heading change both into and away from the VISTA aircraft. The lead deceleration maneuvers will not be presented due to the deceleration rate mismatch previously discussed.

Lead Acceleration.

With the VISTA aircraft in standard formation the lead aircraft was commanded to accelerate 50 knots at a rate of approximately 1.5 knots/second. Two acceleration maneuvers were accomplished with good data and are presented in Figures 57 and 58 in Appendix A. A time delay of less than 1 second is noted as the maneuver is begun. During the acceleration, steady state offsets of approximately 10 feet and 5 feet are realized in the vertical and fore-aft directions respectively. The maneuver is terminated

shortly after the lead aircraft reaches the new final velocity and it is not apparent whether the steady state errors during acceleration would have settled to zero upon the lead aircraft reaching a final airspeed. A data dropout is apparent in Figure 57 as a large hump in the x channel separation at approximately 27 seconds. The rounded nature of the x channel separation immediately following the data dropout is due to the position smoothing algorithm on board the VISTA aircraft. This effectively prevented the data drop-out from being input to the controller as a step, and reduced the possibility of instability.

Lead Climbs and Descents.

With the VISTA aircraft holding in the standard formation, the lead aircraft was commanded to increase altitude by 100 feet with a rate of approximately 6 feet per second. The climbing and descending maneuvers that were accomplished are presented in Appendix A, Figures 49 through 53 and Figures 54 through 56 respectively. The descents had the same formation setup but decreased in altitude 100 feet with a rate of approximately 5 feet per second. Again a slight delay of less than one second was noted as the climb or descent maneuver began. The z-separation error, as a result of this delay, was approximately 10 feet when the leader was increasing g loading to either start a climb or level off from a dive. The error grew to approximately 5 feet when the leader was reducing the g loading to either start a descent or level off from a climb. It was not possible to determine a steady state condition during the climb or descent, as the lead aircraft would begin the level off prior to allowing the dynamics to settle. It was apparent during the climb that enough control authority was available in the vertical direction

since the VISTA aircraft would overshoot lead's altitude by 10 to 15 feet and be in the process of matching leads rate of climb when the level-off would occur.

Lead Turns.

The VISTA aircraft was commanded to hold the standard formation position while the lead aircraft performed turning maneuvers of 10, 20, or 30 degrees heading change. In all cases the lead aircraft would be able to bank up to a maximum of 30 degrees to accomplish the turns. Because of the reduced damping of the lateral channel, and the resulting long settling time, often times there was not enough airspace to conduct the initialization, perform the turning maneuvers, and allow the aircraft to settle fully after the maneuver. The turning maneuvers presented extra difficulty since the above mentioned velocity errors would increase beyond the controller's ability to compensate for them whenever a turn greater than 20 degrees off of the direct crosswind heading was conducted. Depending upon which direction the turn was accomplished the VISTA aircraft would begin to drift forward or aft, until a turn back to the direct crosswind heading was accomplished. If the test team allowed the aircraft to proceed on a heading that was not the direct crosswind heading long enough for the lateral channel to settle, the VISTA aircraft would have drifted forward or aft to the point where acquiring valid data in any channel was questionable. All of the turning maneuver runs are presented in Appendix A, Figures 59 through 67, but a specific multiple turn maneuver run is presented in Figure 66 that displays the standard result. It is apparent from the plot that the controller is commanding the VISTA aircraft back to the commanded position until the above mentioned velocity errors occur. The direct crosswind heading was determined to be -5 degrees and was being flown at the start of the maneuver. At 150 seconds into

the run, the lead heading has been commanded to -28 degrees and the VISTA aircraft followed and began to drift forward in position. At 240 seconds into the run the heading of the lead aircraft has been commanded in the opposite direction and the VISTA aircraft followed the lead to a heading angle of 28 degrees. Now the x channel of the VISTA aircraft begins a slow drift aft from the commanded position. The velocity error that is being introduced is apparent in the velocity traces for the lead and VISTA aircraft on plot a) of Figure 66. It is apparent that the velocity error increases as the heading changes are made off of the direct crosswind heading. A sign change in the velocity error is also apparent as the VISTA heading reversed to the opposite direction. The smooth drifting of the x channel forward and aft when off the direct crosswind heading is only disturbed by the three data dropouts that are apparent on the x channel plot at times 145, 160, and 225 seconds.

Because of the axes setup of the control system, the rolling motion during the turns caused a swapping of y separation for z separation. The lateral motion of the VISTA aircraft was thus characterized by multiple disturbances and a low frequency damping cycle as the different turns were accomplished by lead. The vertical or z channel saw similar induced disturbances due to the axes setup of the control system, but yielded the best performance of all three channels. The disturbances in the z direction are quickly settled to the commanded position with a maximum of one overshoot or less depending upon the magnitude of the disturbance.

Combination Maneuvers.

All lead combination maneuvers were conducted while the VISTA aircraft was commanded to the standard position. All combination maneuvers are presented in

Appendix A, Figures 68 through 78. In general, the same VISTA aircraft responses that were observed during the individual maneuvers were observed in the combination maneuvers, with little apparent coupling. There were no observed instabilities due to the greater amount of maneuvering and the motions in each channel could be directly related to the maneuver that was being accomplished. One interesting result that was observed during the two lead climbs 100 feet and accelerates 50 knots maneuvers, presented in Appendix A, Figures 68 and 69, was that the y channel did not settle to the commanded position. In fact the two same maneuver runs conducted on two different days yielded y channel offsets observed at 5 and 12 feet, but on different sides of the commanded 30 foot position. This occurred despite the fact that the heading angle differences, accounting for the winds aloft, were in the same direction. This offset condition is explored in the analysis portion later in this chapter. Overall, the combination maneuvers displayed an average error of approximately 25-30 feet in the y and z channels. Much of this error was due to the swapping of y- and z-channel separations as rolling corrections were accomplished. The x channel maintained tight control, usually less than 10 feet of error until velocity errors, 3 feet per sec for the 30 degree heading changes, would cause fore or aft drifting.

Formation Change Maneuvers

This section details the results of the formation change maneuvers that were accomplished while the virtual lead aircraft maintained straight, level, and un-accelerated flight. The formation changes included forward and aft, lateral, and vertical position changes out of and back to the standard formation position. The dynamic parameters for

position changes observed during flight test are summarized in Table 11 found in the Summary of Flight Test Results section that follows.

Fore and Aft Position Changes.

Plots of the flight test results for the 30 foot forward and aft position changes are presented in Appendix A, Figures 86 through 89. The 60 foot forward and aft position changes are presented in Appendix A, Figures 94 and 95. The 30 foot position changes had the controller command a 30 foot forward position change from the standard position to a line abreast formation followed by an aft position change back to the standard formation. Looking at Figure 87, plot a it is apparent that the controller increased the VISTA aircraft velocity by approximately 1 knot to affect the position change. Plot d) shows the maneuver was heavily damped and required approximately 12 seconds to complete. There was no perceivable overshoot during the maneuver. Another position change maneuver presented in Figure 86 shows an overshoot when the maneuver is conducted but this test run was accomplished prior to the test team determining the need to fly the direct crosswind heading and was not considered characteristic of the controller's performance. A similar result is found when looking at the aft position changes in Appendix A, Figures 88 and 89. The position change aft presented in Figure 89 shows the same heavily damped move to the standard position with no overshoot that was seen in the forward position change and was characteristic of position changes in these directions. The time to perform the aft maneuver increased slightly, to approximately 17 seconds. The 60 foot position changes started from the same standard formation but moved forward past the line abreast formation to a position 30 feet in front of the lead aircraft and then back to the standard formation position. One maneuver was

accomplished forward and one aft. The forward position change found in Appendix A, Figure 93, is corrupted by a data drop-out that occurred several seconds prior to the maneuver. This caused the x separation to jump 50 feet approximately 5 seconds before the maneuver began. The controller immediately corrects for this and has accelerated 2 knots prior to beginning the maneuver. Because of this, the VISTA aircraft performs the position change maneuver faster than would be expected, approximately 15 seconds. Again the maneuver is highly damped, with no overshoot. The 60 foot aft position change in Figure 94 is also heavily damped with no overshoot, but takes approximately 60 seconds to accomplish. The vertical channel displayed a slight bobble as the controller corrected to maintain altitude during the accelerations, but maintained less than 6 feet of error during all maneuvers. The lateral channel had a lightly damped oscillation that was a function of how much lateral offset from the commanded position the VISTA aircraft had before the controller was engaged, and was relatively unaffected by the fore and aft maneuvering.

Lateral Position Changes.

Plots of the flight test results for 30 foot lateral position changes can be found in Appendix A, Figures 79 and 82. The 60 foot lateral position changes are presented in Appendix A, Figures 92 and 93. The 30 foot lateral position changes commanded the VISTA aircraft to move right, to a position directly behind the lead aircraft and then back to the standard formation position. Figure 81, plot e) shows the y channel displayed the same lightly damped oscillations as it corrected the position step disturbance to the right and then back to the standard formation position. The period of the oscillations was found to be approximately 20 seconds and the damping ratio was found to be less than

0.1. It is apparent that the VISTA aircraft was correcting to a steady state offset approximately 5 feet from all of the commanded positions. This offset was apparent at the maneuver initiation and is analyzed the Analysis of Issues sub-section below. Overshoots for the lateral maneuvers were significant, as would be expected for a lightly damped system. For the 30 and 60 foot position changes, the initial overshoots were 25 and 58 feet respectively. The settling times for both maneuvers was found to be approximately 80 seconds. The x channel remained unaffected by the lateral position change. A data drop-out is observed at approximately 105 seconds in Figure 92 plot d) of Appendix A. The x separation is quickly ramped back to zero by the position smoothing algorithm when good data is received. The z channel again displayed the most desirable performance, and quickly damped the expected disturbances as the VISTA aircraft banked to affect the position changes. All errors in the z direction were maintained at less than 10 feet for all of the lateral maneuvering.

Vertical Position Changes.

Plots of the flight test results for vertical position changes are found in Appendix A, Figures 83 through 85, 90 and 91. The vertical position changes were conducted from the standard formation position and consisted of commanding the VISTA aircraft to either climb 30 feet above or descend 30 feet below the lead aircraft and then descend or climb back to the standard formation position. As in other position changes the commanded position was input to the controller as a step. Looking at Figure 85 plot f), the VISTA aircraft responded to the step input within 2 seconds of the command. The motion was characterized by a second order, moderately damped response with a damping ratio of approximately 0.4 or greater and a period of approximately 15 seconds.

Overshoots for the 30 foot steps were less than 10 feet and 100% rise time occurred approximately 5 seconds after the step. The x channel was unaffected by the vertical maneuvers. The y channel displayed the same low frequency, lightly damped oscillation observed previously.

Summary of Flight Test Results

This section will initially present an overview of the flight test results, and then present a summary of each channel's performance. Table 10 below was taken from AFFTC-TIM-04-08 and presents the maximum errors in each channel during lead maneuvers (14). It also presents the maximum velocity errors and inertial separation errors observed during each maneuver run. It must be noted that Table 10 is presented without consideration for the maneuver being accomplished or the errors that are occurring to include data drop-outs and velocity error issues. It simply presents the greatest errors that were observed in each channel. To help characterize the results for the reader, errors caused by data drop-outs and x-channel errors as a result of system velocity errors are highlighted as indicated at the bottom of Table 10. The majority of excessive error is a result of these two issues. It is apparent from the flight test results that the controller was able to maintain the desired formation throughout lead maneuvering, but at varying levels of precision based on three main external factors. The first was the amount and duration of data drop-outs experienced during the maneuver runs. The second was how well the aircrew were able to begin and keep the aircraft on the direct crosswind heading.

Table 10. Maximum Errors for Lead Maneuvers

Event	Sortie	Record	Maximum Error				
			x (feet)	y (feet)	z (feet)	Velocity (feet/second)	Inertial Sep (feet)
100' Climb	1	4	11.0	19.4	15.0	3.1	19.2
	3	4	107.0**	11.0	18.6	12.8	38.8
	5	1	12.2	23.9	14.1	2.5	24.8
	5	3	77.1 *	4.4	13.1	3.2	69.2
	5	5	11.1	5.9	14.8	3.0	4.3
100' Descent	3	4	166.2 *	56.9	9.8	3.2	96.4 *
	1	5	12.0	18.5	10.5	2.9	20.1
	5	2	7.1	9.9	7.8	1.8	10.4
50Kt Accel	1	6	69.1*	17.5	12.5	2.9	65.3
	5	5	8.1	2.7	16.1	4.1	5.4
10 deg Turn	1	8	33.5	31.4	20.7	4.5	29.5
	4	1	67.4**	38.6	25.9	3.7	59**
10/20/30 deg Turns	3	12	106.8**	80.9	56.5	3.8	102.6**
20 deg Turn	1	10	76.7**	24.7	32.9	3.7	66.6**
10/20/30 deg Turns	4	3	246.2 *	57.5	38.8	2.9	236.2 *
30 deg Turn	1	3	105.3**	50.8	27.7	10.2	50.9**
	1	13	92.0*	132.5	61.4	3.1	125.4*
20 deg Turn	1	11	160.8**	16.5	22.9	3.3	151.9**
30 deg Turn	1	14	37.0	366.5	75.2	3.1	358.3

* error caused by data dropouts

** x-channel divergence due to system velocity errors

Finally, the amount of initial offset from the commanded position when the controller was engaged and whether that offset was allowed to settle prior to lead maneuvering was a factor. If all three of these factors were favorable, the controller's response was well damped and errors were approximately ten feet or less for the x and z channels and lightly damped but stable for the y channel. If data drop-outs were experienced, the controller would be continually fixing position errors. Stability was maintained during

the data drop-outs primarily as a result of the extrapolated position smoothing algorithm and the limits placed on the position errors the controller received. If the data drop-outs became too excessive the virtual lead aircraft could not even be received. Finally, if the aircraft was not within 20 degrees of the direct crosswind heading, the VISTA aircraft would drift forward or aft from the commanded position.

A summary of the dynamic parameters during the formation change maneuvers, taken directly from AFFTC-TIM-04-08 (14), is presented in Table 11 below.

Table 11. Dynamic Parameters for Position Change Maneuvers

Position Change	Overshoot Distance (feet)	Rise Time 100% (Sec)	Damp Ratio	Period of Oscillation (sec)	Settling Time 90% (sec)
Climb/Descend 30 feet	10	5	0.4	15	15
Descend/Climb 30 feet	8	4	0.5	12	12
Lateral 30 feet	25	6	<0.1	20	80
Lateral 60 feet	58	9	<0.1	20	80
Forward 30 feet	2	8	0.7	1.3	8
Forward 60 feet	0	16	0.7	1.4	14
Aft 30 feet	3	19	0.7	9, 1.3	18
Aft 60 feet	1	62	0.7	10, 1.4	58

It was apparent during flight testing that formation change maneuvers were easily accomplished but with the same impacts to the precision of the maneuver as seen during lead maneuvering. The fore and aft and vertical position changes were effective and represented acceptable performance if the VISTA aircraft was flying on the direct crosswind heading. The lateral position changes were stable, but the damping ratio was much less than would be desired or required for close formation flight and would require improvement for safe two-ship formation flight.

Summary of Channel Performance.

The x channel performance is best summarized as a compilation of different oscillations at various frequencies. The previous results presented the overall response, but it must be noted that the signal represented a compilation of approximately three separate frequencies. A very high frequency noise of approximately 2 foot amplitude several times a second was imposed upon all of the responses for all of the flight testing. This noise was assessed to be positional accuracy round-off errors, since this type of motion was not reported by the aircrew and would not be physically possible. A medium frequency response was observed by the aircrew and was apparent in the data when the VISTA aircraft was within ten feet of the commanded position and the proportional control of the algorithm was not limited by the ten foot x-channel error limit. In fact, this oscillation was used by the aircrew to determine that the controller was controlling the VISTA aircraft correctly. The final oscillation had a period of approximately 10 seconds and was representative of the position correction motion that was observed when a disturbance was encountered. When the VISTA aircraft was not on the direct crosswind heading and the x channel was drifting, these errors would be the greatest errors observed in any channel.

The y channel performance was overall characterized by a lightly damped oscillation with a period of about 20 seconds and a steady state offset that is explored in the next section below. There was no significant change to the lateral motion for any of the lead or position change maneuvers.

Finally, the z channel represented the most stable and well damped motion of all the channels. The damping ratio was slightly greater than 0.4 for all of the maneuvers

and displayed one or less overshoots for a given disturbance depending on the amplitude. For the basic maneuvering cases, excepting those where significant data dropout occurred, the z channel maintained errors of approximately 10 feet, and were usually kept to less than 6 feet. For the complex maneuvers, the z-channel error was always maintained less than approximately 30 feet but was mostly a result of the other channels developing errors inducing larger errors in the z channel. The responses to these errors were well damped and represented the best performance of all channels for the complex maneuvers.

Analysis of Results

The results presented above describe the observed performance of the controller during in-flight testing. It is an objective of this work to compare the simulation results presented in previous chapters with the flight test results. An analysis of the possible reasons for differences between the two results is useful for the development of automatic formation flight controllers and for improvements to this work. Several issues and observations presented above will be detailed for analysis in this section. The first such issue is the one that generated the most problems during flight test as well as the greatest error in the flight test results.

Velocity Error.

The velocity error mismatch previously mentioned became apparent in the VISTA state vector due to the actual winds aloft. It has been previously discussed that a mismatch between positions and the integration of velocities in a given direction would cause difficulty for the controller, since even if the velocity is perfectly matched,

generating no velocity commands, the position would still drift. The position and velocity values that were provided to the controller during flight test were analyzed to determine where the velocity errors originated. The positions and velocities from the virtual lead that were sent across the data link had good coherency and showed an error of approximately 0.5 feet per second. This was considered reasonable considering the precision of the data linked position coordinates were 0.25 feet. The VISTA North-South and East-West velocities were integrated at each time step and subtracted from the actual VISTA positions to yield the positional errors over time as shown in Figure 42 below.

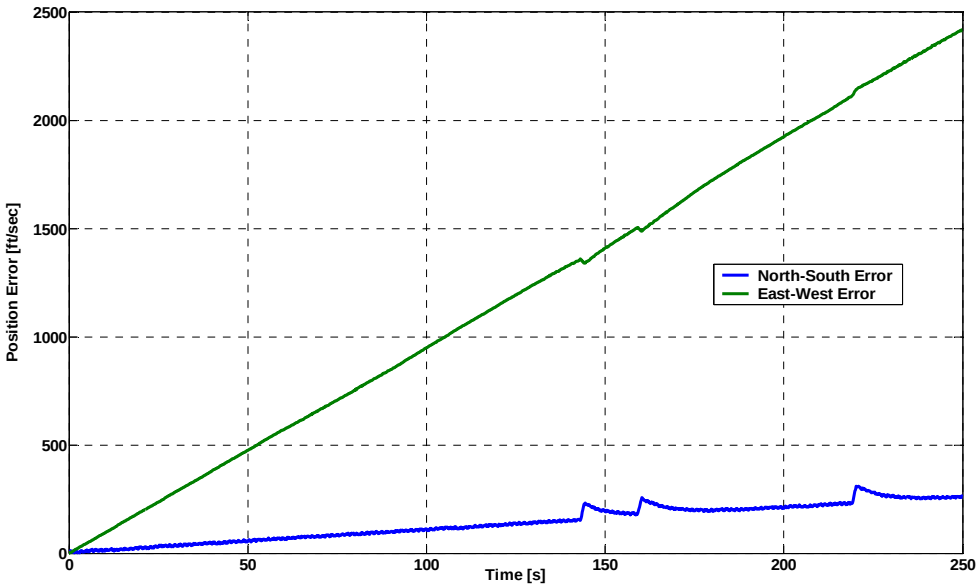

Figure 42. VISTA Integrated Velocity Errors (Sortie 3 Run 12)

It is clear that the North-South direction showed an error of approximately 1 foot per second. This was again considered reasonable for the application. The VISTA East-West positional errors shown above were not reasonable and showed significant inconsistencies of approximately 9.6 feet per second. The large magnitude of the drift in the East-West direction was found in all of the flight test runs. The determination of the

source of these errors is not in the scope of this work, but is suspected to be a result of the VISTA algorithm for blending of INS and GPS data.

To determine if the observed velocity error in the East-West direction was responsible for the x channel drift, the errors in both directions were introduced into the final pre-flight model. The final simulation model presented in Appendix B, used to test the flight test setup, was run with the lead aircraft holding straight, level, un-accelerated flight while the VISTA aircraft held a constant formation. The velocity error of 9.6 feet per second was input as an error into the VISTA aircraft's state vector in the model. An ICE model run was used as the lead aircraft as during flight testing. The simulation results are presented in Figure 43 below. The same forward drift was apparent as the lead aircraft began the left turn, proving the velocity error to be the cause of the x channel drift observed in flight test. It was determined from these simulations that this effect is a result of three competing forces. The first is that the steady state velocity error must cause a corresponding offset in the x direction as a function of the previously discussed balancing nature of the control law. The magnitude of the x position offset is a direct result of the amount of velocity error input to the system. The system would normally seek a steady state balance, but the use of position error limits imposes a limit on how much velocity error can be introduced before its effects cannot be countered. The x position error limit was set at ten feet for flight test and corresponded to a heading change of approximately 20 degrees, since the velocity error was a function of the current heading. In simple terms, if the steady state offset due to the velocity error was greater than the x position error limit, then the aircraft would continue to drift as in Figure 43.

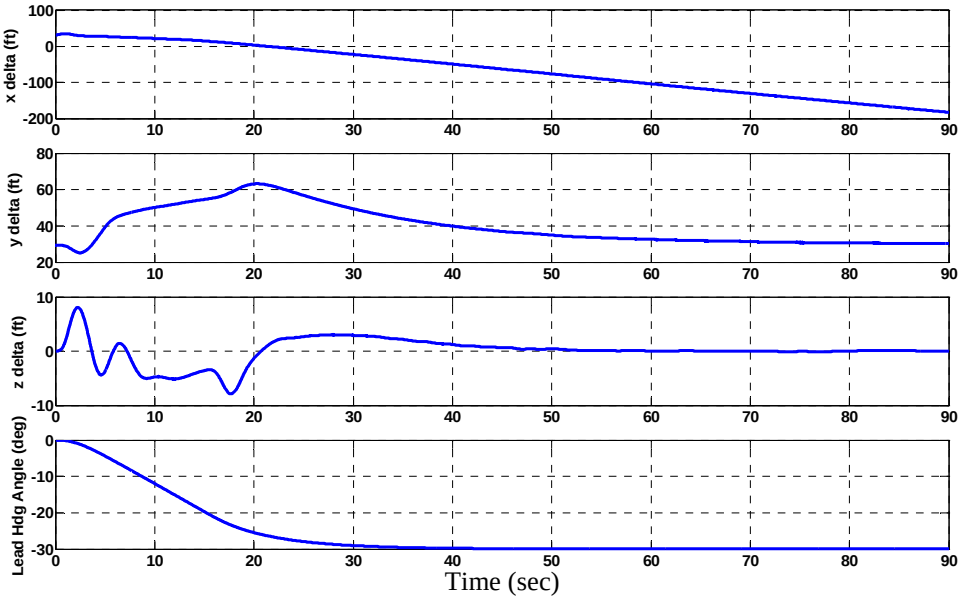

Figure 43. Separations with Velocity Error

Next the velocity error input to the model was reduced to observe the situation where the x position offset did not exceed the x position error limit.

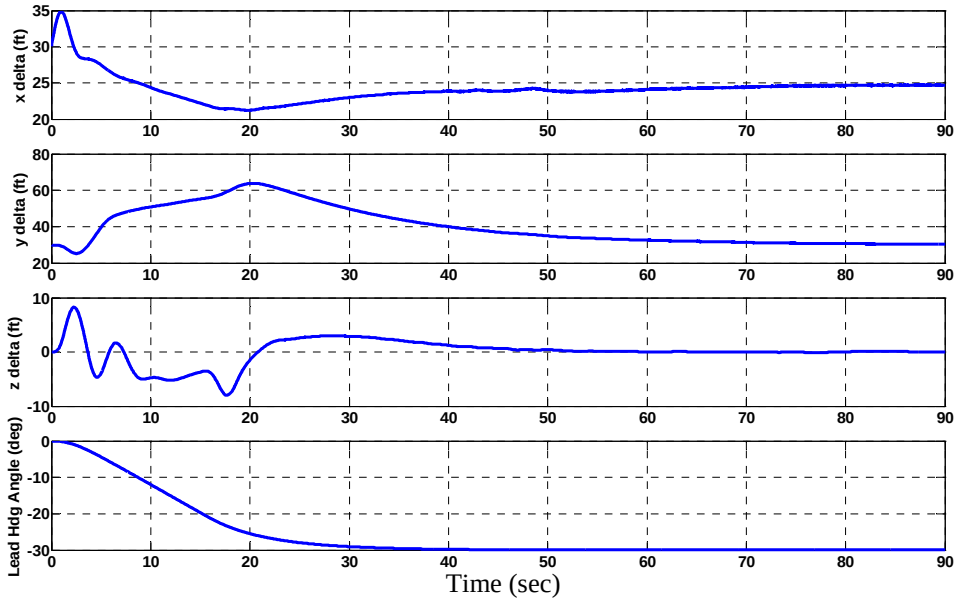

Figure 44. Separations with Reduced Velocity Error

In Figure 44 above it is clear that the velocity error input of 2.4 feet per second induced an x position offset of only 4.9 feet, which is less than the x position error limit of 10 feet.

Assuming it was not possible to make the positions and velocities of the system correlate, an analysis of the problem provided three possible solutions. The first is to accept the error of the offset, similar to the turning flight situation, and make sure the x position error limit is set to a value greater than the maximum steady state error that will be observed. This solution assumes the user can accept the x position offset errors that will be induced. The second option is to counter the velocity error and trim it out of the commanded x position. This would be possible by modeling the errors and applying the model to the commanded x position, or measuring the errors and countering them with a trimming algorithm. The development of a real time trimming algorithm is non-trivial and is left as an area of future work. The final option is to limit the integrated velocity errors to only what is required to reduce the steady state errors. Figure 45 below shows the result when a limit of 10 is placed on the integrated velocity error and the full velocity error of 9.6 feet per second is input into the model. It is apparent from the plots that the impact of the velocity errors is minimized and the x separation is allowed to settle to the commanded 30 foot offset. This option seems to have the greatest benefit and allows the controller to handle larger velocity errors but would require the limit be tuned to the application to avoid upsetting the velocity and x position balancing nature of the velocity control law.

Despite all of the previously provided solutions to this problem, it must be emphasized that the best solution is to ensure the position and velocities are always correlated.

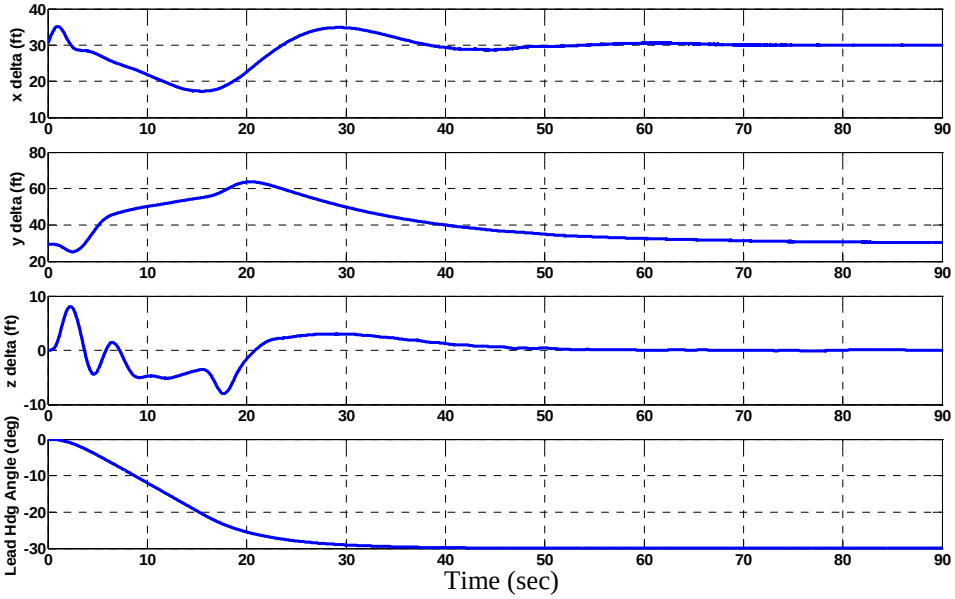

Figure 45. Velocity Errors with Integrated Velocity Errors Limited

Lateral Issues.

The lateral performance observed during flight test was found to be significantly more oscillatory than was desired and usually displayed a steady state offset. Simulations presented previously used a roll rate command system, but during the course of integrating the controller into the VISTA aircraft it was determined that lateral control would be accomplished using roll angle commands instead of roll rate commands. Initial simulations indicated this setup would yield the lesser damped roll response that was observed. Simulation results of a lateral position change were conducted using both a roll rate control law and a roll angle control law. In both cases the lead aircraft is holding straight, level, un-accelerated flight and the VISTA is commanded to a position in trail behind the lead aircraft. Figure 46 below shows the simulated VISTA aircraft response

with a roll rate control law. The position change is commanded at five seconds into the simulation.

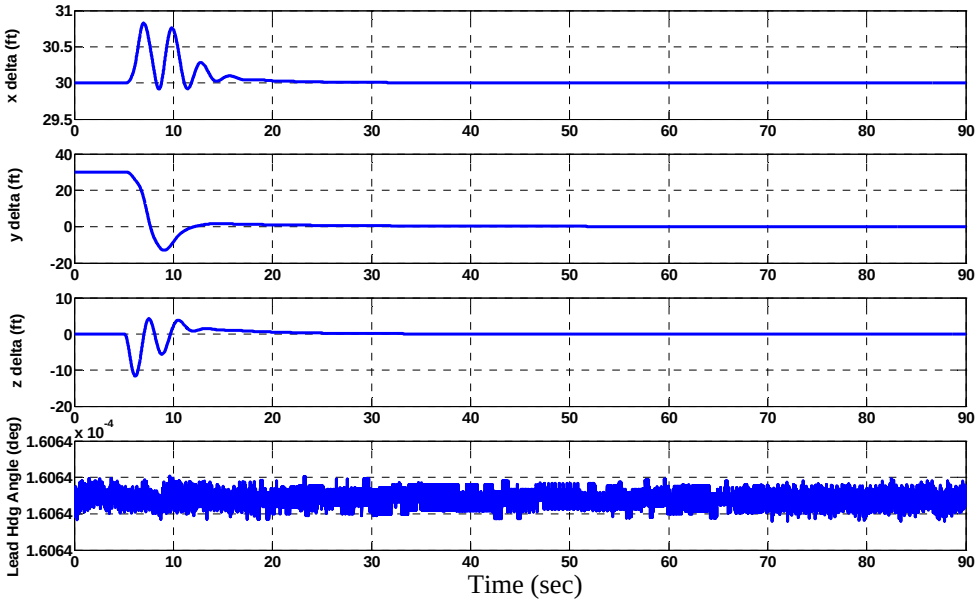

Figure 46. Separations During Position Change: Roll Rate Control Law

Apparent in the y channel plot is a nine foot overshoot followed by a well damped recovery to the zero steady state condition. The response is similar what was observed in earlier simulations but utilizing instead the General Dynamics provided VISTA model. Gain tuning would be required to achieve the optimum performance of minimal overshoot with minimal maneuver time. It must be noted that the optimum performance would have to be balanced between formation hold performance and position change performance. As previously discussed, an overshoot would be expected if the controller was tuned to be a compromise of performance between both tasks. The next plots found in Figure 47 show the same commanded position change, but with a roll angle control law. The gains used for flight test were included in this simulation.

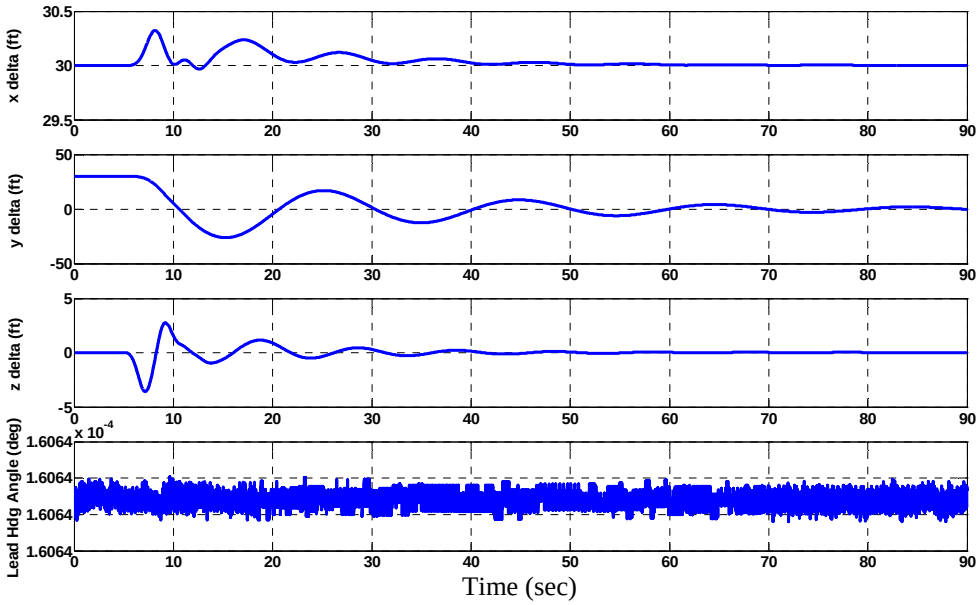

Figure 47. Separations During Position Change: Roll Angle Control

The in-flight y channel performance was very similar to the y channel response of the simulation using the roll angle control law. The overshoot for the 30 foot position change was approximately 25 feet and the period of oscillation was approximately 20 seconds. Both numbers match the flight tested results. Because of the direct compatibility of the simulation and flight test results, it is expected that a roll rate control system as simulated and previously presented would yield better performance and greatly increase lateral damping. Thus, the need to switch to roll angle control because of time and budget constraints significantly contributed to the lateral errors observed in-flight. Gain tuning was performed on the roll angle control system used to produce Figure 47 above in an attempt to decrease errors and increase lateral damping, but was unsuccessful in this task without significantly reducing the performance during formation hold maneuvers. The time delay of the roll angle response of the VISTA aircraft is considered to be the primary reason for the lateral performance issues.

The last lateral issue to be explored was the offset that was observed in-flight. It was previously presented that a lateral offset in the steady state position was observed for most of the flight testing. It was also previously discussed that the actual roll angles of the aircraft had to be utilized in order to minimize calculation errors and reduce the amount of data being transmitted along the data link. Previous simulations had utilized a velocity vector roll angle as the roll angle to match for the two aircraft. In this way, the actual aircraft bank required to generate a given turn rate was not required. The velocity vector roll angle of zero simply meant the velocity vector heading angle was not changing. When using body roll angles, this may not always be the case, since every real aircraft flies differently, and different roll angles may be required to affect a given turn rate for different aircraft. The balancing nature of the control laws assumed that when the two aircraft have the same roll angle there will be no lateral movement between the aircraft. Because of the need to use the actual body roll angles of the two aircraft a certain amount of roll angle mismatch was expected. Roll angle mismatch was introduced into the simulation to observe the response. It was found that a 0.5 degree of angular mismatch produced a steady state lateral offset of seven feet from the command position. Since the simulation gains were those used during flight test, the lateral offset observed in simulation should match the lateral offset observed in-flight when the correct roll angle mismatch is input to the model. It was determined that the five foot lateral offset was a result of a 0.36 degree roll angle mismatch. Figure 48 presented below shows the simulation results of the 0.36 degree mismatch. The five foot lateral offset can be observed in the y channel plot above. As discussed earlier, the lateral offset is a

necessary by-product of the balancing nature of the control law. The most obvious solution to the lateral offset is to use the velocity vector roll angle previously presented.

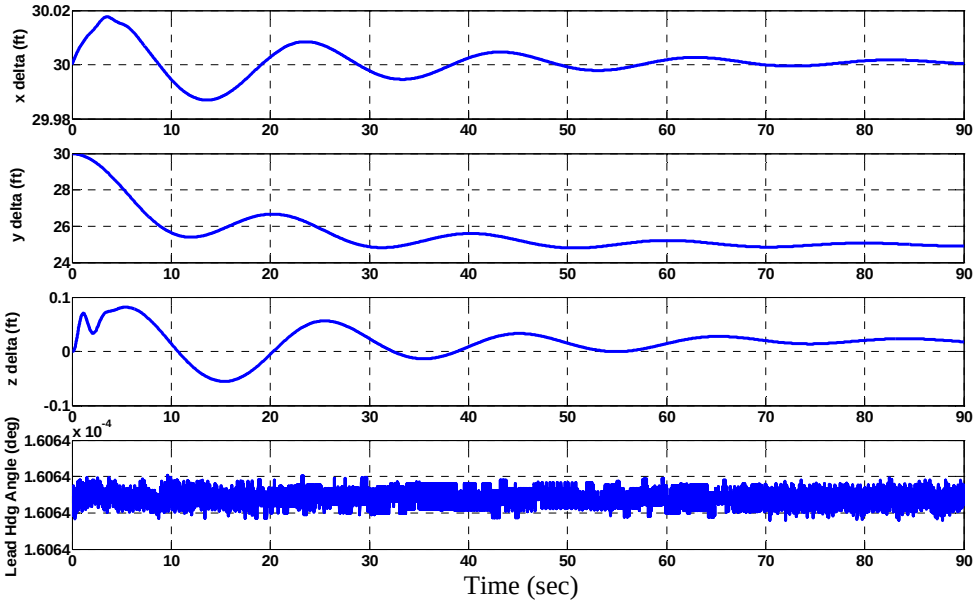

Figure 48. Lateral Offset due to Phi Angle Mismatch

If body phi angles must be used, the possible solutions to the lateral error, if the induced offset is too great for the application, is to use a continuous trimming function or model the error and counter the offset in this way.

VIII. Conclusions and Recommendations

Conclusions

Flight test results were positive in that the controller was proven to be feasible and capable of maintaining and changing the two ship formation. The need to tune the controller to the task became apparent as the testing progressed. The controller gains were chosen to perform both of the tasks of holding a formation during lead maneuvering and making a position change. The best performance would most likely be obtained if the controller was modified to use separate gain sets for each task. It is also necessary to continue to tune the gains as the model of the system changes, or when finally applying the controller to the real system. This is a process of fly, model, predict, and fly again. Time and budget constraints did not allow for this approach. Despite the lack of fine tuning, most of the significant errors that were observed during flight test were a result of changed control laws or errors the controller had to overcome. The one control law change that was required during integration, that caused significant errors during flight test, was the switch to a roll angle control system. The lateral channel displayed significantly less damping and larger overshoots as a result of the roll angle control system and the lack of sideslip control. Controller tuning during post-flight simulations was not able to significantly increase the lateral channel damping, without significantly reducing the formation hold during lead maneuvering performance. The most obvious solution is to utilize a roll rate command system for the lateral control.

Another significant finding was the need to plan for errors in the system information that is input to the controller. Small errors in velocity, roll, and flight path

angles correspond to positional offsets due to the balancing nature of the control laws. Errors expected in these values must be identified and their corresponding offsets determined. Minimizing these errors is the obvious solution, but if they cannot be reduced and the corresponding offset is too large for the application, then they must be overcome. Two possible methods of overcoming the errors is to either model them and introduce opposite inputs to the system to cancel their effects, or develop a continuously trimming function to remove observed errors. The second option is left as an area of further development. It was also determined that a robust data link is required for the successful performance of tight formation flight control. Data link quality during flight testing was marginal at best and completely unusable during some of the sorties. Finally, flight test data proved the controller to be capable of autonomous formation flight, and indicated that tight formation control is possible if the previously mentioned issues are successfully overcome.

Recommendations

Some recommendations based on the results of this study and areas of further work are included in this section. The main recommendation is to develop and utilize, in all automatic formation flight testing, a dedicated data link built for the purpose. The SADL system that was used did not display the level of integrity required for close formation flight. The impact of a poor data link should not be underestimated when performance, capability, and safety of flight is concerned. Areas of further work include developing and applying a continuously trimming function to trim out observed errors. It is also recommended, for peak performance, that the controller be modified to allow

multiple gain sets to be chosen based upon the task to be performed. Another area of further work includes the analysis of limitations placed on the different error states and how they affect the controller's performance.

Appendix A. Flight Test Results (14)

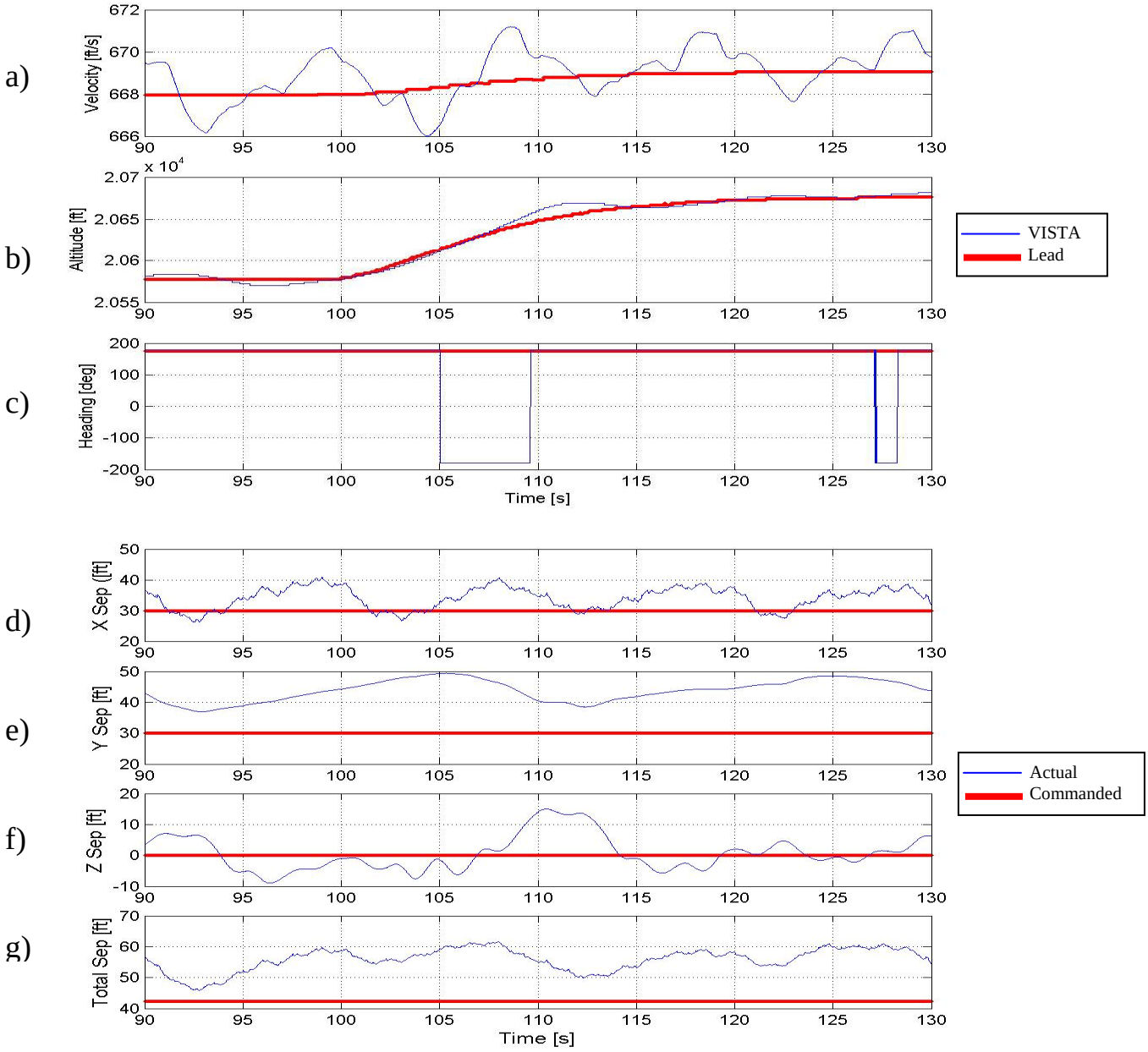

Data Basis: Flight Test; Test A/C: NF-16D #86-00048;
Engine: F110-GE-100; Configuration: Cruise, FCL; Test Date: 25Oct04

	X	Y	Z	Total Separation
Maximum Error (feet)	11.0	19.4	15.0	19.2
Time of maximum error (seconds)	99.0	105.3	110.4	108.0
Lead Maneuver	Climbs 100 feet while VISTA is commanded to maintain standard position (30 30 0)			

Figure 49. Event 3A Run 1 (Sortie 1 Record 4)

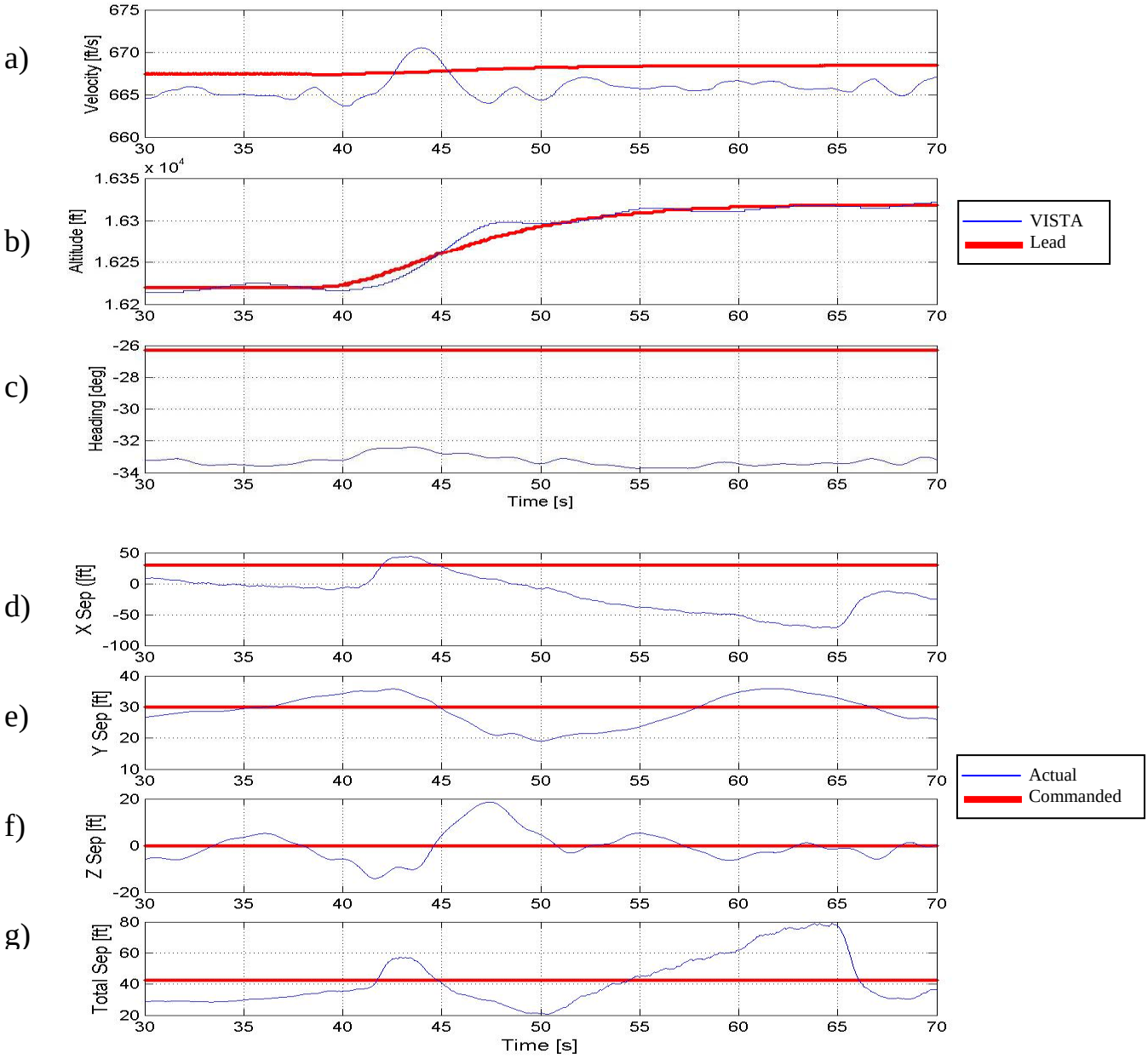

Data Basis: Flight Test; Test A/C: NF-16D #86-00048;
Engine: F110-GE-100; Configuration: Cruise, FCL; Test Date: 26Oct04

	X	Y	Z	Total Separation
Maximum Error (feet)	107.0	11.0	18.6	38.8
Time of maximum error (seconds)	77.1	50.0	47.4	77.1
Lead Maneuver	Climbs 100 feet while VISTA is commanded to maintain standard position (30 30 0)			

Figure 50. Event 3A Run 2 (Sortie 3 Record 4)

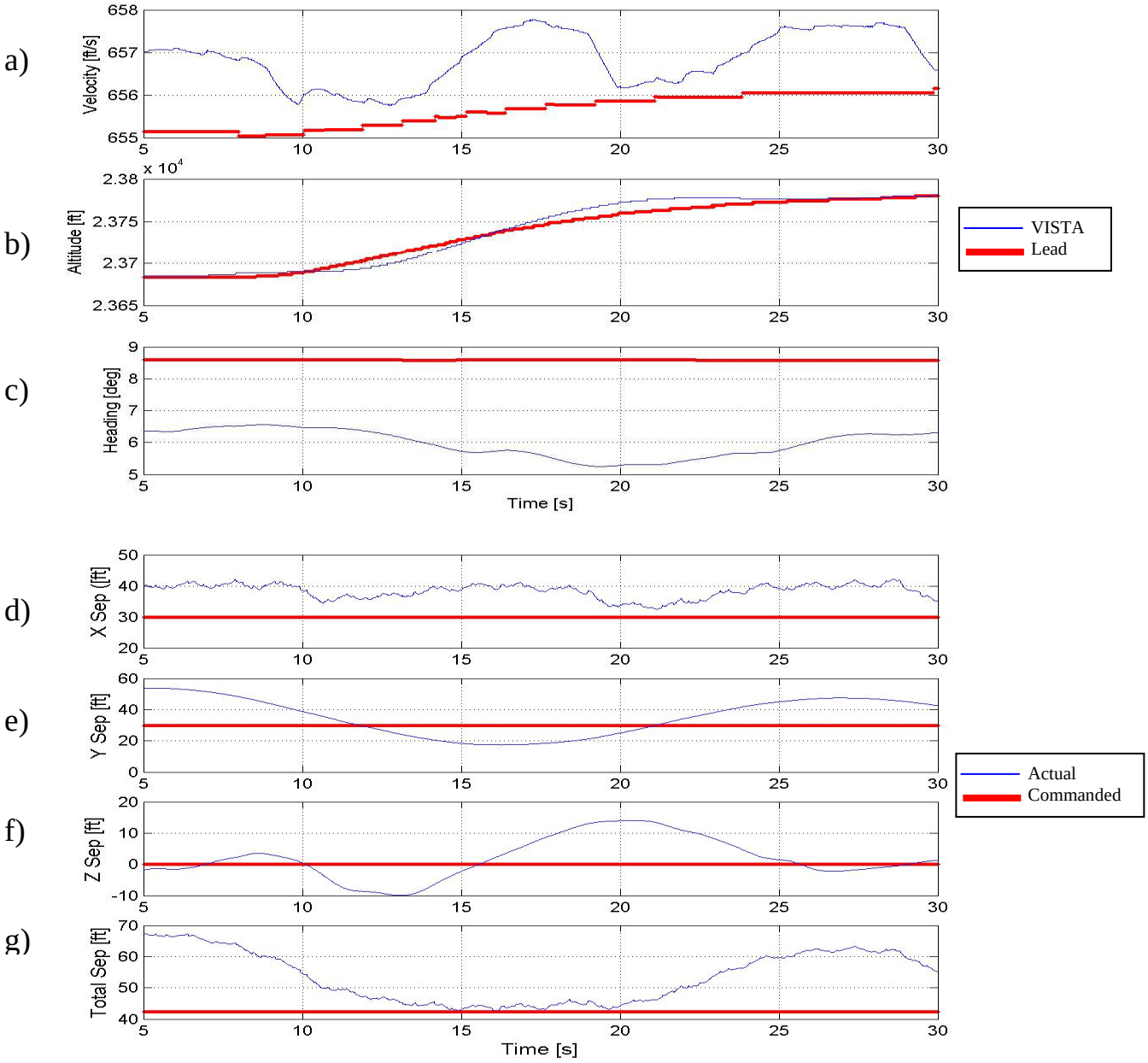

Data Basis: Flight Test; Test A/C: NF-16D #86-00048;
Engine: F110-GE-100; Configuration: Cruise, FCL; Test Date: 27Oct04

	X	Y	Z	Total Separation
Maximum Error (feet)	12.2	23.9	14.1	24.8
Time of maximum error (seconds)	28.6	5.0	20.4	5.1
Lead Maneuver	Climbs 100 feet while VISTA is commanded to maintain standard position (30 30 0)			

Figure 51. Event 3A Run 3 (Sortie 5 Record 1)

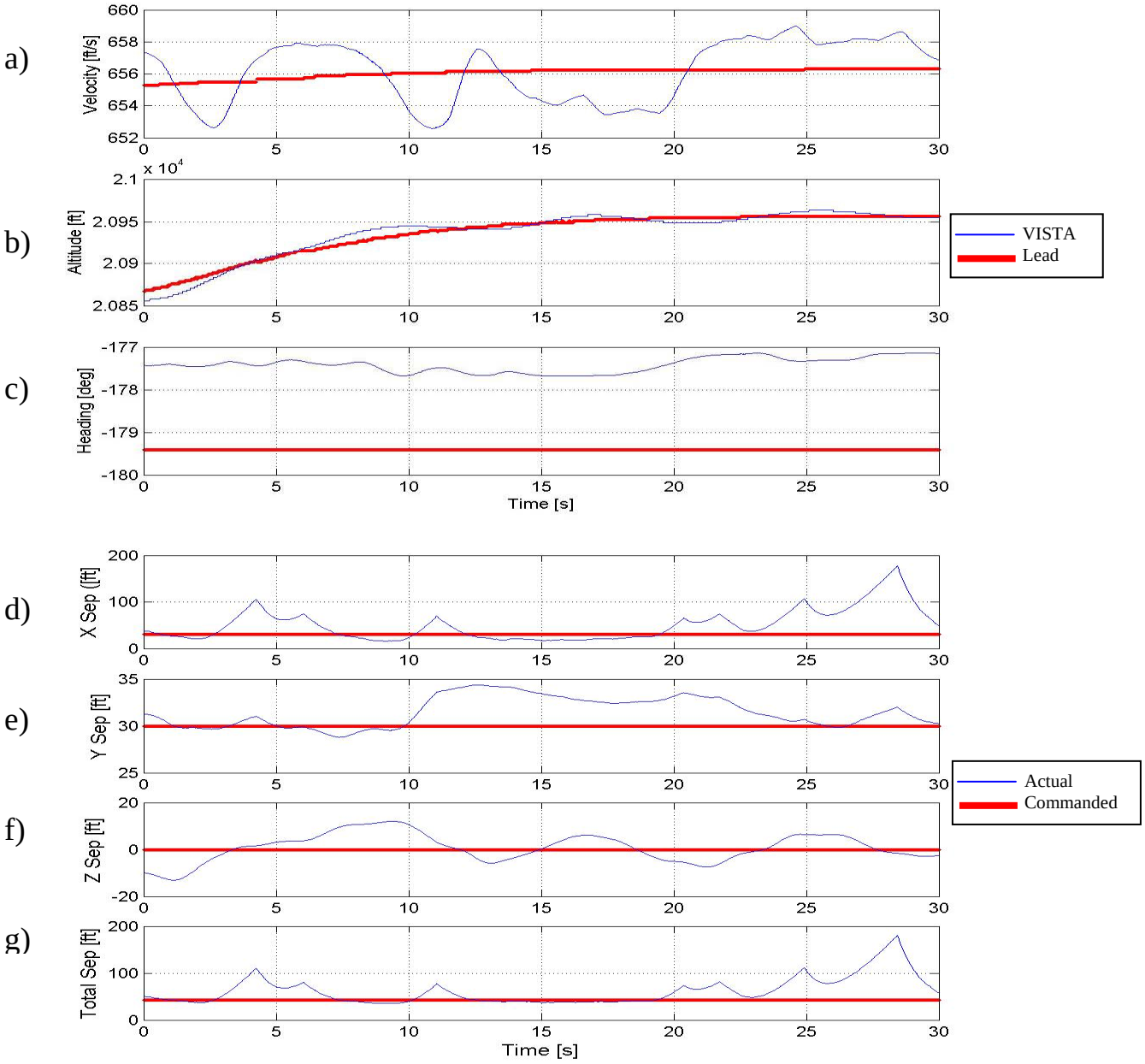

Data Basis: Flight Test; Test A/C: NF-16D #86-00048;
Engine: F110-GE-100; Configuration: Cruise, FCL; Test Date: 27Oct04

	X	Y	Z	Total Separation
Maximum Error (feet)	77.1	4.4	13.1	69.2
Time of maximum error (seconds)	24.9	12.5	1.1	24.9
Lead Maneuver	Climbs 100 feet while VISTA is commanded to maintain standard position (30 30 0)			

Figure 52. Event 3A Run 4 (Sortie 5 Record 3)

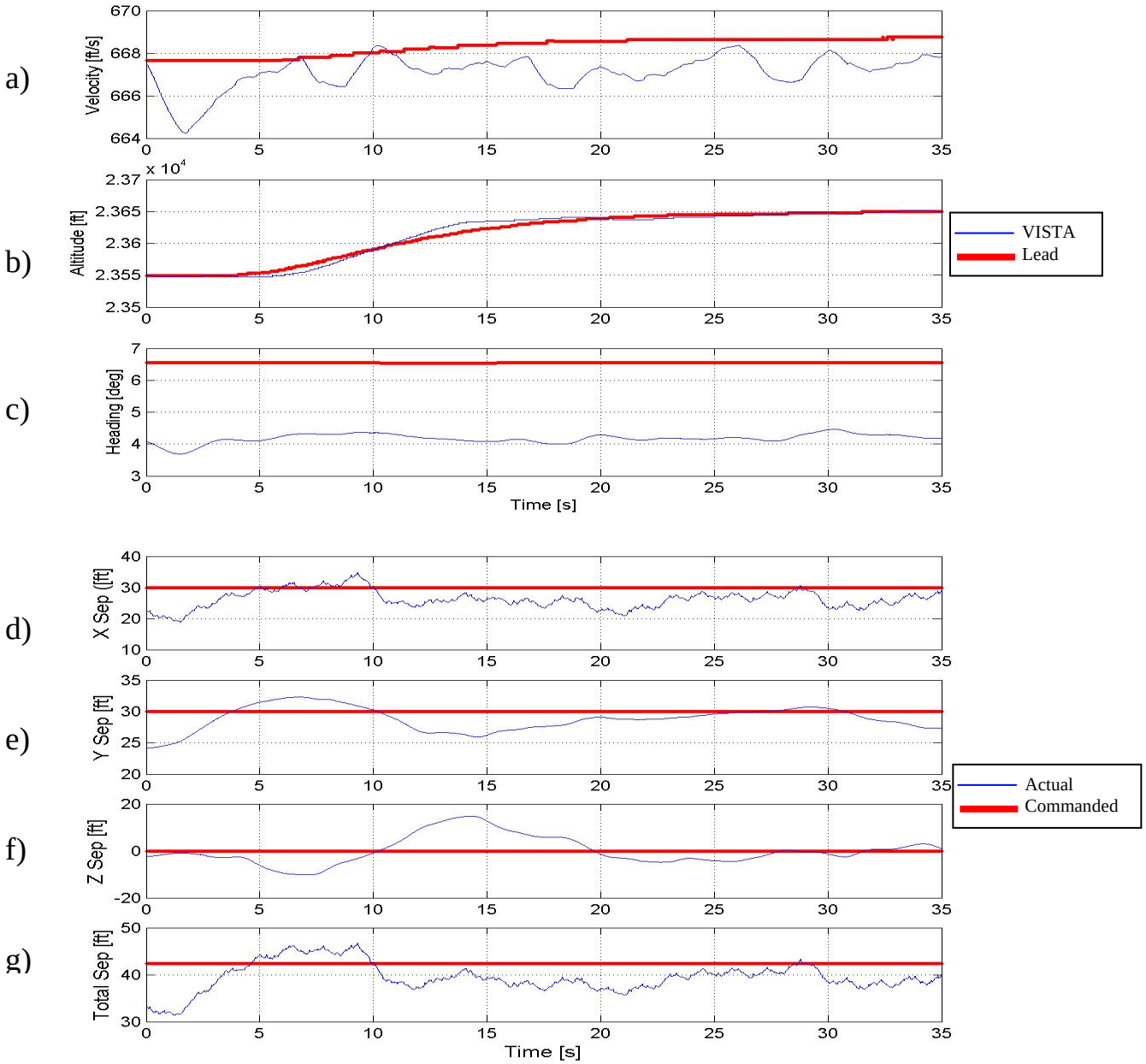

Data Basis: Flight Test; Test A/C: NF-16D #86-00048;
Engine: F110-GE-100; Configuration: Cruise, FCL; Test Date: 27Oct04

	X	Y	Z	Total Separation
Maximum Error (feet)	11.1	5.9	14.8	4.3
Time of maximum error (seconds)	1.5	0	14.3	9.3
Lead Maneuver	Climbs 100 feet while VISTA is commanded to maintain standard position (30 30 0)			

Figure 53. Event 3A Run 5 (Sortie 5 Record 5)

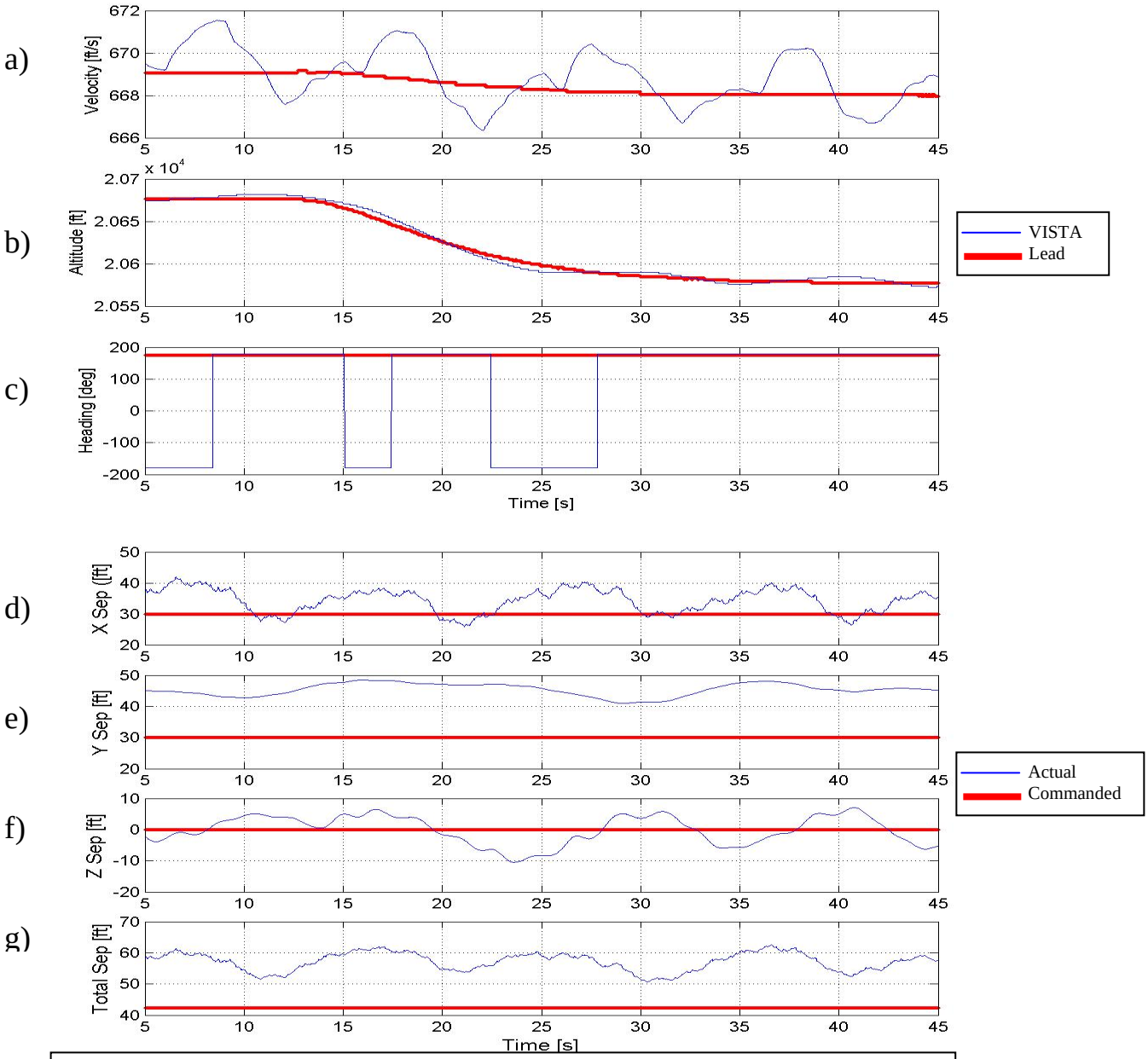

Data Basis: Flight Test; Test A/C: NF-16D #86-00048;
Engine: F110-GE-100; Configuration: Cruise, FCL; Test Date: 25Oct04

	X	Y	Z	Total Separation
Maximum Error (feet)	12.0	18.5	10.5	20.1
Time of maximum error (seconds)	6.6	15.9	23.5	36.6
Lead Maneuver	Descends 100 feet while VISTA is commanded to maintain standard position (30 30 0)			

Figure 54. Event 3B Run 1 (Sortie 1 Record 5)

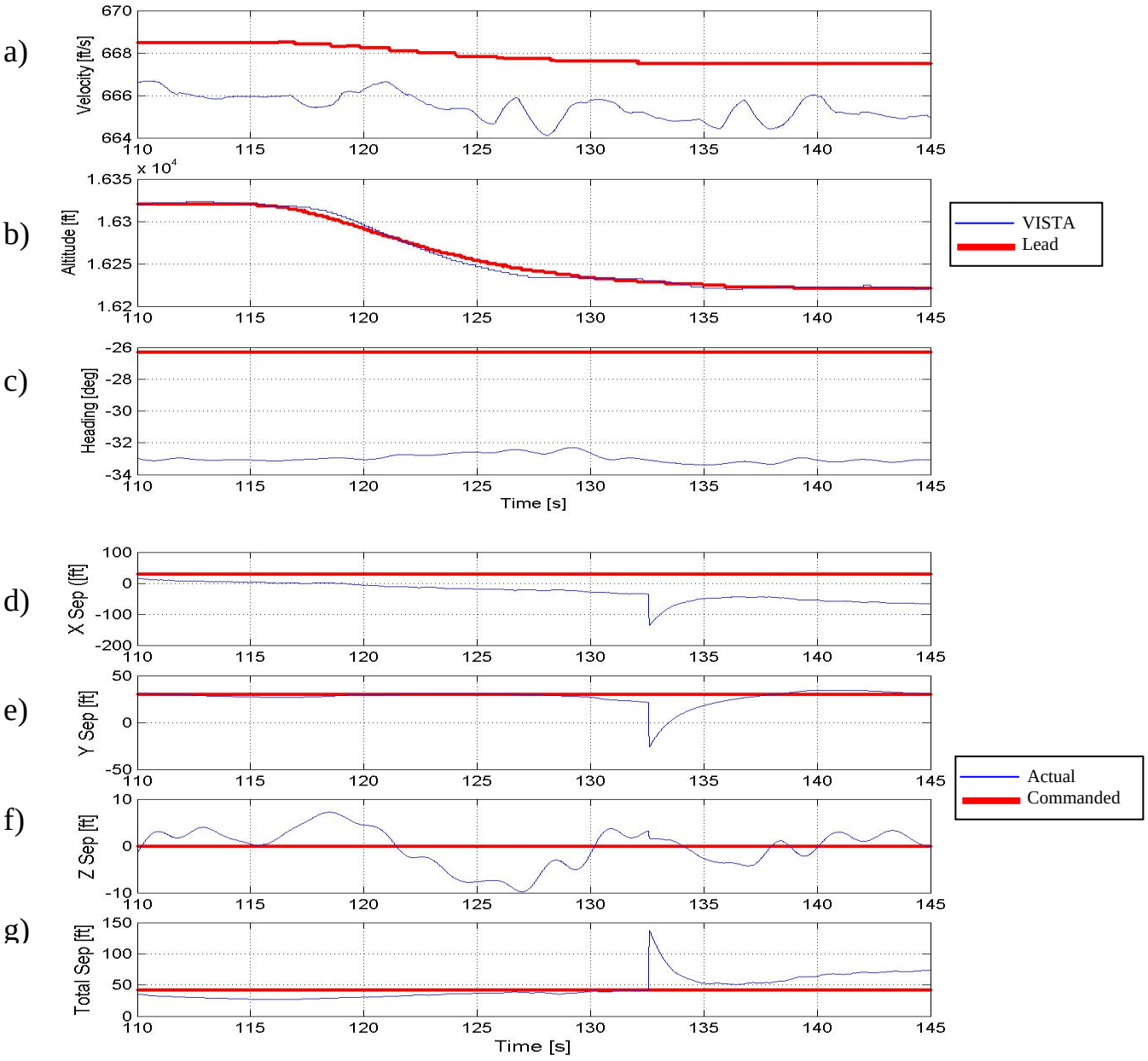

Data Basis: Flight Test; Test A/C: NF-16D #86-00048;
Engine: F110-GE-100; Configuration: Cruise, FCL; Test Date: 26Oct04

	X	Y	Z	Total Separation
Maximum Error (feet)	166.2	56.9	9.8	96.4
Time of maximum error (seconds)	132.6	132.6	127.0	132.6
Lead Maneuver	Descends 100 feet while VISTA is commanded to maintain standard position (30 30 0)			

Figure 55. Event 3B Run 2 (Sortie 3 Record 4)

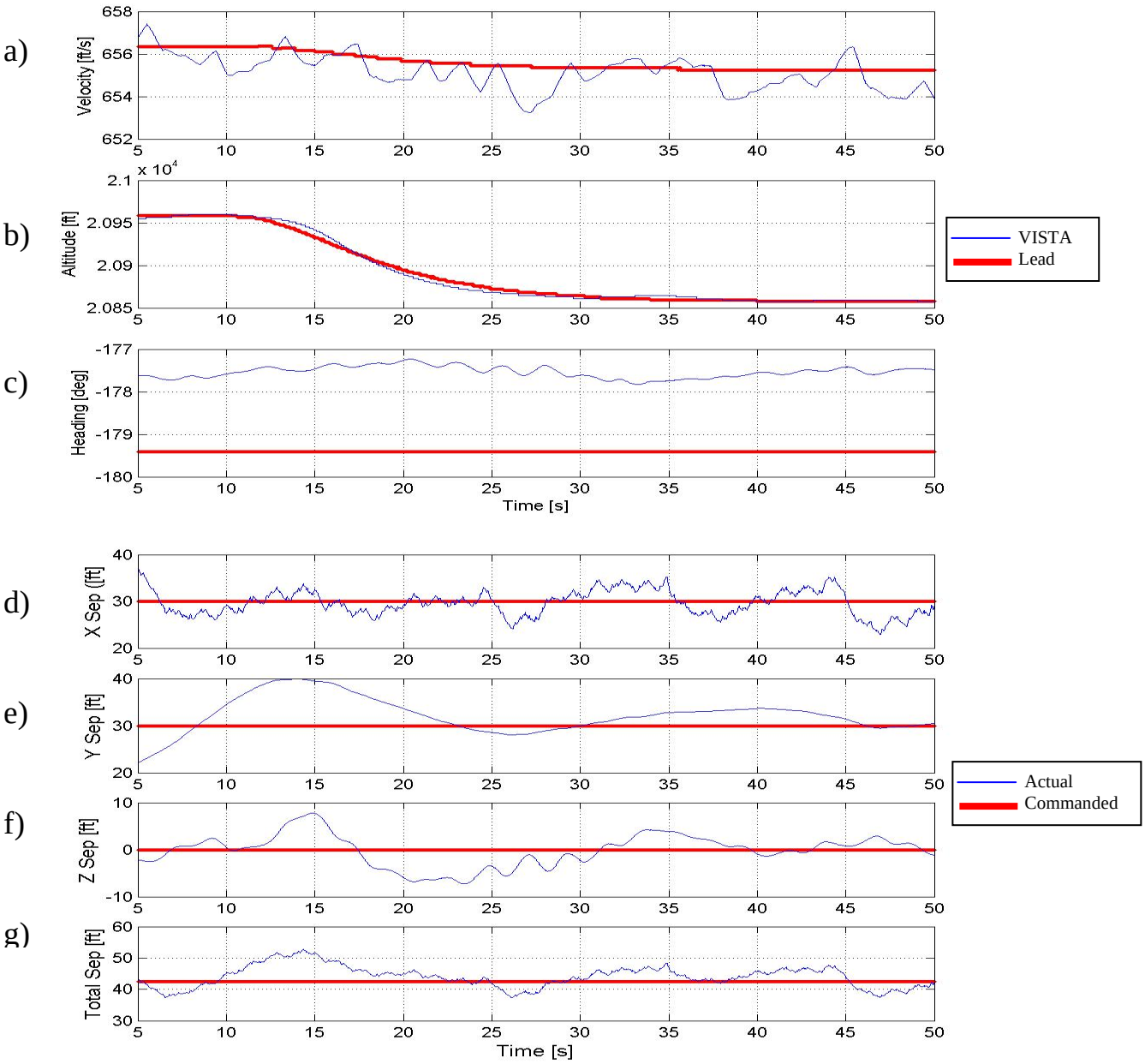

Data Basis: Flight Test; Test A/C: NF-16D #86-00048;
Engine: F110-GE-100; Configuration: Cruise, FCL; Test Date: 27Oct04

	X	Y	Z	Total Separation
Maximum Error (feet)	7.1	9.9	7.8	10.4
Time of maximum error (seconds)	46.9	13.9	14.9	14.4
Lead Maneuver	Descends 100 feet while VISTA is commanded to maintain standard position (30 30 0)			

Figure 56. Event 3B Run 3 (Sortie 5 Record 2)

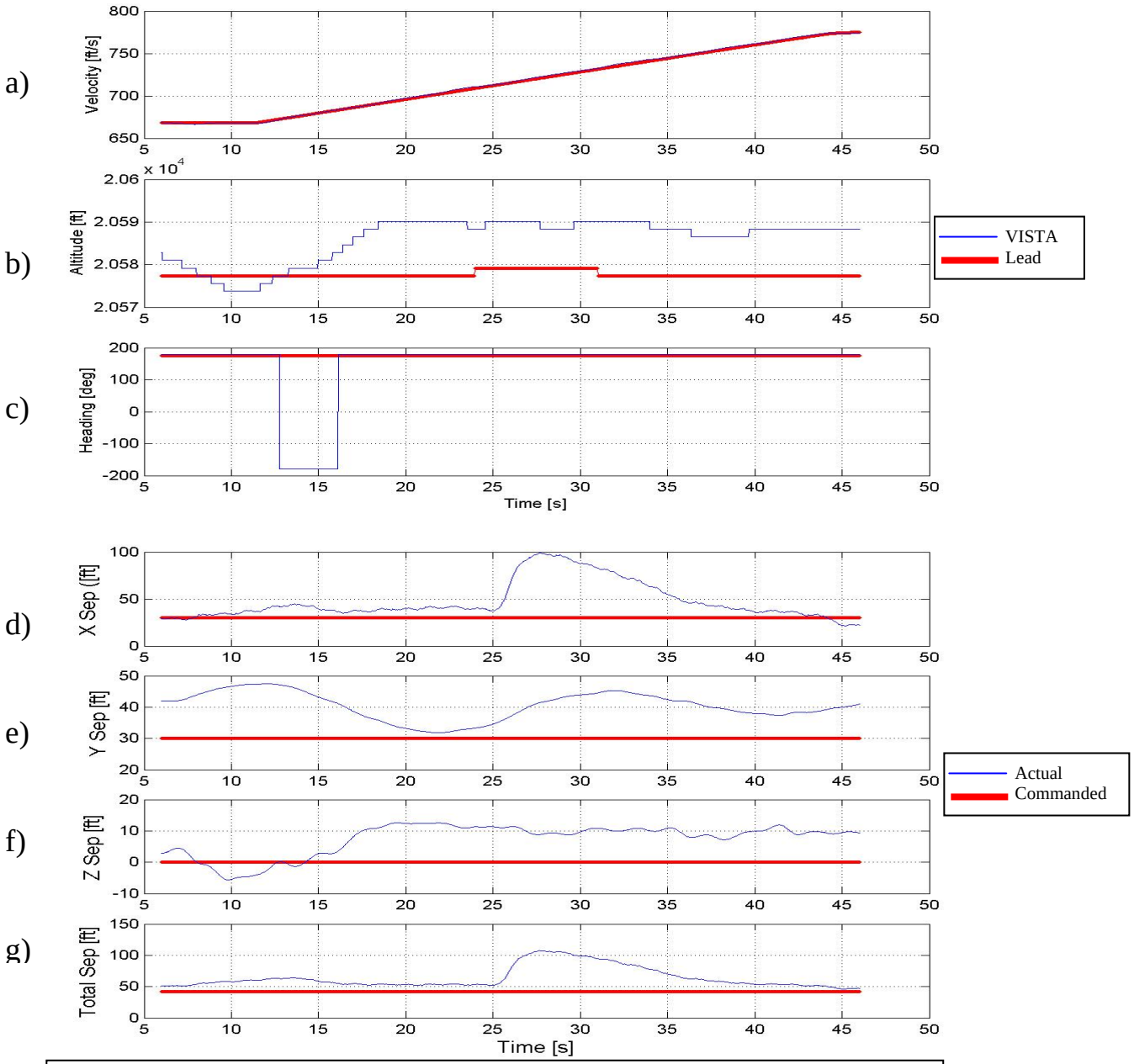

Data Basis: Flight Test; Test A/C: NF-16D #86-00048;
Engine: F110-GE-100; Configuration: Cruise, FCL; Test Date: 25Oct04

	X	Y	Z	Total Separation
Maximum Error (feet)	69.1	17.5	12.5	65.3
Time of maximum error (seconds)	27.7	12.1	19.4	27.7
Lead Maneuver	Accelerates 50 knots while VISTA is commanded to maintain standard position (30 30 0)			

Figure 57. Event 4A Run 1 (Sortie 1 Record 6)

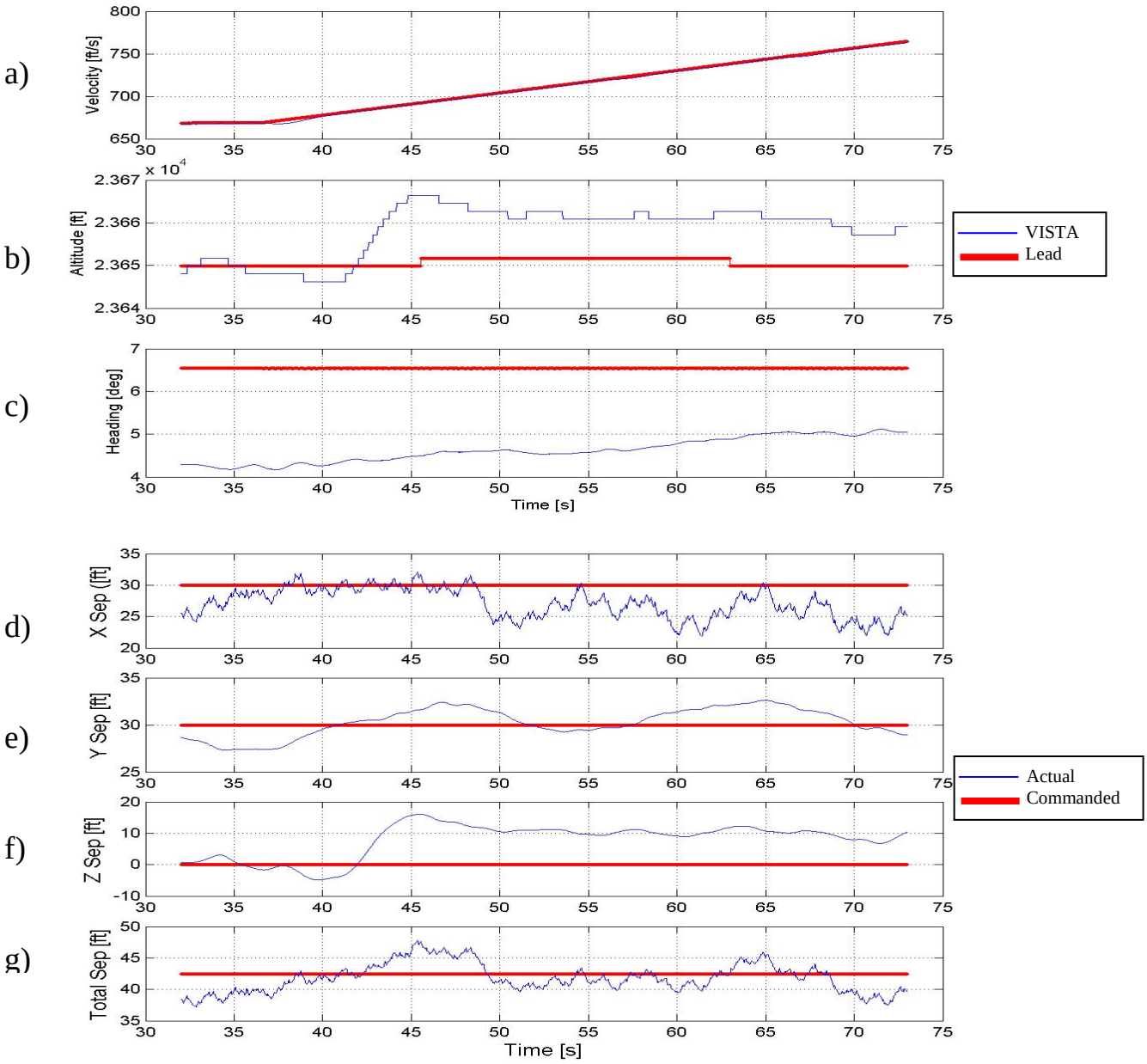

Data Basis: Flight Test; Test A/C: NF-16D #86-00048;
Engine: F110-GE-100; Configuration: Cruise, FCL; Test Date: 27Oct04

	X	Y	Z	Total Separation
Maximum Error (feet)	8.1	2.7	16.1	5.4
Time of maximum error (seconds)	61.4	34.4	45.5	45.4
Lead Maneuver	Accelerates 50 knots while VISTA is commanded to maintain standard position (30 30 0)			

Figure 58. Event 4A Run 2 (Sortie 5 Record 5)

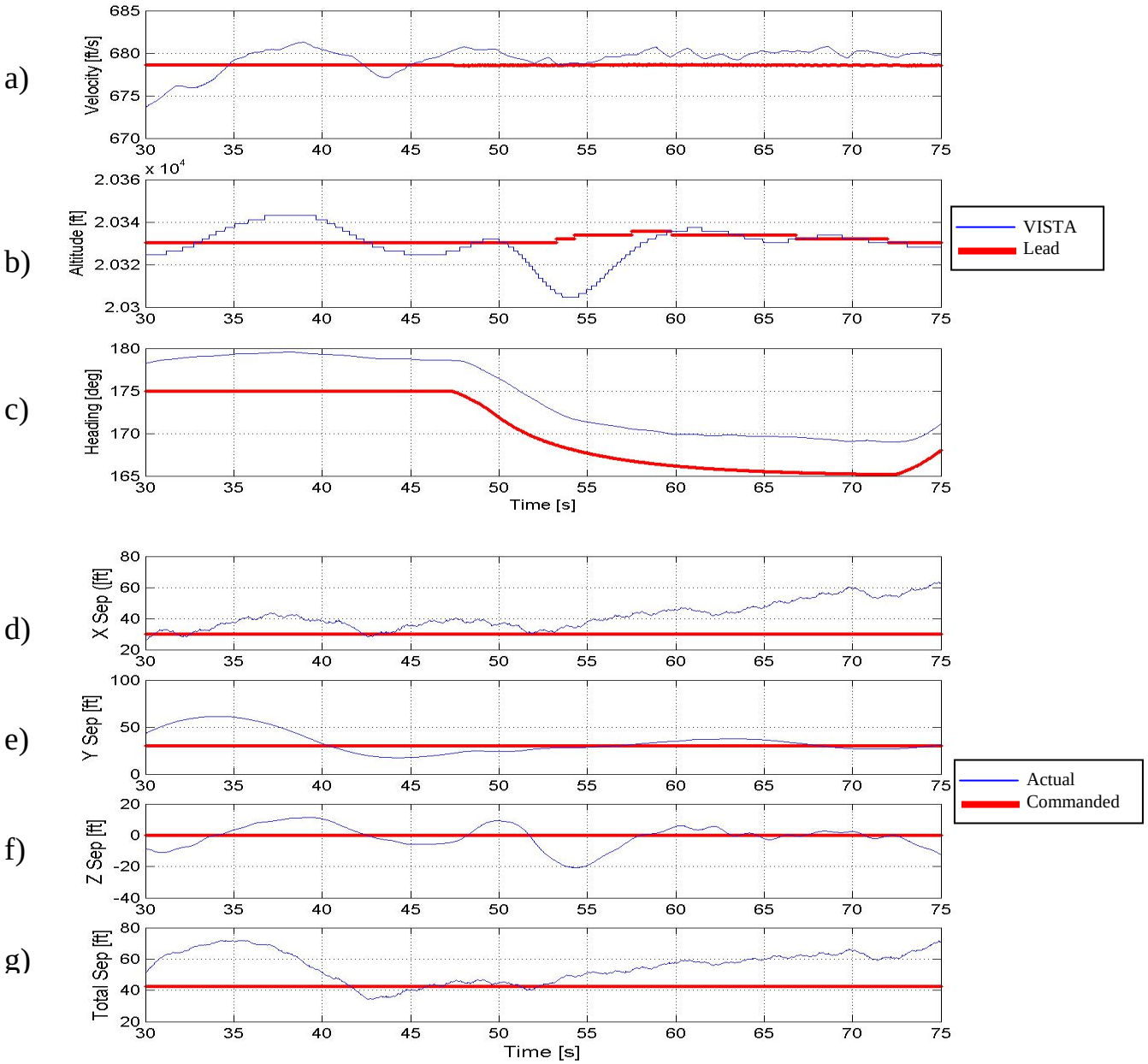

Data Basis: Flight Test; Test A/C: NF-16D #86-00048;
Engine: F110-GE-100; Configuration: Cruise, FCL; Test Date: 25Oct04

	X	Y	Z	Total Separation
Maximum Error (feet)	33.5	31.4	20.7	29.5
Time of maximum error (seconds)	74.9	34.0	54.3	34.3
Lead Maneuver	Turns left 10 degrees while VISTA is commanded to maintain standard position (30 30 0)			

Figure 59. Event 5A Run 1 (Sortie 1 Record 8)

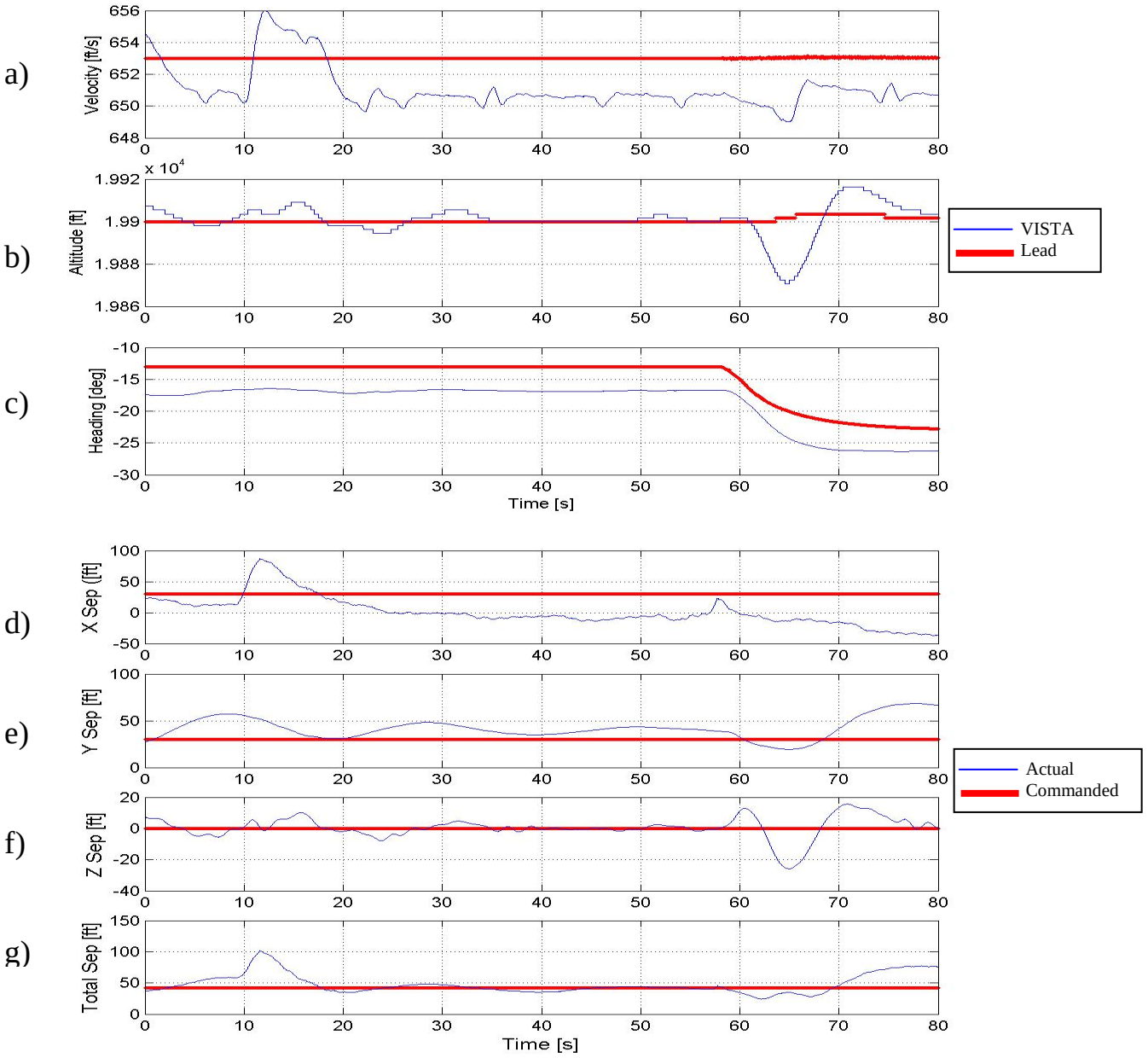

Data Basis: Flight Test; Test A/C: NF-16D #86-00048;
Engine: F110-GE-100; Configuration: Cruise, FCL; Test Date: 27Oct04

		X	Y	Z	Total Separation
Maximum Error (feet)		67.4	38.6	25.9	59.0
Time of maximum error (seconds)		79.6	77.8	65.0	11.6
Lead Maneuver	Turns left 10 degrees while VISTA is commanded to maintain standard position (30 30 0)				

Figure 60. Event 5A Run 2 (Sortie 4 Record 1)

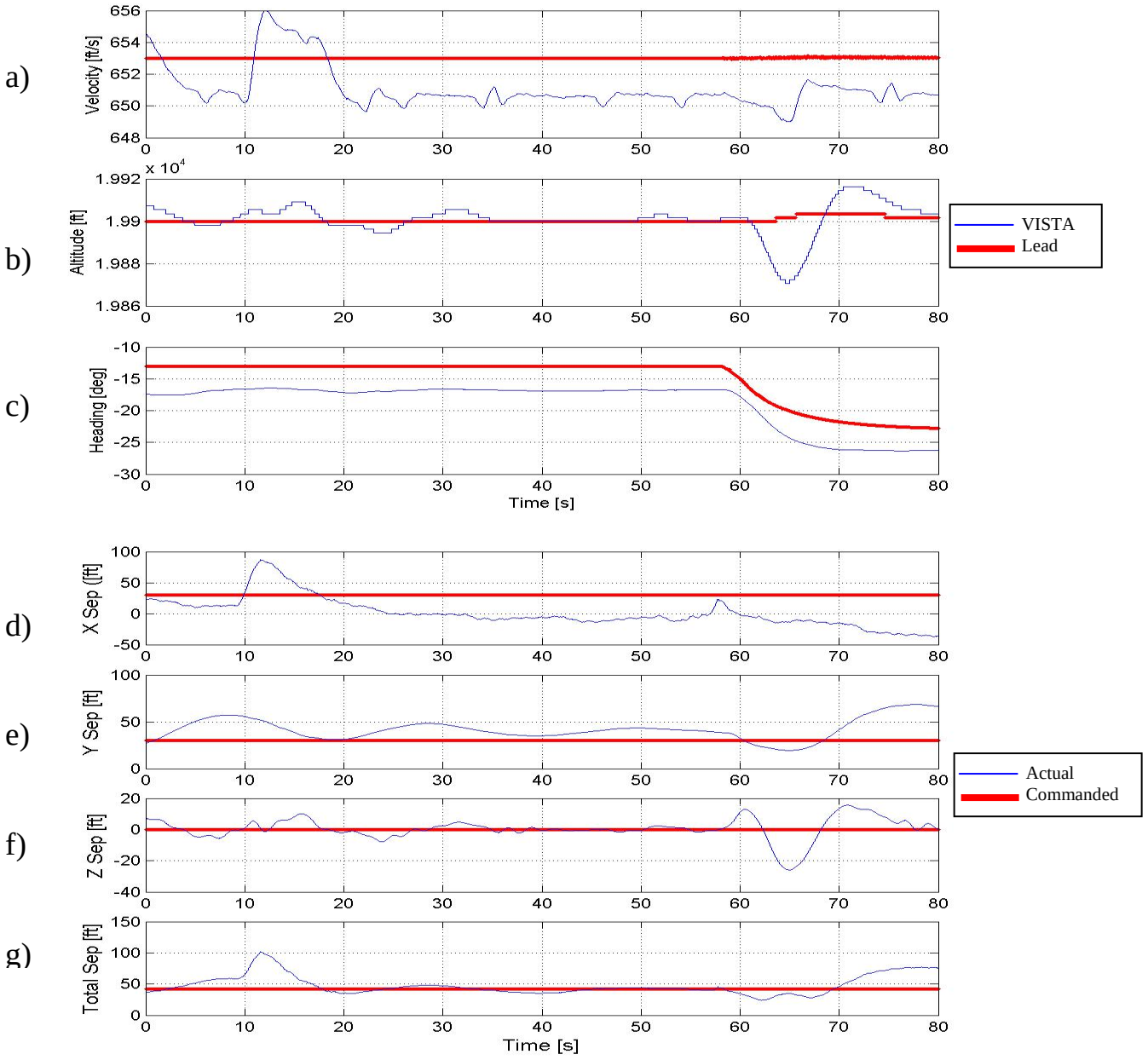

Data Basis: Flight Test; Test A/C: NF-16D #86-00048;
Engine: F110-GE-100; Configuration: Cruise, FCL; Test Date: 25Oct04

	X	Y	Z	Total Separation
Maximum Error (feet)	76.7	24.7	32.9	66.6
Time of maximum error (seconds)	41.8	33.0	23.5	41.8
Lead Maneuver	Turns left 20 degrees while VISTA is commanded to maintain standard position (30 30 0)			

Figure 61. Event 5B Run 1 (Sortie 1 Record 10)

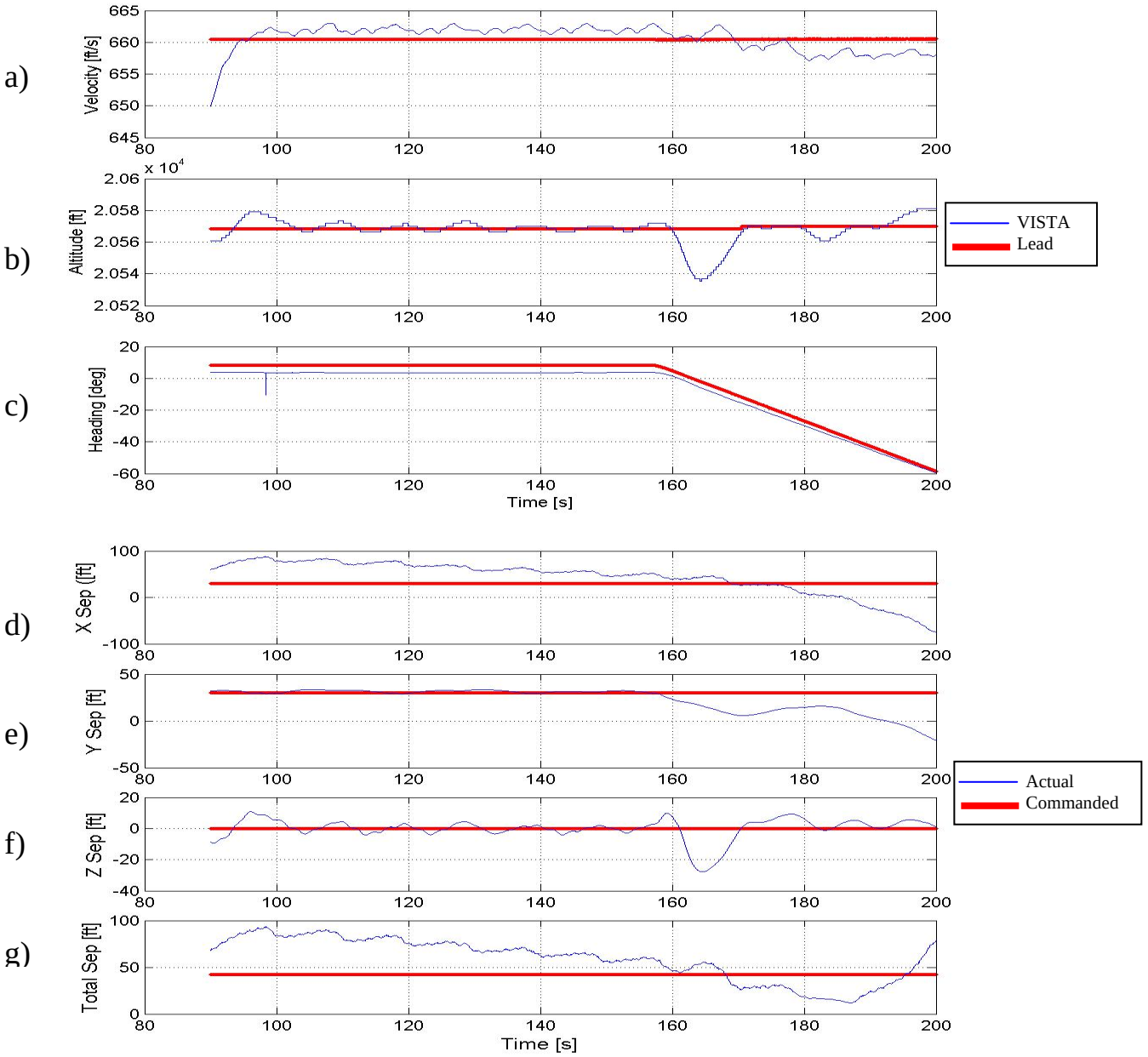

Data Basis: Flight Test; Test A/C: NF-16D #86-00048;
Engine: F110-GE-100; Configuration: Cruise, FCL; Test Date: 25Oct04

	X	Y	Z	Total Separation
Maximum Error (feet)	105.3	50.8	27.7	50.9
Time of maximum error (seconds)	200.0	200.0	164.7	98.3
Lead Maneuver	Turns left 30 degrees while VISTA is commanded to maintain standard position (30 30 0)			

Figure 62. Event 5C Run 1 (Sortie 1 Record 3)

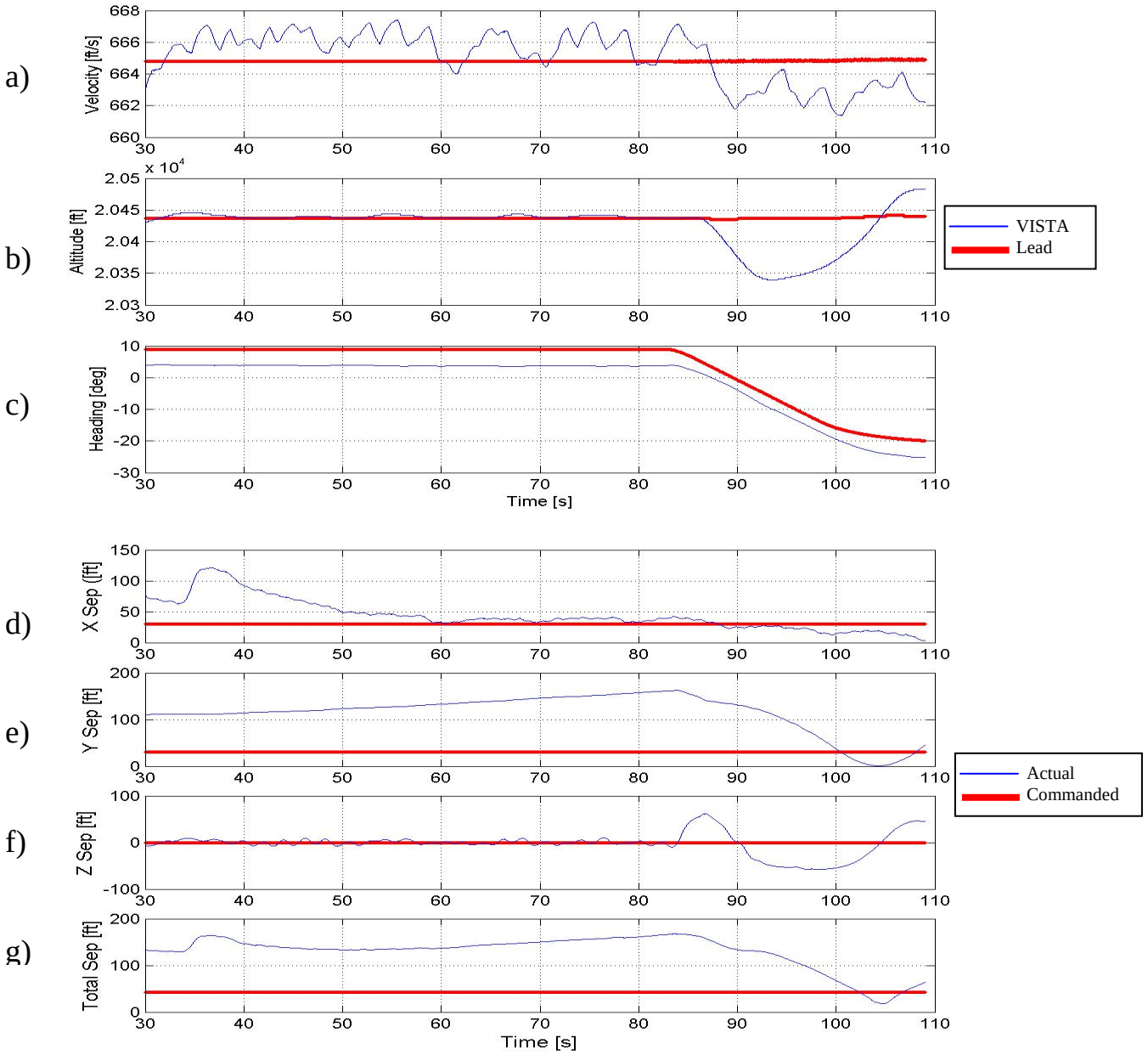

Data Basis: Flight Test; Test A/C: NF-16D #86-00048;
Engine: F110-GE-100; Configuration: Cruise, FCL; Test Date: 25Oct04

	X	Y	Z	Total Separation
Maximum Error (feet)	92.0	132.5	61.4	125.4
Time of maximum error (seconds)	36.8	83.9	86.8	83.6
Lead Maneuver	Turns left 30 degrees while VISTA is commanded to maintain standard position (30 30 0)			

Figure 63. Event 5C Run 2 (Sortie 1 Record 13)

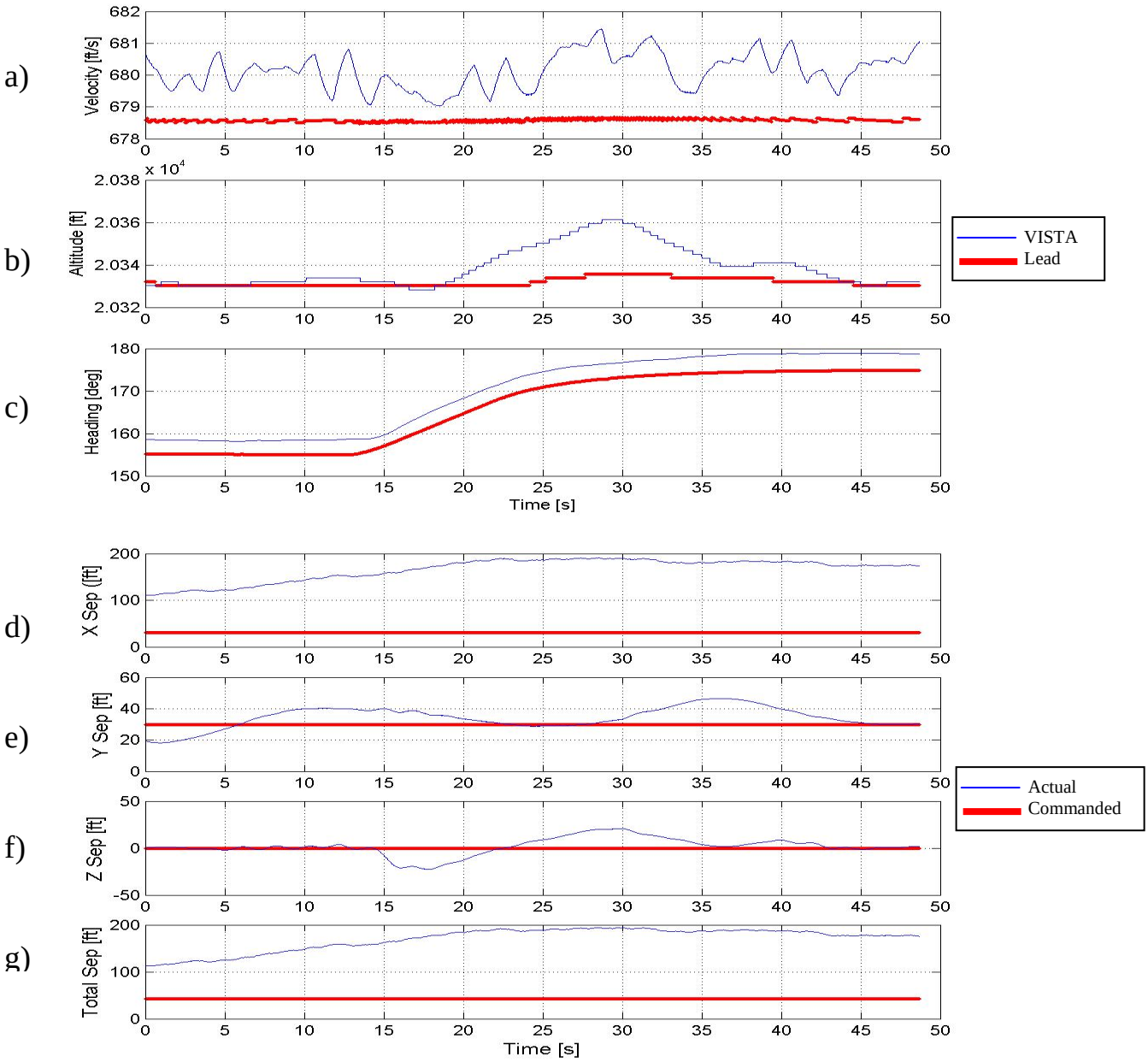

Data Basis: Flight Test; Test A/C: NF-16D #86-00048;
Engine: F110-GE-100; Configuration: Cruise, FCL; Test Date: 25Oct04

		X	Y	Z	Total Separation
Maximum Error (feet)		160.8	16.5	22.9	151.9
Time of maximum error (seconds)		28.5	36.0	17.7	28.5
Lead Maneuver	Turns right 20 degrees while VISTA is commanded to maintain standard position (30 30 0)				

Figure 64. Event 5E Run 1 (Sortie 1 Record 11)

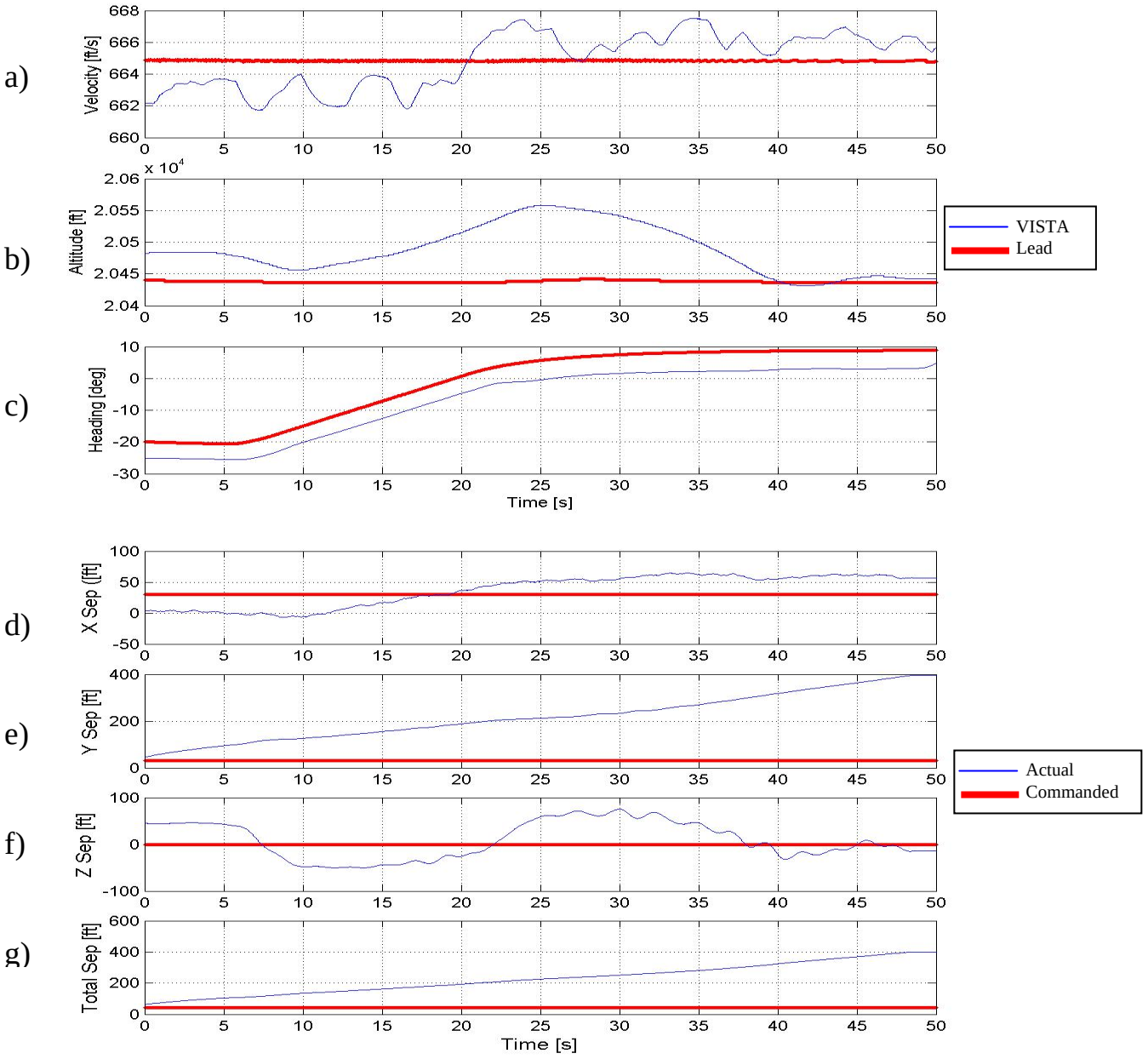

Data Basis: Flight Test; Test A/C: NF-16D #86-00048;
Engine: F110-GE-100; Configuration: Cruise, FCL; Test Date: 25Oct04

	X	Y	Z	Total Separation
Maximum Error (feet)	37.0	366.5	75.2	358.3
Time of maximum error (seconds)	8.7	48.5	29.9	48.5
Lead Maneuver	Turns right 30 degrees while VISTA is commanded to maintain standard position (30 30 0)			

Figure 65. Event 5F Run 1 (Sortie 1 Record 14)

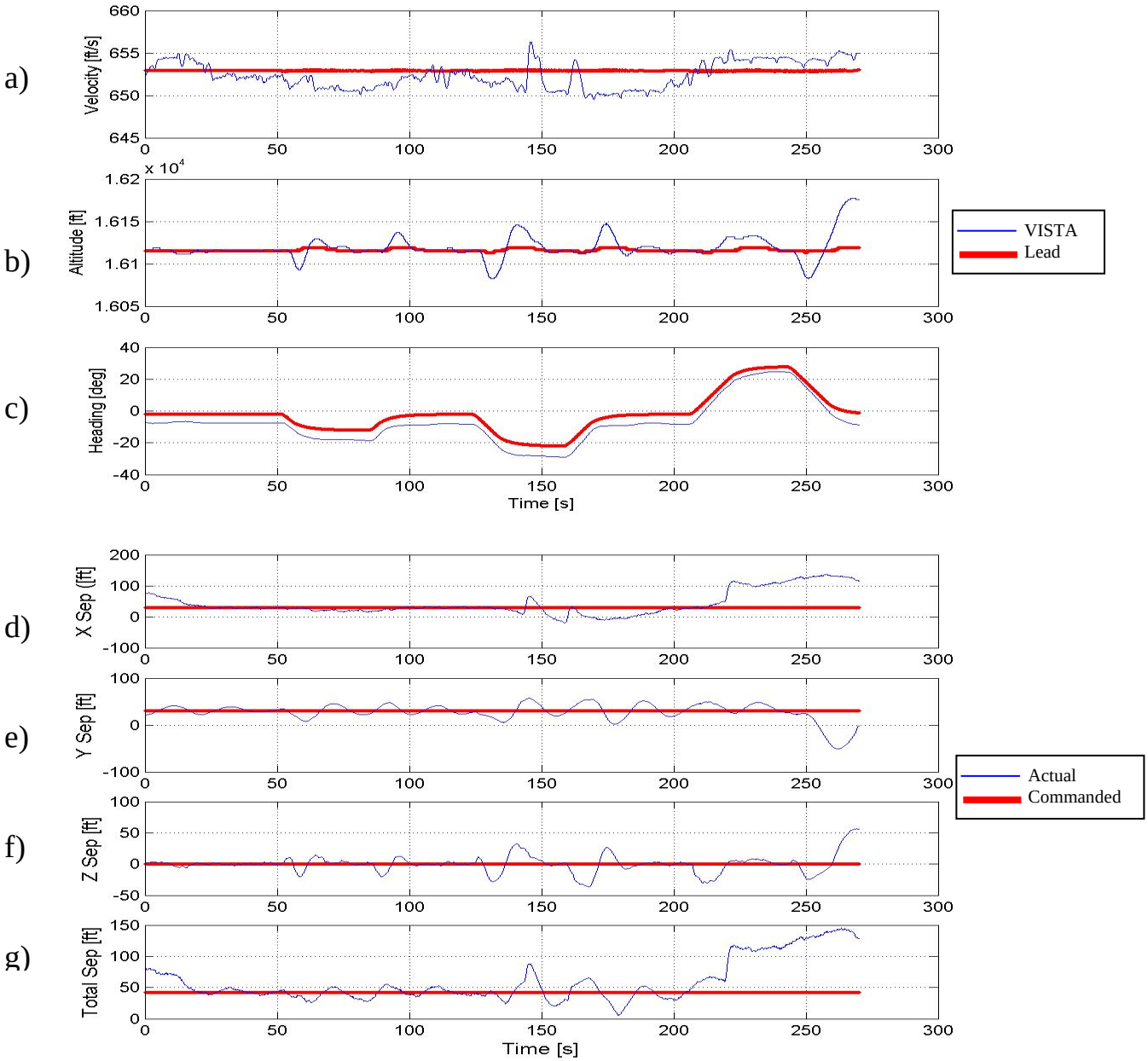

Data Basis: Flight Test; Test A/C: NF-16D #86-00048;
Engine: F110-GE-100; Configuration: Cruise, FCL; Test Date: 26Oct04

	X	Y	Z	Total Separation
Maximum Error (feet)	106.4	80.9	56.5	102.6
Time of maximum error (seconds)	258.1	262.0	269.3	263.4
Lead Maneuver	Turns left 10, right 10, left 20, right 20, left 30, and right 30degrees while VISTA is commanded to maintain standard position (30 30 0)			

Figure 66. Event 5A-F Run 2 (Sortie 3 Record 12)

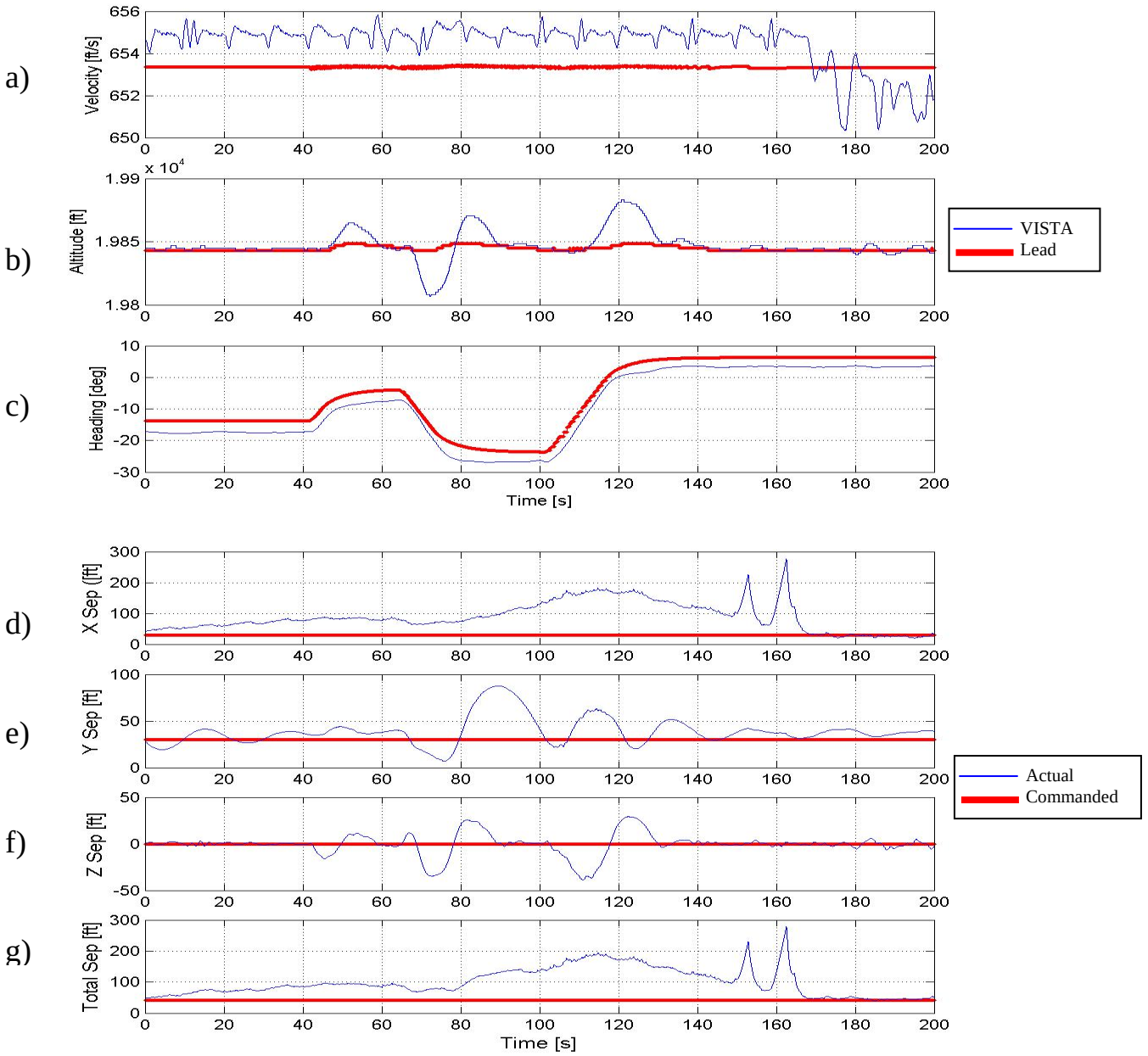

Data Basis: Flight Test; Test A/C: NF-16D #86-00048;
Engine: F110-GE-100; Configuration: Cruise, FCL; Test Date: 27Oct04

	X	Y	Z	Total Separation
Maximum Error (feet)	246.2	57.5	38.8	236.2
Time of maximum error (seconds)	162.6	89.3	111.0	162.6

Lead Maneuver	Turns left 20 degrees, right 10 degrees, right 30 degrees while VISTA is commanded to maintain standard position (30 30 0)

Figure 67. Event 5B,D,F Run 3 (Sortie 4 Record 3)

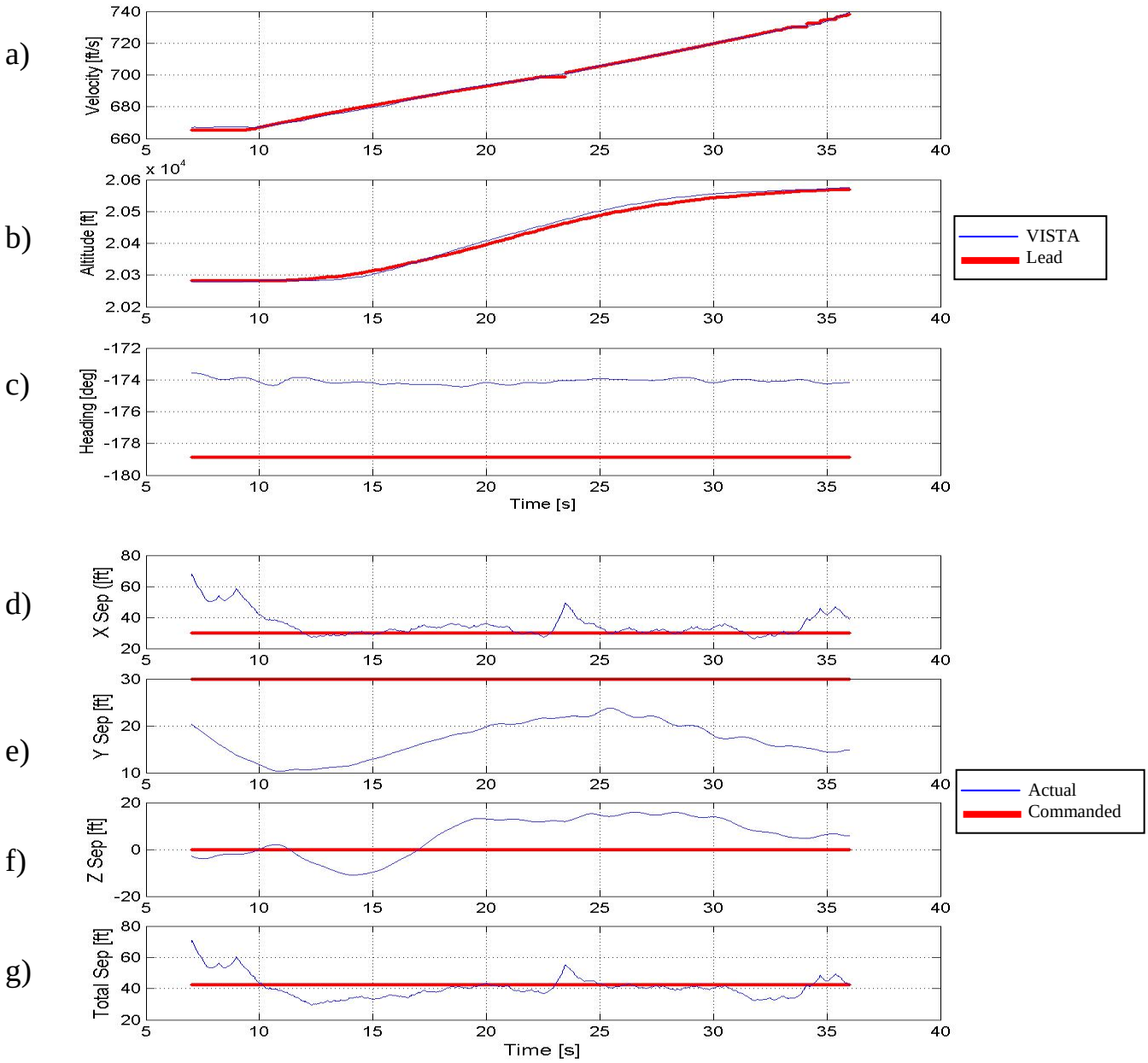

Data Basis: Flight Test; Test A/C: NF-16D #86-00048;
Engine: F110-GE-100; Configuration: Cruise, FCL; Test Date: 25Oct04

	X	Y	Z	Total Separation
Maximum Error (feet)	37.9	19.7	15.9	28.5
Time of maximum error (seconds)	7.0	10.8	26.6	7.0
Lead Maneuver	Climbs 300 feet and accelerates 50 knots while VISTA is commanded to maintain standard position (30 30 0)			

Figure 68. Event 6A Run 1 (Sortie 1 Record 37)

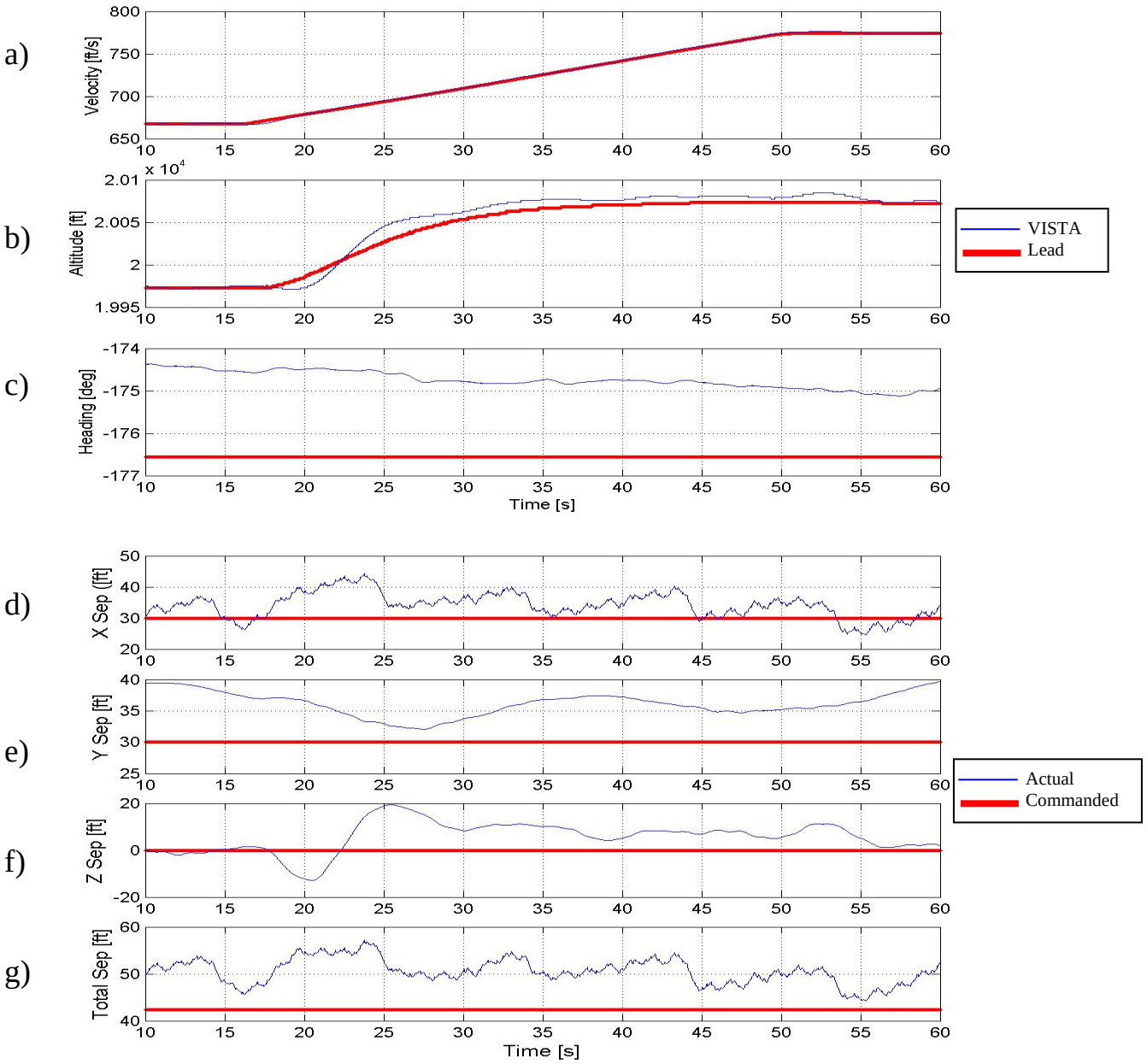

Data Basis: Flight Test; Test A/C: NF-16D #86-00048;
Engine: F110-GE-100; Configuration: Cruise, FCL; Test Date: 27Oct04

	X	Y	Z	Total Separation
Maximum Error (feet)	14.3	9.7	19.4	14.8
Time of maximum error (seconds)	23.8	60.0	25.4	23.8
Lead Maneuver	Climbs 100 feet and accelerates 50 knots while VISTA is commanded to maintain standard position (30 30 0)			

Figure 69. Event 6A Run 2 (Sortie 4 Record 7)

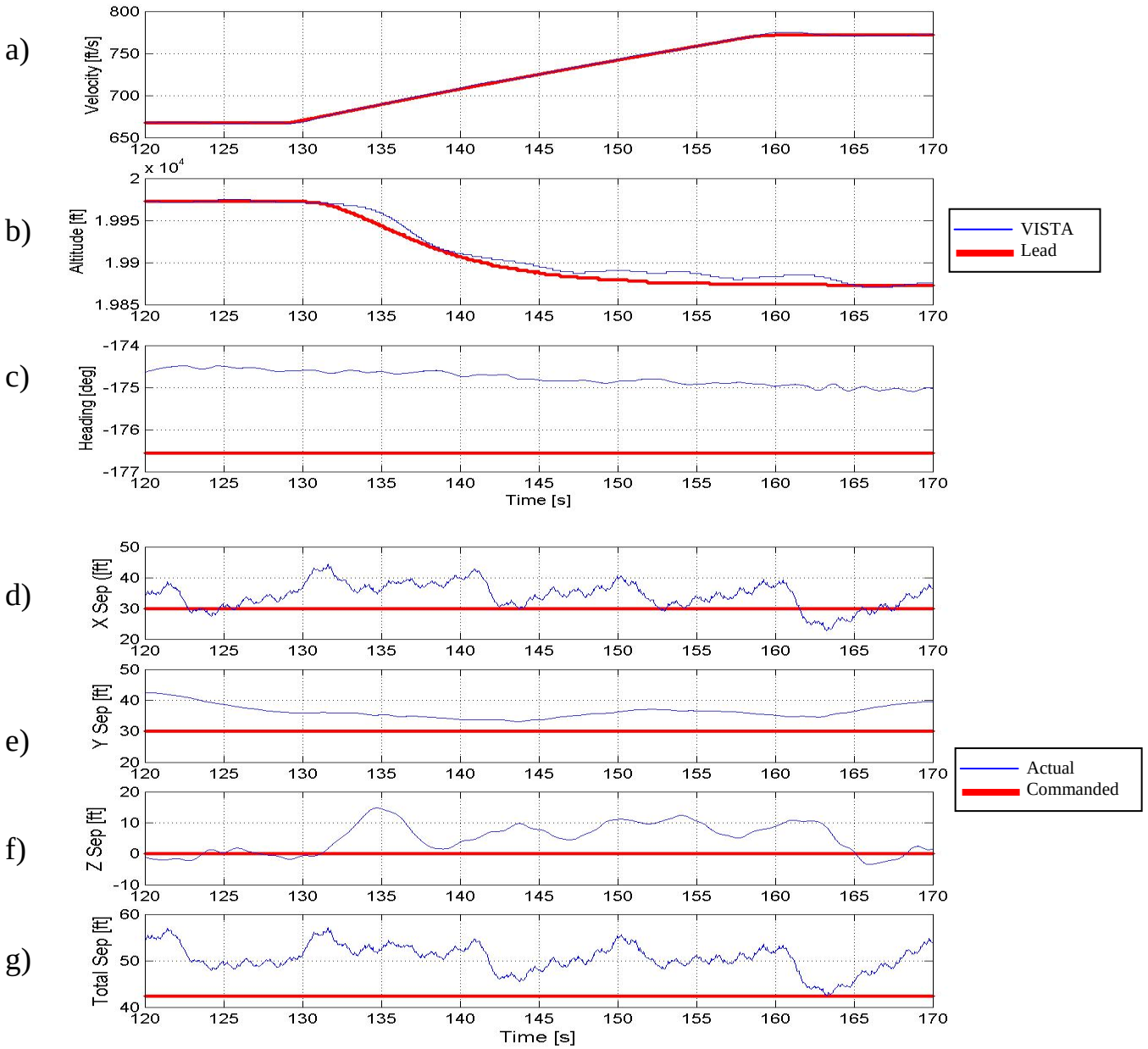

Data Basis: Flight Test; Test A/C: NF-16D #86-00048;
Engine: F110-GE-100; Configuration: Cruise, FCL; Test Date: 27Oct04

	X	Y	Z	Total Separation
Maximum Error (feet)	14.3	12.5	14.8	14.7
Time of maximum error (seconds)	131.6	120.0	134.8	131.6
Lead Maneuver	Descends 100 feet and accelerates 50 knots while VISTA is commanded to maintain standard (30 30 0) position			

Figure 70. Event 7A Run 1 (Sortie 4 Record 7)

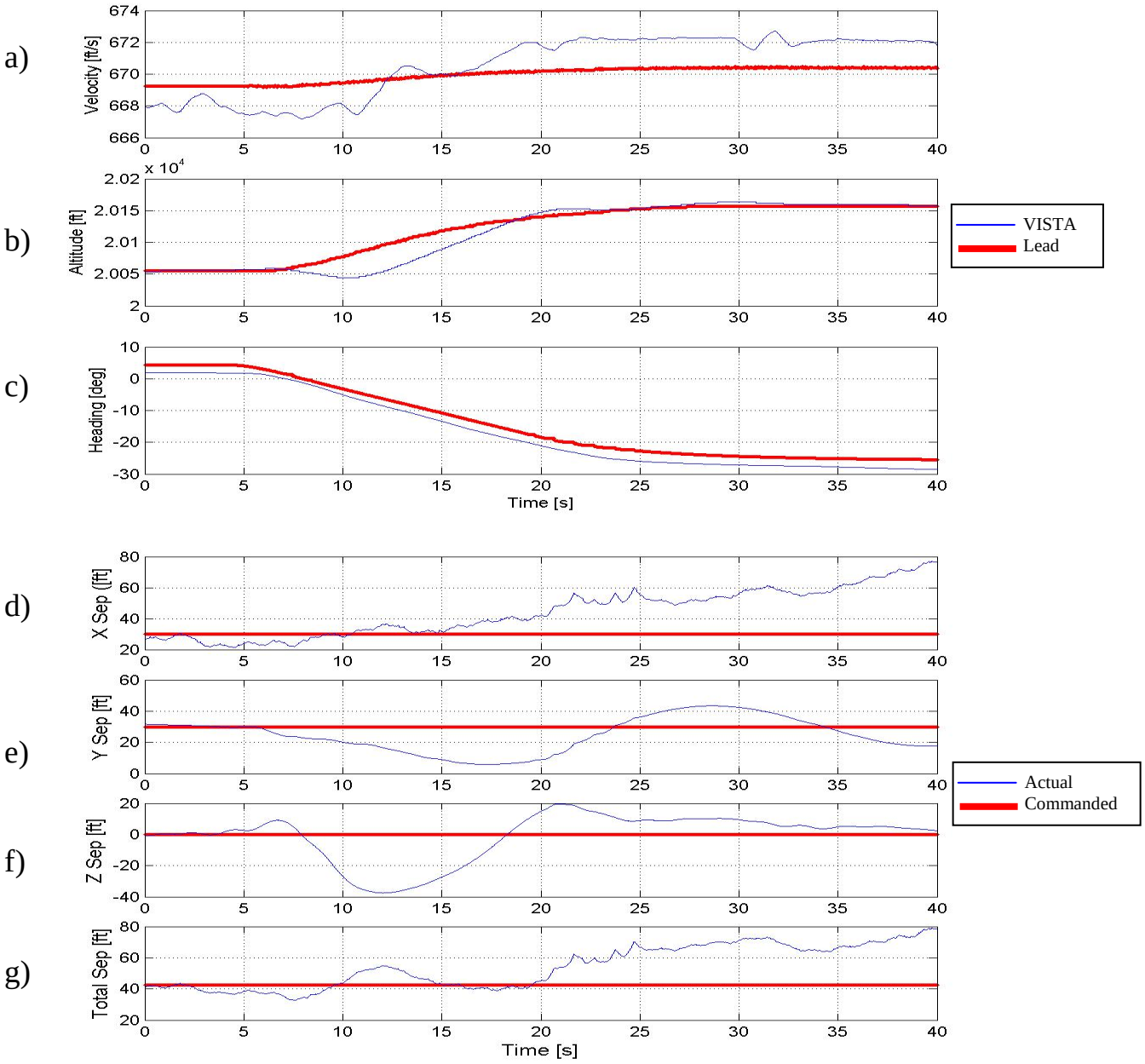

Data Basis: Flight Test; Test A/C: NF-16D #86-00048;
Engine: F110-GE-100; Configuration: Cruise, FCL; Test Date: 27Oct04

	X	Y	Z	Total Separation
Maximum Error (feet)	46.9	24.2	37.6	36.5
Time of maximum error (seconds)	39.6	17.3	12.0	39.6
Lead Maneuver	Climbs 100 feet and turns left 30 degrees while VISTA is commanded to maintain standard (30 30 0) position			

Figure 71. Event 8A Run 1 (Sortie 4 Record 8)

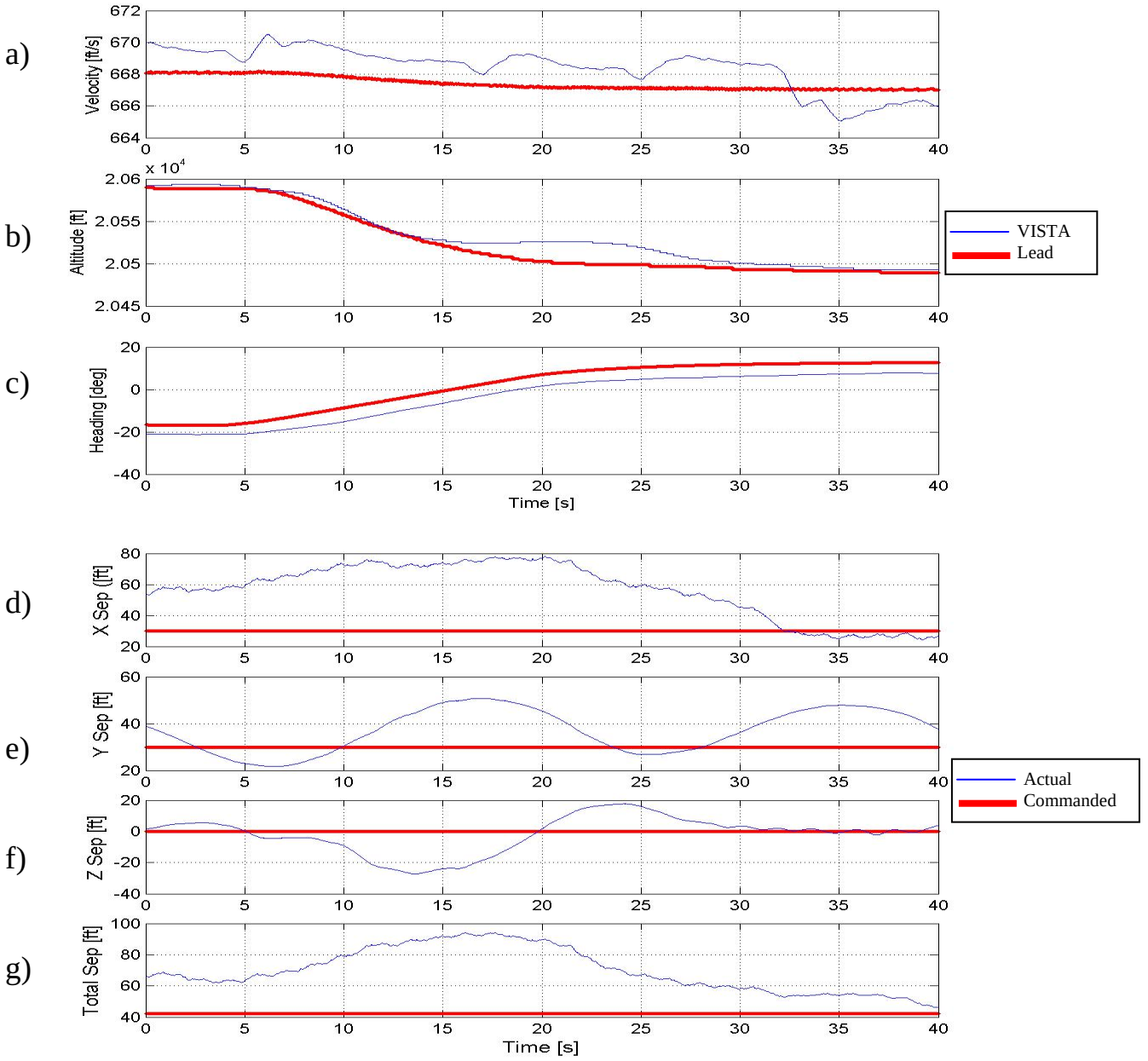

Data Basis: Flight Test; Test A/C: NF-16D #86-00048;
Engine: F110-GE-100; Configuration: Cruise, FCL; Test Date: 25Oct04

	X	Y	Z	Total Separation
Maximum Error (feet)	48.1	20.8	27.3	51.7
Time of maximum error (seconds)	20.2	16.8	13.5	17.4
Lead Maneuver	Descends 100 feet and turns right 30 degrees while VISTA is commanded to maintain standard (30 30 0) position			

Figure 72. Event 8B Run 1 (Sortie 1 Record 47)

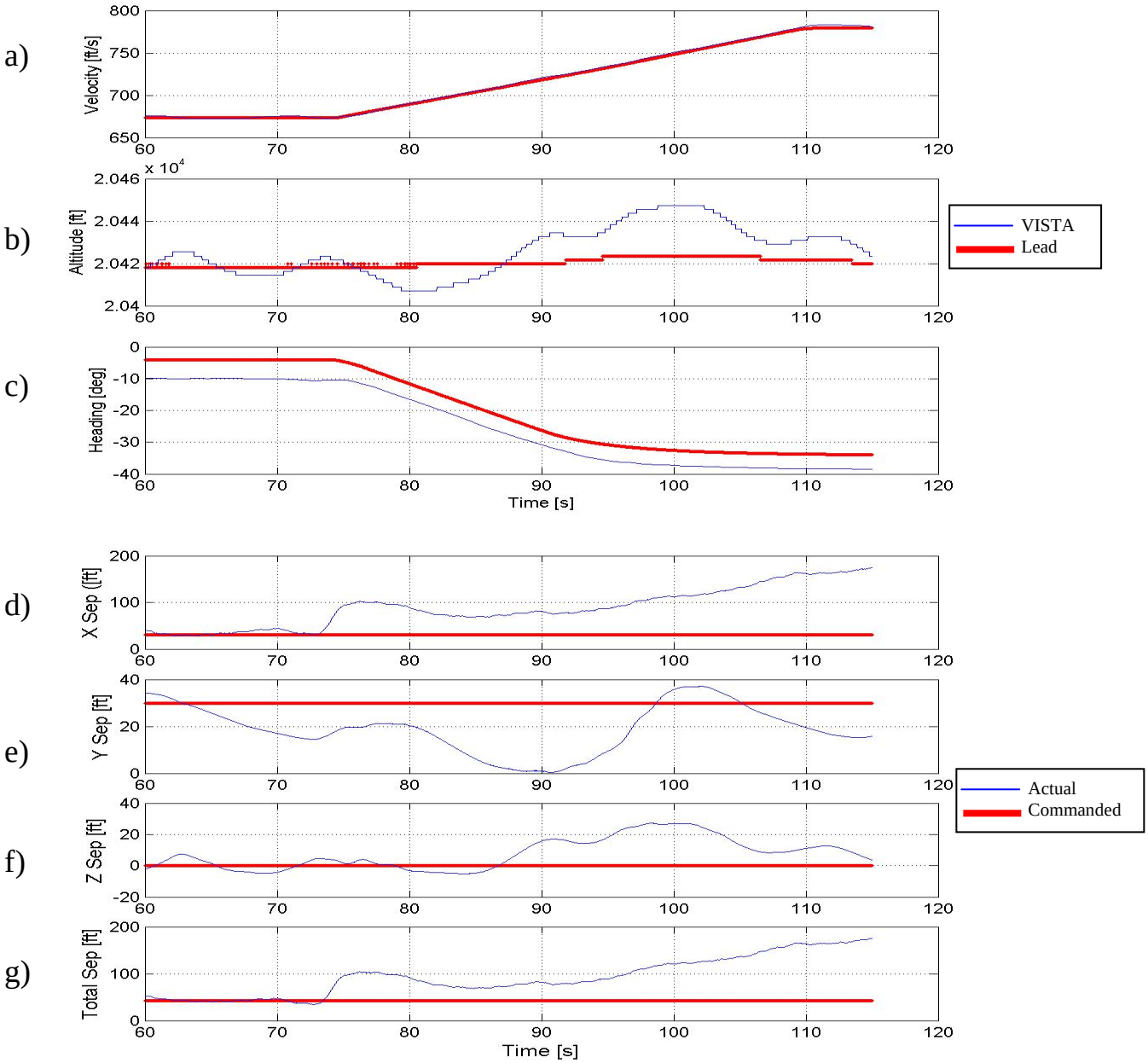

Data Basis: Flight Test; Test A/C: NF-16D #86-00048;
Engine: F110-GE-100; Configuration: Cruise, FCL; Test Date: 25Oct04

	X	Y	Z	Total Separation
Maximum Error (feet)	144.8	29.6	27.1	133.1
Time of maximum error (seconds)	115.0	90.8	98.3	115.0
Lead Maneuver	Accelerates 50 knots and turns left 30 degrees while VISTA is commanded to maintain standard (30 30 0) position			

Figure 73. Event 9A Run 1 (Sortie 2 Record 7)

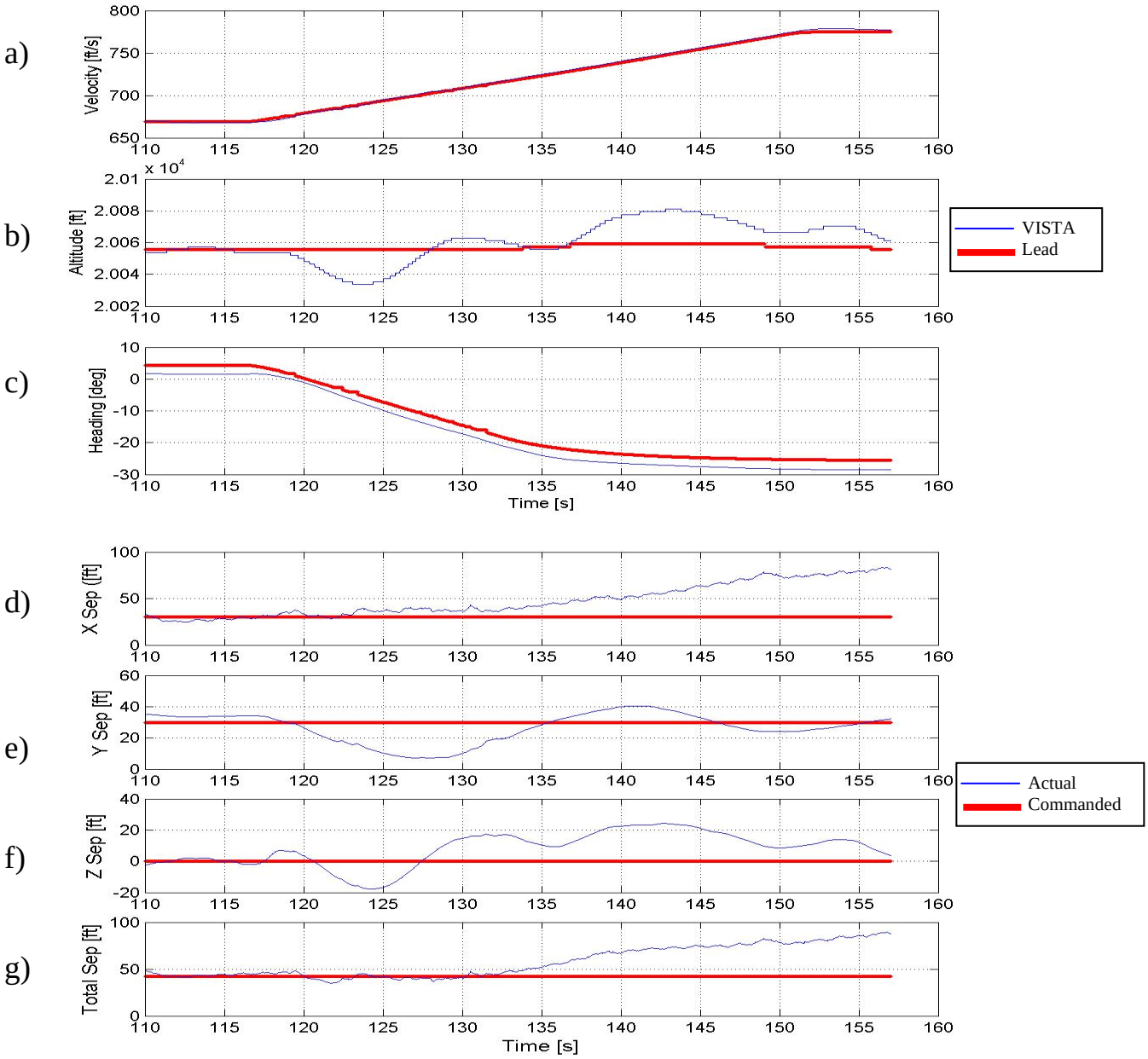

Data Basis: Flight Test; Test A/C: NF-16D #86-00048;
Engine: F110-GE-100; Configuration: Cruise, FCL; Test Date: 27Oct04

	X	Y	Z	Total Separation
Maximum Error (feet)	53.5	23.0	24.3	47.1
Time of maximum error (seconds)	156.8	127.1	142.7	156.8
Lead Maneuver	Accelerates 50 knots and turns left 30 degrees while VISTA is commanded to maintain standard (30 30 0) position			

Figure 74. Event 9A Run 2 (Sortie 4 Record 8)

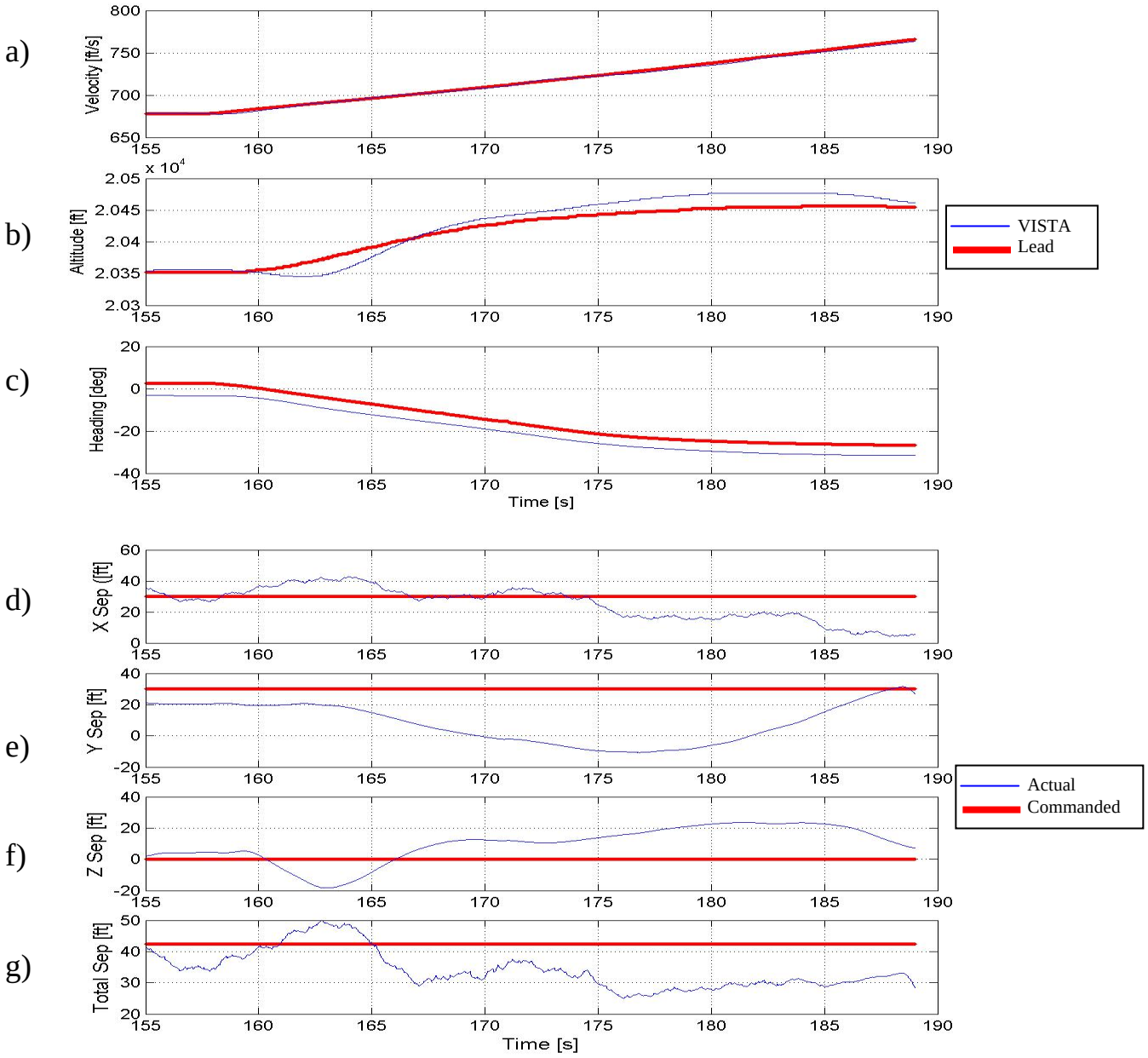

Data Basis: Flight Test; Test A/C: NF-16D #86-00048;
Engine: F110-GE-100; Configuration: Cruise, FCL; Test Date: 25Oct04

	X	Y	Z	Total Separation
Maximum Error (feet)	25.7	40.7	23.6	7.6
Time of maximum error (seconds)	187.9	176.7	181.5	162.8

Lead Maneuver	Climbs 100 feet, accelerates 50 knots, and turns left 30 degrees while VISTA is commanded to maintain standard (30 30 0) position

Figure 75. Event 10A Run 1 (Sortie 2 Record 10)

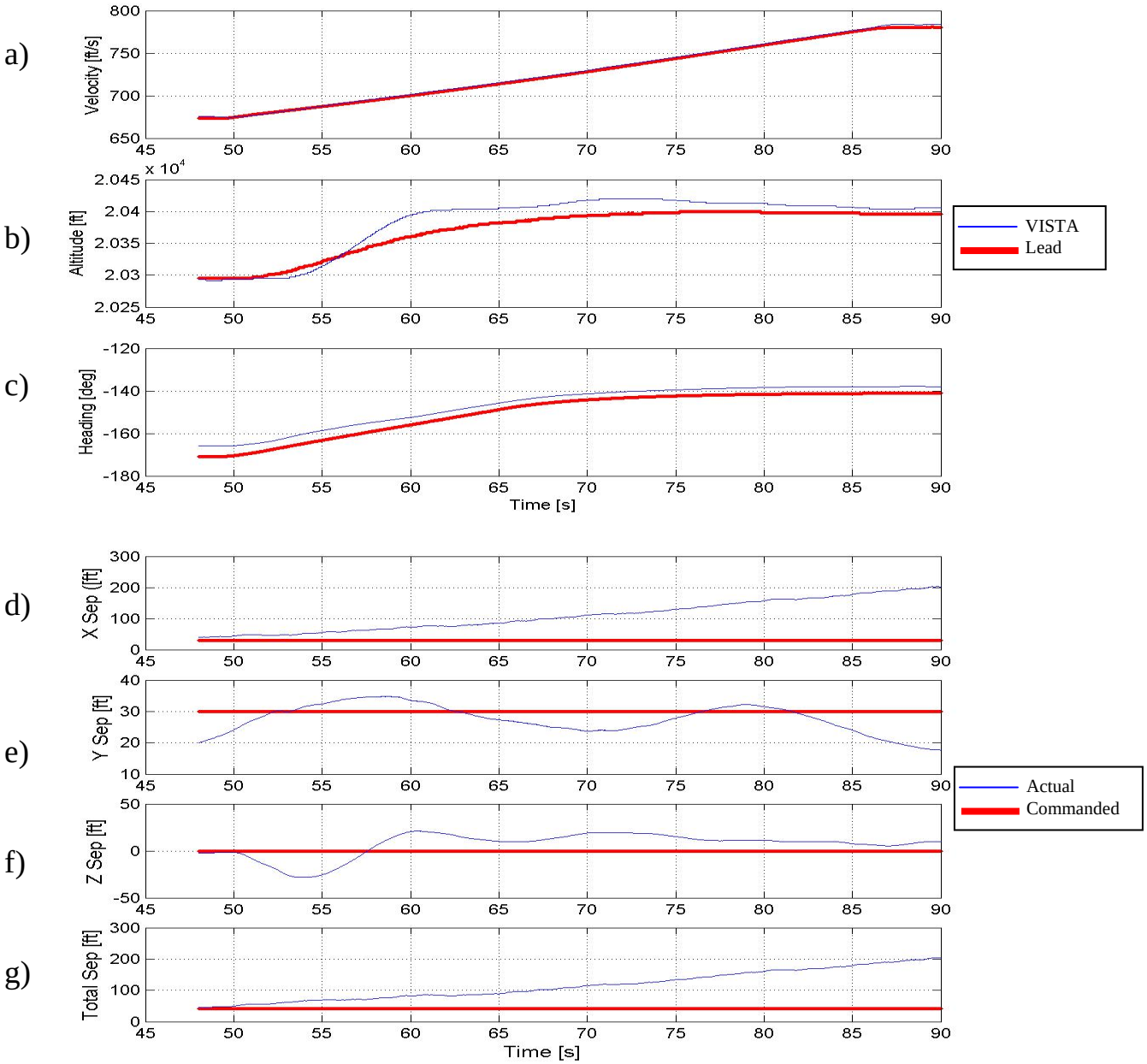

Data Basis: Flight Test; Test A/C: NF-16D #86-00048;
Engine: F110-GE-100; Configuration: Cruise, FCL; Test Date: 25Oct04

	X	Y	Z	Total Separation
Maximum Error (feet)	172.7	12.3	28.4	161.3
Time of maximum error (seconds)	89.8	90.0	53.8	89.8
Lead Maneuver	Climbs 100 feet, accelerates 50 knots, and turns right 30 degrees while VISTA is commanded to maintain standard (30 30 0) position			

Figure 76. Event 12A Run 1 (Sortie 2 Record 13)

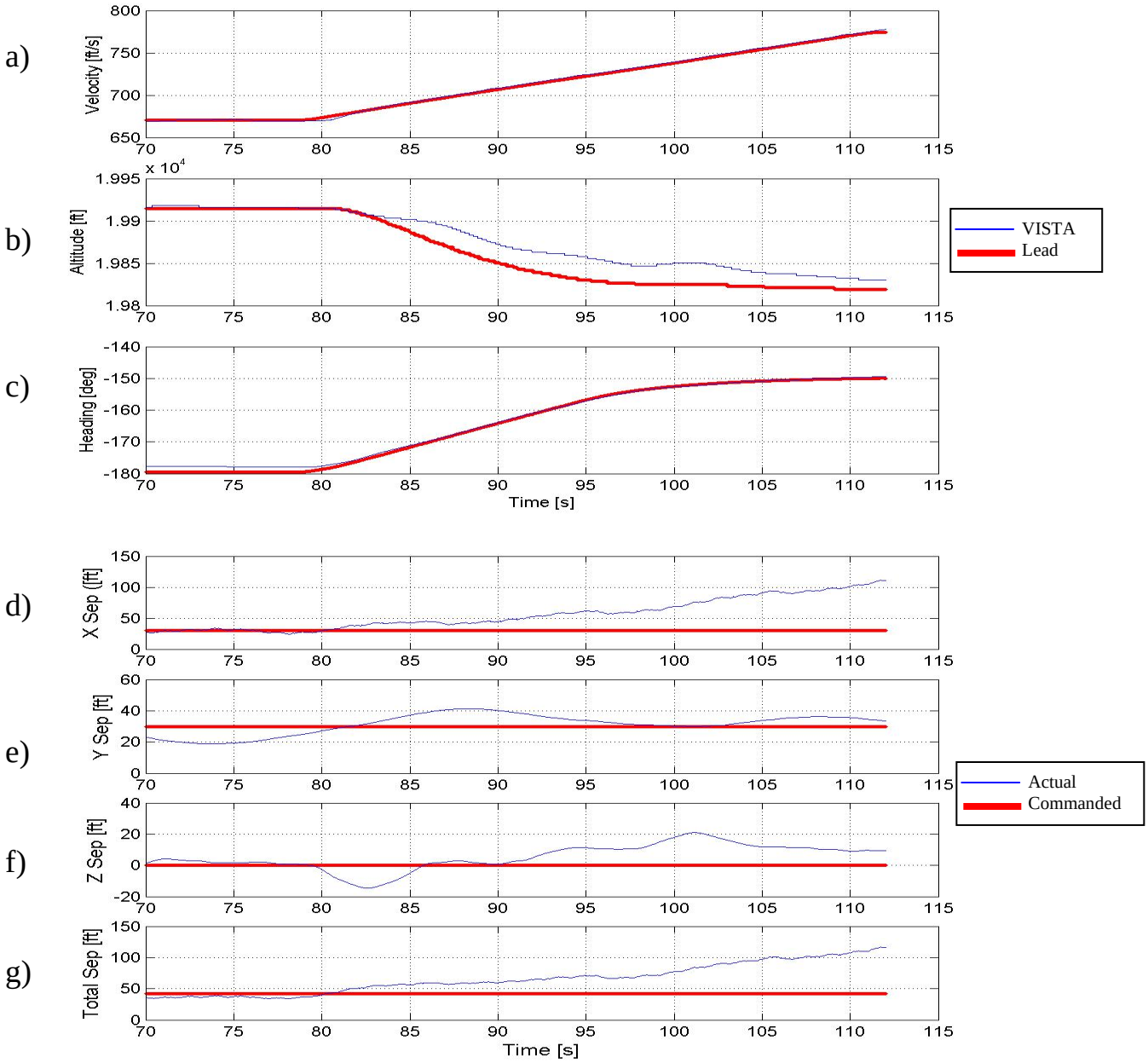

Data Basis: Flight Test; Test A/C: NF-16D #86-00048;
Engine: F110-GE-100; Configuration: Cruise, FCL; Test Date: 27Oct04

	X	Y	Z	Total Separation
Maximum Error (feet)	81.6	11.3	21.0	74.5
Time of maximum error (seconds)	111.7	88.6	101.2	111.7
Lead Maneuver	Descends 100 feet, accelerates 50 knots, and turns right 30 degrees while VISTA is commanded to maintain standard (30 30 0) position			

Figure 77. Event 12B Run 1 (Sortie 4 Record 13)

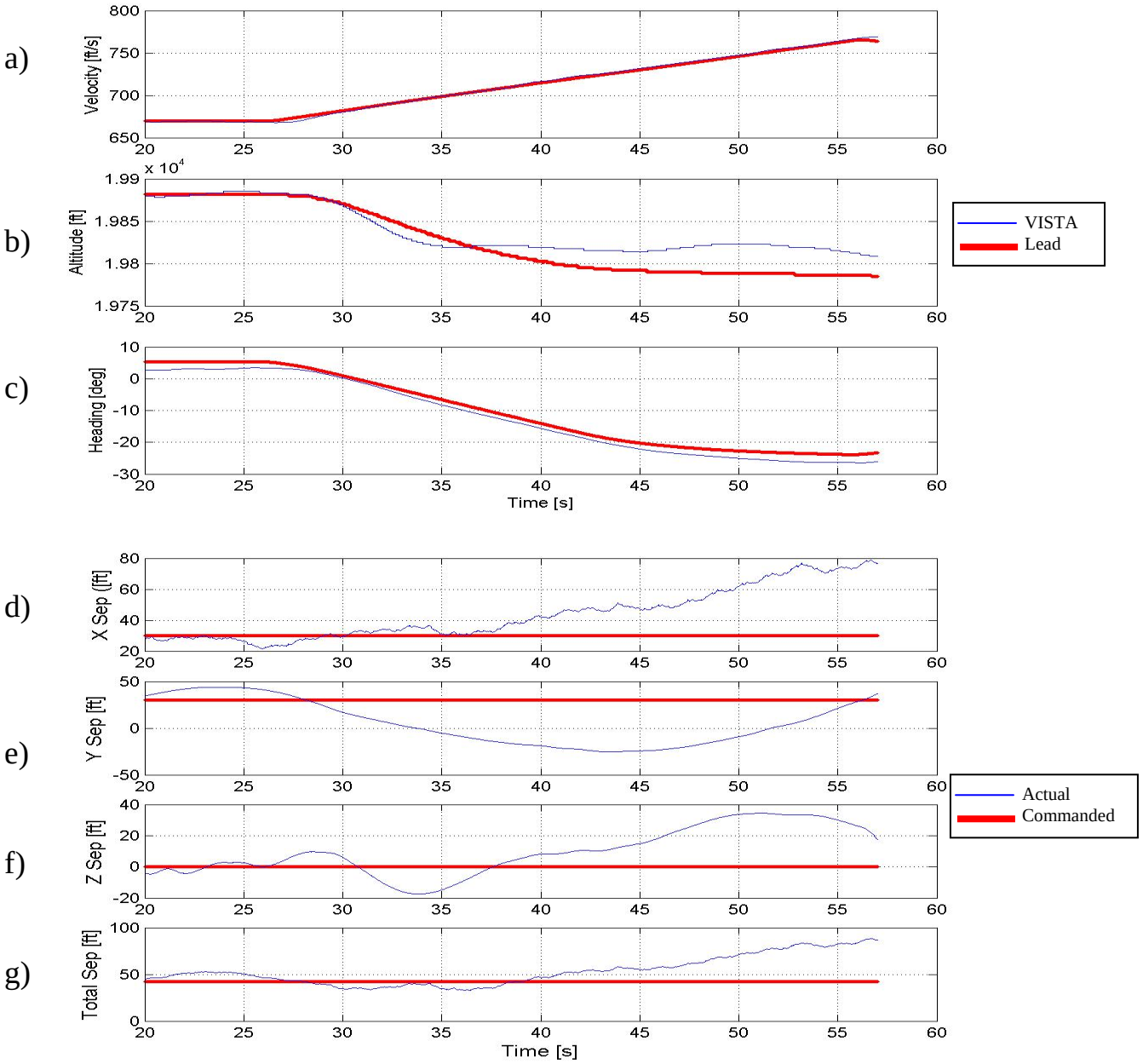

Data Basis: Flight Test; Test A/C: NF-16D #86-00048;
Engine: F110-GE-100; Configuration: Cruise, FCL; Test Date: 27Oct04

	X	Y	Z	Total Separation
Maximum Error (feet)	48.9	55.5	34.5	46.0
Time of maximum error (seconds)	56.7	43.4	51.1	56.7
Lead Maneuver	Descends 100 feet, accelerates 50 knots, and turns left 30 degrees while VISTA is commanded to maintain standard (30 30 0) position			

Figure 78. Event 13B Run 1 (Sortie 4 Record 14)

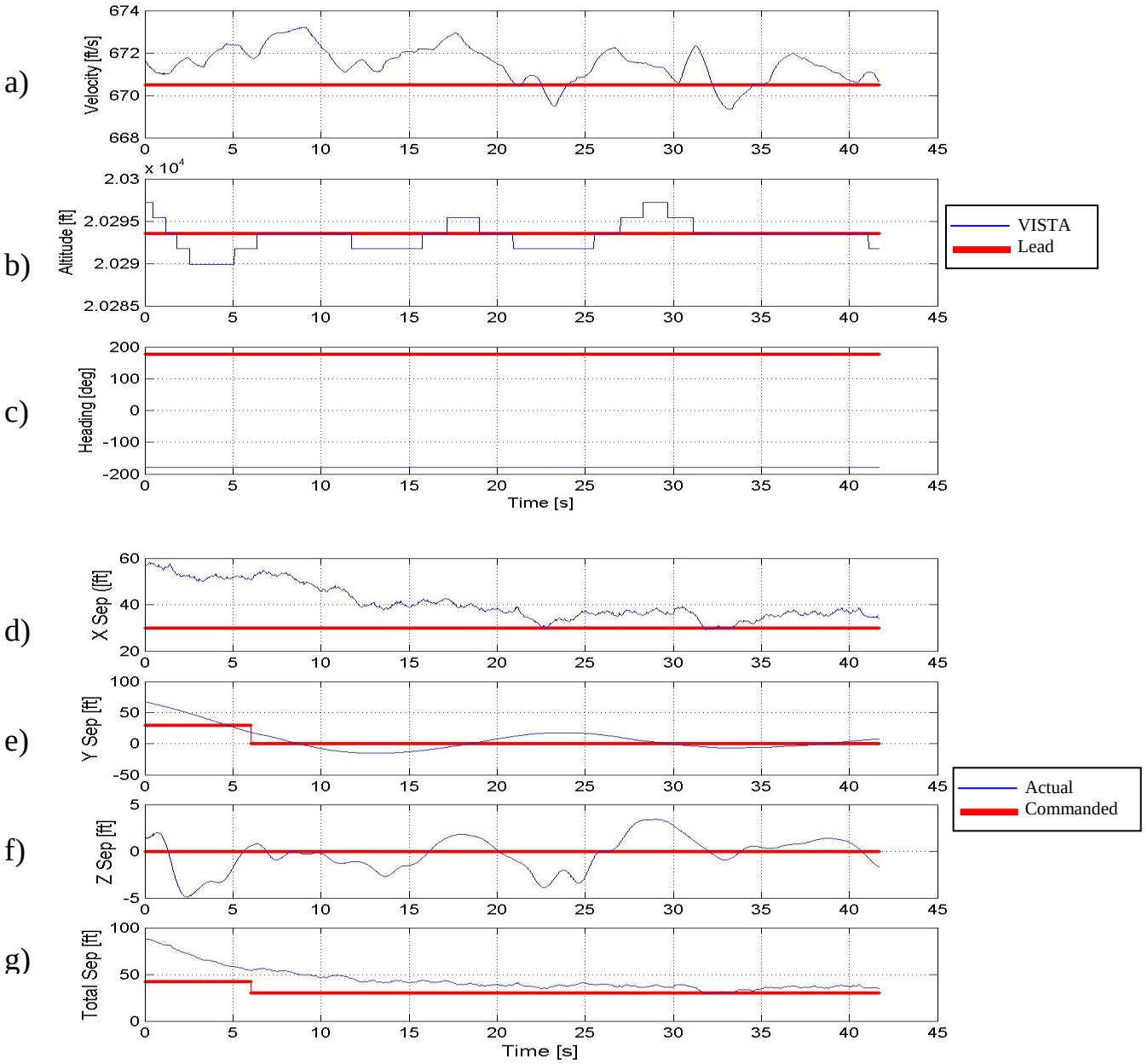

Data Basis: Flight Test; Test A/C: NF-16D #86-00048;
Engine: F110-GE-100; Configuration: Cruise, FCL; Test Date: 25Oct04

	X	Y	Z	Total Separation
Maximum Error (feet)	28.2	37.4	4.9	45.9
Time of maximum error (seconds)	0.3	0	2.4	0
Position Change	VISTA moves right 30 feet to (30 0 0) from standard position (30 30 0)			

Figure 79. Event 14A Run 1 (Sortie 1 Record 16)

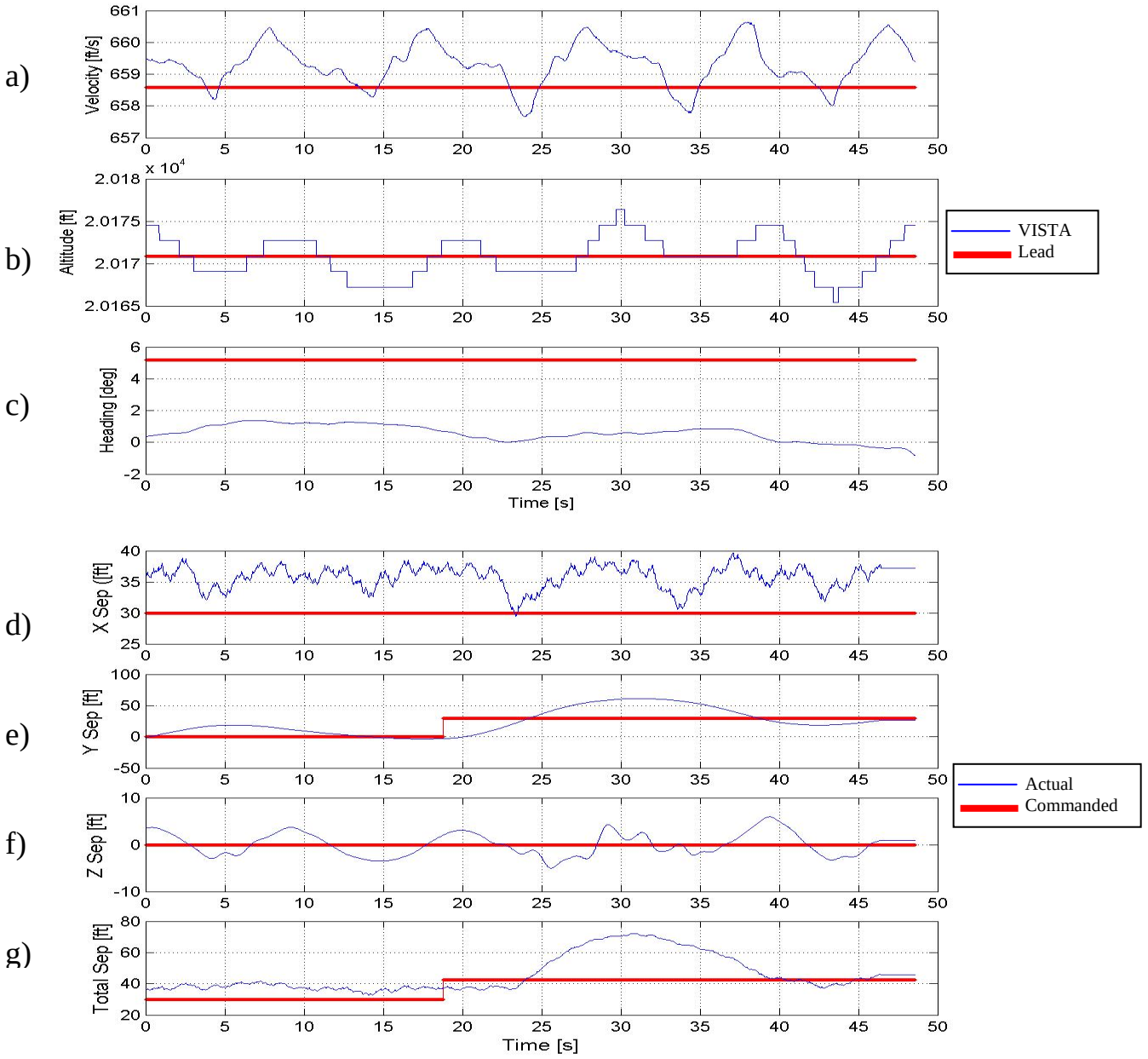

Data Basis: Flight Test; Test A/C: NF-16D #86-00048;
Engine: F110-GE-100; Configuration: Cruise, FCL; Test Date: 25Oct04

	X	Y	Z	Total Separation
Maximum Error (feet)	9.6	33.0	6.0	29.7
Time of maximum error (seconds)	37.0	18.8	39.4	30.8
Position Change	VISTA moves left 30 feet from (30 0 0) back to standard position (30 30 0)			

Figure 80. Event 14B Run 1 (Sortie 1 Record 21)

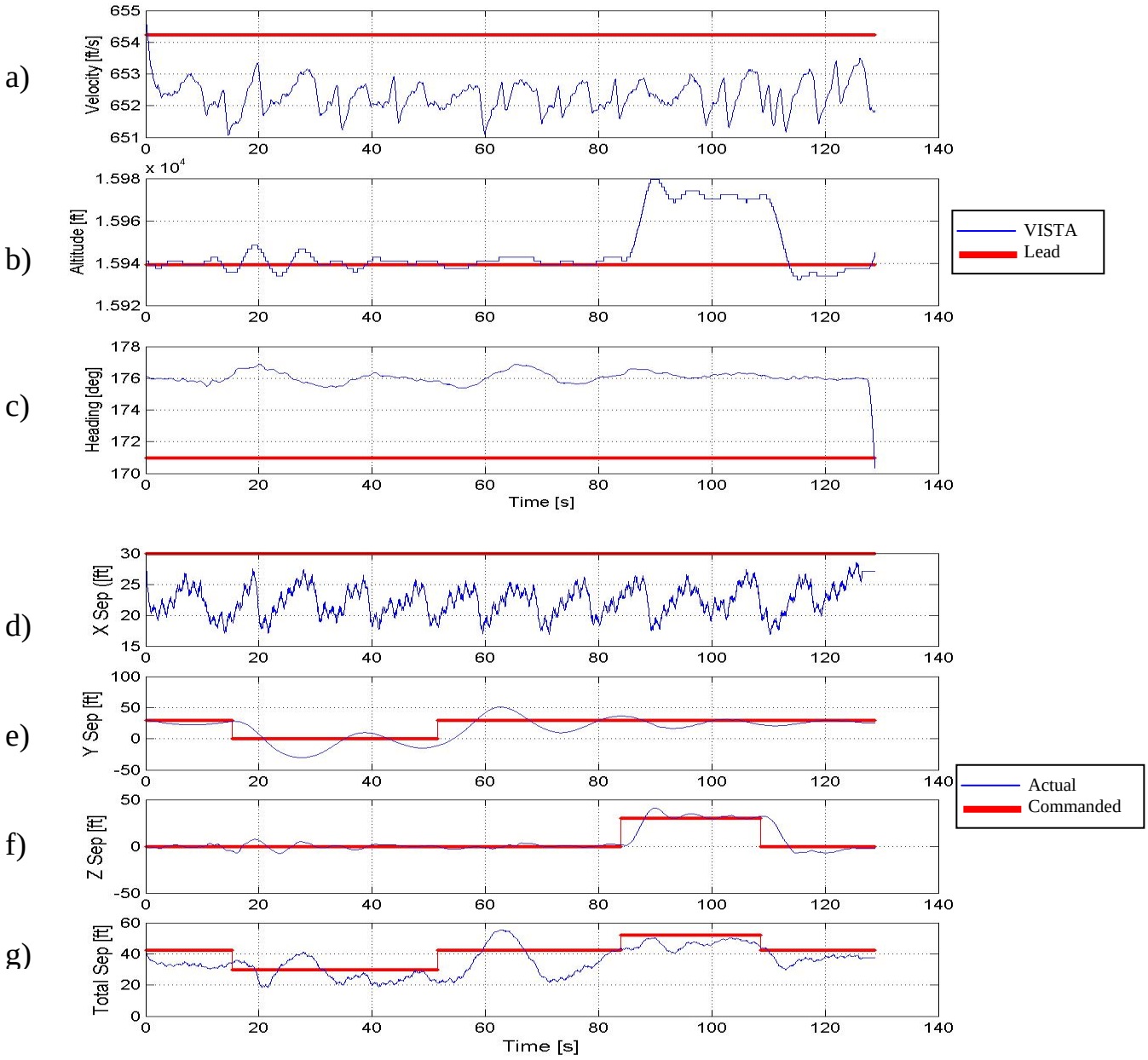

Data Basis: Flight Test; Test A/C: NF-16D #86-00048;
Engine: F110-GE-100; Configuration: Cruise, FCL; Test Date: 26Oct04

	X	Y	Z	Total Separation
Maximum Error (feet)	13.2	41.2	32.1	13.3
Time of maximum error (seconds)	71.3	51.5	108.8	62.8
Position Change	VISTA moves right 30 feet to (30 0 0) from standard position (30 30 0) and then back to standard position (30 30 0)			

Figure 81. Event 14A & B Run 2 (Sortie 3 Record 13)

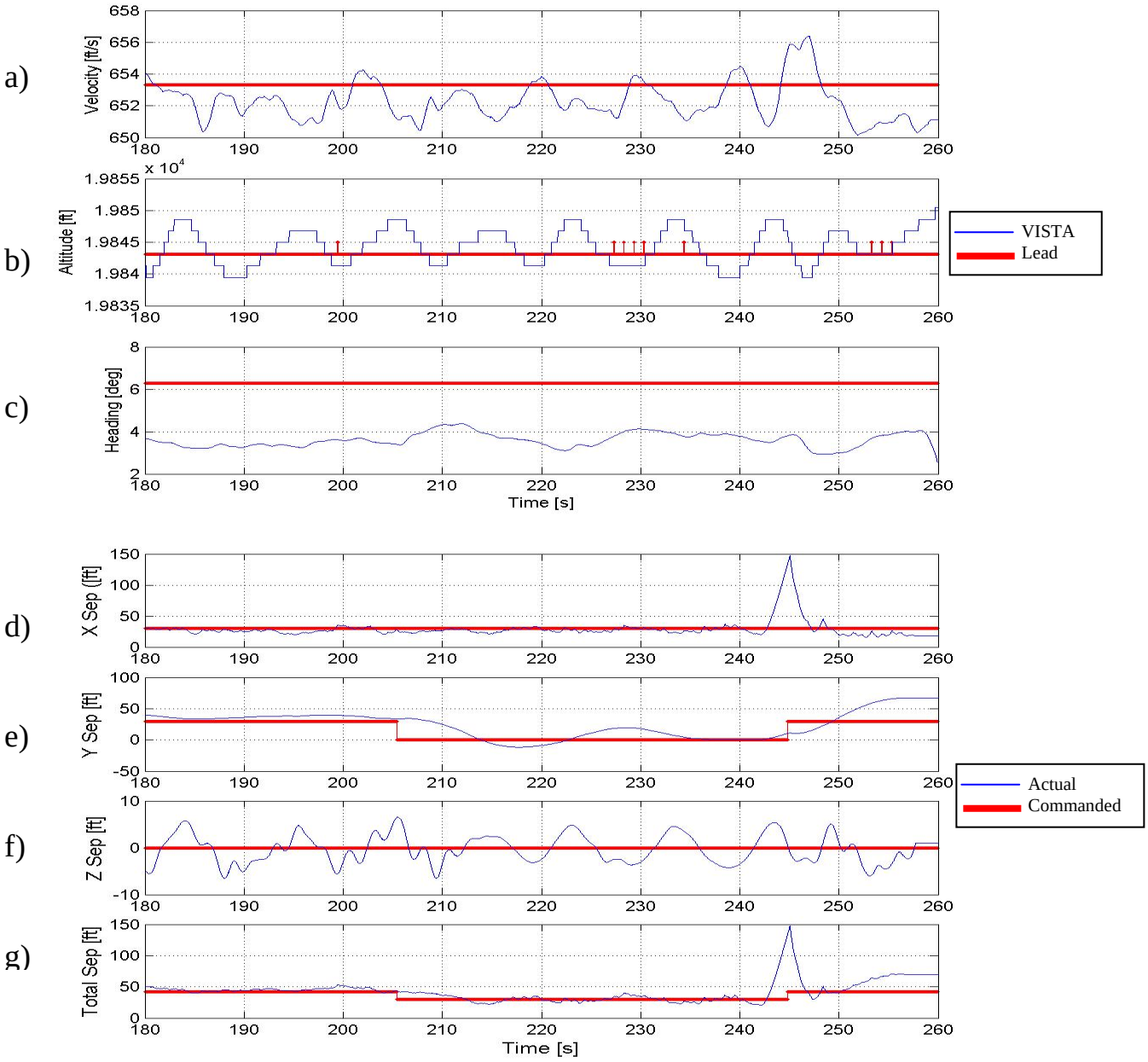

Data Basis: Flight Test; Test A/C: NF-16D #86-00048;
Engine: F110-GE-100; Configuration: Cruise, FCL; Test Date: 27Oct04

	X	Y	Z	Total Separation
Maximum Error (feet)	117.5	37.2	6.6	105.5
Time of maximum error (seconds)	245.0	256.7	188.0	245.0
Position Change	VISTA moves right 30 feet to (30 0 0) from standard position (30 30 0) and then back to standard position (30 30 0)			

Figure 82. Event 14A & B Run 3 (Sortie 4 Record 3)

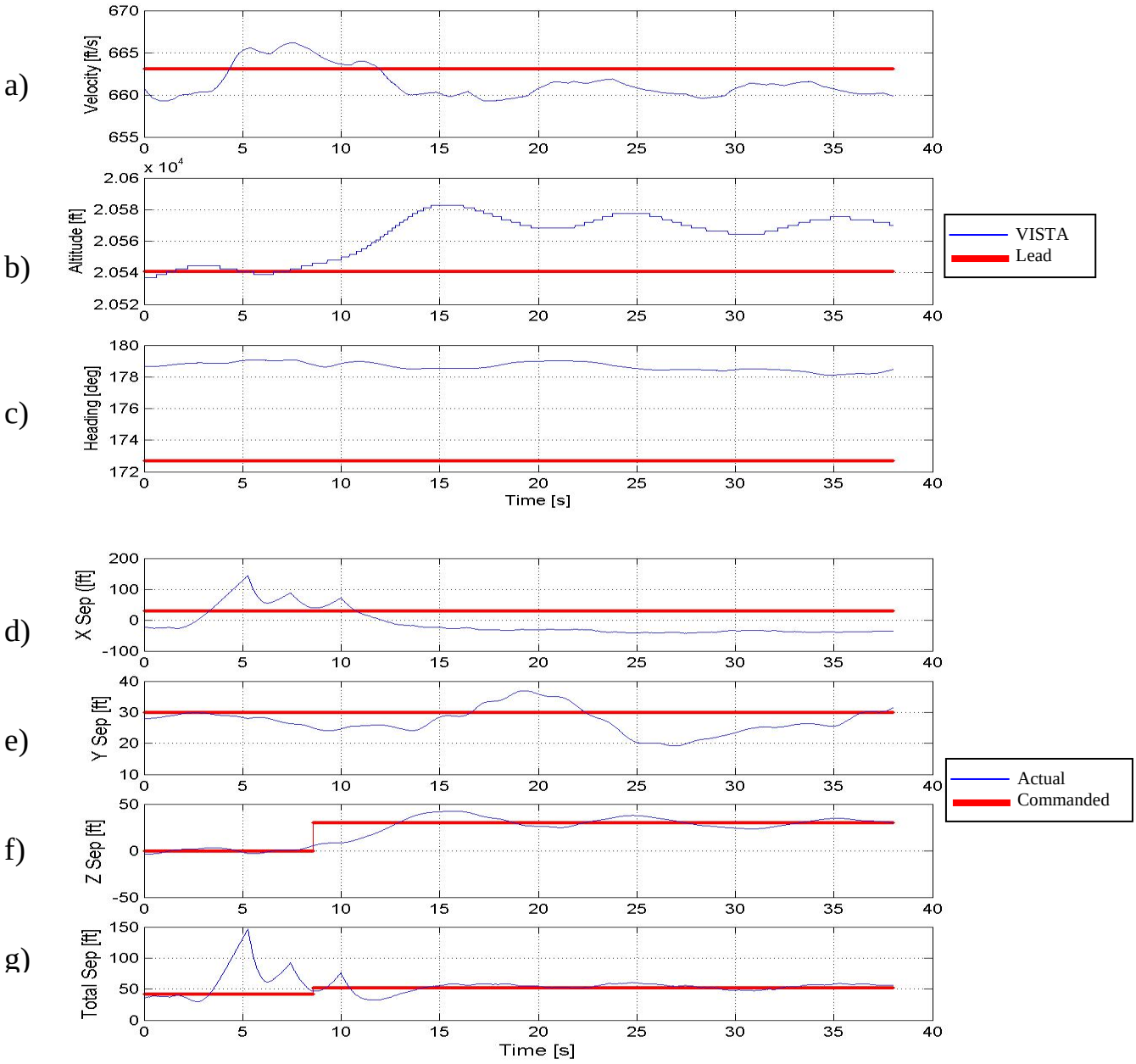

Data Basis: Flight Test; Test A/C: NF-16D #86-00048;
Engine: F110-GE-100; Configuration: Cruise, FCL; Test Date: 25Oct04

	X	Y	Z	Total Separation
Maximum Error (feet)	72.8	10.9	24.6	8.9
Time of maximum error (seconds)	5.3	26.9	8.6	24.8
Position Change	VISTA climbs 30 feet to (30 30 -30) from standard (30 30 0) position			

Figure 83. Event 15A Run 1 (Sortie 2 Record 5)

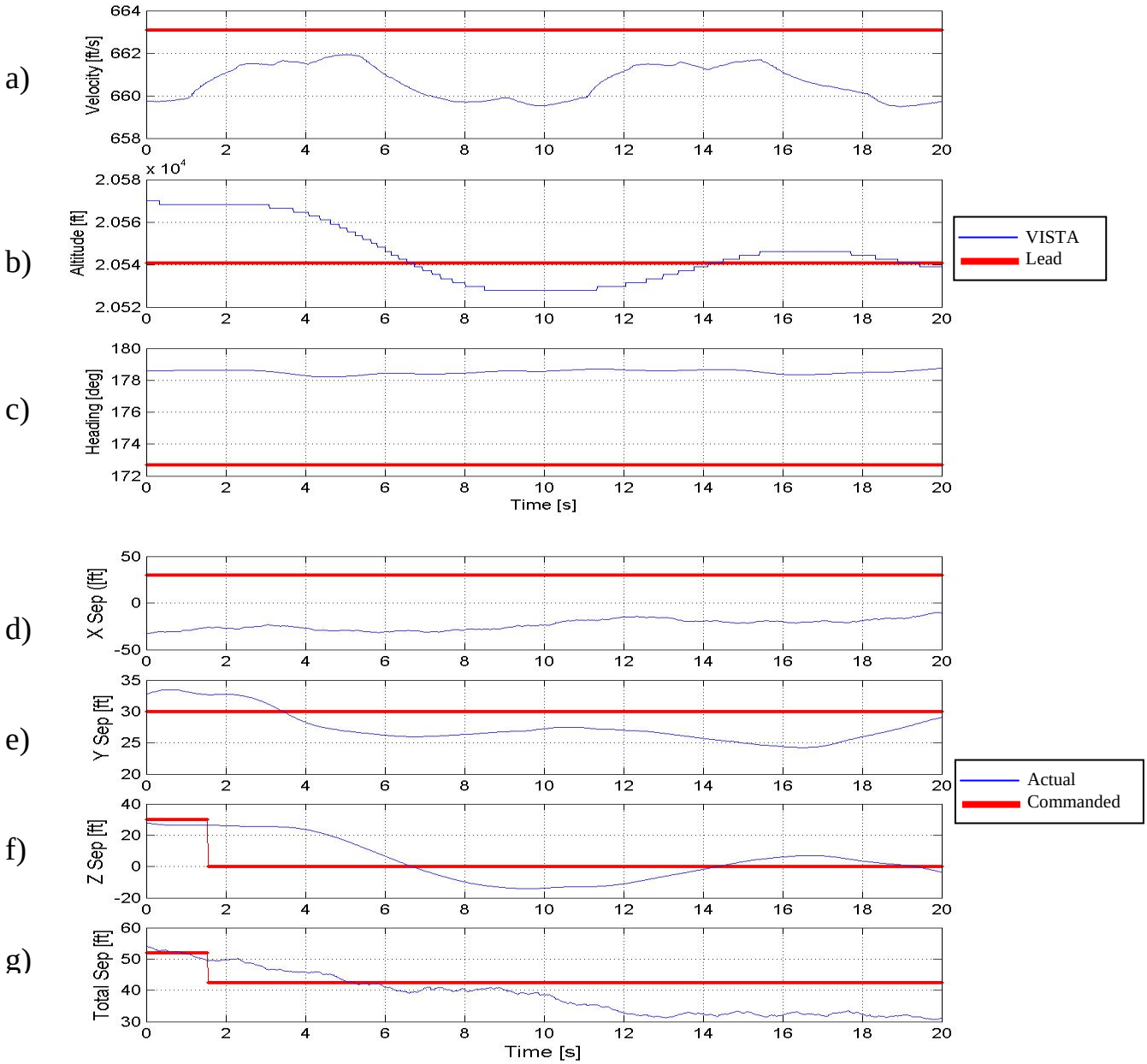

Data Basis: Flight Test; Test A/C: NF-16D #86-00048;
Engine: F110-GE-100; Configuration: Cruise, FCL; Test Date: 25Oct04

	X	Y	Z	Total Separation
Maximum Error (feet)	62.7	5.8	26.5	2.1
Time of maximum error (seconds)	0	16.5	1.6	0
Position Change	VISTA descends 30 feet from (30 30 30) back to standard (30 30 0) position			

Figure 84. Event 15B Run 1 (Sortie 2 Record 6)

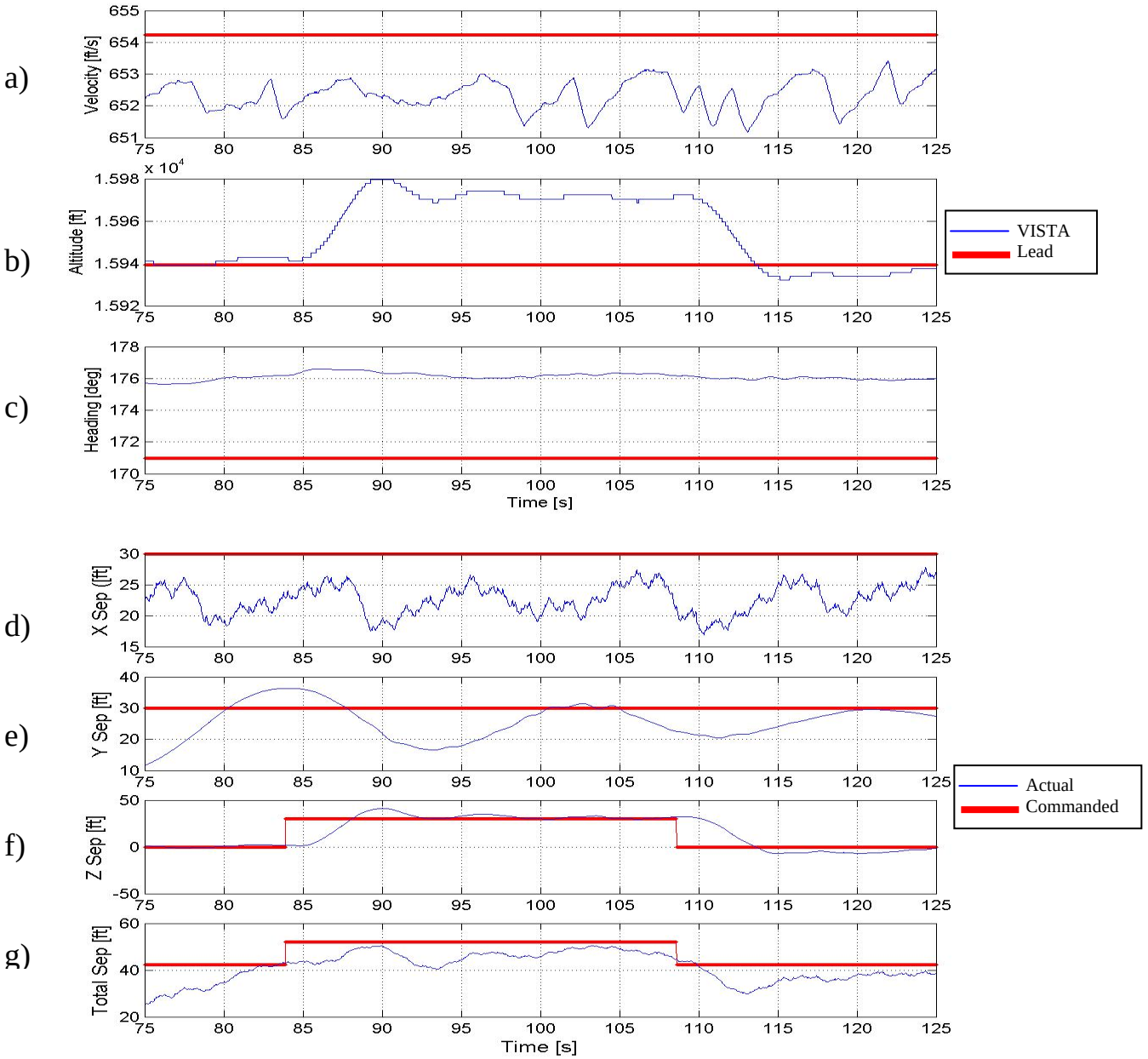

Data Basis: Flight Test; Test A/C: NF-16D #86-00048;
Engine: F110-GE-100; Configuration: Cruise, FCL; Test Date: 26Oct04

	X	Y	Z	Total Separation
Maximum Error (feet)	13.1	13.5	32.1	12.7
Time of maximum error (seconds)	110.3	93.2	108.8	113.1
Position Change	VISTA climbs 30 feet to (30 30 30) from standard (30 30 0) position and then descends back to standard position (30 30 0)			

Figure 85. Event 15A & B Run 2 (Sortie 3 Record 13)

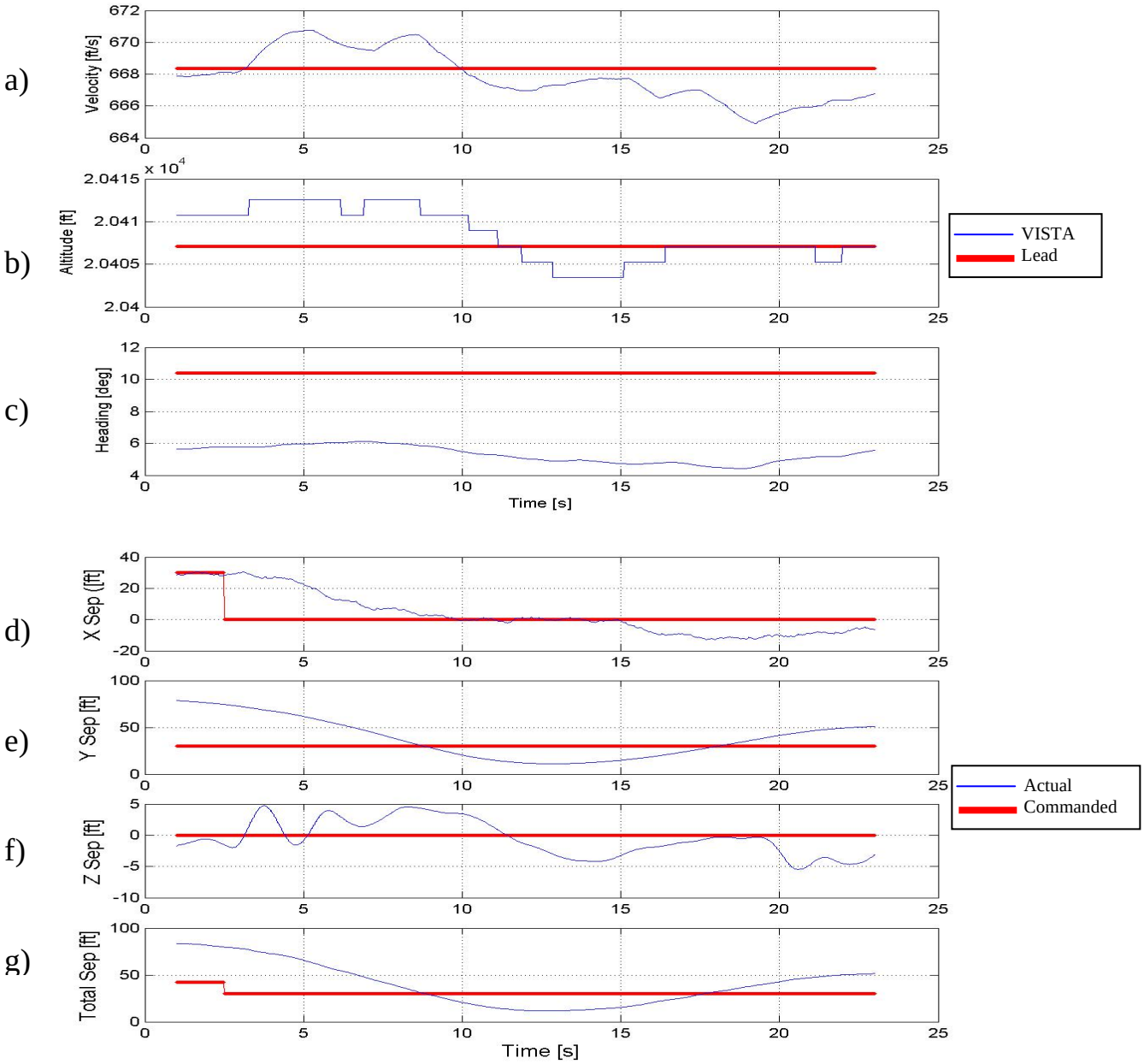

Data Basis: Flight Test; Test A/C: NF-16D #86-00048;
Engine: F110-GE-100; Configuration: Cruise, FCL; Test Date: 25Oct04

	X	Y	Z	Total Separation
Maximum Error (feet)	30.5	48.6	5.5	41.2
Time of maximum error (seconds)	3.1	1.0	20.6	1.1
Position Change	VISTA moves forward 30 feet to (0 30 0) from standard position (30 30 0)			

Figure 86. Event 16A Run 1 (Sortie 1 Record 31)

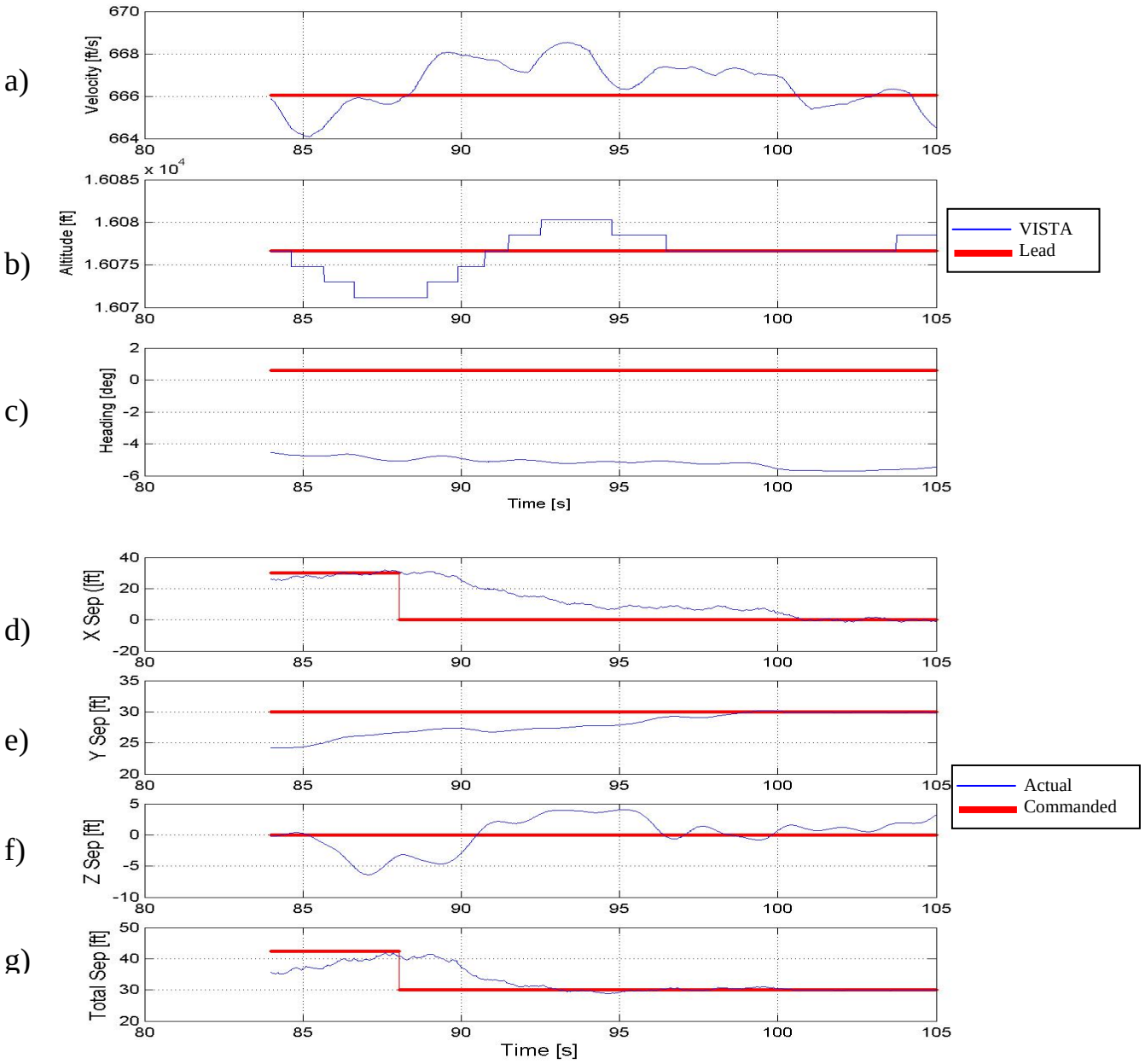

Data Basis: Flight Test; Test A/C: NF-16D #86-00048;
Engine: F110-GE-100; Configuration: Cruise, FCL; Test Date: 26Oct04

	X	Y	Z	Total Separation
Maximum Error (feet)	31.0	5.8	6.4	30.5
Time of maximum error (seconds)	89.0	84.0	87.1	87.6
Position Change	VISTA moves forward 30 feet to (0 30 0) from standard position (30 30 0)			

Figure 87. Event 16A Run 2 (Sortie 3 Record 14)

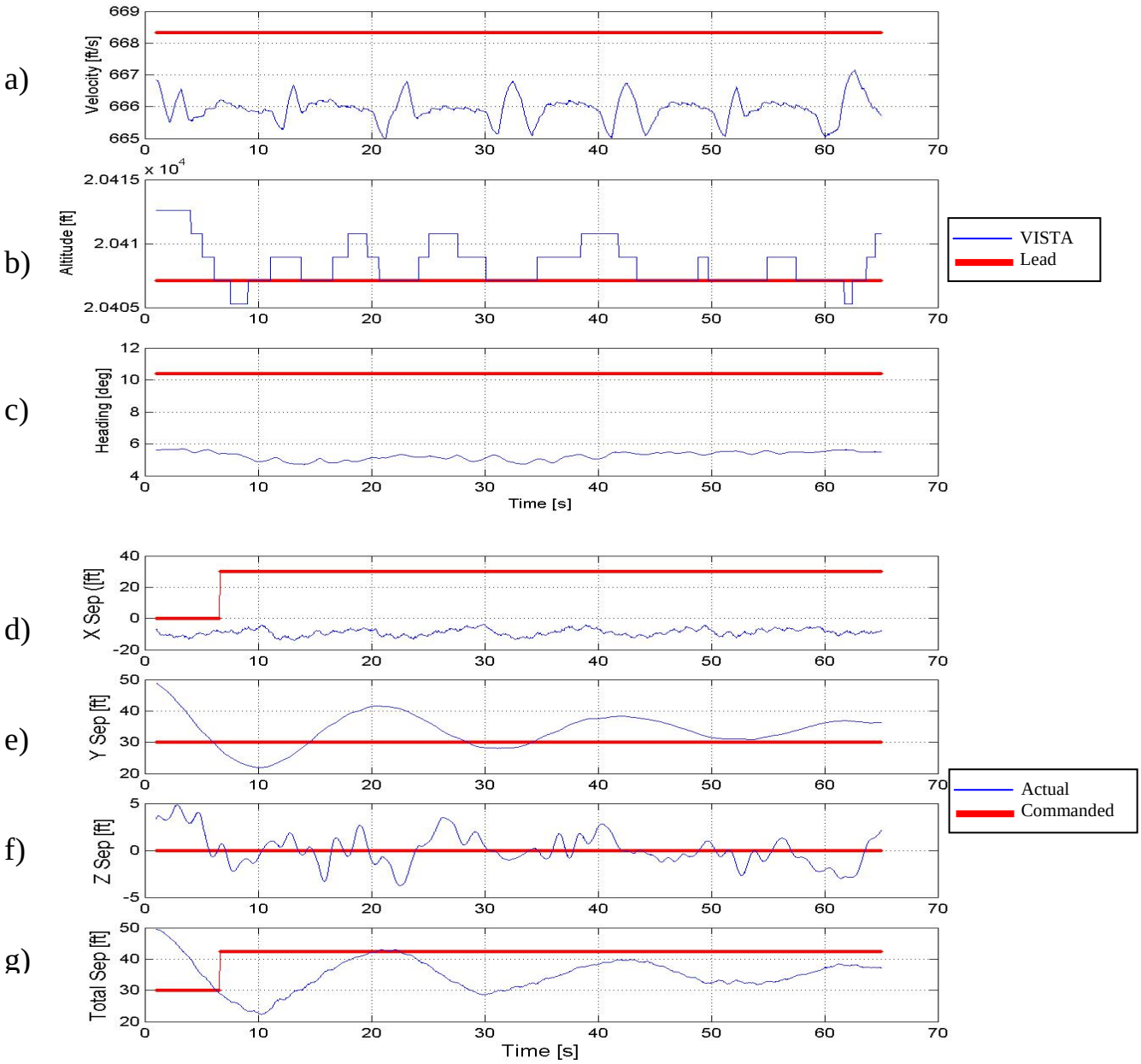

Data Basis: Flight Test; Test A/C: NF-16D #86-00048;
Engine: F110-GE-100; Configuration: Cruise, FCL; Test Date: 25Oct04

	X	Y	Z	Total Separation
Maximum Error (feet)	44.0	19.0	4.9	19.6
Time of maximum error (seconds)	13.2	1.0	2.8	1.0
Position Change	VISTA moves back 30 feet from (0 30 0) back to standard position (30 30 0)			

Figure 88. Event 16B Run 1 (Sortie 1 Record 32)

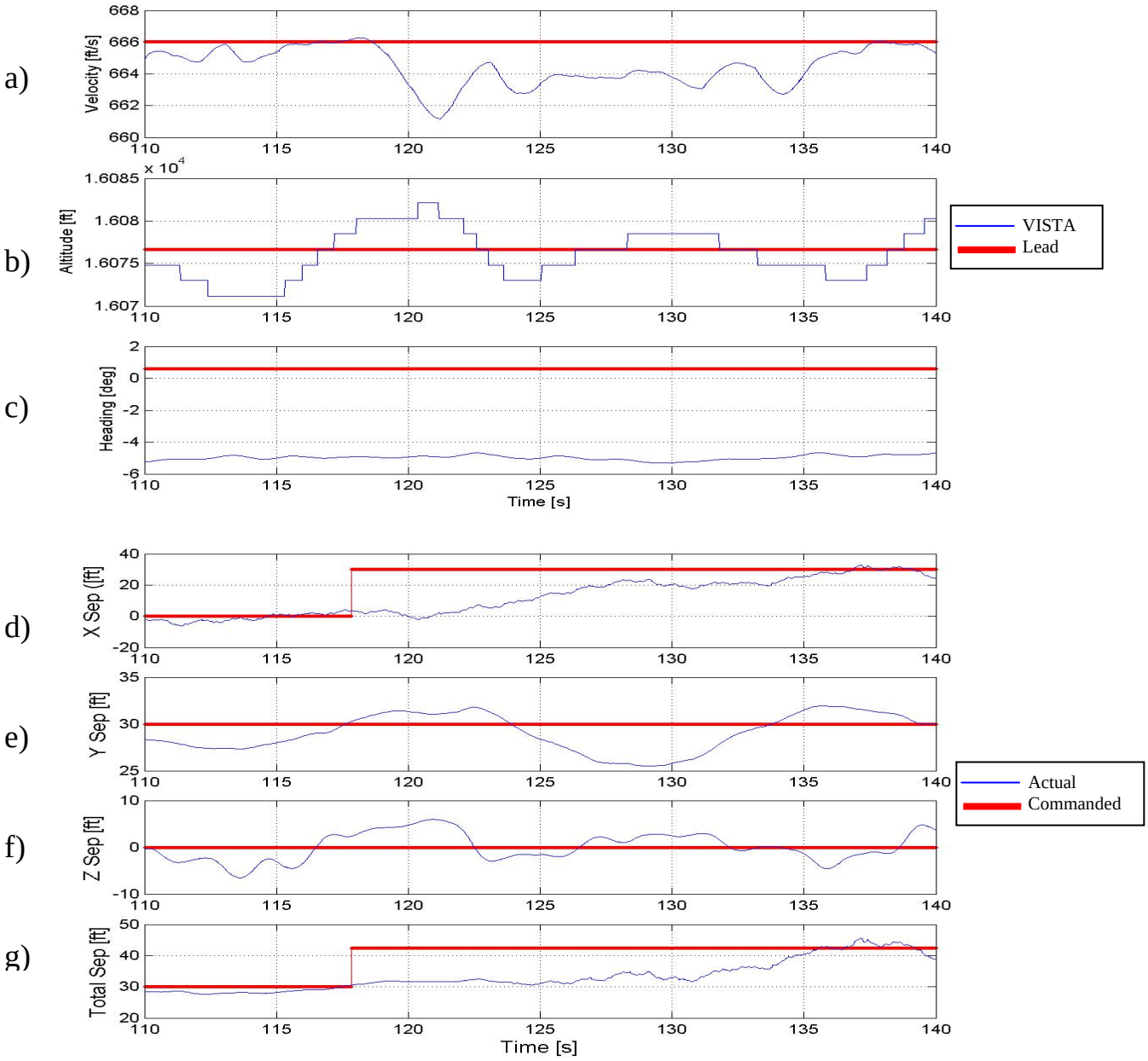

Data Basis: Flight Test; Test A/C: NF-16D #86-00048;
Engine: F110-GE-100; Configuration: Cruise, FCL; Test Date: 26Oct04

	X	Y	Z	Total Separation
Maximum Error (feet)	32.0	4.5	6.5	12.0
Time of maximum error (seconds)	120.4	128.9	113.6	137.2
Position Change	VISTA moves back 30 feet from (0 30 0) back to standard position (30 30 0)			

Figure 89. Event 16B Run 2 (Sortie 3 Record 14)

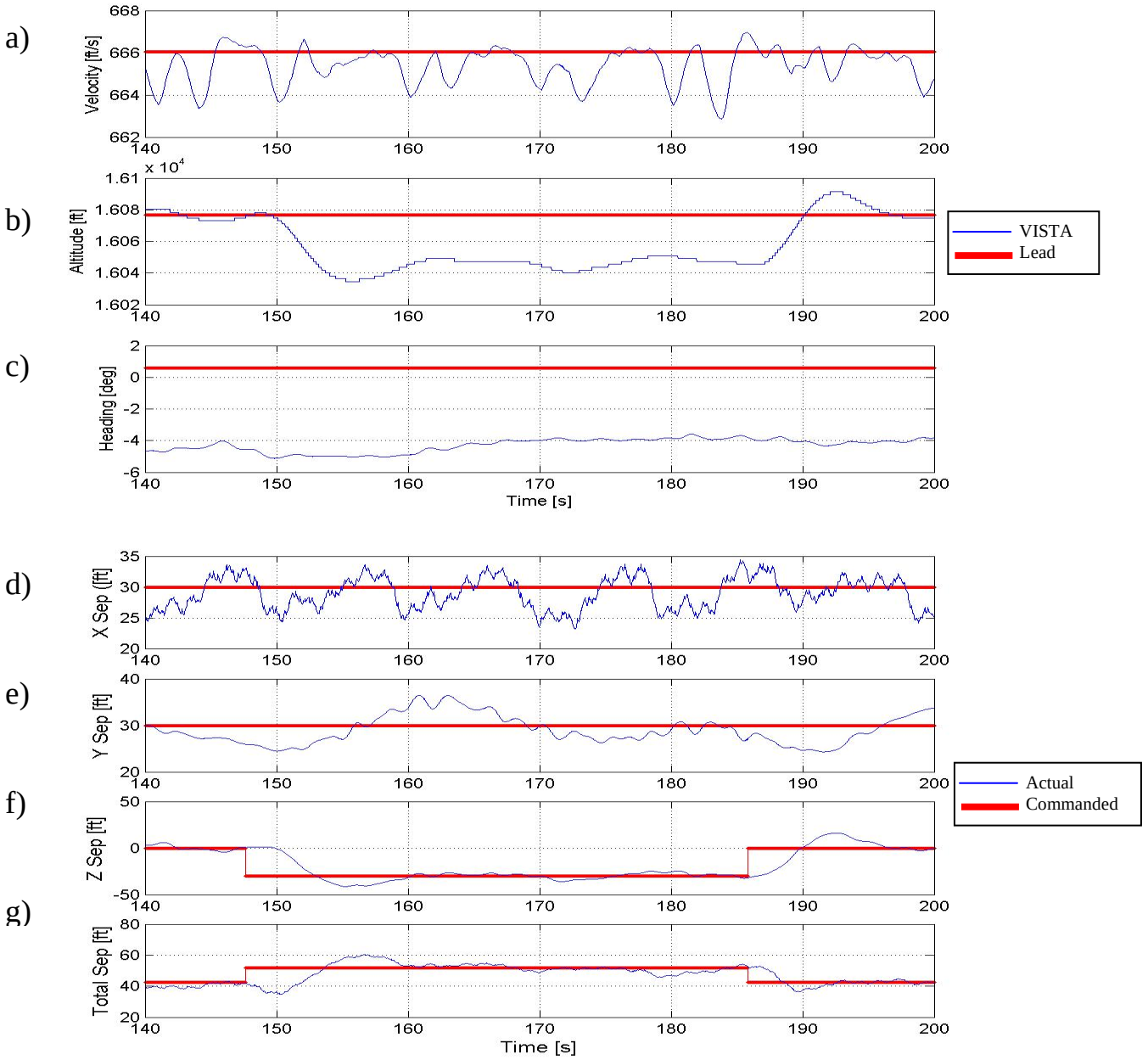

Data Basis: Flight Test; Test A/C: NF-16D #86-00048;
Engine: F110-GE-100; Configuration: Cruise, FCL; Test Date: 26Oct04

	X	Y	Z	Total Separation
Maximum Error (feet)	6.8	6.4	32.1	8.5
Time of maximum error (seconds)	172.7	160.8	185.8	156.7
Position Change	VISTA descends 30 feet to (30 30 -30) from standard position (30 30 0) and then climbs 30 feet back to standard position (30 30 0)			

Figure 90. Event 17A & B Run 1(A) 2(B) (Sortie 3 Record 14)

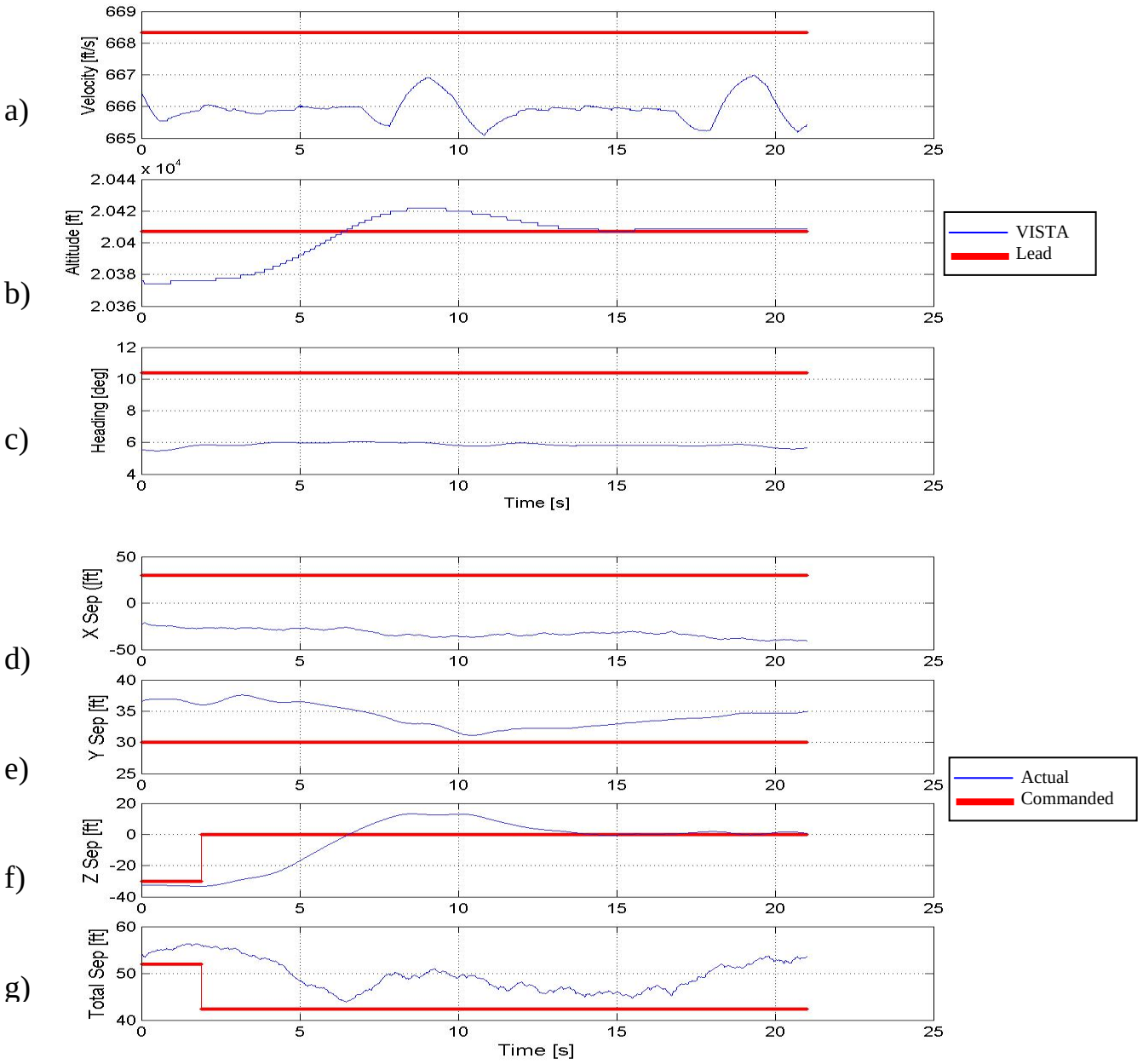

Data Basis: Flight Test; Test A/C: NF-16D #86-00048;
Engine: F110-GE-100; Configuration: Cruise, FCL; Test Date: 25Oct04

	X	Y	Z	Total Separation
Maximum Error (feet)	71.0	7.6	33.3	4.4
Time of maximum error (seconds)	19.8	3.2	1.9	1.4
Position Change	VISTA climbs 30 feet from (30 30 -30) back to standard position (30 30 0)			

Figure 91. Event 17B Run 1 (Sortie 1 Record 34)

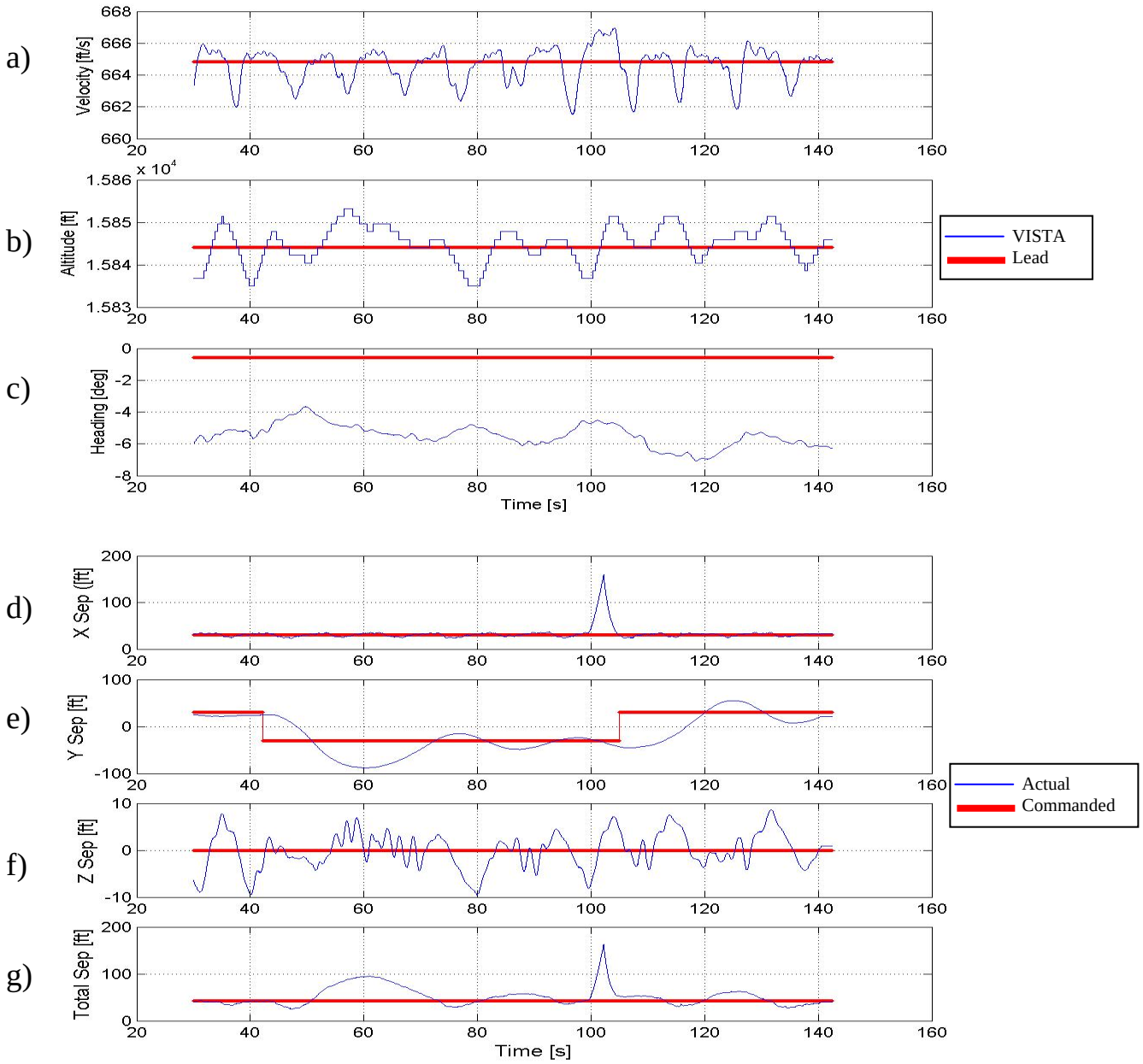

Data Basis: Flight Test; Test A/C: NF-16D #86-00048;
Engine: F110-GE-100; Configuration: Cruise, FCL; Test Date: 26Oct04

	X	Y	Z	Total Separation
Maximum Error (feet)	129.3	75.6	9.5	120.3
Time of maximum error (seconds)	102.2	107.0	79.9	102.2
Position Change	VISTA moves right 60 feet to (30 -30 0) from standard (30 30 0) position and then moves left 60 feet back to standard position (30 30 0)			

Figure 92. Event 18A & B Run 1 (Sortie 3 Record 16)

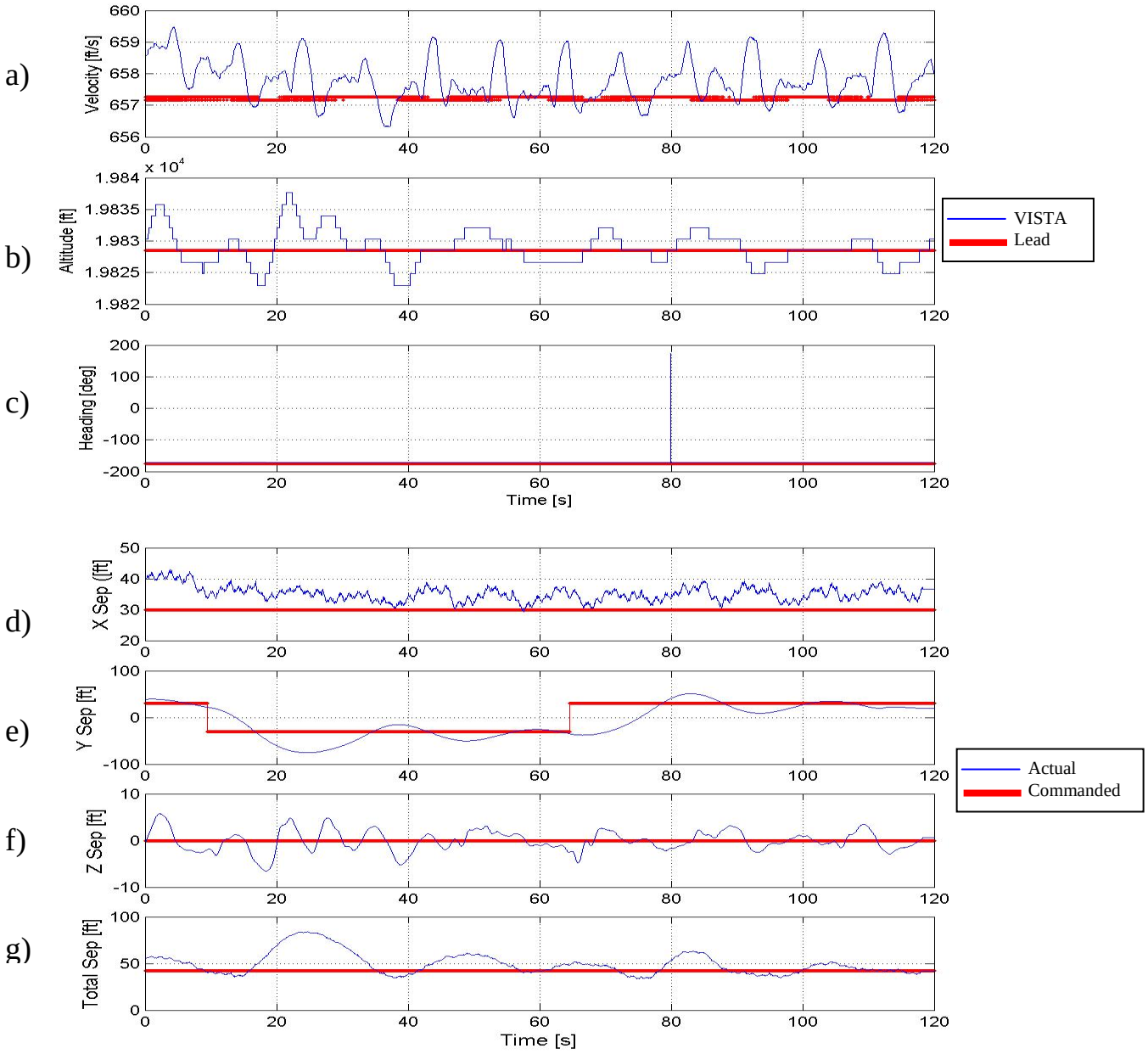

Data Basis: Flight Test; Test A/C: NF-16D #86-00048;
Engine: F110-GE-100; Configuration: Cruise, FCL; Test Date: 27Oct04

	X	Y	Z	Total Separation
Maximum Error (feet)	12.9	67.8	6.6	41.5
Time of maximum error (seconds)	3.8	66.5	18.4	24.8
Position Change	VISTA moves right 60 feet to (30 -30 0) from standard (30 30 0) position and then moves left 60 feet back to standard position (30 30 0)			

Figure 93. Event 18A & B Run 2 (Sortie 4 Record 15)

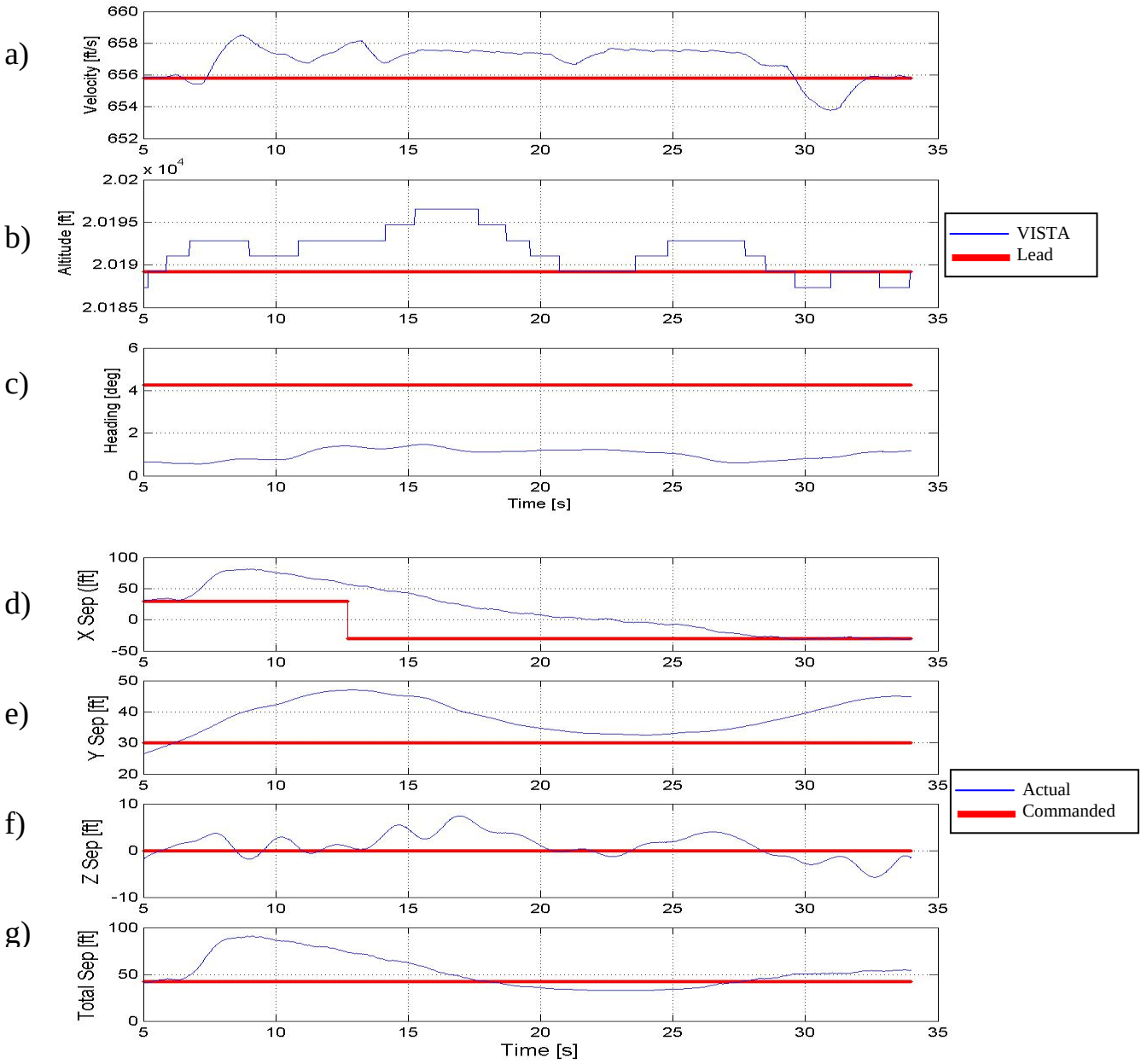

Data Basis: Flight Test; Test A/C: NF-16D #86-00048;
Engine: F110-GE-100; Configuration: Cruise, FCL; Test Date: 27Oct04

	X	Y	Z	Total Separation
Maximum Error (feet)	86.6	17.0	7.4	48.5
Time of maximum error (seconds)	12.8	12.7	16.9	9.1
Position Change	VISTA moves forward 60 feet to (-30 30 0) from standard position (30 30 0)			

Figure 94. Event 19A Run 1 (Sortie 4 Record 6)

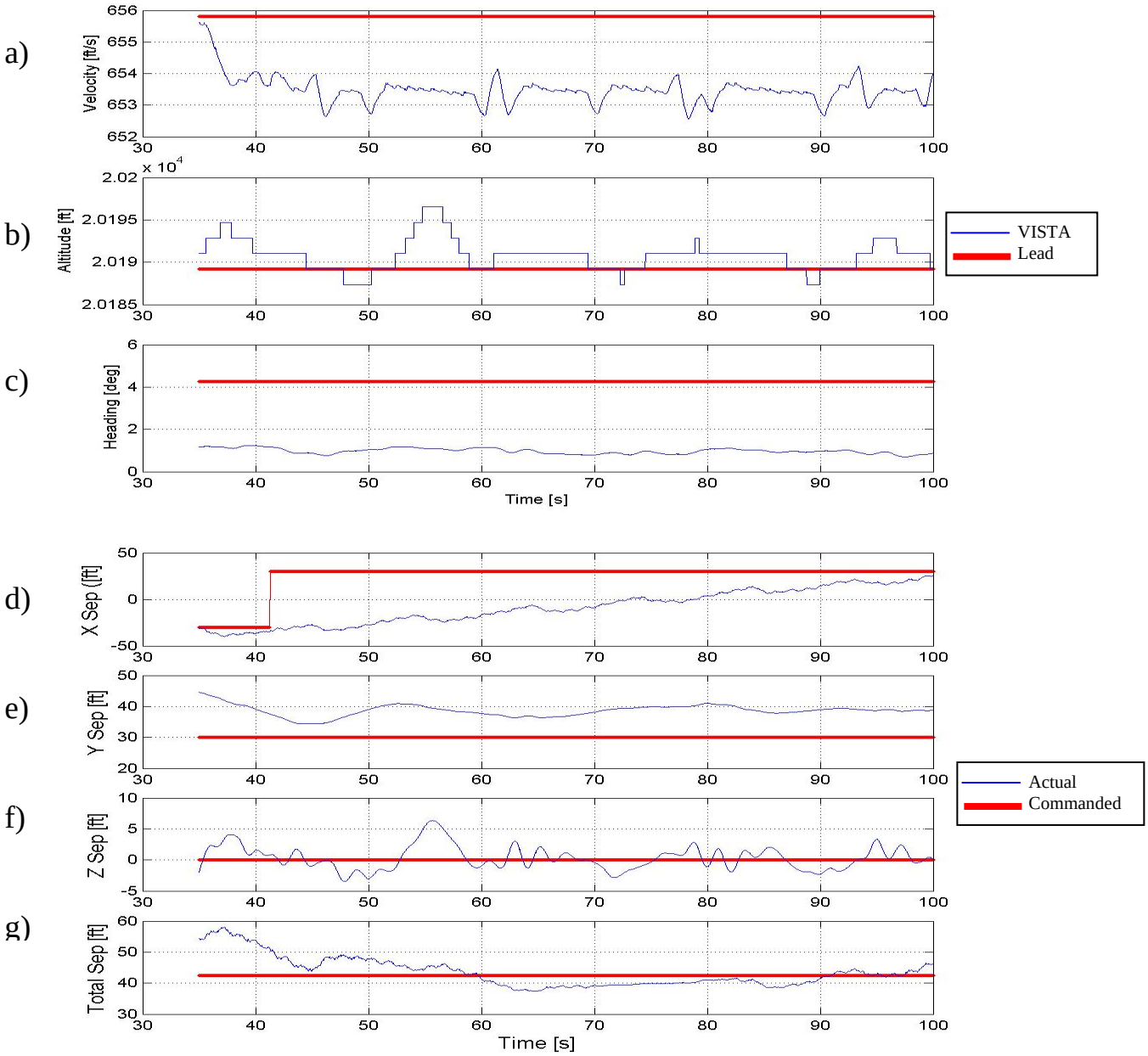

Data Basis: Flight Test; Test A/C: NF-16D #86-00048;
Engine: F110-GE-100; Configuration: Cruise, FCL; Test Date: 27Oct04

	X	Y	Z	Total Separation
Maximum Error (feet)	64.8	14.6	6.4	15.7
Time of maximum error (seconds)	41.3	35.0	55.7	37.3
Position Change	VISTA moves aft 60 feet from (-30 30 0) back to standard position (30 30 0)			

Figure 95. Event 19B Run 1 (Sortie 4 Record 6)

Appendix B. Diagrams of Controller and Model For Simulation

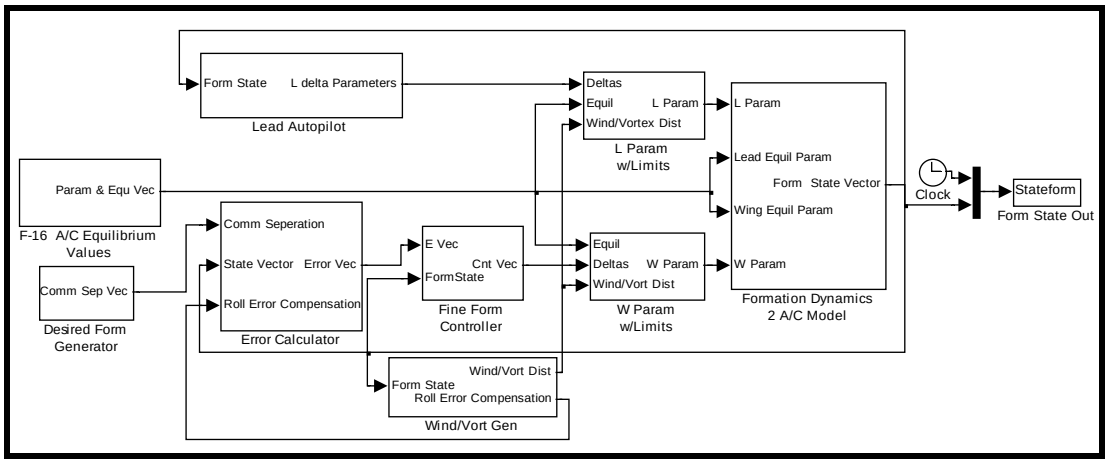

Figure 96. Main Controller and System Model

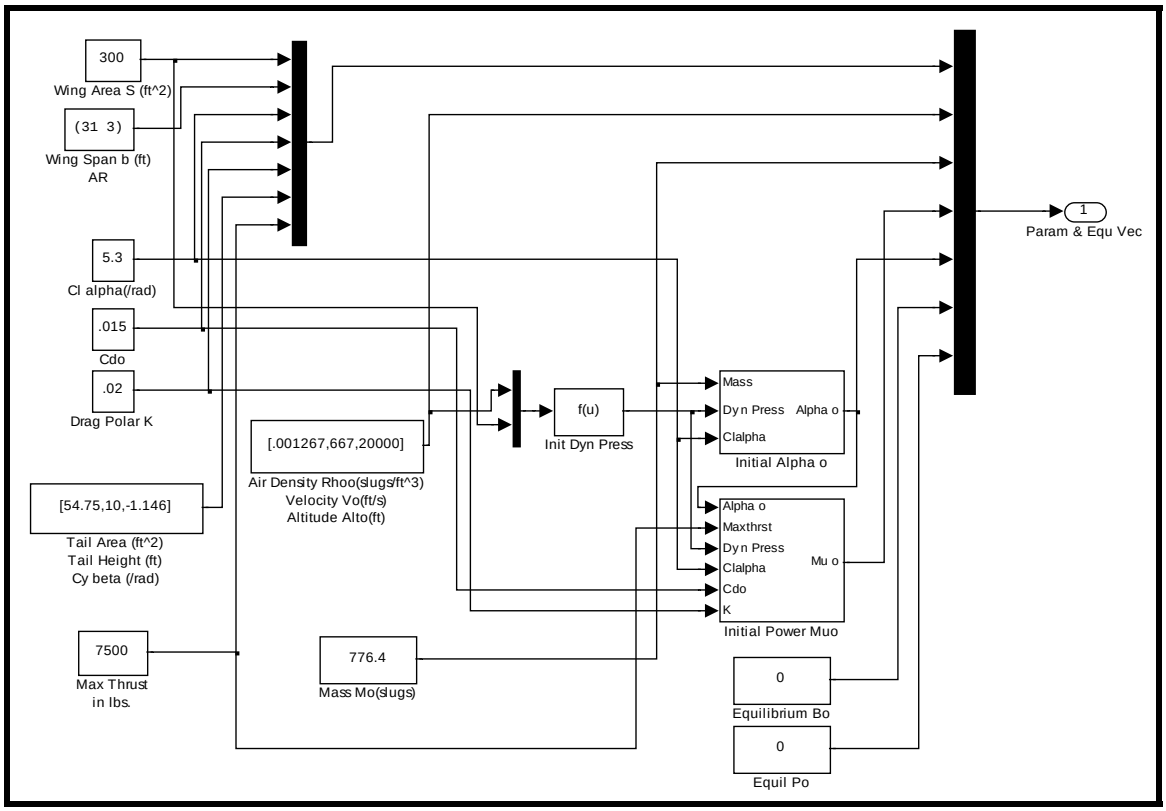

Figure 97. F-16 A/C Equilibrium Values Block

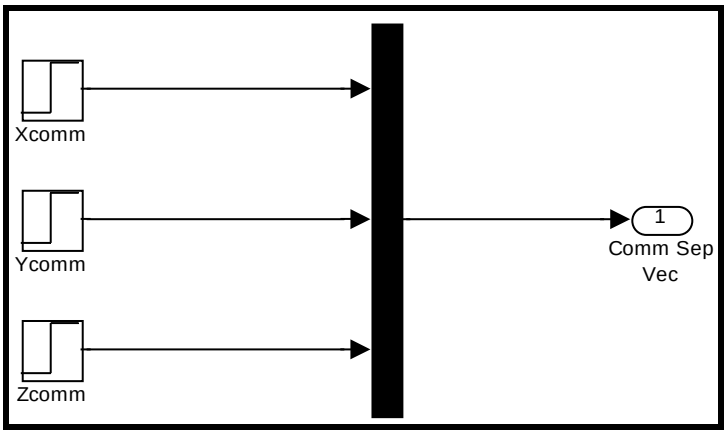

Figure 98. Desired Form Generator Block

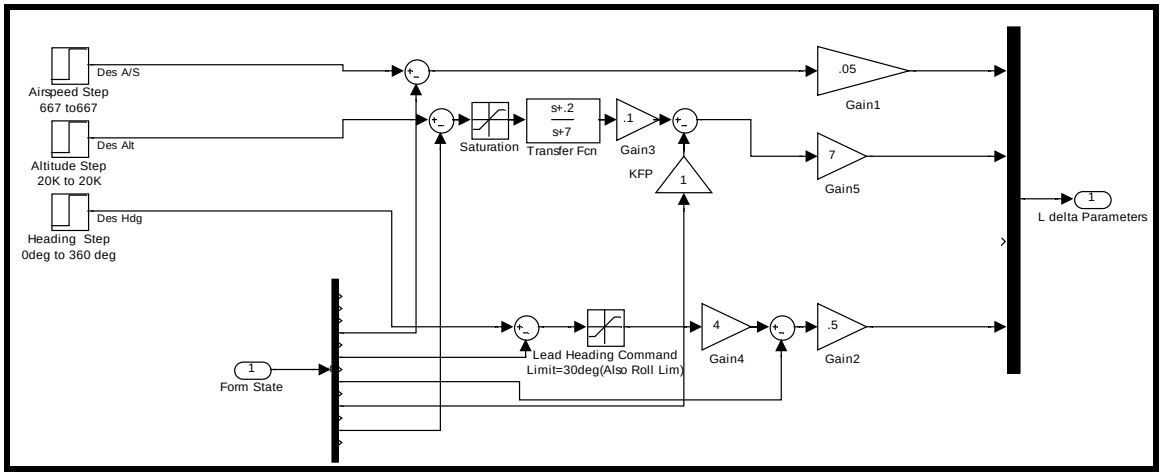

Figure 99. Lead Autopilot Block

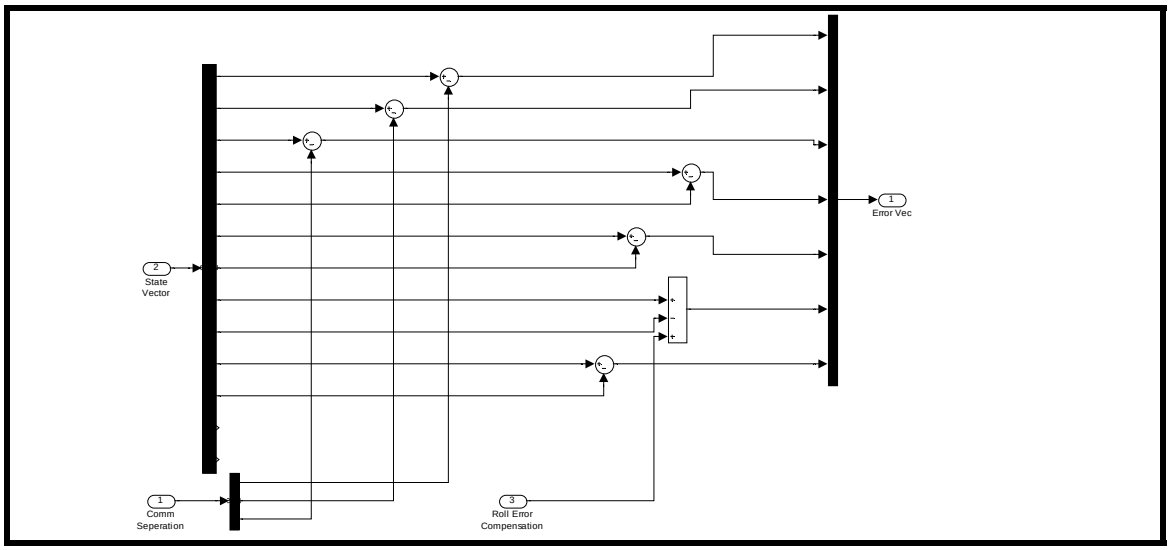

Figure 100. Error Calculator Block

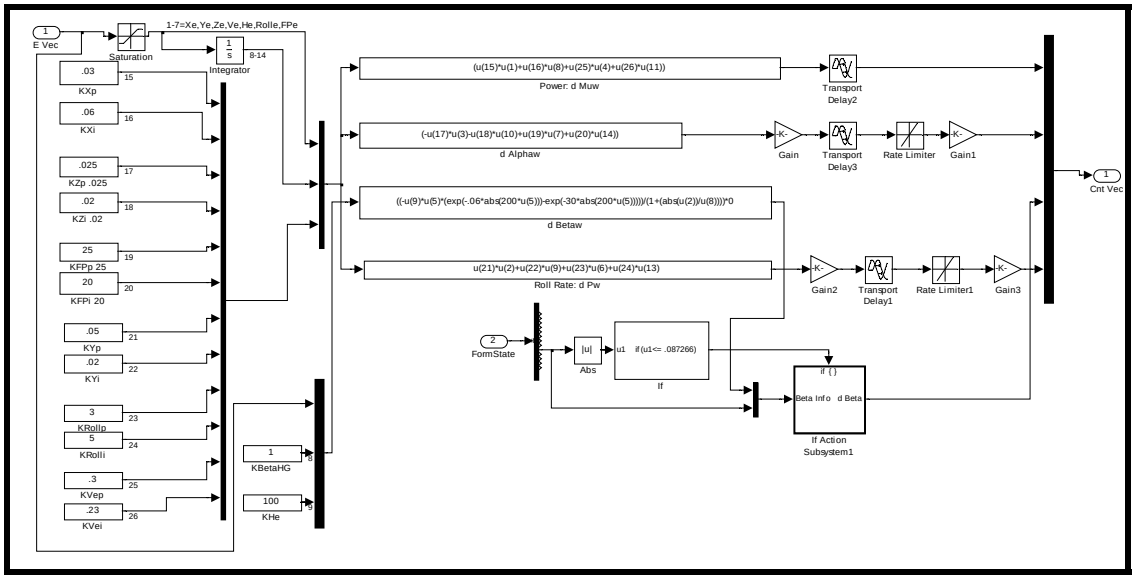

Figure 101. Fine Form Controller Block

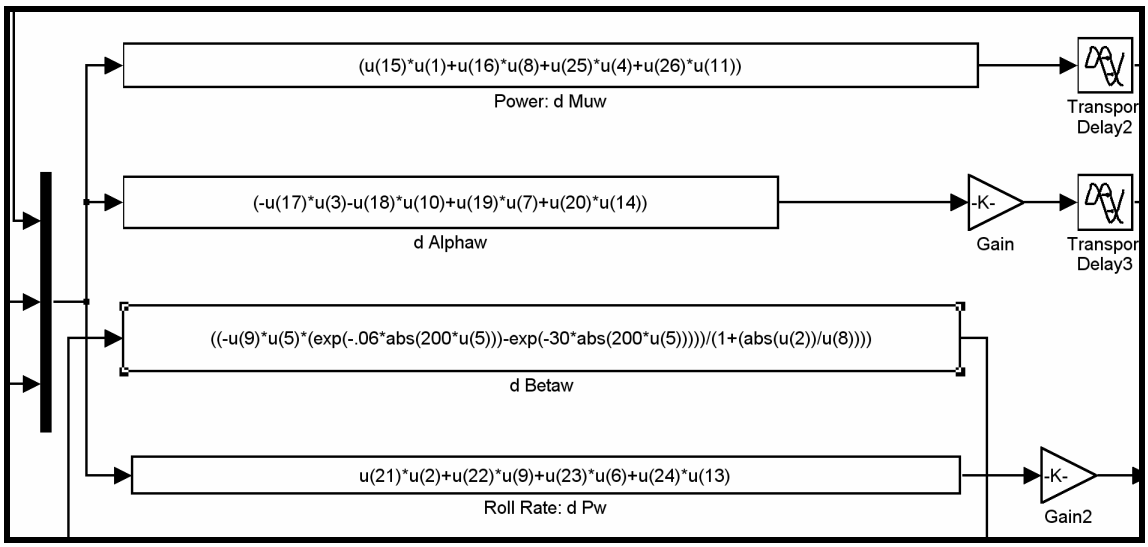

Figure 102. Close Up of Control Laws in Fine Form Controller Block

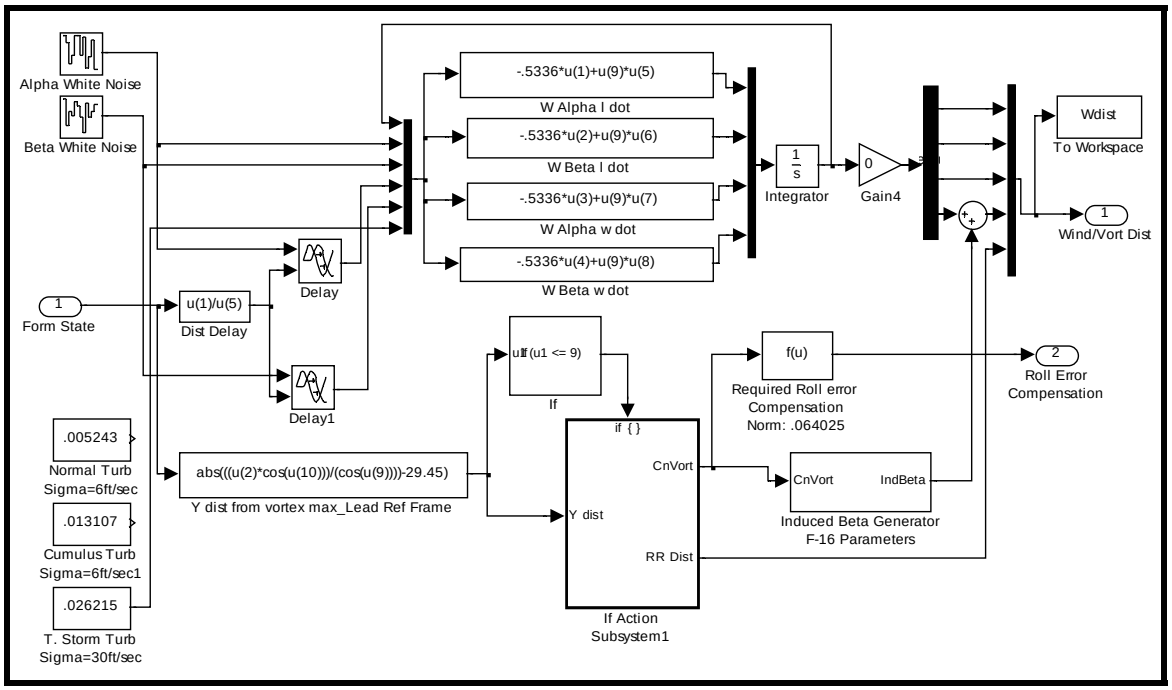

Figure 103. Vortex Generator Block

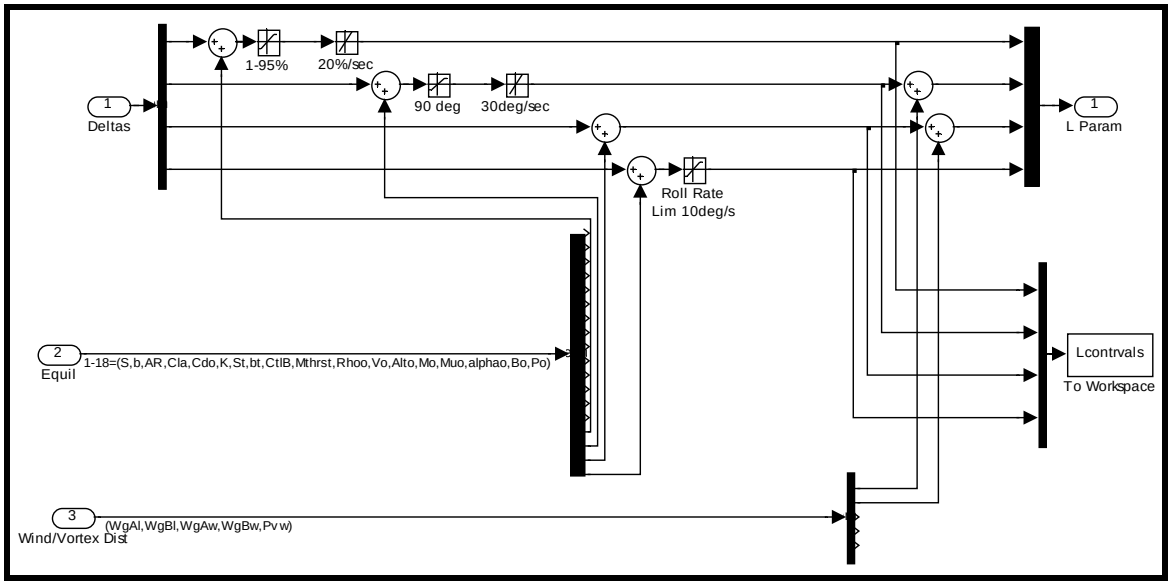

Figure 104. L Param w/ Limits Block

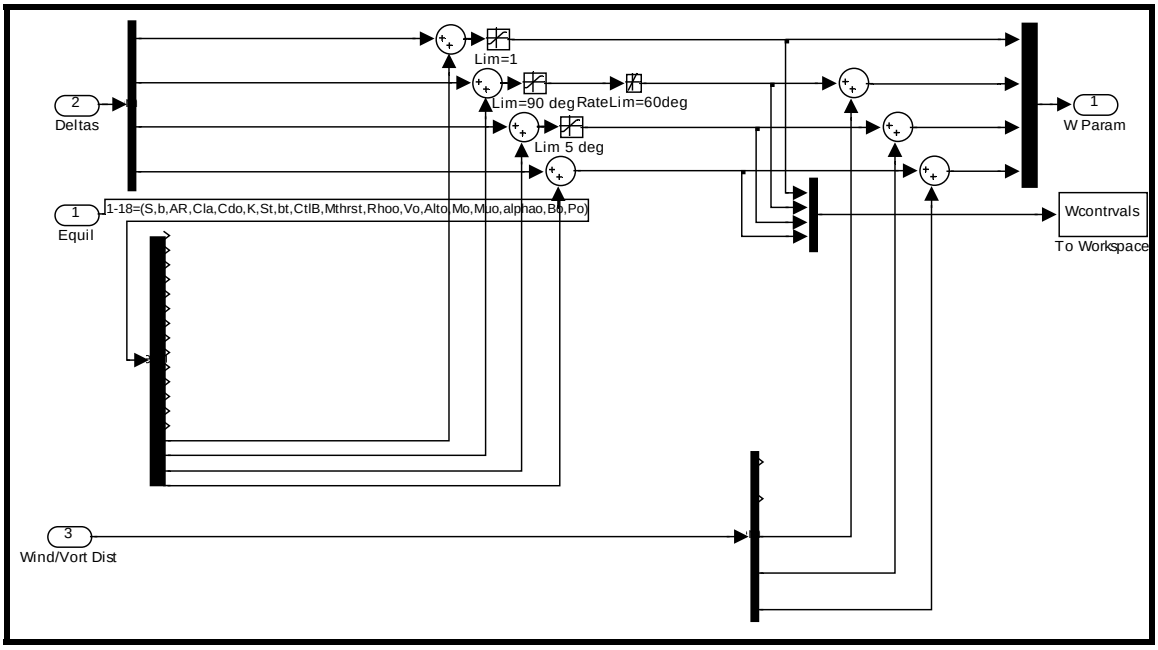

Figure 105. W Param w/ Limits Block

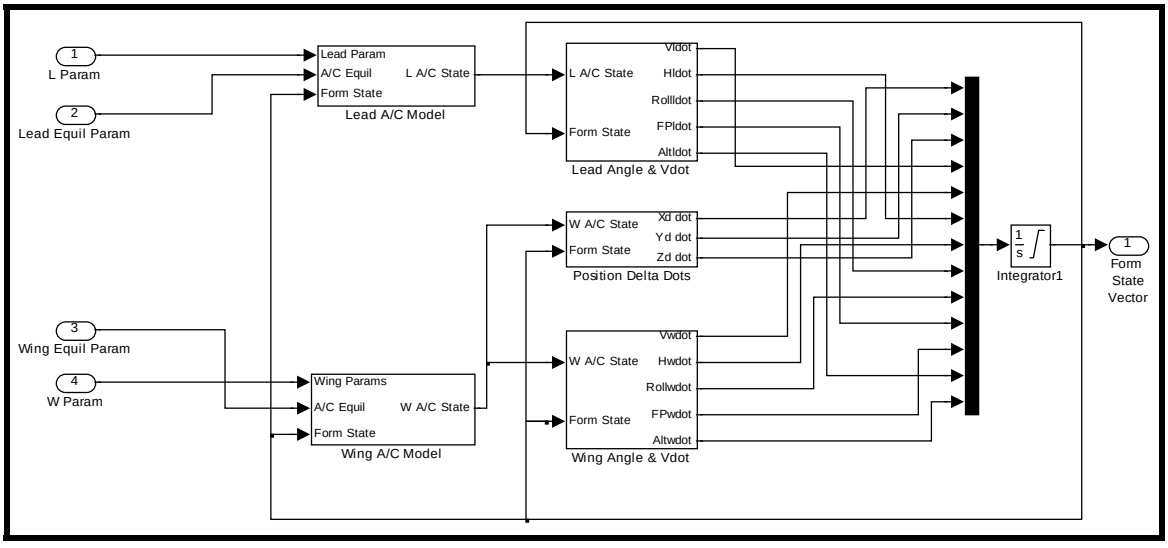

Figure 106. Formation Dynamics 2A/C Block

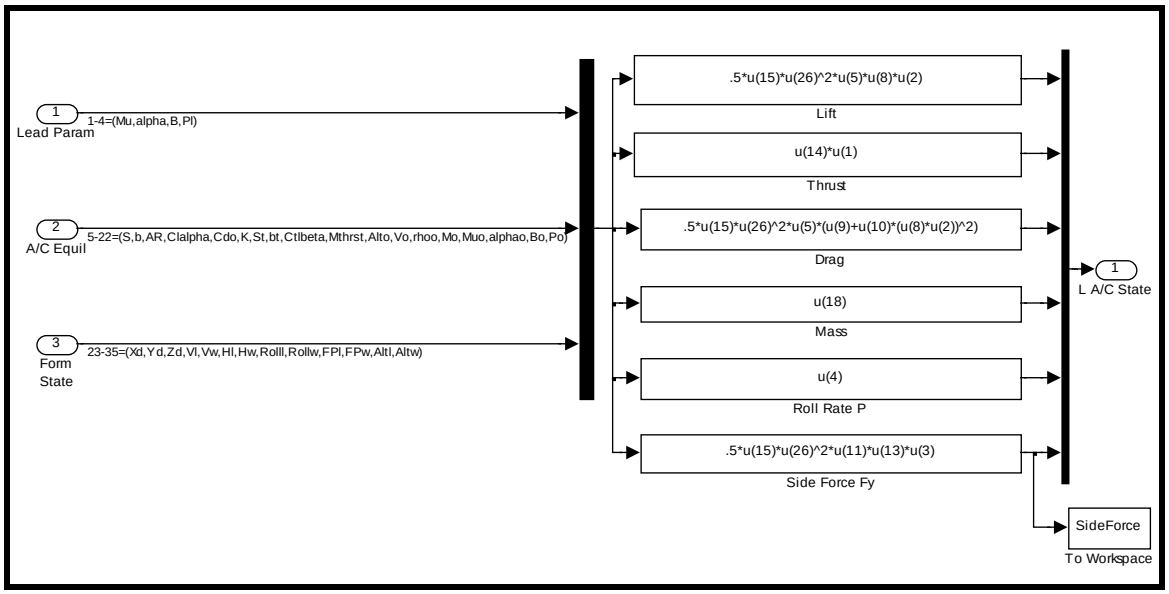

Figure 107. Lead A/C Model Sub-Block

The Wing A/C Model Sub-Block is the same layout as Figure 106 above and will not be shown.

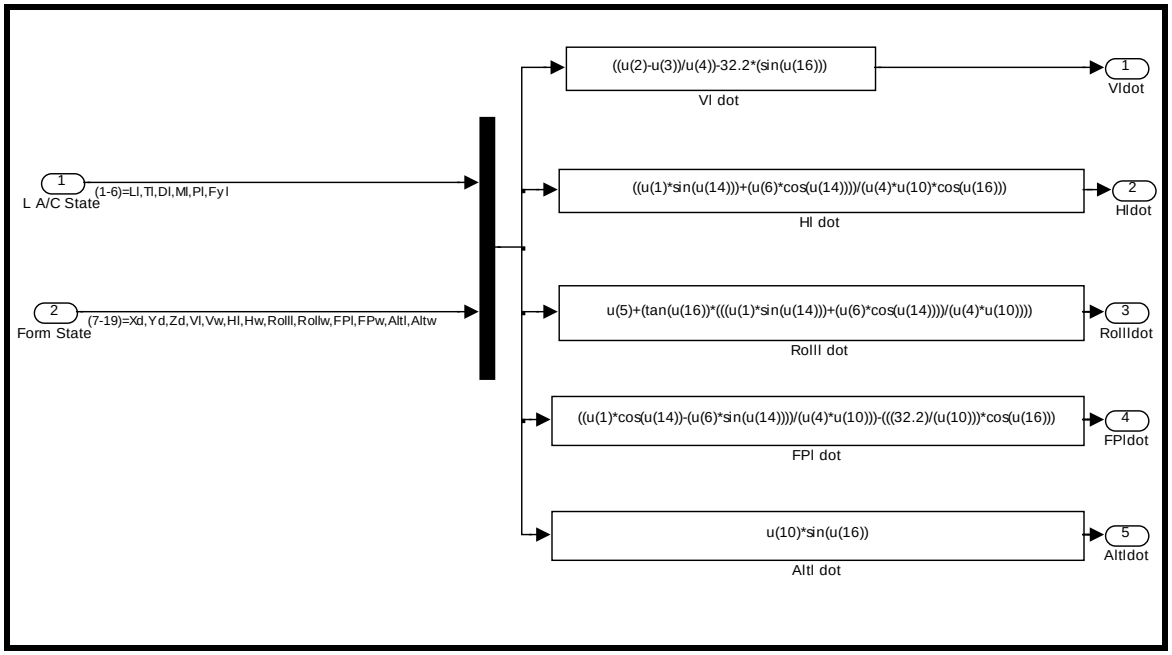

Figure 108. Lead Angle and Vdot Sub-Block

The Wing Angle and Vdot Sub-Block is the same layout as Figure 107 above and will not be shown.

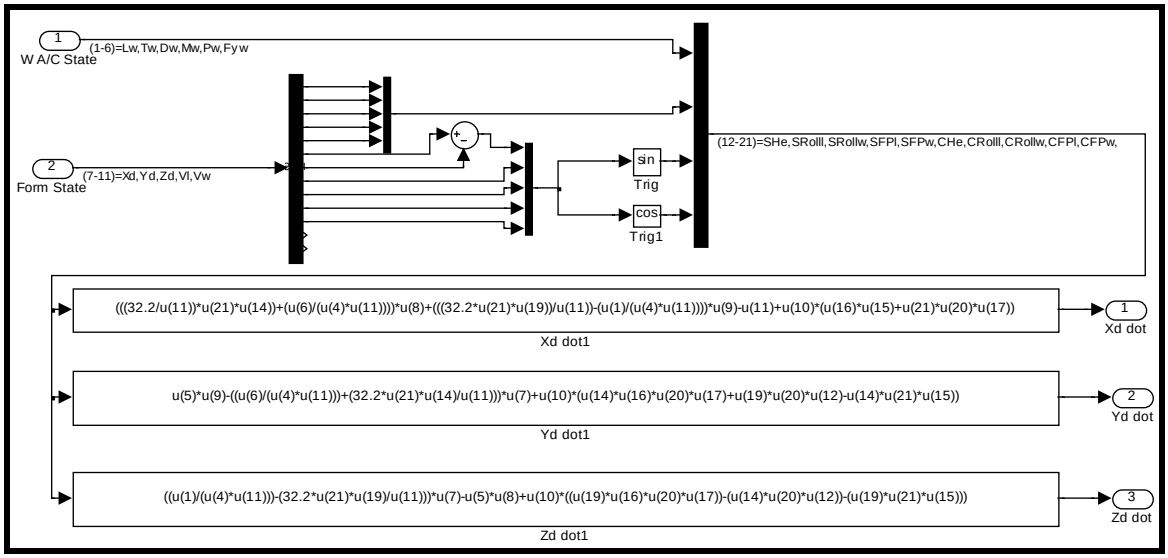

Figure 109. Position Delta Dots Sub-Block

Appendix C. Modified Controller For Flight Test

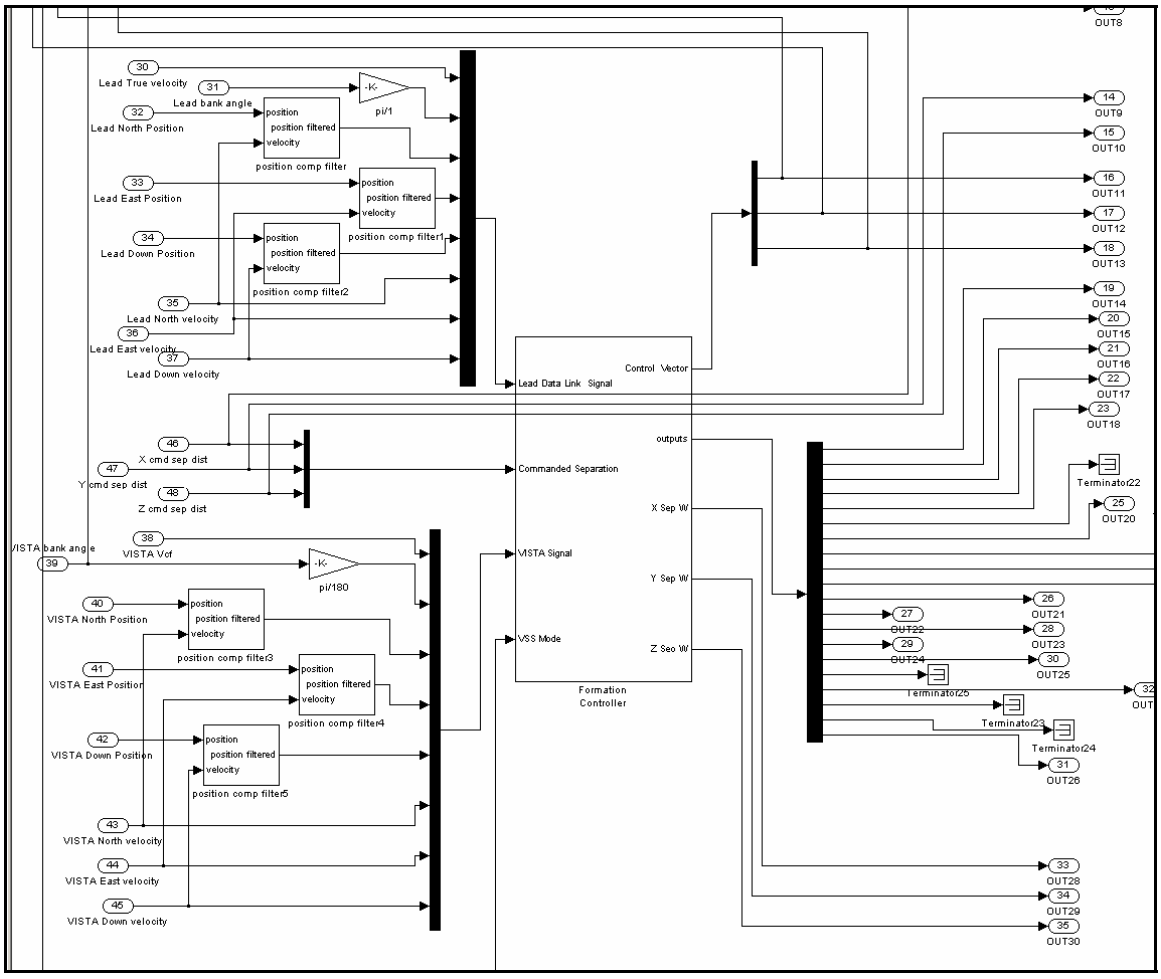

Figure 110. Formation Controller Embedded in VISTA Logic

The formation flight controller is embedded in the VISTA logic that feeds and receives the inputs and outputs of the modified controller. For information outside of this diagram, the reader is advised to contact General Dynamics, Aeronautical Information Systems.

The smoothing blocks for both the lead and VISTA positions are apparent in the above diagram. Velocities in the appropriate directions are used to smooth the positions as presented in Figure 111 below.

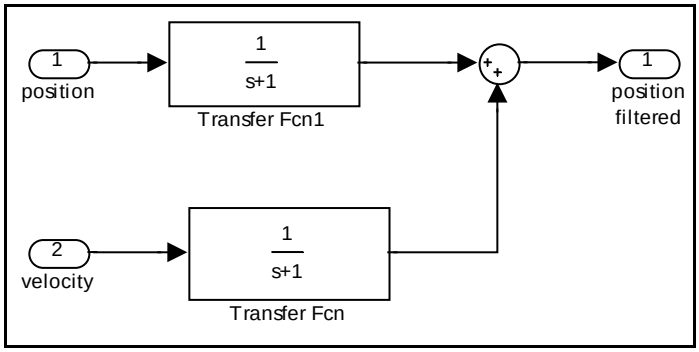

Figure 111. Position Smoothing Block

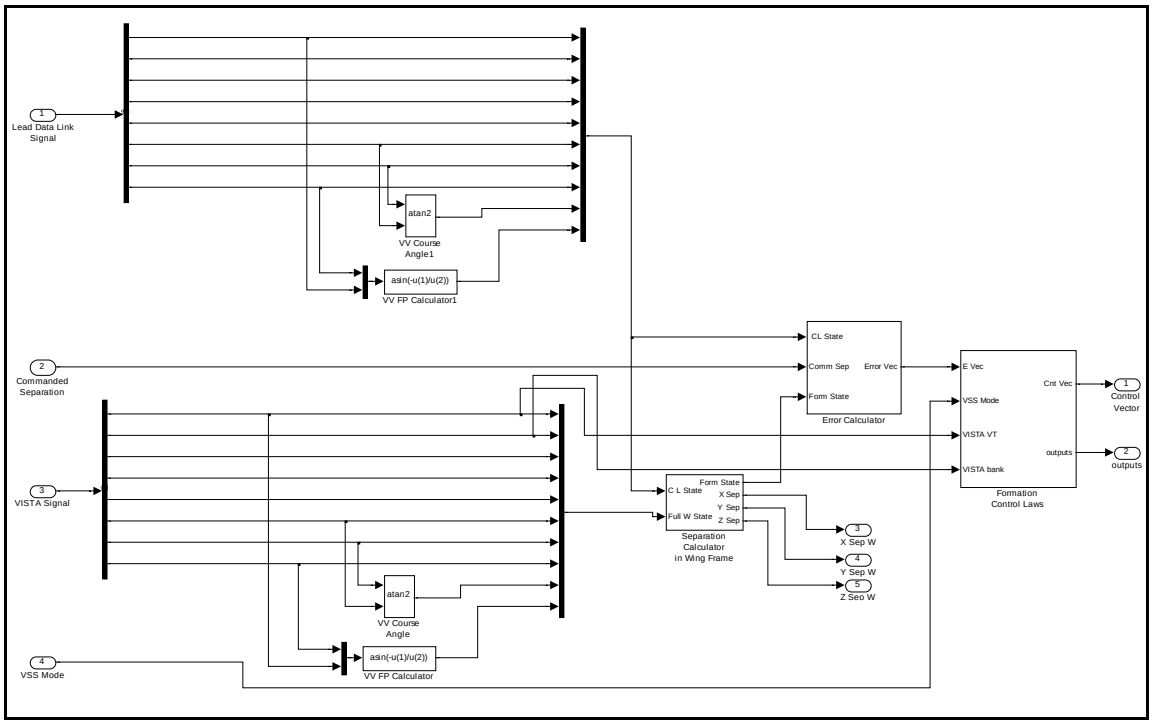

Figure 112. Formation Controller Block

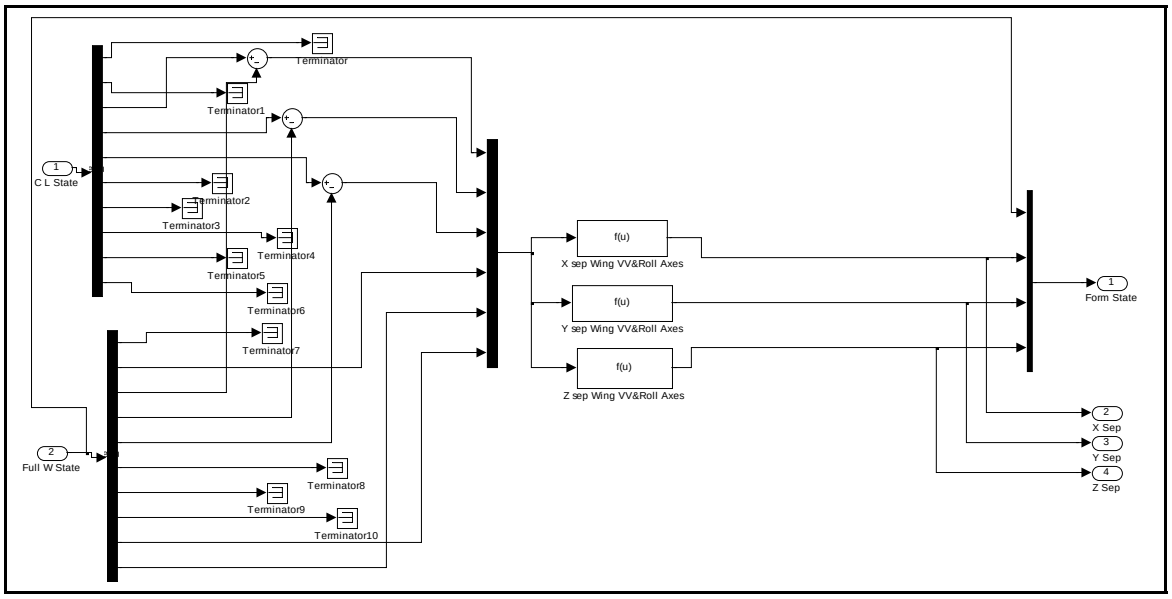

Figure 113. Separation Calculator in Wing Frame Block

The Wing VV & Roll Axes blocks represent the DCM equations required to express the separation vector rotated about the velocity vector heading and flight path angles and finally about the wing body roll angle.

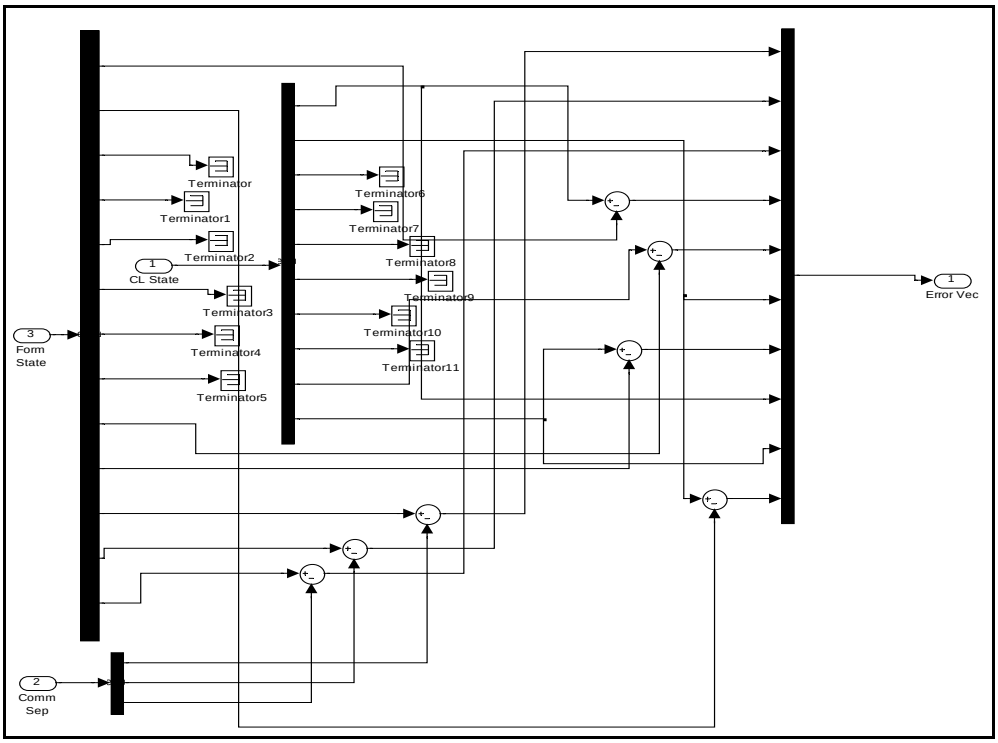

Figure 114. Error Calculator Block

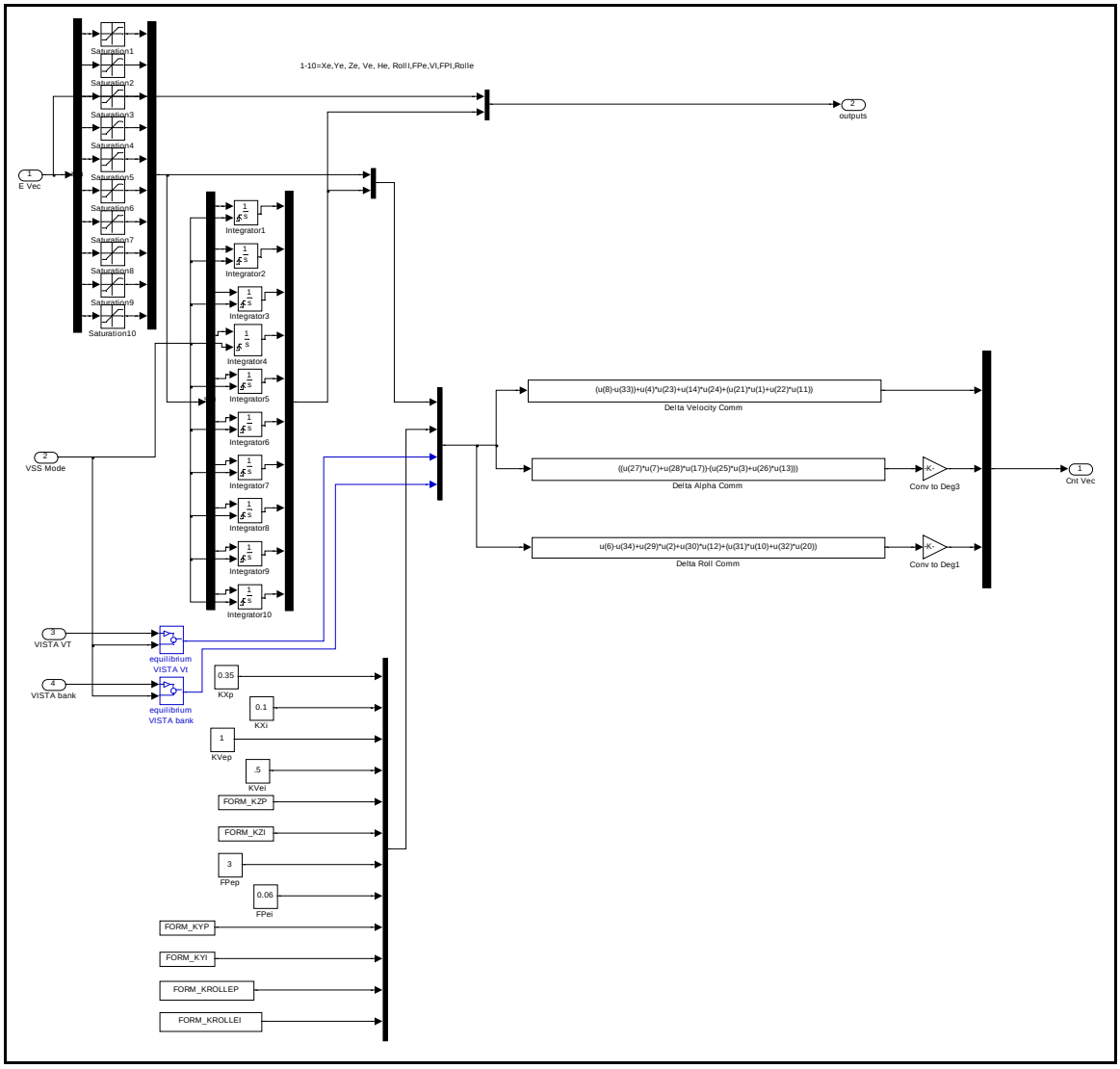

Figure 115. Formation Control Laws Block

This is the overview of the formation control law block. Close-ups of this diagram of each of the areas of interest follow in Figures 116 and 117. The error vector that enters from the top input port on the left is ten elements long and consists of: X error, Y error, Z error, Velocity error, Heading error, Roll Angle of lead, Flight Path error, Velocity of lead, Flight Path of lead, and Roll Angle error.

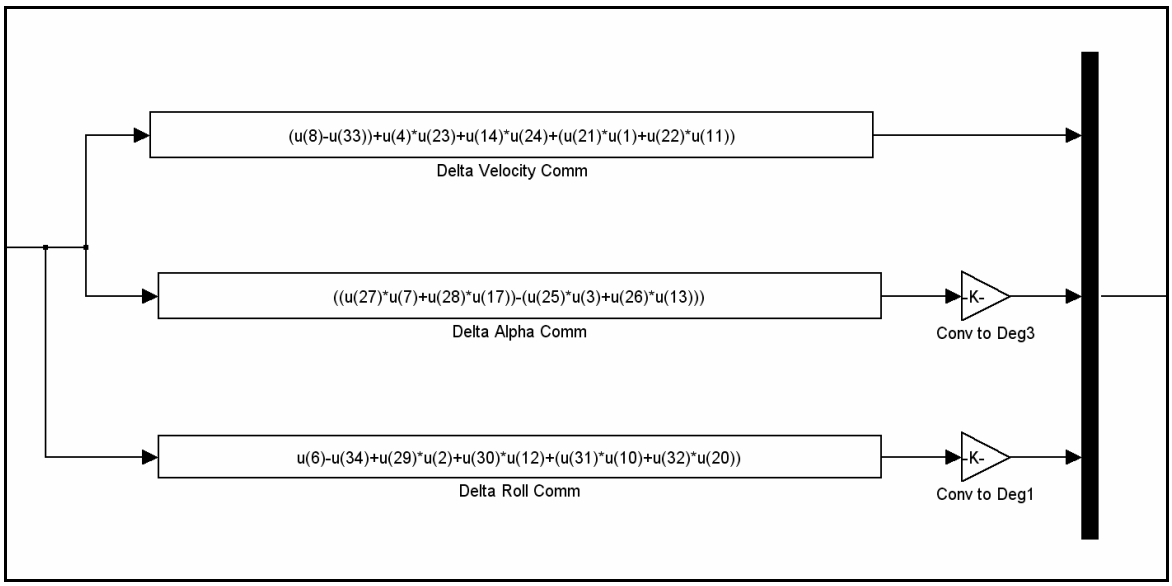

Figure 116. Control Law Blocks

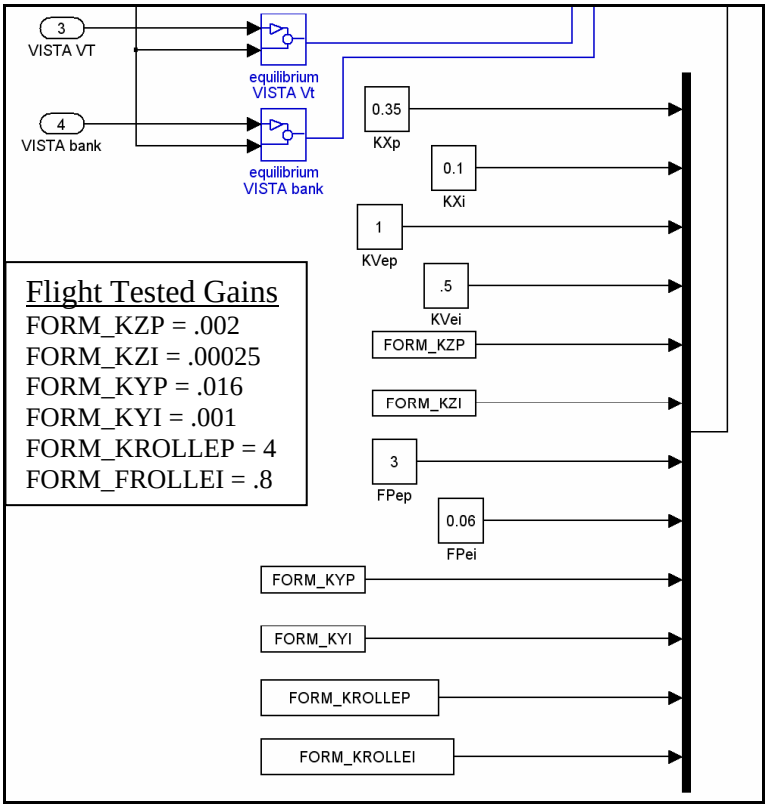

Figure 117. Controller Gain and Equilibrium Hold Blocks

Bibliography

1. Athans, Michael, David Castañon, Keh-Ping Dunn, Christopher S. Greene, Wing H. Lee, Nils R. Sandell Jr., and Alan S. Willsky. *The Stochastic Control of the F-8C Aircraft Using a Multiple Model Adaptive Control(MMAC) Method-Part I: Equilibrium Flight.* IEEE Transactions on Automatic Control, Vol AC-22, No. 5:768-780, (October 1977).

2. Bihrle Applied Research, *D-Six User's Manual*, Hampton VA, 2004

3. Buzogany, Louis E., *Automated Control of Aircraft in Formation Flight*, MS thesis, AFIT/GE/ENG/92D-07, School of Engineering, Air Force Institute of Technology (AU), Wright-Patterson AFB OH, December 1992.

4. Dargan, John L., *Proportional Plus Integral Control of Aircraft for Automated Maneuvering Formation Flight*, MS thesis, AFIT/GE/ENG/91D-14, School of Engineering, Air Force Institute of Technology (AU), Wright-Patterson AFB OH, December 1991.

5. Department of the Air Force, USAF NF-16D 86-0048 Modification Flight Manual, WI-FARG-NF16D-0071-R05, 6 December 2002.

6. Gingras, D. R. *Flight Model of a Generic High Performance Air Vehicle [ICE101]*. BAR02-05. Bihrle Applied Research, Hampton VA, September 2002.

7. Hall, James K., *Three Dimensional Formation Flight Control*, MS thesis, AFIT/GAE/ENY/00M-06, School of Engineering, Air Force Institute of Technology (AU), Wright-Patterson AFB OH, March 2000.

8. Hummel, D. *The Use of Aircraft Wakes to Achieve Power Reductions in Formation Flight*. in Proceedings of the AGARD FDP Symposium on "The Characterization and Modification of Wakes from Lifting Vehicles in Fluid", Trondheim, Norway, May 1996 and published in CP-584.

9. Kuethe, Arnold M. and Chuen-Yen Chow. *Foundations of Aerodynamics* (5th Edition). New York: John Wiley & Sons, Inc., 1998.

10. Maskew, Brian; *Formation Flying Benefits Based on Vortex Lattice Calculations.* NASA-CR-151974. 4 April 1977.

11. McCamish, Sean J., *Optimal Formation Flight Control*, MS thesis, AFIT/GE/ENG/95D-16, School of Engineering, Air Force Institute of Technology (AU), Wright-Patterson AFB OH, December 1995.

12. Morgan, Michael , *A Study in the Drag Reduction of Close Formation Flight Accounting for Trim Actuation and Dissimilar Formation*, MS thesis, AFIT/GAE/ENY/05-M13, School of Engineering, Air Force Institute of Technology (AU), Wright-Patterson AFB OH

13. Nelson, Robert C. *Flight Stability and Automatic Control* (2nd Edition). Boston: McGraw-Hill Companies, Inc., 1998.

14. Osteroos, Ryan K. *Limited Evaluation of the Automatic Flight Controller: Project Solo Form.* Air Force Flight Test Center Technical Information Memorandum. AFFTC-TIM-04-08. Edwards Air Force Base, California. December, 2004.

15. Proud, Andrew W., *Close Formation Flight Control*, MS thesis, AFIT/GE/ENG/99M-24, School of Engineering, Air Force Institute of Technology (AU), Wright-Patterson AFB OH, March 1999.

16. Reyna, Vincent P., *Automation of Formation Flight Control*, MS thesis, AFIT/GE/ENG/94M-01, School of Engineering, Air Force Institute of Technology (AU), Wright-Patterson AFB OH, March 1994.

17. Rohs, Paul R., *A Fully Coupled, Automated Formation Control System for Dissimilar Aircraft in Maneuvering, Formation Flight*, MS thesis, AFIT/GE/ENG/91M-03, School of Engineering, Air Force Institute of Technology (AU), Wright-Patterson AFB OH, March 1991.

18. Stevens, Brian L. and Frank L. Lewis. *Aircraft Control and Simulation.* New York: John Wiley & Sons, Inc., 1992.

19. Veth, Michael J., *Advanced Formation Flight Control*, MS thesis, AFIT/GE/ENG/94D-30, School of Engineering, Air Force Institute of Technology (AU), Wright-Patterson AFB OH, December 1994.

20. Wagner, Eugene H. Jr., *An Analytical Study of T-38 Drag Reduction in Tight Formation Flight*, MS thesis, AFIT/GAE/ENY/02-2, School of Engineering, Air Force Institute of Technology (AU), Wright-Patterson AFB OH, March 2002.

Vita

Major Ryan K. Osteroos was born in Valdosta, Georgia. He graduated from Longmont High School in Longmont, Colorado in 1990. He entered the US Air Force Academy immediately after graduation and earned a Bachelor of Science degree in Astronautical Engineering and was commissioned in May of 1994.

His first assignment was at Sheppard AFB as a student in Euro Nato Joint Jet Pilot Training (ENJJPT) in November of 1994. Upon graduation of ENJJPT in November of 1995 Major Osteroos was assigned to Introduction to Fighter Fundamentals (IFF) in Columbus AFB, MO. Following this assignment he was sent to Seymour Johnson AFB to fly F-15E's. He was subsequently assigned to the 334th, 336th, and 333rd Fighter Squadrons, leaving Seymour Johnson as a 4-ship Flight Lead, IP, Mission Commander, and Functional Check Flight Pilot. In March of 2002 Major Osteroos was selected to attend AFIT as part of the AFIT/TPS program to receive a Masters of Science Degree in Aeronautical Engineering. Upon completion of academic coursework, Major Osteroos proceeded to the USAF Test Pilot School (TPS) at Edwards AFB, California and completed a year of training to become a test pilot. He graduated TPS in December 2004 and graduated from AFIT in March of 2005.

REPORT DOCUMENTATION PAGE

Form Approved
OMB No. 074-0188

The public reporting burden for this collection of information is estimated to average 1 hour per response, including the time for reviewing instructions, searching existing data sources, gathering and maintaining the data needed, and completing and reviewing the collection of information. Send comments regarding this burden estimate or any other aspect of the collection of information, including suggestions for reducing this burden to Department of Defense, Washington Headquarters Services, Directorate for Information Operations and Reports (0704-0188), 1215 Jefferson Davis Highway, Suite 1204, Arlington, VA 22202-4302. Respondents should be aware that notwithstanding any other provision of law, no person shall be subject to an penalty for failing to comply with a collection of information if it does not display a currently valid OMB control number.
PLEASE DO NOT RETURN YOUR FORM TO THE ABOVE ADDRESS.

1. REPORT DATE *(DD-MM-YYYY)*	**2. REPORT TYPE**	**3. DATES COVERED** *(From – To)*
21-03-2005	Master's Thesis	Sep 2002 – Mar 2005

4. TITLE AND SUBTITLE

Full Capability Formation Flight Control

5a. CONTRACT NUMBER

5b. GRANT NUMBER

5c. PROGRAM ELEMENT NUMBER

6. AUTHOR(S)

Osteroos, Ryan, K., Major, USAF

5d. PROJECT NUMBER

5e. TASK NUMBER

5f. WORK UNIT NUMBER

7. PERFORMING ORGANIZATION NAMES(S) AND ADDRESS(S)

Air Force Institute of Technology
Graduate School of Engineering and Management (AFIT/EN)
2950 Hobson Way
Wright Patterson AFB, OH 45433-7765

8. PERFORMING ORGANIZATION REPORT NUMBER

AFIT/GAE/ENY/05-M16

9. SPONSORING/MONITORING AGENCY NAME(S) AND ADDRESS(ES)

United States Air Force Test Pilot School (USAFTPS)
Attn: Maj. Russell G. Adelgren
220 S. Wolfe Ave.
Edwards AFB, CA 93523 DSN: 277-3000

10. SPONSOR/MONITOR'S ACRONYM(S)

11. SPONSOR/MONITOR'S REPORT NUMBER(S)

12. DISTRIBUTION/AVAILABILITY STATEMENT

APPROVED FOR PUBLIC RELEASE; DISTRIBUTION UNLIMITED.

13. SUPPLEMENTARY NOTES

14. ABSTRACT :

The subject of automatic formation flight control is of current interest to the development of Unmanned Aerial Vehicles (UAV). Previous control approaches have been refined in this work to allow more robust maneuvering and to include a fourth control parameter. The equations of motion for each aircraft as a point mass, expressed in a wind-axis coordinate system, are coupled into differential equations that model the two aircraft system dynamics. Control laws are developed that include proportional and integral action. Gains are determined based on formation performance. Lead maneuvers are simulated and the controller is gauged on its ability to maintain the commanded formations in and out of the vortex wake generated by the lead aircraft. A Dryden wind model at varying intensities is applied to the system. In simulation the controller maintained acceptable performance in all maneuvers tested. A slightly modified controller was applied to a USAF NF-16D aircraft for flight testing. Utilizing a data link system and a virtual lead aircraft generated from a ground based control station, the NF-16D was able to flight test the controller. In-flight, the controller was stable, and able to perform all of the desired formation hold and change maneuvers.

15. SUBJECT TERMS

Variable Stability In-Flight Simulator Test Aircraft (VISTA), Automatic Formation, Formation Control, UAV

16. SECURITY CLASSIFICATION OF:			**17. LIMITATION OF ABSTRACT**	**18. NUMBER OF PAGES**	**19a. NAME OF RESPONSIBLE PERSON**
REPORT	**ABSTRACT**	**c. THIS PAGE**			**David R. Jacques, Dr. (SYE)**
U	**U**	**U**	**UU**	205	**19b. TELEPHONE NUMBER** *(Include area code)* (937) 255-7777, ext 3329; email: David.Jacques@afit.edu

Standard Form 298 (Rev: 8-98)
Prescribed by ANSI Std.